Investigating the biological importance of Dipeptidyl Peptidase 9 enzymatic activity using a mouse model

This Thesis is Submitted By

Margaret Gall

In Fulfilment of the requirements for the degree of

Doctor of Philosophy

Sydney Medical School

University of Sydney

December 2016

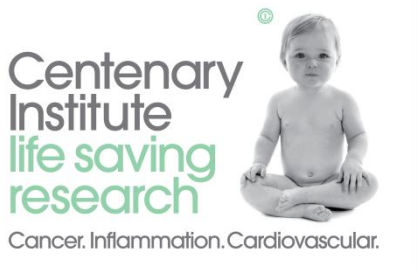

Table of contents

Preface

The work presented in this thesis was undertaken personally by the author between March 2012 and December 2016 under the guidance of Associate Professor Mark Gorrell, Dr Fiona Keane and Dr Adam Cook at the Centenary Institute, Sydney Medical School, University of Sydney. Design of DPP9 enzyme-inactive mice was done by Dr Denise Yu in collaboration with Ozgene (WA, Australia) and generation of heterozygous DPP9$^{wt/S729A}$ mice was performed by Ozgene. This work is original and has not been submitted previously for the purpose of obtaining any other degree. Any collaborative experiments are noted in the thesis where appropriate.

This thesis contains one published work and one work in press, author contributions for this publication are acknowledged in Appendices.

Chapter 1 is in press:

Margaret G Gall and Mark D Gorrell (2016) The multifunctional post-proline dipeptidyl peptidase, DPP9, in mice, cell biology and immunity. In: Pathophysiological aspects of proteases. Editors: Sajal Chakraborti and Naranjan S. Dhalla. Publisher: Springer, New York. In press.

Chapter 3 has been published:

Gall MG, Chen Y, Vieira de Ribeiro AJ, Zhang H, Bailey CG, Spielman DS, Yu DMT, Gorrell MD (2013) Targeted Inactivation of Dipeptidyl Peptidase 9 Enzymatic Activity Causes Mouse Neonate Lethality. PLoS ONE 8(11): e78378. doi:10.1371/journal.pone.0078378

Acknowledgements

I dedicate my thesis to my grandchildren, Azucena, Cooper and Tomas, in hope that they will always remember that you can teach an old dog new tricks.

Even though the past 4 ½ years has had its fair share of extremely stressful moments, I have never regretted embarking on this PhD journey. It has been an experience worth having and I'm grateful to all the people who made it possible for me and those that made it enjoyable and entertaining.

Thank you to my supervisor, Associate Professor Mark Gorrell, and assistant supervisors, Dr Fiona Keane and Dr Adam Cook. Mark, I can't thank enough for your unwavering faith that I was worth persevering with on my journey from student to research assistant to PhD student after my late return to science. You encouraged me to get back up to speed by letting me to attend seminars and conferences. You endured my highs and lows, my ongoing need to deal with family matters and my slow writing of this thesis with patience and good grace.

Also, enormous thanks to you Fiona, who spurred me on when I needed it and, absolutely always, was available for scientific technical guidance, brainstorming and, most importantly, a supportive chat over coffee when things got too much. Throughout my whole time at Centenary Institute, you were and still are an amazing person and a true friend.

Thanks to Dr Adam Cook, who stepped in as assistant supervisor and helped me with the chimera experiments. His depth of knowledge, extreme patience and willingness to assist allowed me to greatly broaden my technical skills and scientific expertise and

made these experiments possible. I would also like to acknowledge the fantastic job done by the Animal Facility staff at CI through my long years of mouse work, especially Rona, Danielle, Marisa, Sarah and Maria.

The other members of our lab, both past and present, have helped in so many ways I couldn't list them and it has been a pleasure being part of such a great team. Special thanks to Libby, Emma, James, Brenna, Sumaiya, Ana Julia, Yiqian and Stef from our lab and Jess, Emily, Nick, Bramilla and Alastair from our floor for, not only helping me with the science, but being a fantastic group of people who made working at Centenary Institute fun.

And last, but by no means least, thanks to my family. The unconditional support I have received from the very first day I announced I was going back to uni until now has been immeasurable. My wonderful husband Phil, my amazing children and their partners, Adam and Ana, Megan and Rossy, Amy and Dean and Chris and Brigitte and my devoted parents, Len and Betty, have shared the journey, shown enthusiasm for my excitement when science answered my questions, tolerated the whining when science didn't cooperate and happily listened to me drone on about my experiments whether they understood what I was talking about or not. This was done with encouragement and love and I don't think I would have got through without all of you. I love every one of you heaps xxxx.

Publications

Publications generated from this thesis

Margaret G Gall and Mark D Gorrell (2016) The multifunctional post-proline dipeptidyl peptidase, DPP9, in mice, cell biology and immunity. In: Pathophysiological aspects of proteases. Editors: Sajal Chakraborti and Naranjan S. Dhalla. Publisher: Springer, New York. In press.

Gall MG, Chen Y, Vieira de Ribeiro AJ, Zhang H, Bailey CG, Spielman DS, et al. (2013) Targeted Inactivation of Dipeptidyl Peptidase 9 Enzymatic Activity Causes Mouse Neonate Lethality. PLoS ONE 8(11): e78378. doi:10.1371/journal.pone.0078378

Other publications

XM Wang, L Holz, S Chowdhury, SP Cordoba, KA Evans, **MG Gall**, AJ Vieira de Ribeiro, YZ Zheng, MT Levy, DMT Yu, N Polak, CJ Jolly, P Bertolino, GW McCaughan, MD Gorrell (2017) Profibrotic role of dipeptidyl peptidase 4 in a carbon tetrachloride induced experimental liver injury. *Immunology and Cell Biology* 95(5), 443-453.

Yiqian Chen, **Margaret G Gall**, Hui Zhang, Fiona M Keane, Geoffrey W McCaughan, Denise M Yu and Mark D. Gorrell (2016) Dipeptidyl Peptidase 9 Enzymatic Activity Influences the Expression of Neonatal Metabolic Genes *Experimental Cell Research* **342**(1): 72-82.

Pok Fai Wong, **Margaret G. Gall**, William W. Bachovchin, Geoffrey W. McCaughan, Fiona M. Keane, Mark D. Gorrell (2016) Neuropeptide Y is a physiological substrate of fibroblast activation protein: enzyme kinetics in blood plasma and expression of Y2R and Y5R in human liver cirrhosis and hepatocellular carcinoma. *Peptides* **75**:80-95. doi:10.1016/j.peptides.2015.11.004

Keane, F M, Yao, T-W, Seelk, S, **Gall, M G**, Chowdhury, S, Poplawski, S E, Lai, J H, Li, Y, Wu, W, Farrell, P, Vieira de Ribeiro, A J, Osborne, B, Yu, D M T, Seth, D, Rahman, K, Haber, P, Topaloglu, A K, Wang, C, Thomson, S, Hennessy, A, Prins, J, Twigg, S M, McLennan, S V, McCaughan, G W, Bachovchin, W W, and Gorrell, M D (2014). Quantitation of Fibroblast Activation Protein (FAP)-specific protease activity in mouse and primate fluids and organs using novel substrate 3144-AMC *FEBS open bio* **4**, 43-54.

Keane, F. M., Chowdhury, S., Yao, T-W., Nadvi, N. A., **Gall, M. G**., Chen, Y., Osborne, B., Ribeiro, A. J. V., Church, W. B., McCaughan, G. W., Gorrell, M. D. and Yu, D. M. T. (2012) Targeting Dipeptidyl Peptidase-4 (DPP-4) and Fibroblast Activation Protein (FAP) for Diabetes and Cancer Therapy, in *Proteinases as Drug Targets* RSC Drug Discovery Series Vol 18. Cambridge, UK: ISBN 978-1-84973-049-5 Royal Society of Chemistry Chapter 5, 119-145.

Conference presentations of work from this thesis

Margaret Gall, Yiqian Chen, Hui Zhang, Elizabeth Hamson, Fiona Keane and Mark Gorrell (2015) Investigating biological roles of Dipeptidyl Peptidase 9 enzyme activity in mice using targeted enzyme inactivation The 15th Hunter Meeting, Australia's Premier Cellular Biology Meeting. Hunter Valley, NSW, Australia 16th-20th March. **Poster presentation**

Margaret Gall, Yiqian Chen, Ana Julia Vieira de Ribeiro, Hui Zhang, Elizabeth Hamson, Fiona Keane, Derek Spielman, Denise Yu and Mark Gorrell (2014) Targeted inactivation of Dipeptidyl Peptidase 9 enzyme activity in mice: neonate lethality and potential roles in epithelia Gordon Research Conference 22nd-27th June. Lucca, Italy. **Poster presentation**

Margaret G Gall, Yiqian Chen, Ana Julia Vieira de Ribeiro, Derek Spielman, Denise MT Yu and Mark D Gorrell (2013) The role of Dipeptidyl Peptidase 9 enzymatic activity in early postnatal mouse survival. The 13th Hunter Meeting, Australia's Premier Cellular Biology Meeting. Hunter Valley, NSW, Australia 19th-22nd March. **Poster presentation**

Margaret G Gall, Yiqian Chen, Ana Julia Vieira de Ribeiro, Derek Spielman, Denise MT Yu and Mark D Gorrell (2013) Targeted inactivation of DPP9 enzyme activity. The 38th Lorne Conference on Protein Structure and Function, Lorne, Vic, Australia 10th - 14th Feb. **Poster presentation**

Margaret G Gall, Yiqian Chen, Ana Julia Vieira de Ribeiro, Hui Zhang,Derek Spielman, Denise MT Yu and Mark D Gorrell (2013). The enzymatic activity of dipeptidyl peptidase 9 is necessary for mouse neonate survival. *International Proteolysis Society 8th General Meeting.* Capetown, South Africa 20th-24th October. **Oral presentation**

List of figures

Chapter 1

Chapter 3

Chapter 4

Chapter 5

Chapter 6

List of Tables

Chapter 2

Chapter 3

Chapter 4

Chapter 6

List of Abbreviations

°C	Degrees Celcius
Bis-Tris	1,3-Bis[tris(hydroxymethyl)methylamino]propane
bp	Base pair
BSA	Bovine serum albumin
CD	Cluster of differentiation
cDNA	Complementary DNA
Da	Dalton
DAB	Diaminobenzidine tetrahydrochloride
DIGE	Differential in-gel electrophoresis
DMEM	Dulbecco's modified eagle media
DMSO	Dimethyl sulfoxide
DNA	deoxyribonucleic acid
DNAse	Deoxyribonuclease
DPL	Dipeptidyl peptidase like protein
DPL-1	Dipeptidyl peptidase like protein 1
DPL-2	Dipeptidyl peptidase like protein 2
DPP	Dipeptidyl peptidase
DPP4	Dipeptidyl peptidase 4
DPP10	Dipeptidyl peptidase 10
DPP6	Dipeptidyl peptidase 6
DPP8	Dipeptidyl peptidase 8
DPP9	Dipeptidyl peptidase 9
ECM	Extracellular matrix
EDTA	Ethylene diamine tetracetic acid
ESFT	Ewing sarcoma family tumour
FACS	Fluorescence-activated cell sorting
FAP	Fibroblast activation protein
GFP	Green fluorescent protein
GIP	Glucose insulinotropic peptide
GKI	Gene knock-in
GKO	Gene knockout
GLP-1	Glucagon-like peptide 1
h	Hour

HRP	Horseradish peroxidase
HSC	Hematopoietic stem cell
kDa	Kilodalton
LC3	Microtubule-associated protein 1 light chain 3
LCFA	Long chain fatty acid
MALDI-TOF	Matrix assisted laser desorption ionisation time-of-flight
MAP1LC3	Microtubule-associated protein 1 light chain 3
MEF	Mouse embryonic fibroblast
min	Minute
mRNA	Messenger ribonucleic acid
MS	Mass spectrometry
MW	Molecular weight
NBF	Neutral buffered formalin
NEM	n-ethylmaleimide
NK	Natural killer
NPY	Neuropeptide Y
PBS	Phosphate buffered saline
PDVF	Polyvinylidene difluoride
RNA	Ribonucleic acid
RNAse	Ribonuclease
rpm	Revolutions per minute
RT	Room temperature
s	Second
SD	Standard deviation
sDPP4	Soluble dipeptidyl peptidase 4
SDS-PAGE	Sodium dodecyl sulfate polyacrylamide gel electrophoresis
SEM	Standard error of the mean
sFAP	Soluble fibroblast activation protein
SUMO1	Small ubiquitin-like modifier 1
TDW	Triple distilled water
TG	Triglyceride
V	Volts
WT	Wild-type

Abstract

Dipeptidyl peptidase 9 (DPP9) is an atypical post-proline serine protease of the DPP4 enzyme family which has ubiquitous expression and DPP4-like enzymatic activity. It is localised intracellularly and has roles in antigen processing and epidermal growth factor signalling. It interacts with H-Ras and small ubiquitin-like modifier-1 and influences cellular interactions with extracellular matrix. Our lab made the first DDP9 gene knock-in (gki) mouse with a DPP9 active site (S729A) mutation which results in a lack of DPP9 enzymatic activity. This thesis investigated the biological properties of DPP9 using this genetically modified mouse model.

Mice lacking DPP9 proteolytic activity die in the early neonatal stage. This study validated that the DPP9 protein, while present in the gki mouse, is enzyme-inactive and the DPP9-S729A protein and wild-type DPP9 have similar subcellular localisation. A range of investigations were undertaken to determine if obvious histological and/or physiological differences exist between early neonate DPP9$^{S729A/S729A}$ homozygotes from their heterozygous and wild-type littermates and involved analysis of organ morphology, histology and function and investigation of autophagy. The novel findings of this study show that DPP9 enzymatic activity is essential for early neonatal survival in mice and suggest that there is dysregulated autophagy in the DPP9-enzyme-activity-deficient neonatal mice that may contribute to the lethal phenotype.

Other members of the DPP4 protein family are implicated in wound healing with

fibroblast activation protein expressed in the granulation tissue of healing wounds and DPP4-positive T cells involved in regulation of granulation tissue formation. As there is a heterozygous effect on survival to weaning and DPP9 immunoreactivity was shown in the skin of both WT and DPP9$^{S729A/S729A}$ neonates, the skin of adult mice was studied using a model of cutaneous wound healing. This involved analysis of wound closure rates, tensile strength and collagen levels of both wounded and steady state tissue in adult DPP9$^{wt/S729A}$ mice and their wild-type littermates. It was found that adult heterozygous DPP9-GKI mice display reduced skin collagen levels compared to their WT littermates, but that the rate of skin wound healing appeared unaffected.

DPP9 has *in vivo* expression in normal immunological tissues and major lymphocyte populations that alters with chronic liver injury, suggesting a role in immune function. To investigate the importance of DPP9 in immune regeneration and function, primary and secondary mixed chimeric mice were created using DPP9$^{S729A/S729A}$ and WT fetal liver cells and adult bone marrow, respectively, injected into irradiated recipients. The process of regeneration of the immune system in these mice was assessed at several time-points and the immune cells present in the regenerated immune systems were compared between DPP9$^{S729A/S729A}$ -origin and WT-origin chimeras. These chimeric mice were then subjected to an immune challenge by influenza virus infection. The novel findings of this study suggest that DPP9-enzyme-activity-deficient secondary chimeric mice may have an enhanced ability to recover from an immune challenge with influenza virus. Therefore, DPP9 appears to influence immune function in that viral infection.

Together, these studies underline the biological significance of DPP9 *in vivo* in both neonatal and adult mice. These data contribute to the expanding knowledge of the role of DPP9, building upon recent discoveries *in vitro* of its involvement in multiple biological processes. By providing physiologically relevant results, this study has enhanced the knowledge of DPP9 enzyme function and the overall biological roles of DPP9.

CHAPTER 1:

Introduction

Statement

Chapter 1 is currently in press:

Margaret G Gall and Mark D Gorrell (2016) The multifunctional post-proline dipeptidyl peptidase, DPP9, in mice, cell biology and immunity. In: Pathophysiological aspects of proteases. Editors: Sajal Chakraborti and Naranjan S. Dhalla. Publisher: Springer, New York. In press.

Chapter 1 is mostly contained in the final submission for publication, except for minor additions and corrections. The written permission and statement of contribution by the co-author is attached in Appendix 1

1 Introduction

1.1 The Dipeptidyl Peptidase 4 (DPP4) Family

Proteases are important regulatory and modifying molecules which are responsible for the dynamic upkeep of many cellular physiological processes. The DPP4 family of enzymes are serine proteases of the S9b protease subfamily which are ubiquitously expressed and contain a conserved catalytic triad of serine, aspartate and histidine (Gorrell and Yu, 2005). They possess a rare ability to cleave a post-proline peptide bond near the N-terminus of a protein (Abbott et al., 2000a, Ajami et al., 2004, Qi et al., 2003). The presence of a proline near the N-terminus of a peptide (*Figure 1.1*) confers resistance against protease degradation and occurs in many different biologically active peptides, including chemokines, incretins and neuropeptides. Thus,

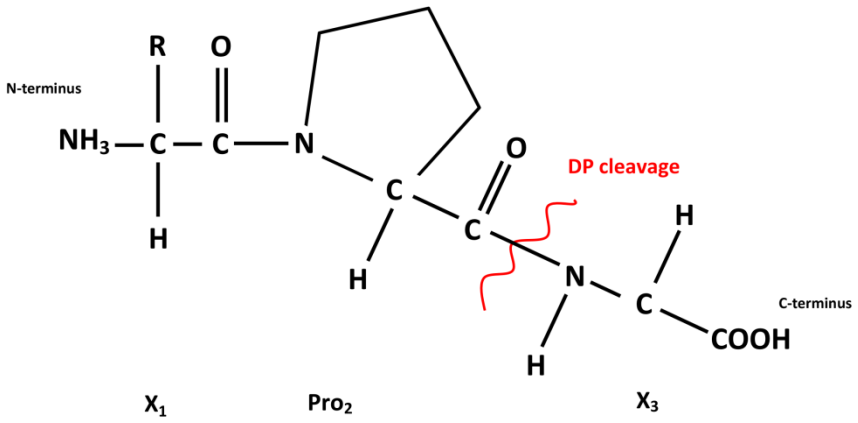

Figure 1.1: Cleavage of a post-proline bond.

A tri-peptide containing a proline at position two creating a bend in the peptide chain. Dipeptidyl peptidase cleavage occurs C-terminal to the proline residue.

the specialised ability of dipeptidyl peptidases to cleave these bonds is useful for processing and degradation of such peptides (Cunningham and O'Connor, 1997).

The DPP4 protein family consists of six members: four enzymatic members and two non-enzymatic members. DPP4, DPP8, DPP9 and fibroblast activation protein (FAP) have dipeptidyl peptidase activity while FAP is also an endopeptidase. The two non-enzymatic members are dipeptidyl peptidase like protein (DPL)-1 and DPL-2. (*Figure 1.2*)

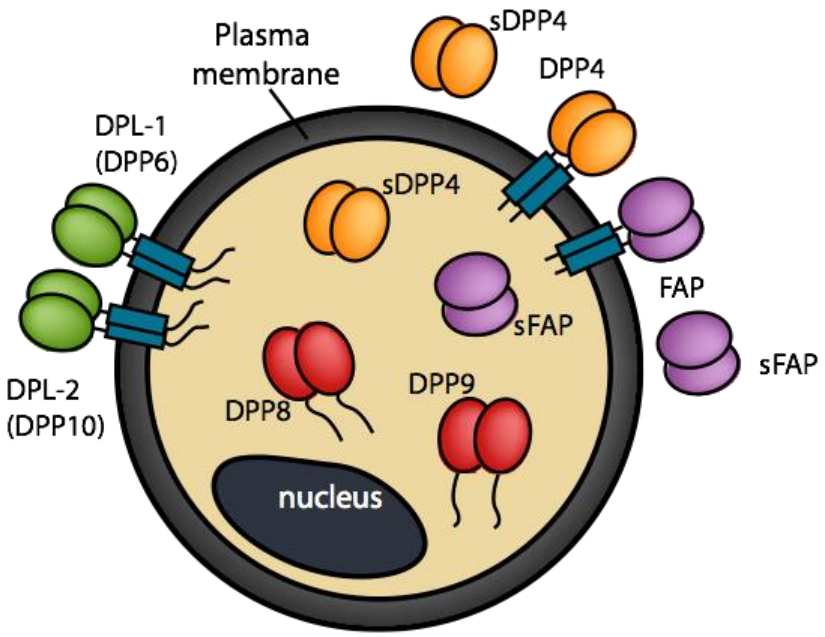

Figure 1.2.: Cellular localisation of the six members of the DPP4 family. DPP4 and FAP are membrane-bound cell surface proteases and also exist in soluble forms both inside and outside the cell. DPP8 and DPP9 are intracellular proteases. DPL1- and DPL-2 are membrane-bound, non-enzymatic proteins. Adapted from (Kirby et al., 2010)

1.1.1 DPP4

DPP4 is the prototypical and most well characterised member of the family. It displays enzymatic activity in both the dimeric cell-surface membrane-bound form and in the soluble circulating form (Gorrell, 2005). In the bound form, DPP4 is expressed by epithelial cells in the liver, gut, uterus and kidney; by capillary endothelium of all organs examined; by acinar cells of mucous, salivary glands and pancreas and by immune organs (Gorrell et al., 2001). The soluble form is present in serum, seminal fluid, saliva, kidney, liver and bile (Keane et al., 2012, Keane et al., 2014).

Functionally, DPP4 is involved in numerous processes throughout the body, including immunological, endocrine, haematological and metabolic (Yu et al., 2010). These include the ability to participate in chemokine inactivation and also to have a role in apoptosis, lymphocyte activation and cell migration, along with the capacity to cleave a wide range of small bioactive proteins (Keane et al., 2012, Waumans Y et al., 2015). Most noted of these is the ability of DPP4 to rapidly inactivate the incretins glucagon-like peptide-1 (GLP-1) and glucose insulinotropic peptide (GIP) (Mentlein et al., 1993) leading to the inhibition of DPP4 as a successful type 2 diabetes therapy. DPP4 inhibitors are now implicated in a wide range of physiological and metabolic benefits and potential benefits including improved cardiac health, improved glucose uptake, improved energy metabolism and less fat accumulation (Keane et al., 2012). DPP4 is also known as CD26 and, as such, has roles in the immune system in T cell activation and proliferation and T helper 1 responses to foreign antigens. Cell surface expression on T cells greatly increases following stimulation with antigen or mitogens (Gorrell et al., 1991, Gorrell et al., 2001, Chowdhury et al., 2013).

1.1.2 FAP

FAP, which is also known as seprase, also displays enzymatic activity as a transmembrane protein or a soluble protease. Although DPP4 and FAP share 52% amino acid sequence identity, these proteins differ in their enzyme activities and expression profiles. FAP possesses both dipeptidyl peptidase and endopeptidase activites, which enables it to cleave a prolyl bond two or more amino acids from the N-terminus of a protein (*Figure 1.3*) (Aertgeerts et al., 2005).

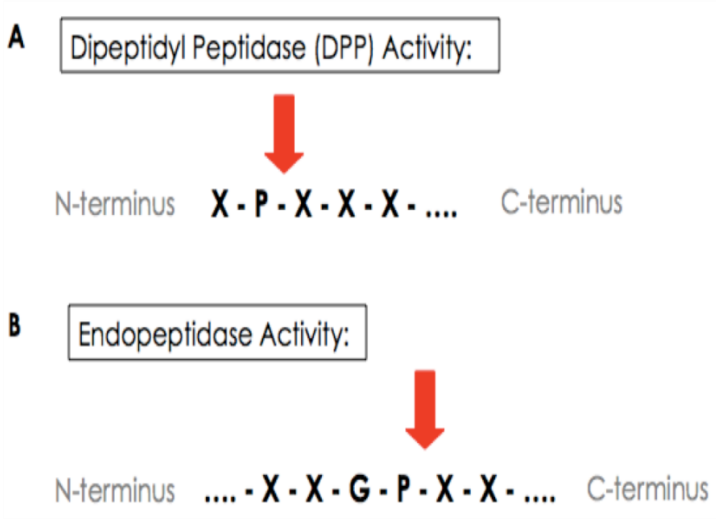

Figure 1.3: Enzyme activity of FAP

A Dipeptidyl peptidase activity involves the cleavage of two amino acids off the N-terminus of a protein following a proline residue.

B Endopeptidase activity involves the cleavage of a post-proline bond that is more than two amino acids from the N-terminus of a protein.

While DPP4 is abundant in most tissues, FAP is at very low levels (Keane et al., 2014) with high level expression being limited to sites of tissue remodelling and areas of stromal activation, such as in wound healing, tissue damage and inflammation (Garin-Chesa et al., 1990), during mouse embryogenesis (Niedermeyer et al., 2001) and in activated hepatic stellate cells in cirrhotic liver (Levy et al., 1997, Wang et al., 2005). FAP has, however, also been isolated in a truncated form from human plasma (Lee et al., 2006b) and bovine serum (Collins et al., 2004). FAP activity levels in normal and diseased tissue from humans, mice and baboons, has been extensively analysed by our group using the novel FAP-specific substrate, 3144-AMC. In mice, uterus, pancreas, submaxillary gland and skin showed the highest levels of FAP activity (Keane et al., 2014).

While FAP has been shown to cleave some DPP4 substrates *in vitro* (Keane et al., 2011), until recently there were no known physiological substrates of FAP's dipeptidyl peptidase activity. This lab carried out the first study to characterize the physiological DPP substrate repertoire of endogenous FAP in mammalian plasma, thereby revealing a potential function of FAP in neuropeptide signaling within liver and cancer biology (Wong et al., 2016). In addition to its dipeptidyl peptidase activity, FAP also has endopeptidase activity cleaving known substrates α2-antiplasmin (Lee et al., 2006b) and denatured type I collagen (Park et al., 1999). The gelatinase activity of FAP most likely contributes to extracellular matrix degradation.

Because of its pattern of expression on activated stromal fibroblasts in many cancers, FAP has been studied as a therapeutic target in tumours. This role in cancer biology

has been reviewed previously (Sulda et al., 2010, Hamson et al., 2014). Strategies for targeting FAP for cancer therapy include the use of inhibitors, antibodies, prodrugs and T-cell immunotherapy however, as the role of FAP seems to be highly contextual, the expression pattern of FAP requires greater definition to better predict the effects of targeting this protease.

1.1.3 DPL-1 and DPL-2

DPL-1 (DPP6) and DPL-2 (DPP10) have 53% amino acid similarity with each other and are highly homologous to DPP4 with sequence identities of 33% and 32% respectively (Qi et al., 2003, Chen et al., 2005). While they both have dimeric forms, they lack the catalytic serine and a nearby tryptophan that are essential for enzymatic activity. DPL-1 has a wide tissue distribution but DPL-2, in contrast, has expression limited to human brain, adrenal gland and pancreas (Abbott and Gorrell, 2002, Qi et al., 2003, Chen et al., 2005). The functional effects of these proteins appear to be through binding interactions and there is evidence of an association between DPL-1 and DPL-2 and neuronal diseases (Chen et al., 2008) and asthma (Cronin et al., 2008) with DPL-2 being indicated in a possible role in excitability of neurons in the lung airway (Ren et al., 2005).

1.1.4 DPP8 and DPP9

DPP8 and its closest relative DPP9 are the most recently discovered members of the DPP4 gene family (Abbott et al., 2000b, Olsen and Wagtmann, 2002, Qi et al., 2003,

Ajami et al., 2004). As DPP4, DPP8 and DPP9 all have DPP4-like enzymatic activity and ubiquitous expression, the discovery of DPP8 and DPP9 has called for the reinterpretation of previous DPP4 data (Abbott et al., 2000b, Ajami et al., 2004). This was necessary to determine which functions had been attributed to DPP4 which may instead be accounted for by DPP8 and DPP9.

Unlike DPP4, DPP8 and DPP9 are intracellular proteins and are therefore likely to have different biological roles. As there are currently no substrates or inhibitors that distinguish DPP8 from DPP9, their characteristics are usually outlined together. DPP8 and DPP9 are currently under study in many fields including cell biology, immune-biology and tumour biology (Zhang et al., 2013).

1.1.4.1 Structure of DPP8 and DPP9

DPP8 and *DPP9* are located on human chromosome 15q22 and 19p13.3 (Abbott et al., 2000b, Olsen and Wagtmann, 2002) and mouse chromosome 9 and 17 respectively. In *DPP4* and *FAP*, the sequence adjacent to the active-site serine is encoded by two exons while the homologous region in *DPP8* and *DPP9* is encoded by a single exon which suggests that the *DPP8* and *DPP9* genes arose at an earlier evolutionary stage.

Although located on different chromosomes the resultant proteins have a closely related sequence, sharing 58% overall identity to each other and 72% in the catalytic region (Ajami et al., 2004) suggesting that they may have arisen by gene duplication (Olsen and Wagtmann, 2002). There is a high homology between the amino acid sequences of human and mouse DPP8 and DPP9, with 95% and 92% identity

respectively (Olsen and Wagtmann, 2002, Ajami et al., 2004). Currently, no crystal structures of DPP8 or DPP9 exist but homology models have been built using the known structures of DPP4, DPL-1 and FAP (Park et al., 2008, Rummey and Metz, 2007). In these models, DPP8/9 is depicted with an α/β-hydrolase domain containing a Ser-Asp-His catalytic triad and an 8-blade β-propeller domain containing two glutamic

Figure 1.4: A putative model of DPP9 protein structure.

DPP9 residues 51 to 863 are depicted in ribbon representation of the monomer. The α/β-hydrolase domain is in red and the 8-blade β-propeller domain in green. The catalytic triad (Ser-Asp-His) is shown as blue spheres in the hydrolase domain and the 2 glutamates essential for catalysis as yellow spheres in the propeller domain. An extended arm (^{285}VEVIHVPSPALEERKTDSYR^{304}) in the propeller surface of DPP9 that is critical in SUMO1–DPP9 interaction is colored pink. Modified from (Zhang et al., 2013)

acids essential to functionality of the catalytic pocket (*Figure 1.4*).

While structurally similar to DPP4 and FAP, DPP8 and DPP9 lack a transmembrane domain and are translated as intracellular proteins (Abbott et al., 2000b, Ajami et al., 2004). Another structural difference between DPP4 and DPP8 and 9 is that selective point mutations in the C-terminal loop of both proteases can result in their inactivation but the integrity of their dimeric structure is maintained (Tang et al., 2009). This confirms the importance of the C-terminal loop for DPP8 and DPP9 enzymatic function. Finally, since DPP8 has been shown to have a larger substrate pocket than DPP4 (Pitman et al., 2010), there is some suggestion that DPP8 and DPP9 might have a larger β-propeller domain and/or contain a separate element of tertiary structure at the N-terminus of the protein.

1.1.4.2 Expression profiles and tissue distribution of DPP8 and DPP9

DPP8 and DPP9 are cytoplasmic enzymes that are ubiquitously expressed in tissues at both the mRNA (Olsen and Wagtmann, 2002, Bjelke et al., 2006, Qi et al., 2003) and protein levels (Yu et al., 2009) and both DPP8 and DPP9 occur in different isoforms.

Human DPP8 has several mRNA transcripts identified, one is abundant in testis, prostate and muscle (Abbott et al., 2000b, Qi et al., 2003) while another longer transcript variant has intense signals in adult testis (Zhu et al., 2005). Bioinformatics analysis of NCBI database sequences has identified at least two other isoforms (Abbott and Gorrell, 2013).

DPP9 cDNA was cloned in two forms with the short form encoding 863 amino acids (Olsen and Wagtmann, 2002, Ajami et al., 2004) and the longer full-length form encoding 971 amino acids (Ajami et al., 2004). The short form is ubiquitously expressed including high levels in liver, heart and skeletal muscle, while the long form is much less abundant and is predominantly expressed in skeletal muscle. It has been recently shown that the N-terminal extension of the long form of DPP9 contains a nuclear localisation signal (NLS) allowing it to preferentially localise to the nucleus (Justa-Schuch et al., 2014).

In canine and porcine small intestine, lung, kidney and pancreas, differential relative abundance of DPP8 and DPP9 has been measured by RT-PCR analysis with DPP9 having the greater expression (Wagner et al., 2006b). In adult mice, greater numbers of DPP9 transcripts are in brain, skin, colon and thymus compared with DPP4 (Helmuth et al., 2006, Ansorge et al., 2009, Wagner et al., 2006a).

DPP8 mRNA is in human testes and upregulated in adult testis compared to fetal testis (Zhu et al., 2005). DPP8 and DPP9 is also present in the male reproductive tissue of different mammals with bovine and rat testis showing DPP8/9 localised in spermatozoids embedded in the epithelium of the seminiferous tubules (Dubois et al., 2009). DPP9 has been purified from bovine testes and identified and characterised as the short form isoform (Dubois et al., 2010). Taken together, these studies suggest a role for DPP8 and DPP9 in spermatogenesis and male fertility.

Using *in situ* hybridisation, immunohistochemistry and enzyme assays on baboon and human tissues, the ubiquitous expression and distribution of DPP8 and DPP9 has been

validated in lymphocytes and epithelial cells in the brain, muscle, gastrointestinal tract, liver, lung, spleen, lymph node and skin, as well as in pancreatic acinar cells, adrenal gland, spermatogonia and spermatids of testis and Purkinje cells and the granular layer of the cerebellum (Yu et al., 2009). These findings are in agreement with related studies (Stremenova et al., 2007, Schade et al., 2008, Dubois et al., 2009).

More recently, data on mRNA and protein levels in Sprague-Dawley rat and cynomolgus monkey showed similar ubiquitous expression and tissue distribution correlation with specific enzymatic activity in those species (Harstad et al., 2013). DPP8 and DPP9 have been shown to be in rat primary endothelial cells of aortic, endocardial and cardiac microvascular origin (Matheeussen et al., 2011) with a greater abundance of DPP8 protein over DPP9. However, in human carotid artery endothelial cells, DPP9 is the only DPP4-like enzyme detected using immunohistochemistry suggesting a regulated expression of DPPs in endothelial cells.

Both DPP8 and DPP9 expression has been shown to be present in tumour tissues (Ajami et al., 2004, Yu et al., 2009), hepatocytes (Yu et al., 2009, Yao et al., 2011, Chowdhury et al., 2013) and lymphocytes (Maes et al., 2007, Yu et al., 2009, Chowdhury et al., 2013) but absent from activated stellate cells (Yu et al., 2009). Recent reviews provide more detailed information regarding the expression and distribution of DPP8 and/or DPP9 (Yu et al., 2010, Wilson and Abbott, 2012b, Zhang et al., 2013, Waumans Y et al., 2015).

1.1.4.3 Enzymatic activity and substrate specificity of DPP8 and DPP9

Although originally identified as monomers, both DPP8 and DPP9 are now known to be catalytically active as dimers in their dominant conformation (Bjelke et al., 2006, Lee et al., 2006a, Tang et al., 2009). Both DPP8 and DPP9 have optimum activity at neutral to basic pH of 7.0 – 8.5 (Abbott et al., 2000b, Qi et al., 2003, Tang et al., 2009) which is consistent with cytoplasmic localisation. DPP8 and DPP9 have reversible variation in

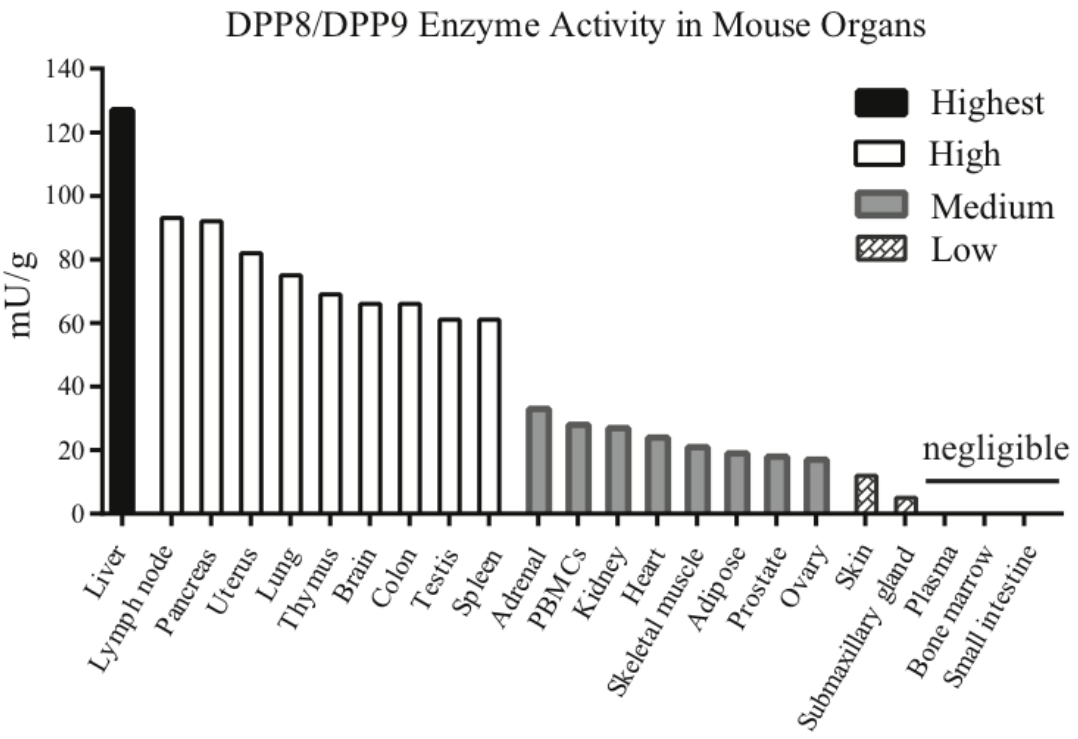

Figure 1.5: DPP8/DPP9 enzyme activity in mouse organs.

The approximate intensity of DPP8 and DPP9 enzyme activity was measured by Yu and colleagues (Yu et al., 2009) from mouse organs in DPP4-gene knockout mice with/without the addition of N-ethylmaleimide (NEM), which modifies thiols and inhibits DPP8/9. NEM-inhibited activity was subtracted from total DPP activity to estimate the activity derived from DPP8 and DPP9. From (Zhang et al., 2013)

enzymatic activity dependent on the redox state of their cysteine moieties with activity decreased by oxidation and increased by reduction (Park et al., 2008, Geiss-Friedlander et al., 2009). DPP9 is also allosterically activated by SUMO1 (Pilla et al., 2012), however the small peptide region of SUMO1 which interacts with DPP9 was also shown to act as a non-competitive inhibitor of DPP9 activity with inhibition dependent on the residues in the DPP9 arm motif (Figure 1.4) (Pilla et al., 2013).

Both enzymes have similar substrate specificity, preferring a proline in the penultimate P1 position and small or basic amino acid residues at the P2 position of synthetic substrates (Lee et al., 2006a, Geiss-Friedlander et al., 2009, Tang et al., 2009). This was confirmed by an *in vivo* substrate study which showed DPP8 and DPP9 favoured natural substrates with a P1 proline preceeded by an alanine in the P2 position (Wilson et al., 2013). Ala-Pro- and Gly-Pro-containing fluorogenic and chromogenic substrates have been routinely used to determine DPP8/9 enzymatic activity derived from DPP8 and DPP9 (Figure 1.5), but Arg-Pro is also hydrolysed (Ajami et al., 2004, Yu et al., 2009).

DPP8 and/or DPP9 are able to cleave a number of naturally occurring peptides and chemokines *in vitro* but with reduced rates of hydrolysis compared to DPP4 (Ajami et al., 2008). Whether these predominantly extracellular substrates have physiological relevance, however, when considering the intracellular location of DPP8 and DPP9, is unclear. It has previously been shown that neuropeptide Y (NPY) can be cleaved by DPP4, DPP8, DPP9 and FAP (Mentlein, 1999, Bjelke et al., 2006, Frerker et al., 2007, Keane et al., 2011). NPY extracted from rat brain can be cleaved in the presence of a

DPP4 inhibitor, suggesting that DPP8 and DPP9 can cleave NPY *in vivo* (Frerker et al., 2007). A later study of dipeptidyl peptidases in tumour cells showed that NPY could act as a substrate for DPP8 and DPP9 in intact cells, not just cell extracts. Cleavage of releasable NPY by DPP4, DPP8 and DPP9, but not FAP, regulates Ewing Sarcoma family tumour cells (ESFT) by reducing NPY-induced cell death (Lu et al., 2011).

A role of DPP9 in antigen presentation and peptide turnover was shown by the identification of the antigenic peptide $RU1_{34-42}$ as its first natural substrate. This peptide is degraded *in vitro* by both DPP8 and DPP9, however, silencing of DPP8 and DPP9 using siRNA resulted in increased RU1 presentation only in DPP9-silenced cells, which indicated that the $RU1_{34-42}$ antigen is a substrate of DPP9 (Geiss-Friedlander et al., 2009). DPP9 substrates have been sought using a degradomic approach and resulted in the identification and validation *in vitro* of adenylate kinase 2 and calreticulin as DPP8 and DPP9 substrates. That study suggested a role for DPP8 and DPP9 in cellular metabolism and homeostasis (Wilson et al., 2013).

By targeting the DPP9 protein active site with a serine to alanine point mutation, we were able to create a DPP9 gene knock-in mouse (DPP9-GKI) that lacks DPP9 enzymatic activity while maintaining normal DPP9 protein structure. This mouse exhibits neonate lethality suggesting that DPP9 enzymatic activity is essential for early neonatal survival in mice (Gall et al., 2013)(Chapter 3 of this thesis). Further studies using neonatal liver and gut from DPP9-GKI mice compared to WT have shown that DPP9 enzymatic activity influences the expression of neonatal metabolic genes. Differential gene expression patterns of genes involved in cell growth, innate immunity, lipid

metabolism and gluconeogenesis were found suggesting a role for DPP9 enzymatic activity in regulation of metabolic pathways in the neonate (Chen et al., 2016).

Most recently, two-dimensional differential in-gel electrophoresis (DIGE) was used *in vitro* on cells lacking endogenous DPP9 activity to identify novel DPP9 substrates (Zhang et al., 2015b), with nine being confirmed as substrates by MALDI-TOF or immunoblotting. This study also identified a DPP9-specific consensus site for cleavage (Val-Ala) that was not recognised by DPP8, suggesting that these two proteases have different *in vivo* roles.

1.1.4.4 Non-enzymatic functions of DPP8 and DPP9

Early investigations showed potential roles for DPP8 and DPP9 in apoptosis, wound healing and cell migration. *In-vitro* over-expression of DPP8 and DPP9 resulted in impaired cell adhesion, migration and monolayer wound healing for DPP9 and impaired migration and wound healing for DPP8, suggesting that those outcomes may result from direct protein-protein interactions or via altered expression of other proteins involved in cell adhesion and migration (Yu et al., 2006b). Both DPP8 and DPP9 also enhanced apoptosis. Using enzyme-negative mutants of each protein, in which enzyme activity was absent, the role of DPP8 and DPP9 in apoptosis appeared to be independent of enzymatic activity.

Recent work supported the finding of the previous study (Yu et al., 2006b) that apoptosis and cell death were unaffected by DPP9 knockdown or enzyme inhibition, but has provided contrary data on cell adhesion and migration compared to the part of

that earlier work that examined protein over-expression in 293T cells (Zhang et al., 2015b). Inhibition or silencing of DPP9 in Huh7 cells resulted in less cell mobility and adhesion compared to control cells (Zhang et al., 2015a), indicating that DPP9 enzymatic function is important for these processes. The mechanistic roles of DPP8 and DPP9 require further study.

1.1.4.5 Inhibition of DPP8 and DPP9

Many early DPP4 inhibitors were later found to also inhibit DPP8 and DPP9, raising the question of which functions attributed to DPP4 activity, should be attributed to DPP8 and/or DPP9. This has led to the development of many inhibitors that are selective for DPP8 and DPP9 over DPP4 and FAP (Lankas et al., 2005, Wu et al., 2009, Jiaang et al., 2005, Van der Veken et al., 2008, Van Goethem et al., 2011) but are not selective for DPP8 or DPP9 alone. While some isoindoline inhibitors were originally thought to inhibit DPP8 alone (Jiaang et al., 2005, Van der Veken et al., 2007), these were later shown to inhibit both DPP8 and DPP9 (Wu et al., 2009).

The safety of targetting DPP8/9 activity for therapeutic use has been controversial with toxic effects reported in rats with the use of the DPP8/9 selective inhibitor, UAMC00132 (Lankas et al., 2005), while a later study on rats and mice using vildagliptin at high doses showed no toxicity or mortality of animals (Burkey et al., 2008). Using the compound 1G244, Wu *et al* did not discover any pathological symptoms of inhibiting DPP8 and DPP9 (Wu et al., 2009). With the recent design of two analogues of 1G244 which have shown a 10-fold selectivity for DPP8 over DPP9

(Van Goethem et al., 2011), there is good progress towards selectively differentiating between these two enzymes by inhibition of either DPP8 or DPP9, rather than both.

An alternative approach to chemical inhibitors has been studied in other DPPs, namely DPP4 and FAP. As these proteases also have non-enzymatic functions, there have been attempts to treat disease by blocking protein-binding interactions using immunotherapy, with several studies undertaken to demonstrate the efficacy of immunotargetting DPP4 (Ohnuma et al., 2002, Ho et al., 2001, Inamoto et al., 2006, Inamoto et al., 2007). Another study involved the use of a non-substrate nonapeptide, the HIV-1 Tat protein, which was identified as the first natural inhibitor of DPP4, as an immunosuppressor (Wrenger et al., 2008). However, whether these nonapeptides can enter the cell and act on DPP8 and DPP9 was not shown.

More recently, it was found that, while the small ubiquitin-like protein modifier SUMO1 interacts with DPP9 leading to allosteric activation of the peptide (Pilla et al., 2012), the E67-interacting loop peptide acts as a non-competitive inhibitor (Pilla et al., 2013). This highlights the potential modulation of enzyme activity by peptides that mimic interaction surfaces. Development of therapeutics which target the non-enzymatic activities of DPP8 and DPP9 as a therapeutic approach will require further research aimed at identifying protein-binding partners.

1.1.4.6 Biological functions of DPP8 and DPP9

Knowledge of the precise physiological functions of DPP8 and DPP9 is emerging with further research into their roles in normal homeostasis and pathophysiological

conditions. Data on enzymatic activity, substrate specificity and cell and tissue distribution of these proteases provide some clues to their biological functions, such as cell survival and cell biology, disease and inflammation and both cell-mediated and humoral immunity.

1.1.4.6.1 DPP8 and DPP9 in immunity

1.1.4.6.1.1 DPP8 and DPP9 in innate immunity

The innate immune system consists of cells and proteins that are always present and ready to activate and attack when exposed to alien elements. The non-specific defence mechanisms which initiate after exposure to foreign substances can include physical barriers, such as skin, blood-borne chemicals and immune cells, such as phagocytic leukocytes, dendritic cells and natural killer (NK) cells. DPP8 and DPP9 have been shown to have extensive *in vivo* expression in epithelial cells of the gut and skin and normal immunological tissues (Yu et al., 2009) and also are expressed by all major lymphocyte populations (Abbott et al., 2000b, Chowdhury et al., 2013).

Natural killer (NK) cells play a major role in host-rejection of both tumours and virally infected cells in the innate immune system. An early study showed that inhibition of DPP4 enzyme activity resulted in the suppression of certain stimulatory cytokines causing a reduction of DNA synthesis and cell cycle progression (Buhling et al., 1994). However, the inhibitors used in that study were later shown to also inhibit DPP8/9 activity (Lankas et al., 2005), therefore those effects were possibly DPP8/9 mediated. Further support for that conclusion derives from the finding that the presence or absence of DPP4 on the cell surface of NK cells does not influence the natural

cytotoxicity of these cells (Madueno et al., 1993). Interestingly, in a lung metastasis model using DPP4-deficient rats, NK cytolytic function against tumour cells is lessened (Shingu et al., 2003).

1.1.4.6.1.2 DPP8 and DPP9 in adaptive immunity

The antigen-specific adaptive immune response is more complex and includes a "memory" that improves the efficiency of future responses and depends upon antigen presentation and recognition. DPP9 has been shown to be involved in the degradation *in vitro* of the antigenic peptide $RU1_{34-42}$ and, hence, down-regulation of DPP9 results in increased presentation of this antigen (Geiss-Friedlander et al., 2009).

DPP8 and DPP9 have also been shown to be up-regulated upon B or T cell activation (Chowdhury et al., 2013). Several T cell leukemia cell lines highly expressed DPP8 and DPDP9 mRNA transcripts (Tadje et al., 2008), while CD3+ T cells isolated from healthy human donors showed up-regulation of DPP9 mRNA after T cell activation (Heimburg et al., 2008).

DPP8/9 enzyme activity has been found in human lymphocytes, monocytes and also in human and mouse primary leukocytes and monocytes, B and T cell lines (Abbott et al., 2000b, Lankas et al., 2005, Maes et al., 2007, Bank et al., 2011). While thought to be only located intracellularly, one study suggested that DPP8 and DPP9 may also be present on the surface of immune cells under certain conditions (Bank et al., 2011), although they indicated that there was uncertainty whether this externalisation of DPP8 and DPP9 was undertaken actively by viable cells or passively by stressed, apoptotic or necrotic cells. In a rat model of cerebral ischemia, an association was

found between DPP8 and active microglia and macrophages (Röhnert et al., 2012) and a study of atherosclerosis showed an abundance of DPP8 and DPP9 in the macrophage-rich regions of atherosclerotic plaques (Matheeussen et al., 2013).

While mouse-spleen derived B lymphocytes express little DPP4 mRNA, DPP8 and DPP9 mRNA are expressed at greater levels and stimulation with pokeweed mitogen and lipopolysaccharide of mouse splenocytes, Jurkat T- and Raji B-cell lines up-regulates both proteins (Chowdhury et al., 2013). DPP8 and DPP9 mRNA are down-regulated after dithiothreitol (DTT) treatment and up-regulated upon mitomycin c treatment in Raji cells. Contrary to this, Jurkat cells or peripheral blood mononuclear cells stimulated with phytohaemagglutinin does not change DPP8 or DPP9 expression levels (Tang et al., 2009).

DPP8 and DPP9 has been detected by *in-situ* hybridisation in lymphocytes in the mantle and paracortical zones of human lymph node and baboon spleen and DPP8/9 activity was detected in interfollicular T-cells of baboon spleen and Jurkat cells (Yu et al., 2009). Activation and proliferation of immune cells appears to be affected by DPP8 and DPP9 enzymatic activity and selective DPP8/9 inhibition can reduce cytokine production due to the induction of TGF-β secretion, as well as DNA synthesis and T cell proliferation (Lankas et al., 2005, Reinhold et al., 2009). This is suggestive of DPP8/9 enzyme activity having important roles in the regulation of immune function.

1.1.4.6.2 DPP8 and DPP9 in cell biology and cell survival

In an early study, both DPP8 and DPP9 were involved in cell-extracellular matrix interactions and influenced apoptosis but DPP8 did not influence cell adhesion and

only DPP9 was a primary trigger of apoptosis (Yu et al., 2006b). Overexpression of DPP8 and DPP9 in HEK293T epithelial cells showed impaired cell adhesion, migration and monolayer wound healing *in vitro* which appeared to be independent of enzyme activity. While DPP8 and DPP9 are very similar intracellular enzymes and both ubiquitously expressed, DPP9, as suggested by the literature, appears to have a more pronounced role in cell biology.

DPP9 mRNA expression is up-regulated after activation in human T-cells, in contrast to DPP8 (Heimburg et al., 2008, Tadje et al., 2008) and DPP9 mRNA was also elevated in cartilage from osteoarthritis patients (Milner et al., 2008). A study of normal and keloid-derived skin fibroblasts *in vitro* showed that inhibitors of DPP8 and DPP9 could suppress proliferation, decrease fibrogenic cytokine transforming growth factor-β_1 and secretion of procollagen type 1, which is seen as a major therapeutic goal in the treatment of fibrotic skin disorders and keloids (Thielitz et al., 2008).

In sarcoma cell lines, NPY-driven tumour cell death, mediated by the nuclear protein modifying enzyme poly(ADP-ribose) polymerase (PARP-1) and apoptosis-inducing factor, can be abolished by the overexpression of DPP8 and DPP9 and enhanced by their own down-regulation (Lu et al., 2011). In contrast, overexpression of DPP9 in epithelial tumour cell lines is anti-proliferative and enhances intrinsic apoptosis (Yu et al., 2006a, Yao et al., 2011). DPP9 overexpression was also shown to result in significantly less epidermal growth factor(EGF)-mediated Akt pathway activation in HepG2 cells but not observed in cells stimulated with other growth factors, suggesting that this activation was growth factor dependent (Yao et al., 2011). Since experiments

in which DPP9 is overexpressed, gene-silenced or inhibited have resulted in conflicting data, the pro- or anti-apoptotic activity of this enzyme may depend on its *in vitro* culture environment and/or the cell type in which the experiment is undertaken.

While studying the antileukemic activity of the chemotherapy drug, parthenolide, and using a high-throughput screen, it has been found that the DPP inhibitor vildagliptin synergistically enhances parthenolide's action in leukemia, lymphoma and primary human acute myeloid leukemia cell lines (Spagnuolo et al., 2013). This synergy is due to the inhibition of DPP8 and DPP9 rather than DPP4 suggesting that this inhibition might be used as a chemosensitising strategy for leukemia cells.

Primary endothelial cells from aortic, endocardial and cardiac microvascular regions of the rat heart contain DPP8/9 enzymatic activity, with DPP8 protein more abundant than DPP9 (Matheeussen et al., 2011). In that study, the localisation of DPP8 and DPP9 showed spatial heterogeneity, with DPP8 more abundant in the cardiac microvascular endothelium and DPP9 predominant in human carotid artery endothelial cells.

More recently, that research group focussed on the expression of DPPs in human atherosclerotic plaques by using the monocyte cell line U937 differentiated into either M1 or M2 macrophages, and showed that DPP8 and DPP9 are abundant in the macrophage-rich regions of plaques (Matheeussen et al., 2013). Another study used the mouse macrophage cell line J774, as well as monocytes and macrophages derived from mouse bone marrow, to show that the inhibition of DPP8/9 lessens M1 macrophage activation in mice. As DPP8 and DPP9 are abundantly present in atherosclerotic plaques, it has been suggested that the mouse could become a valid

model species for therapeutic targeting of DPPs in atherosclerosis (Waumans et al., 2016). The use of a wide variety of cell lines and tissues can provide insights into the physiological and pathological roles of DPP8 and DPP9 in cell behaviour and survival.

1.1.4.6.3 DPP8 and DPP9 in disease and inflammation

There is increasing evidence in the literature that DPP8 and DPP9 may be associated with disease pathogenesis. In a gene expression profile study using human hepatocellular carcinoma (HCC) tissue, mRNA of DPP9 has shown differential expression and upregulation between non-tumour liver tissue adjacent to tumours and normal liver tissue (Kurokawa et al., 2003), suggesting a possible role in disease progression.

Expression profiling of breast and ovarian carcinoma cell lines, along with 293T and HeLa cell lines, showed ubiquitous but differential expression of DPP8 and DPP9 mRNA and protein across these cell lines. There was, however, a lack of correlation between mRNA transcript and protein levels for both DPP8 and DPP9 which suggests that DPP8 and DPP9 may be regulated post-transcriptionally in breast and ovarian cancer cell lines (Wilson and Abbott, 2012a).

DPP8 mRNA expression is greater than other DPPs in breast and ovarian cancer cell lines (Wilson and Abbott, 2012a), DPP9 mRNA is abundant in chronic myelogenous leukemia (K-562) and immortalised cervical cancer (HeLa) cells (Olsen and Wagtmann, 2002) and DPP8 and DPP9 mRNA can be detected in tumour infiltrating lymphocytes

with upregulation of DPP9 mRNA levels in human testicular tumours (Yu et al., 2009), thus suggesting that DPP8 and DPP9 may have roles in tumour pathogenesis.

DPP activity inhibition partially attenuates dextran sulphate sodium (DSS) - induced colitis in mice, and DPP8 mRNA levels exhibit differential regulation during colitis development, which is suggestive of role of DPP8 in inflammatory bowel disease (Yazbeck et al., 2010). DPP8 mRNA and protein expression is significantly up-regulated in B-cell chronic lymphocytic leukemia (B-CLL) lymphocytes compared to normal tonsil B lymphocytes in B-CLL patients (Sulda et al., 2010). These findings suggest that DPP expression may have biological relevance in disease states.

Meningiomas are inter-cranial tumours that are derived from the arachnoid cap cells and include a wide variety of subtypes. A study of the expression of all DPPs, including DPP8 and DPP9, has shown enzymatic activity of both was present in all benign meningiomas, with elevated levels in atypical meningiomas that are associated with higher cell proliferation (Stremenova et al., 2010). An aggressive group of human paediatric malignancies, Ewing sarcoma family of tumours, are driven by an aberrant transcription factor that up-regulates specific target genes, such as NPY. ESFT cell death is stimulated by exogenous and endogenous NPY, however, this effect is prevented by cleavage of NPY by both membrane-bound DPP4 and intracellular DPP8 and 9. Thus, DPPs act as survival factors for EFST and may become potential therapeutic targets for these tumours (Lu et al., 2011).

A pathophysiologically significant role in asthma has been shown when DPP8 and DPP9 enzymatic activity is regulated in a rat asthma model. The sites of expression of DPP8

and DPP9 were investigated in rat lungs, with and without an allergic-like inflammation status. Considering bronchi and lung parenchyma, DPP8 and DPP9 were primarily detected in the bronchial epithelium of the airways (Schade et al., 2008). DPP8 and DPP9, along with other DPPs, are elevated in human articular cartilage in osteoarthritis patients, which implicates these enzymes in the cascades leading to cartilage breakdown and/or collagenolysis that occurs in arthritis (Milner et al., 2008).

Using a model of transient and unilateral cerebral ischemia in rats, another group studied the expression, localisation and activity patterns of DPP8 and DPP9 and several other proteases to gain insight into the action of cerebral inflammation and neuronal degeneration (Röhnert et al., 2012). It has been shown that mRNA expression of DPP9 is diminished in the ischemic region of the brain at 6 hours and 3 days after induced ischemia whereas DPP8 levels remain the same at all time points. Also, DPP8 is present in activated microglia and macrophages at day 3 post-ischemia and in astroglial cells at day 7 post-ischemia, suggesting that DPP8 and DPP9 have potential roles in cerebral inflammation.

As a role for DPP4 in atherosclerosis emerged (Matsubara et al., 2012), it was necessary to investigate the expression and role of DPP8 and DPP9. More recently, it has been shown that DPP8 and DPP9 are abundant in macrophage-rich regions of human atherosclerotic plaques (Matheeussen et al., 2013). That study showed that, while DPP4 is only present in endothelial cells of plaque, DPP8 and DPP9 are highly expressed in macrophages with a significant up-regulation of DPP9 protein expression in both pro-inflammatory M1 and anti-inflammatory M2 macrophages during

monocyte-to-macrophage differentiation. Since M1 macrophages play a role in atherogenesis, there may be future therapeutic prospects in the reduction of atherosclerosis and/or plaque rupture by inhibition of DPP9. Activation of macrophages in atherosclerotic plaques can cause indiscriminate tissue damage and attenuation of activiation by DPP8/9 inhibition would be a desirable outcome.

A genome-wide association study which focused on human pulmonary fibrosis identified *DPP9* as one of several novel susceptibility loci. Although the evidence for higher expression of *DPP9* in lung tissue of pulmonary fibrosis cases compared to controls was slight, this group speculated that DPP9 may be involved in the integrity of lung epithelia via cell-to-cell adhesion (Fingerlin et al., 2013). This finding would need further investigation to show if DPP9 does have a role in the development of pulmonary fibrosis.

The current understanding of the role of DPP8 and DPP9 in atherosclerosis has been reviewed (Waumans et al., 2015). Most recently, the role of DPPs in atherosclerosis was further studied focusing on macrophage activation in a mouse model and human M1 macrophages *in vitro* (Waumans et al., 2016). While, DPP8 and DPP9 expression was relatively low in mouse monocytes and macrophages, DPP8/9 inhibition was confirmed to attenuate macrophage activation and the viability of both mouse and human macrophages was unaffected by this inhibition.

Overall, DPP8 and DPP9 are becoming increasingly implicated in disease pathogenesis. Increased understanding of the role they play may make them candidates future therapeutic targeting.

1.2 DPP4 family mouse phenotypes

1.2.1 Mouse models

As the mouse genome is amenable to genetic manipulation, there are great benefits to using mouse models. Many studies involve the use of gene knockout (GKO) mice as models for investigation of the biological properties of proteins in a physiological and/or pathophysiological context. In GKO mice, the protein of interest is absent from the resultant mouse. In the DPP4 gene family, GKO mice have been created for both DPP4 and FAP. The DPP4-GKO mouse was produced by a targeted inactivation in the *DPP4* gene and resulted in healthy mice (Marguet et al., 2000). Similarly, the FAP-GKO mouse was constructed through exon deletion and also created fertile mice with no overt developmental defects or increased cancer susceptibility (Niedermeyer et al., 2000). It has been speculated that, in the absence of these proteins, other proteins are up-regulated and have compensatory roles (Marguet et al., 2000, Niedermeyer et al., 2000). To date, no DPP8-GKO mice have been reported.

1.2.2 DPP9 gene knock-in (GKI) mouse

Unlike in the case of GKO mice where the entire protein is absent from the mouse, in a GKI mouse the protein of interest is present but inactivated by a single amino acid change, thus it is still able to fulfill non-enzymatic functions, such as structural roles and protein-protein interactions. This study utilised a DPP9-GKI mouse which was found to display early neonatal lethality suggesting that enzyme activity of DPP9 has a

crucial role in neonate mouse survival. Those findings are published (Gall et al., 2013) and are the basis of Chapter 3 of this thesis.

1.3 PhD project aims

As outlined above, DPP9 has been implicated in the immune system, cell behaviour and survival, disease pathogenesis and inflammation, however clear physiological roles remain to be determined. There is a need to gain a greater understanding of the functional and biological properties of this ubiquitously-expressed protein.

AIM 1: To demonstrate the importance of DPP9 enzymatic activity *in vivo*

The creation of GKO mice lacking the other DPP4 family proteins, DPP4 and FAP, resulted in healthy mice with indications that the absence of these proteins have protective effects. The absence and/or inactivation of DPP9 enzymatic activity had not previously been reported when this thesis work began, so the importance of DPP9 activity in mice was explored.

AIM 2: To elucidate the biological roles of DPP9 in DPP9-GKI neonate and adult mice

Concurrent to this thesis, *in vitro* studies using DPP9-GKI mouse embryonic fibroblasts (MEFs) and neonatal tissues isolated from wild-type (WT) or DPP9-GKI mice explored the role of DPP9 in neonate metabolism which later resulted in a publication from this

lab (Chen et al., 2016). As there have been no reported DPP9-enzyme-activity-deficient mice used in any *in vivo* studies, the potential causes of lethality in neonate mice and other possible physiological or pathological effects in adult heterozygous mice were investigated. The main areas of focus were potential defects in heart and autophagy in the neonate and the possible role of DPP9 enzymatic activity in adult heterozygous mouse skin as compared to WT.

AIM 3: To explore the role of DPP9 in the regeneration of the mouse immune system

DPP9 has been detected in immune cells and tissues *in vitro* and *in vivo*, however no study exists where the role of DPP9 in the regenerating immune system has been examined. This study used the creation of primary and secondary chimeras to investigate the role of DPP9 enzyme activity on the developing immune system of WT mice. These chimeras were produced using irradiated mice injected with WT and DPP9-GKI mouse fetal liver cells for primary chimeras in the first instance and then, subsequently, bone marrow cells from the primary chimeric mice.

CHAPTER 2:

General Materials and Methods

2 General Materials and Methods

2.1 Buffers, media, chemical reagents and antibodies

2.1.1 General buffers

1 x PBS

Made from 10 x Dulbecco's Phosphate-buffered saline (Cellgro).

FACS wash

10 ml FCS (5%), 800 µl of 0.5 M EDTA (2mM) and 200 µl of 10% NaN_3 (0.01%) to a total volume of 200 ml with PBS.

50 x TAE buffer

242 g of Tris-base, 57.1 ml of acetic acid (glacial), 100 ml of 0.5 M EDTA (pH 8.0) was made up to 1 L with triple distilled H_2O. A working solution of 1 x TAE was made by diluting 20 ml of 50 x TAE buffer in 980 ml of triple distilled H_2O.

0.5 M EDTA (pH 8.0)

186.1 g of EDTA.$2H_2O$ was dissolved in 800 ml H_2O under vigorous stirring. The pH was adjusted to 8.0 with NaOH and H_2O was added to give a final volume of 1 L.

1 M TrisXHCl (pH 7.6)

121.14 g of Tris-base was dissolved in 1 L of H2O (buffer 1).

157.64 g of Tris-HCl was dissolved in 1 L of H2O (buffer 2).

Buffer 1 was added to buffer 2 until the pH reached 7.6.

Red cell lysis (RBC) buffer

8.26 g ammonium chloride (NH_4Cl), 1 g potassium bicarbonate ($KHCO_3$) and 0.037 g EDTA were dissolved in 1 L of dH_2O.

ACK/ RBC lysis solution

5 ml FACS wash added to 95 ml RBC lysis buffer.

Hydroxyproline assay reagents:

Citrate-Acetate buffer

34 g sodium acetate, 37.5 g sodium citrate and 5.5 g citric acid monohydrate were mixed with 385 ml isopropanol and dissolved in dH_2O up to 1 L.

Chloramine T

7 g chloramine T was added to 100 ml of dH_2O and stored in a dark bottle at 4^0C

Ehrlich's reagent

25 g p-dimethylaminobenzaldehyde and 37.5 ml 60% perchloric acid mixed well and stored in a dark bottle at 4^0C

Chloramine T solution (Solution A)

Mix 1 part chloramine T with 4 parts citrate-acetate buffer. Make up fresh for each experiment.

Ehrlich's solution (Solution B)

Mix 3 parts Ehrlich's reagent with 13 parts isopropanol and store at 4^0C

10M sodium hydroxide

400 g sodium hydroxide in 1 L of dH_2O mixed in a plastic beaker on ice.

3M hydrochloric acid

25.5 ml 37% hydrochloric acid in 100 ml of dH_2O

Liver cell buffer

5 ml Glutamax, 10 ml Penistrep and 50 ml FCS were added to 500ml of Dulbecco's Modified Eagle's Medium (DMEM)

Cell freezing solution

10 ml DMSO added to 90 ml FCS

2.1.2 Source of media and chemical reagents

Table 2.1: List of media and chemical reagents

Chemical Name	Catalogue No.	Supplier
Agarose I	0710	AMRESCO
Acetic Acid	100015N	BDH Chemicals
Ammonium Chloride	A9434	Sigma Chemical Co
Bovine Serum Albumin (BSA)	A7906	Sigma Chemical Co
Chloramine T hydrate	C9887	Sigma Aldrich PL
Citric Acid Monohydrate	C7129	Sigma Aldrich PL
4',6-diamidino-2-phenylindole (DAPI)	D8417	Sigma Aldrich PL
p-dimethylaminobenzaldehyde	D2004	Sigma Aldrich PL
Dimethyl Sulphoxide (DMSO)	D2650	Sigma Chemical Co
Dulbecco's Modified Eagle's Medium (DMEM)	12430	Invitrogen Australia PL
Dulbecco's Phosphate-Buffered Saline (10×DPBS)	98-317-LB	Cellgro
Ethanol Absolute	ET00162500	Scharlau
Ethylene Diamine Tetraacetic Acid Disodium Salt (EDTA)	E5134	Sigma Chemical Co
Fetal Calf Serum (FCS)	FBS500-S	AusGeneX
GelRed Nucleic Acid Stain	41003	Biotium
GlutaMAX, 100×	35050	Invitrogen Australia PL
Glycerol	G7757	Sigma Chemical Co

HEPES	0511	AMRESCO
Hydrogen Peroxide (H_2O_2)	28694.5B	BDH Chemicals
Instant Skim Milk Powder	3549	BonlacFoods
Imidazole	10125	Sigma Chemical Co
Isopropanol	I-9516	Sigma Aldrich Pty Ltd
Lipofectamine LTX and PLUS	15338-100	Invitrogen Australia PL
Magnesium Chloride ($MgCl_2$)	M1028	Sigma Chemical Co
Methanol	M3641	BDH Chemicals
Neutral Buffered Formalin, 10%	HT5011	Sigma Chemical Co
Penicillin-Streptomycin (P/S), 100×	15140	Invitrogen Australia PL
Potassium Bicarbonate	237205	Sigma Chemical Co
Proteinase K, recombinant, PCR Grade	03115852001	Roche
Sodium Acetate	S2889	Sigma Chemical Co
Sodium Azide (NaN_3)	E8751	Sigma Chemical Co
Sodium Chloride (NaCl)	465	Ajax Chemicals
Sodium citrate tribasic dihydrate	C8532	Sigma Chemical Co
Sodium Hydroxide (NaOH)	10252	BDH Chemicals
Tris-Base	0497	AMRESCO
Tris-EDTA buffer solution (100×)	T9285	Sigma
Tris-HCl	0234	AMRESCO
Triton X-114	X-114	Sigma Chemical Co
Trizol Reagent	15596	Invitrogen Australia PL
Trypan Blue	T8154	Sigma Chemical Co

TrypLE Express	12605	Invitrogen Australia PL
Tween-20	P1379	Sigma Chemical Co

2.1.3 Antibodies

Table 2.2: List of antibodies

Primary antibodies

Antibody	Supplier	Catalogue No.	Working Conc.
β-Actin	Sigma	A2103	1:1000
AF647 Ly6G	BioLegend	#127610	1:250
Anti-LC3B	GeneTex	#GTX127375	1:100
APC.Cy7 CD8a	BD Biosciences	#557654	1:250
BUV395 CD19	BD Biosciences	#563557	1:200
BV421 CD3e	BD Biosciences	#562600	1:250
DPP9 - Catalytic domain	Abcam Inc	Ab42080	1:2000
APC TER-119	BD Biosciences	#557909	1:250
FITC CD11b	BD Biosciences	#557396	1:250
GAPDH	EnCor Biotechnology	MCA-1D4	1:1000
PE NK1.1	BD Biosciences	#557391	1:250
PerCP-Cy5.5 CD45.1	eBioscience	#45-0453	1:250
V500 CD45.2	BD Biosciences	#562129	1:250

Secondary antibodies

Antibody	Supplier	Catalogue No.	Working Conc.
Anti-Rabbit IgG-HRP	DAKO	PO448	1:100

2.1.4 Source of specialty mouse supplies

Table 2.3: List of specialty mouse treatment products

Item Name	Purpose	Supplier
Ampicillin	Antibiotic	Sandoz
Isoflurane	Anaesthetic	I.S.O.
Nair	Hair removal	Church & Dwight Co Inc
Povidine-iodine	Antiseptic lotion	Betadine
Temgesic	Analgesic	Reckitt Benckiser
Tegaderm	Wound dressing	3M Company

2.2 General molecular biology methods

Standard molecular biology techniques were used. Techniques specific to one experiment are detailed in the respective chapters. All water (H_2O) used was commercially obtained sterile water (Baxter, NSW, Australia).

2.2.1 Genomic DNA extraction

Mammalian genomic DNA (neonate mouse tail samples and mouse embryonic head samples) was extracted using the Wizard® Genomic DNA Purification Kit (Promega #A1120), according to the manufacturer's instructions.

Mouse tissues were resuspended using a tip in 600 μL of pre-chilled EDTA/Nuclei Lysis Solution (120 μL of a 0.5 M EDTA solution to 500 μL of Nuclei Lysis Solution). 17.5 μL of 20 mg/mL Proteinase K was added to the sample and incubated overnight at 55°C with gentle shaking to make sure the tissues were completely digested. 3 μL RNAse Solution was added to the nuclear lysate followed by inversion 2-5 times. The mixture was incubated at 37°C for 15-30 min and cooled to room temperature. 200 μL of Protein Precipitation Solution was added to the cooled sample and vortexed vigorously for 20 s before the samples were chilled on ice for 5 min and centrifuged at 14,000 rpm for 4 min, with the appearance of a tight pellet of precipitated protein. The supernatant was transferred to a new tube containing 600 μL isopropanol and mixed gently by inversion until DNA threads formed a mass. The DNA was pelleted at 14,000 rpm for 1 min and washed with 600 μL of 70% ethanol before spinning again at 14,000 rpm for 1 min. The ethanol was carefully aspirated and the DNA pellet dried by inversion of the tube on absorbent paper for 15 min. 50 μL of DNA Rehydration Solution was added and the DNA dissolved at 65°C for 1 h or overnight at 4 °C.

2.2.2 Polymerase Chain Reaction (PCR)

The PCR machine used was a DNA Engine (MJ Research, Bio-Rad Laboratories, Hercules, CA, USA). PCR reactions were set up in 0.2 mL thin walled PCR tubes. The reaction contained the designed forward and reverse primers (1 µL of 20 µM), 50 ng double-stranded template, dNTPs (1 µL of 10 mM; Roche), 1 unit (U) Advantage 2 Polymerase Mix (Clontech #639201), 1 ×Advantage 2 SA PCR buffer (1.5 µL; Clontech #639147) and sterile water to a final volume of 15 µL. Cycling parameters comprised an initial 2 min hot start at 95°C to activate the DNA polymerase, followed by 39 cycles, each comprising of 95°C for 30 sec to denature DNA strands and 64°C for 30 sec to reanneal strands and 68°C for 30 sec to permit extension, and final extension at 68°C for 10 min.

2.2.3 Agarose gel electrophoresis

Horizontal gel electrophoresis was performed in HORIZON® 58 Gel tanks (Gibco BRL, Life Technologies, Gaithersburg, MD, USA) attached to an EPS 601 power pack (Amersham Pharmacia Biotech, Piscataway, NJ, USA). GelRed Nucleic Acid Gel Stain (1:10000) was added to agarose gels prior to pouring to enable visualisation under UV light. 6 × DNA Loading Dye (Fermentas) was added to DNA samples. Molecular weight markers used were GeneRuler™ 1 kb DNA ladder (Fermentas #SM0311) or GeneRuler™ Low Range DNA ladder (Fermentas #SM1191). Gels were run at 120 Volts for 30 min or as needed. Gels were photographed using a Polaroid® camera or an UVT-400M transilluminator (International Biotechnologies, New Haven, CT, USA).

1% Agarose Gel

1 g of agarose was dissolved in 100 mL of 1×TAE buffer, with heating.

3% Agarose Gel

3 g of agarose was dissolved in 100 mL of 1×TAE buffer, with heating.

2.2.4 Protein Analysis

2.2.4.1 Protein sample preparation

Triton Lysis Buffer (pH 7.6)

500 µL of 1 M Tris-HCl (50 mM), 20 µL of 0.5 M EDTA (1 mM), 10 µL of 1 M MgCl2 (1 mM), 300 µL of 5 M NaCl (150 mM), 100 µL of Triton-114 (1%) and 1 mL of Glycerol (10%)was made up to 10 mL with Baxter H_2O. The lysis buffer was stored at -20^{0}C as aliquots. 1X Roche complete protease inhibitor cocktail was added to the lysis buffer prior to use.

2.2.4.2 Protein preparation for mouse tissues

Frozen mouse tissues were weighed and homogenised in ice-cold lysis buffer, at the ratio of 1 mg tissue/ 10 µL lysis buffer, using a bead-based homogeniser (TissueLyser, Qiagen) for 2 min at 4^{0}C. The homogenates were sonicated on ice for 10 min, followed by spinning at 14000 rpm for 10 min at 4^{0}C to remove cell debris. The supernatants were collected and stored at -80^{0}C prior to analysis.

2.2.4.3 Protein quantitation

Protein concentrations were determined using the Micro BCA™ Protein Assay Reagent Kit (Pierce Biotechnology). 70 µL of each standard or test sample was added into each well of a clear 96-well plate followed by 70 µL of working reagent. The plate was incubated at 37^0C for 30 min. The absorbance was measured at 570 nm on microplate reader (BMG Labtech) and the protein concentration estimated by comparing it to a standard curve generated with known BSA concentrations (1–40 µg/mL).

2.2.4.4 SDS polyacrylamide gel electrophoresis (SDS-PAGE)

Protein samples were heated at 95°C for 10 min in the presence of 1×NuPAGE LDS Sample Buffer (Invitrogen) and 1×NuPAGE Reducing Agent (Invitrogen) before being cooled on ice prior to loading. NuPAGE pre-cast gels (Invitrogen) were applied to resolve proteins for immunoblot analysis. An XCell SureLock Mini-cell electrophoresis unit (Invitrogen) was used for gel runs. 3-8% Tris-Actetate SDS-PAGE gels were run at 150 V for approximately 60 min with 1×Tris-Acetate SDS Running Buffer, whereas 4-12% Bis-Tris SDS-PAGE gels were run at 200 V for 45 min in 1×MOPS SDS Running Buffer. 500 µL of 1×NuPAGE Antioxidant (Invitrogen) was added to 200mL 1×SDS Running Buffer in the Upper (inner) Buffer Chamber. Relative molecular masses were estimated by comparison to PageRuler^{TM} Prestained Protein Ladder (Thermo Scientific) and MagicMark XP Western Protein Standard (Invitrogen).

2.2.4.5 Immunoblotting

Transfer of proteins from the gel to a polyvinylidene difluoride (PVDF) membrane was performed using an XCell SureLock Mini-cell with XCell II Blot module (Invitrogen). The gel was removed from the gel cartridge and then placed on a piece of Whatman 3 M paper. A piece of PVDF membrane was placed on top of the gel and a piece of Whatman 3 M paper was placed against the PVDF. This assembly was sandwiched between six sponges and the final assembly placed into the tank containing 1× Transfer Buffer (Invitrogen) such that the gel was facing the cathode and the PVDF was facing the anode. Transfer was carried out at 30 V for 2 h. The success of protein transfer was determined by the degree of transfer of the pre-stained protein standard markers. The PVDF was then removed from the assembly and blocked by incubations in Blotto for 1 h at RT, followed by primary antibody at 4°C for overnight on rocker with gentle shaking. Following washing with Blotto for 10 min, PVDF membrane was incubated with a horseradish peroxidase (HRP) conjugated secondary antibodies for 1.5 h at RT. Finally, the membrane was rinsed in PBST before incubating in Chemiluminescent HRP Substrate (Immobilin^{TM}, Millipore, Bedford, MA) for 5 min and detecting by ChemiDOC MP system (BIO-RAD).

PBST

100 µL Tween 20 was added to 1 L PBS.

Blotto

45 g instant skim milk powder and 200 µL Tween 20 was dissolved in 1 L PBS.

2.3 Mouse handling and maintenance

All mice were maintained in the Centenary Institute of Cancer Medicine and Cell Biology animal facility under specific pathogen free conditions and exposed to a 12 h light-dark cycle. DPP9-GKI mice were bred on-site. C57BL/6J and PTPRC^{A} mice were purchased from either Animal Resource Centre (Perth, WA, Australia) or Australian BioResources (Moss Vale, NSW, Australia). After arrival, the animals were housed four to six mice per cage with ad libitum access to rodent chow and water for a one week acclimation period before using them for experimental purposes. All the mice used for chimera experiments were at least 8 weeks old (adult age). All animal handling and experimental procedures were approved by Sydney Local Health District Animal Welfare Committee under ethics protocols Protocol No. 2013/ 017C – The biological roles of dipeptidyl peptidases (K75/5-2012/3/5754) and/or Protocol No. 2013/ 017D – The biological roles of dipeptidyl peptidases (K75/5-2012/3/5754).

2.4 Statistics

Where statistical analysis was used, the data were presented as mean ± standard deviation of the mean (SD) or mean ± standard error of the mean (SEM). Statistical analysis was performed using GraphPad Prism (GraphPad Software, La Jolla, CA, USA). Groups were compared by unpaired t-test or Mann-Whitney test. Specific details of statistical methods used for each analysis is contained in the Materials and Methods section of each data chapter.

CHAPTER 3:

DPP9 enzyme deficiency in the mouse

Statement

Section **3.2** in this chapter has been published:

Gall MG, Chen Y, Vieira de Ribeiro AJ, Zhang H, Bailey CG, Spielman DS, Yu DMT, Gorrell MD (2013) Targeted Inactivation of Dipeptidyl Peptidase 9 Enzymatic Activity Causes Mouse Neonate Lethality. PLoS ONE 8(11): e78378. doi:10.1371/journal.pone.0078378

Section **3.2** of this chapter is identical to the final submission, except for minor corrections. The written permission and statement of contribution by co-authors is attached in Appendix 2

3 *DPP9 enzyme deficiency in the mouse*

3.1 General Introduction

As discussed in Chapter 1, the use of mouse models is beneficial for providing *in vivo* data to assist in the understanding of normal and pathological biological conditions. Genetic manipulation of the mouse genome has enabled the creation of GKO and GKI mice which result in the deletion or inactivation, respectively, of one or more proteins of interest. GKO mice have been produced for both DPP4 (Marguet et al., 2000) and FAP (Niedermeyer et al., 2000) and are healthy and fertile. Thus, there was an expectation in our group that GKO mice for similar enzymes, such as DPP9, would be similarly healthy.

In our lab, we created a DPP9-GKI mouse to study the loss of DPP9 enzymatic activity without altering other non-enzymatic interactions and characteristics of the DPP9 protein. Surprisingly, the DPP9-GKI mouse displayed neonate lethality, which suggested a crucial role for this enzyme activity in early mouse survival.

3.1.1 Aims

The aims of the work in this chapter are:

- to show that the DPP9-GKI mouse, bearing the DPP9-S729A mutation, displays a lethal phenotype and determine the developmental timing of death
- to validate that DPP9-S729A and wild-type DPP9 have similar subcellular localisation and that the DPP9 protein is enzyme-inactive

- to investigate obvious histological and/or physiological differences between early neonate DPP9$^{S729A/S729A}$ homozygotes from their heterozygous and wild-type littermates

3.2 Targeted inactivation of dipeptidyl peptidase 9 enzymatic activity causes mouse neonate lethality

(Section 3.2 of this chapter is published as presented with minor amendments. Section 3.3 contains supplementary data not included in the published paper but undertaken as part of the neonate mouse studies to identify the lethal phenotype.)

3.2.1 Introduction

The DPP4 family of enzymes gained prominence with the success of oral DPP4 inhibitors as type 2 diabetes therapeutics (Deacon, 2011, Kirby et al., 2010). This enzyme family is unusual because its members, DPP4, FAP, DPP9 and DPP8, can hydrolyze the post-proline bond two residues from the N-terminus of substrates. FAP, the closest relative of DPP4, is a potential target for cancer therapy (Yu et al., 2010, Brennen et al., 2012, Keane et al., 2012, Christiansen et al., 2013). DPP9 and its closest relative, DPP8, are primarily under study in cell biology, immunobiology and tumour biology (Zhang et al., 2013). Medicinal chemistry has generated selective inhibitors of DPP4 and FAP but not of DPP9 and DPP8. However, some compounds inhibit DPP9 and DPP8 while not inhibiting DPP4 or FAP (Van Goethem et al., 2011, Wu et al., 2012).

DPP9 overexpression impairs cell adhesion (Yu et al., 2006b), is pro-apoptotic (Yu et al., 2006b, Yao et al., 2011) and causes less Akt phosphorylation following EGF-stimulation (Yao et al., 2011). The role for DPP9-mediated proteolysis in antigen presentation involves DPP9 being rate-limiting for degradation of antigenic proline-containing peptides including the tumour-related antigen $RU1_{34-32}$ (Geiss-Friedlander et al., 2009). DPP9 is in B cells and both CD4+ and CD8+ lymphocytes and is upregulated by mitogen stimulation (Yu et al., 2009, Chowdhury et al., 2013). Inhibiting DPP9 and DPP8 enzymatic activity dampens lymphocyte proliferation (Lankas et al., 2005, Reinhold et al., 2009) making DPP9 important in immunobiology. DPP9 and DPP8 enzymatic activity can protect Ewing sarcoma cells from neuropeptide Y (NPY)-driven death (Lu et al., 2011). The potential importance of DPP9 in tumour biology has also been shown by inhibition of DPP9 and DPP8 enhancing parthenolide's anti-leukemic activity in primary acute myeloid leukemia samples and lymphoma and leukemia cell lines (Spagnuolo et al., 2013). Moreover, an adjuvant effect triggered by inhibition of DPP9 and DPP8 appears to be a mechanism by which the compound Val-boro-Pro mediates tumour regression (Walsh et al., 2013). DPP9 binds to the oncogene and GTPase H-Ras, but the functional consequences are unclear (Yao et al., 2011). Many cancers display upregulated DPP9 expression (Yu et al., 2009, Olsen and Wagtmann, 2002, Ajami et al., 2004, Stremenova et al., 2010).

While DPP4 and FAP are predominantly expressed on the cell surface, DPP9 and DPP8 are intracellular enzymes that are ubiquitously expressed in tissues and most cell lines

(Yu et al., 2010, Yu et al., 2009). DPP9 and DPP8 are strongly expressed in lymphocytes and epithelial cells and in lymph node, thymus, spleen, liver, lung, intestine, pancreas, muscle and brain (Yu et al., 2009, Chowdhury et al., 2013, Schade et al., 2008, Harstad et al., 2013). Little is known of the natural substrates of DPP9 but it can cleave the DPP4 substrates glucagon-like peptide (GLP)-1, GLP-2, peptide YY and NPY *in vitro* and may cleave NPY inside cells (Lu et al., 2011). Some very recently identified potential DPP9 substrates, including adenylate kinase 2 and calreticulin, suggest a potential role in energy homeostasis (Wilson et al., 2013). These data suggest that the biological roles of DPP9 *in vivo* are probably diverse such that the major role of DPP9 may be elusive.

Until now, no lethal gene knockout (GKO) mouse for a protein that possesses DPP activity has existed (Yu et al., 2010). The DPP4-GKO and FAP-GKO mice are phenotypically healthy (Yu et al., 2009, Niedermeyer et al., 2001, Marguet et al., 2000). DPP4-GKO mice have improved glucose tolerance after a glucose challenge and resist diet-induced obesity (Marguet et al., 2000, Conarello et al., 2003). Both DPP4- and FAP-GKO mice have reduced fibrosis in liver injury (Wang et al., 2007). The knockout mice have been useful tools in evaluating the therapeutic potential of DPP4 and FAP enzyme inhibitors. However, care is necessary in evaluating such studies, as these animals have complete ablation of all protein function, rather than specific ablation of the enzymatic function alone (Yu et al., 2010, Keane et al., 2012).

A report that certain DPP inhibitors that inhibit DPP9 and DPP8 activity are toxic *in vivo* (Lankas et al., 2005) is controversial (Kirby et al., 2010). Several subsequent studies

indicate that DPP9 and DPP8 (Wu et al., 2009) or DPP9, DPP4 and DPP8 (Wang et al., 2012, Burkey et al., 2008) can be inhibited in adult rodents without harm.

Structurally, DPP9 is predominantly a dimer (Tang et al., 2011) and has high sequence and topological homology with DPP4 (Ajami et al., 2004), as best seen by protein structure modeling (Park et al., 2008). Human recombinant DPP9 and natural bovine DPP9 protein have been characterized (Ajami et al., 2004, Park et al., 2008, Dubois et al., 2010). Interestingly, DPP9 protease activity may be influenced by several natural processes. It is redox-responsive; in oxidizing conditions the enzymatic activity is inhibited, likely due to reversible intra-molecular disulfide bonding between cysteine residues (Park et al., 2008). DPP9 is acetylated (Choudhary et al., 2009), which might influence activity. DPP9 has a novel SUMO1-specific interacting motif that, when engaged, allosterically upregulates DPP9 enzymatic activity (Pilla et al., 2012). Such changes in DPP9 enzymatic activity would be expected to influence downstream signaling pathways.

DPP9 has an active-site catalytic triad that is conserved across the DPP4 protein family and can hydrolyse the post-proline bond two residues from the N-terminus of peptide substrates. The DPP4 family proteins are atypical serine proteases that have the catalytic triad in the reverse order to trypsin and are unusual in that the catalytic pocket is buried within the protein. In the 863 amino acid isoform (short form) of DPP9, the triad consists of Ser729, Asp807 and His839. We showed that mutation of the catalytic serine of DPP9 to alanine in amino acid position 729 of the short form of DPP9 (S729A) ablates enzymatic activity without affecting other characteristics of this protein (Yao et

al., 2011, Ajami et al., 2003). To examine the *in vivo* significance of DPP9 enzymatic activity, the first GKI mouse was generated containing the S729A point mutation. This biological strategy is expected to mimic the effect of a non-toxic selective DPP9 inhibitor administered from the time of fertilisation.

3.2.2 Materials and Methods

3.2.2.1 Ethics statement

The animal experiments were approved by the local Animal Ethics Committee of the University of Sydney (Ethics protocols K75/6-2012/3/5753 'Production of mice for studies on dipeptidyl peptidases' and K75/5-2012/3/5754 'The biological roles of dipeptidyl peptidases') and conducted in accordance with all applicable laws and guidelines.

3.2.2.2 Generation of DPP9 enzyme-inactive mice

Generation of DPP9 enzyme-inactive mice was performed by Ozgene (Bentley, Western Australia) using standard techniques. The DPP9 targeting construct was generated by cloning polymerase chain reaction (PCR) products of the 5' and 3' homology arms, as well as a short loxP arm containing the S729A mutation (Figure 3.1A), into the plasmid backbone, FLSniper (Ozgene), which contained the Phosphoglycerate Kinase (PGK) - Neo cassette flanked by Flippase Recognition Target (FRT) sites. The S729A mutation was generated by point mutagenesis of the sequence TCC TAC to GCA TAT, which introduced an NdeI restriction enzyme site for Southern blot screening. To allow for conditional deletion of DPP9 gene expression, the same exon containing the S729A

point mutation was flanked with loxP sites (exon 20 in the DPP9 short form), providing the option of exon deletion using Cre-recombinase and hence disruption of the entire protein molecule. In this study, this built-in strategy for exon excision was not utilised.

The targeting construct was electroporated into C57BL/6 Bruce 4 embryonic stem (ES) cells and clones were selected for neomycin resistance. Southern blot analyses (Figure 3.1B, Table 3.1) identified successfully targeted DPP9$^{wt/flox}$ ES cells. The clone chosen for generating the mutant mice, 1G6, was analysed by Southern blot and verified to be correctly targeted at each end of the construct (Figure 3.1B). Probing the blot with a neomycin probe confirmed a single integration event (data not shown).

The DPP9$^{wt/flox}$ ES clone was microinjected into BALB/c blastocysts which were implanted into pseudo-pregnant foster mothers. Chimeric male mice from the resultant litters were mated with C57BL/6 wild-type females and offspring with coat-colour transmission were genotyped for germline transmission of the S729A mutation by Southern blot of tail DNA (Figure 3.1B). Genotyping confirmed germline transmission of the DPP9 serine-to-alanine point mutation locus.

The neo cassette was FLPe-deleted *in vivo* using the FRT sites by mating heterozygous DPP9$^{wt/flox}$ mutant males with transgenic female wt/FLPe mice expressing the enzyme Flp recombinase. Southern blot genotyping of offspring confirmed deletion of the PGK-neo selection cassette. Resultant positive offspring (DPP9$^{wt/S729A}$) were mated with C57BL/6 mice for removal of the FLPe gene.

Routinely, DPP9$^{wt/S729A}$ intercross progeny were genotyped by Southern Blot using the 5' or 3' probes (Figs. 3.1A and 3.1B, Table 3.1), or by PCR using primers (Figure 3.1C, Table

3.2) and Advantage2 Taq Polymerase (Clontech, Mountain View, CA). The PCR cycles used were 94^0C for 2 min, then 94^0C for 30 sec, 60^0C for 30 sec, 68^0C for 30 sec repeated 39 times followed by 68^0C for 10 min and 10^0C on hold. Sequencing of gel-isolated PCR product confirmed the correct amplification of the mutant allele region

and the presence of the S729A mutation in the 349 bp PCR fragment

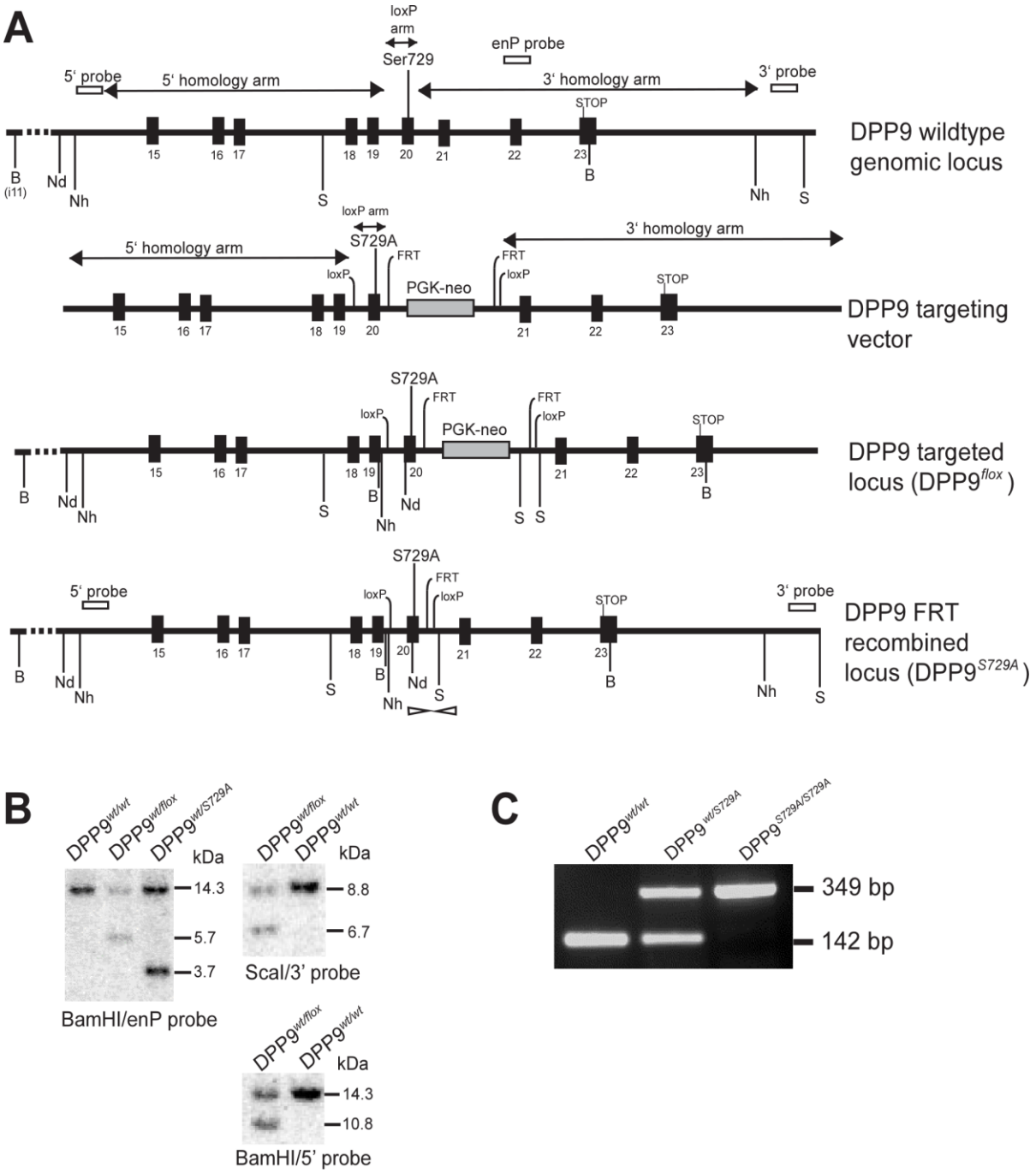

Figure 3.1: Generation of DPP9wt/S729A mice.

(**A**) Representation of the DPP9 wild-type locus, targeting vector, targeted locus, and FRT recombined locus. 5' probe, 3' probe, enP probe, approximate PCR screening primer positions (open arrowheads) and restriction sites (Nh- NheI, S- ScaI, Nd- NdeI, B-BamHI) are indicated.

(**B**) Southern blot screening confirming targeted recombination at each end of DPP9 locus: enP probe on BamHI digest (DPP9$^{wt/wt}$, DPP9$^{wt/flox}$ and DPP9$^{wt/S729A}$ offspring from a wt/flox x FLPe mating), 3' probe on ScaI digest and 5' probe on BamHI (ES cell clone 1G6 used for microinjection). Expected sizes for wild-type and DPP9 targeted locus were detected (Table 3.1).

(**C**) PCR screen distinguishing wild-type, DPP9$^{S729A/S729A}$ homozygote and DPP9$^{wt/S729A}$ heterozygote ED17.5 littermate embryos (wt allele, 142 bp; DPP9^{S729A} allele, 349bp).

Probe	enP probe	5' probe	3' probe	5' probe	5' probe
Restriction enzyme	BamHI	BamHI	Sca I	Nhe I	Nde I *
DPP9^{wt} allele (kb)	14.3	14.3	8.8	13.6	23.0
DPP9^{flox} allele (kb)	5.7	10.8	6.7	7.5	9.4
DPP9^{S729A} allele (kb)	3.7	10.8	6.7	7.5	9.4

Table 3.1: Southern blot strategy for screening of DPP9^{S729A} mice.

Southern blot analyses identified successfully targeted DPP9$^{wt/flox}$ embryonic stem cells using probes described in this table. *NdeI restriction site was inserted during introduction of DPP9^{S729A} mutation.

Primer name	mDPP9_E20.F	mDPP9_i20.R
Sequence (5' - 3')	AAGTATGGCTTCATTGACTTGAGC	GGTGGGCATCAGGCTGCAGGTGG
Wild-type allele (bp)	142	
DPP9^{S729A} allele (bp)	349	
Annealing temp. (ºC)	64	

Table 3.2: PCR primers for routine screening of DPP9^{S729A} mice/ embryos/ MEFs.

DPP9$^{wt/S729A}$ intercross progeny and MEFs generated from these progeny were genotyped by PCR using primers and PCR cycle outlined above.

3.2.2.3 Embryonic and early neonate studies

Embryonic day (ED) 12.5 (ED12.5), ED13.5, ED15.5 and ED17.5 embryos were harvested from DPP9$^{wt/S729A}$ intercrosses. Umbilical cord or embryonic tail was proteinase K-treated for genotyping, while the rest of the embryo was formalin fixed overnight.

For post-natal studies, both observational and experimental studies were undertaken to define the phenotype. In observational studies, hourly litter examinations from birth ensured retrieval of non-surviving pups for genotyping and formalin fixation. All pups were closely observed for physical activity, breathing difficulties and unusual behaviours or appearance. In litters used for experimental studies, all pups were euthanised within six hours of birth, tails retained for genotyping and head and body fixed in 10% neutral buffered formalin.

3.2.2.4 Histochemical studies

To undertake histological observations, paraffin-embedded pups were sectioned at 5 µm and H&E stained. To immunolocalise DPP9 protein, the anti-DPP9 antibody (Abcam; Cambridge, UK, #ab42078, 1:100) was used which bound to both the wild-type and S729A DPP9 proteins. Briefly, 5 µm sections were deparaffinised and rehydrated and then a pressure cooker and Universal Decloaker solution (Biocare Medical, Concord, CA) was used to retrieve antigen. Sections were then covered with Background Sniper (Biocare Medical) for 10 mins, rinsed in PBS and incubated at room temperature for 1 h with primary antibody with 1% BSA in PBS and Renaissance Background Reducing Diluent (Biocare Medical). After thorough washing in PBS, sections were incubated for 30 mins with goat anti-rabbit conjugated to HRP (Dako, Glostrup, Denmark, #P0448, 1:100), washed and then stained in 3,3-diaminobenzidine (DAB) with H_2O_2. Bright-field imaging was performed using a Leica DM6000B microscope.

3.2.2.5 Immunofluorescence Imaging

DPP9-WT-EGFP and enzyme-inactive mutant DPP9-S729AEGFP constructs [10] were transiently transfected into human hepatocarcinoma cell line (Huh7) cells using Lipofectamine® 2000 (Invitrogen, Carlsbad, CA, USA) at 0.4 mg/mL. Forty hours post-transfection, cells were fixed with 4% paraformaldehyde as described previously (Yu et al., 2006b). Immunostaining used rabbit anti- DPP9 antibody (Abcam, #ab42080, 1:200), Alexa Fluor® 647 goat anti-rabbit IgG (Invitrogen, #A-21245, 1:200) and DAPI counterstain. Z-stack images were captured on a Leica TCS SP5 confocal microscope and

the stacks above and below the nucleus were removed. The remaining stacks were reconstructed into a z-projection with ImageJ software.

3.2.2.6 SDS-PAGE urine analysis

In litters used for detection of protein in urine, pups were euthanised within 6 hours of birth by decapitation, then urine collected and analysed by a method modified from Putaala et al (Putaala et al., 2001). Briefly, 3 µL of urine from each pup together with 1 µL of SDS-sample buffer was run on a 4-12% Bis-Tris SDS-PAGE gel (Invitrogen) under non-reducing conditions. Gels were stained with Coomassie Blue.

Supplementary to the data contained in this section, additional SDS-PAGE analysis of urine samples was carried out to identify low molecular weight proteins and is described in Section 3.3.2.

3.2.2.7 Generation and immortalisation of mouse embryonic fibroblasts (MEFs)

ED13.5 embryos from DPP9$^{wt/S729A}$ intercrosses were harvested under sterile conditions and MEFs prepared using standard protocols (Xu, 2005). Briefly, the uterus of each pregnant mouse was removed post mortem and each embryo separated from its placenta and surrounding membranes and placed in complete growth medium (DMEM with 10% FCS). The embryonic liver and head were removed and then the body was homogenised in TrypLE (Life Technologies, Mulgrave, Victoria, Australia) using a syringe and 23 G needle. The homogenate was incubated at 37^{0}C for 10 min before transfer to complete growth medium and culturing at 37^{0}C with 5% CO_2 as passage zero.

Genotyping by PCR was performed on DNA isolated from embryonic head treated with proteinase K using the Wizard® Genomic DNA isolation kit (Promega, Madison, WI, USA).

After the third passage, primary MEFs from wild-type and DPP9$^{S729A/S729A}$ littermates were infected with SV40 large T antigen-expressing lentivirus to generate immortal cell lines (Vince et al., 2007). Briefly, primary MEFs were transduced with the pFU-SV40-LT-puro lentiviral vector encoding the SV40 large T antigen pseudotyped with the Moloney murine leukemia virus ecotropic envelope (pCAG4-Eco) and the structural component (pCMV δ R8.2). Cells ($1x10^5$) plated out 24 h earlier were transduced in 6-well culture plates containing 2 mL complete growth medium and 8 µg/mL Polybrene (Sigma-Aldrich, Castle Hill, Australia), 'spinoculated' at 1,500 rpm for 1 h and then cultured for 4 days at 37^0C. Puromycin selection (1 µg/mL) was added for 3 days to remove non-transduced cells. Colonies of immortalised MEFs emerged after 10 days.

3.2.2.8 Enzyme assays

DPP8/9 enzyme assay using the DPP fluorogenic substrate H-Gly-Pro-AMC (Mimotopes, Clayton, Victoria, Australia) was adapted from described methods (Yu et al., 2009, Keane et al., 2011). Briefly, $3x10^4$ MEF cells or 10 µg of liver sample lysate per well were added to black 96-well plates (Greiner Bio One, Frickenhausen, Germany) in triplicate in the presence or absence of a selective DPP4 inhibitor, sitagliptin (Merck, Rahway, NJ, USA), at 1 µM and TE buffer to a volume of 50 µL per well. 50 µL of substrate was added to a final reaction concentration of 1 mM in TE buffer (pH 7.6) with 5% methanol. The

fluorescence produced by substrate cleavage was monitored every 5 min over 1 h at 37^{0}C in a Polarstar Omega microplate reader (BMG Labtech, Offenburg, Germany) with excitation at 355 nm and emission at 450 nm.

3.2.2.9 Immunoblotting

For immunoblot sample preparation, MEFs were harvested by trypsinisation and washed with ice-cold PBS before re-suspension in ice-cold lysis buffer (50 mM Tris-HCl, 1 mM EDTA, 1 mM $MgCl_2$, 150 mM NaCl, 1% Triton-114, 10% glycerol, 1 x Roche complete protease inhibitor cocktail (Roche Applied Science, Indianapolis, IN, USA; pH 7.6) and stored at -20^{0}C. Frozen neonate mouse liver samples were homogenised in lysis buffer using a bead-based homogeniser (TissueLyser, Qiagen Venlo, Netherlands) at 4^{0}C. Protein concentration was determined using the Micro BCA Protein Assay Kit (Thermo Scientific, Waltham, Massachusetts, USA) following the manufacturer's protocol.

Whole cell lysates (50 µg protein per track) were resolved on 4–12% Bis-Tris SDS-PAGE (Invitrogen) followed by immunoblotting with anti-DPP9 antibody (1:2000) (Yao et al., 2011) and anti-β-Actin (Sigma-Aldrich, #A2103, 1:5000). Relative band intensities were quantitatively analysed using ImageJ and normalised against control proteins as indicated.

3.2.2.10 Quantitative real-time PCR (qPCR)

Total RNA was isolated using Trizol (Invitrogen) and cDNA synthesis was performed using SuperScript VILO cDNA Synthesis Kit (Invitrogen). qPCR was performed as described previously (Chowdhury et al., 2013) using Taqman gene expression assays (Applied Biosystems, Foster City, CA, USA) for mouse DPP4 (Mm00494548_m1), DPP8 (Mm00547049_m1), DPP9 (Mm00841122_m1) and FAP(Mm00484254_m1), with β-Actin (Mm00607939) as a standard.

3.2.3 Results

3.2.3.1 DPP9$^{S729A/S729A}$ homozygotes die in the neonatal period

Heterozygous DPP9$^{wt/S729A}$ mice on a C57BL/6 background were generated and supplied to our lab where sequencing of purified PCR products verified the presence of the S729A mutation in the DPP9 allele (Figure 3.1). However, intercrossing of DPP9$^{wt/S729A}$ mice and subsequent absence of any detectable DPP9$^{S729A/S729A}$ homozygote offspring at weaning was suggestive of lethality.

To determine the time of death, litters were observed and genotyped at embryonic and early neonatal stages. Live homozygote embryos and pups were detected in ED 12.5, 13.5, 15.5, 17.5 and early neonate (Day 1) litters. Analysis of embryo genotype numbers (n =41) confirmed that the DPP9 S729A allele was present in the expected Mendelian frequency (Section 3.3.1, Table 3.6). Thus, it appeared that enzyme-active DPP9 is not essential for development of the mouse embryo to term.

Directly after birth, normal cyanosis was present and all pups breathed normally and became pink (n=92). Littermates were of a similar size and weight with no significant gender or genotype difference found for Day 1 neonates (p>0.05) (Table 3.3). All appeared to feed normally with milk in the stomach shown by a milk spot and later by histological examination of whole neonate sections. At this early stage, pups showed no discernible behavioral differences, however, after several hours, some pups were found dead or showing weak respiratory movements and lethargy. There were no visual differences between genotypes in skin color or hydration.

	Genotype				Gender		
	$DPP9^{S729A/S729A}$	$DPP9^{wt/S729A}$	$DPP9^{wt/wt}$	Total	♂	♀	Total
Neonate number	21	53	18	92	40	52	92
Observed average weight	1.09 ± 0.13	1.12 ± 0.13	1.16 ± 0.11		1.13 ± 0.13	1.09 ± 0.12	
Expected average weight	1.12	1.12	1.12		1.12	1.12	
	$\chi^2 = 0.002$ $p = 0.999$				$\chi^2 = 0.003$ $p = 0.959$		

Table 3.3: Average neonate weights (in grams) for genotype and gender on Day 1 after birth.

Observed weights are expressed as the mean ± standard deviation.

Investigating the mortality of newborn pups revealed that, of the 27 found dead in the first 24 hours, all were either DPP9$^{S729A/S729A}$ or DPP9$^{wt/S729A}$. This suggested a negative effect on survival to weaning for offspring carrying the S729A mutation.

Subsequent genotyping of newborn DPP9$^{wt/S729A}$ intercross pups showed that the DPP9 S729A allele occurred in the expected Mendelian ratios. From 33 litters from DPP9$^{wt/S729A}$ breeding pairs, 317 pups were produced with 68 DPP9$^{S729A/S729A}$, 167 DPP9$^{wt/S729A}$ and 82 DPP9$^{wt/wt}$. Chi-square analysis confirmed no significant deviation from a 1:2:1 ratio (p>0.05). Similarly, a lack of significant gender bias shown in neonates precludes a gender effect by the DPP9 S729A allele on embryonic development (Table 3.4).

	Genotype				**Gender**		
	DPP9$^{S729A/S729A}$	**DPP9$^{wt/S729A}$**	**DPP9$^{wt/wt}$**	**Total**	♂	♀	**Total**
Observed number	68	167	82	317	123	147	270
Expected number	79.25	158.5	79.25		135	135	
Expected ratio	0.25	0.5	0.25		0.5	0.5	
Actual ratio	0.21	0.53	0.26		0.46	0.54	
	χ^2 = 2.148 p = 0.342				***χ^2 = 2.133 p = 0.144***		

Table 3.4: Neonate mouse genotype and gender numbers and ratios compared to expected Mendelian ratios.

At weaning, from 110 tracked DPP9$^{wt/S729A}$ intercross litters resulting in 563 weaned pups, only DPP9$^{wt/S729A}$ and DPP9$^{wt/wt}$ pups were present with no DPP9$^{S729A/S729A}$ pups. Interestingly, Chi-square analysis showed a significant bias towards DPP9$^{wt/wt}$ pups (p =0.008), rather than an expected 2:1 genotype ratio (Table 3.5). This confirmed a heterozygous effect on survival to weaning. The group of surviving DPP9$^{wt/S729A}$ heterozygous pups also showed a slight variation from a 1:1 ratio of males to females (Table 3.5), however this result is consistent with previous studies on mouse sex ratios (Rugh, 1968, Hardy, 1997, Schlager and Roderick, 1968) and, thus, not attributable to the heterozygous effect. There was no gender bias amongst pups that did not survive to weaning.

	Genotype			**Gender**		
	DPP9$^{wt/S729A}$	**DPP9$^{wt/wt}$**	**Total**	♂	♀	**Total**
Observed number	346	217	563	307	256	563
Expected number	375.5	187.5		281.5	281.5	
Expected ratio	0.67	0.33		0.50	0.50	
Actual ratio	0.62	0.38		0.55	0.45	
	χ^2 = 6.969 p = 0.008			***χ^2 = 4.620 p = 0.032***		

Table 3.5: Weaned mouse genotype and gender numbers and ratios compared to expected Mendelian ratios.

Therefore, while the DPP9$^{S729A/S729A}$ embryos and neonates were indistinguishable morphologically from their wild-type and heterozygote littermates, neonates died shortly after birth indicating that DPP9 enzymatic activity is required for neonatal survival.

3.2.3.2 Early neonate DPP9S729A/S729A homozygotes show no histological, histochemical or urinary protein difference from their heterozygous and wild-type littermates

Light microscopic observations of H&E-stained whole neonate sections (Day 1) by a trained pathologist (Derek S Spielman) revealed no histological differences between DPP9$^{S729A/S729A}$ pups (n =4) and their DPP9$^{wt/S7\ 29A}$ (n= 2) and DPP9$^{wt/wt}$ (n= 4) littermates. Organs examined were gut, heart, lung, brain and skin (Figure 3.2A) along with kidney, liver, thymus (Figure 4.5), pancreas, muscle and cartilage (Figure 4.6).

Immunohistochemistry using an antibody specific to DPP9 (Harstad et al., 2013) that has been used extensively by us (Yao et al., 2011, Yu et al., 2009, Chowdhury et al., 2013) and others (Harstad et al., 2013, Dubois et al., 2009), showed no DPP9 localisation differences between DPP9$^{wt/wt}$, DPP9$^{wt/S729A}$ or DPP9$^{S729A/S729A}$ on early whole neonate sections. Many neonate organs were strongly immuno-positive for DPP9 protein, most notably kidney, skin, liver (Figure 3.2B), brain and thymus. Overall, the immunostaining was consistent with published data (Yu et al., 2009, Schade et al., 2008).

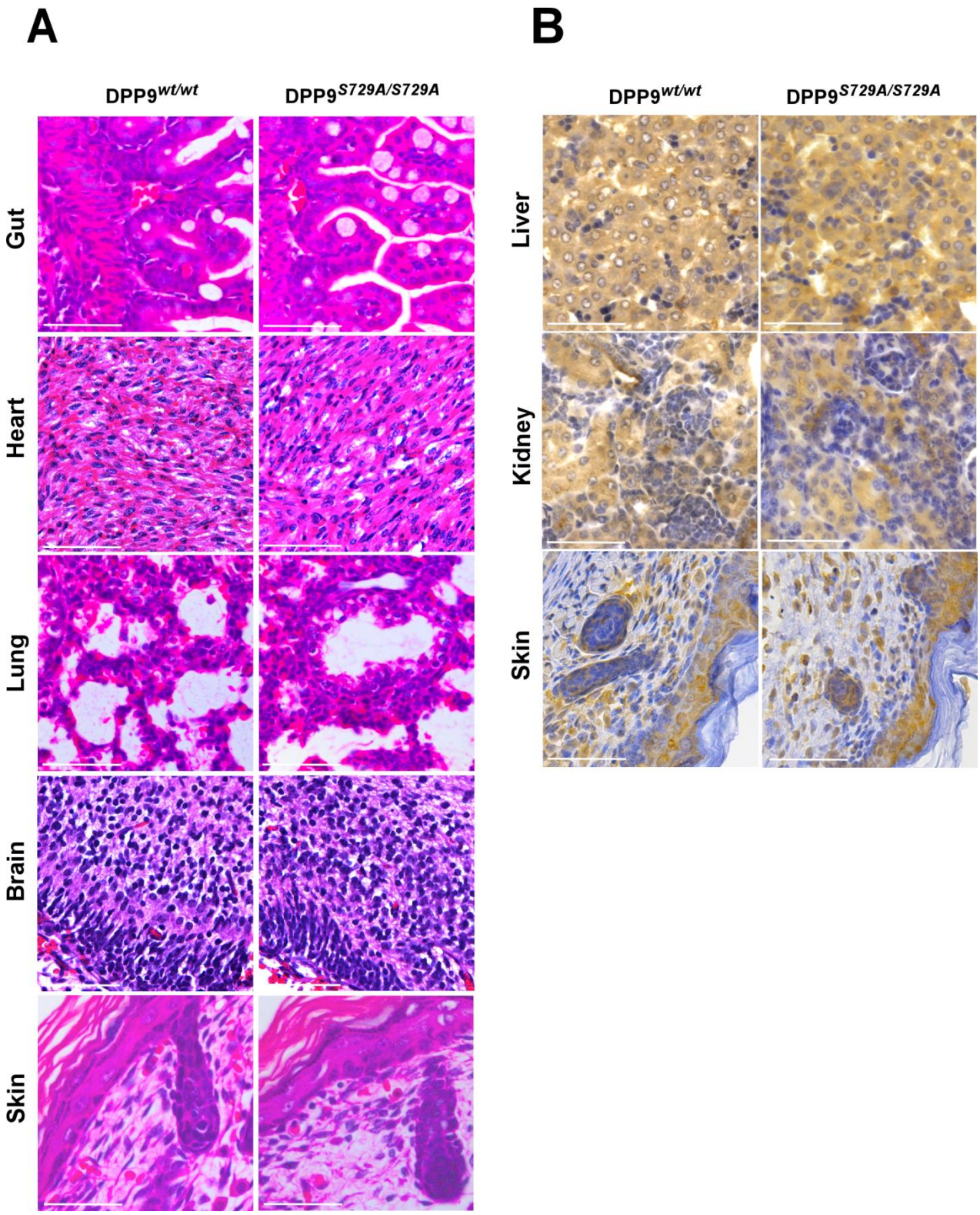
A
DPP9wt/wt
DPP9S729A/S729A
Gut
Heart
Lung
Brain
Skin
B
DPP9wt/wt
DPP9S729A/S729A
Liver
Kidney
Skin

Figure 3.2: Histology and immunohistochemistry of early neonate tissues are comparable between genotypes.

(A) Light micrographs of H&E-stained DPP9$^{S729A/S729A}$ lung, heart, gut, brain and skin tissue compared to DPP9$^{wt/wt}$ show no differences in histological structure and (**B)** Anti-DPP9 antibody staining showed no DPP9 localisation differences between DPP9$^{wt/wt}$ and DPP9$^{S729A/S729A}$ early neonate sections. Scale bar 50μm.

Neonatal death of mice within 24 hours of birth can be due to nephrin deficiency and, hence, massive proteinuria (Putaala et al., 2001). SDS-PAGE analysis of urinary protein in early neonates (Section 3.3.2) showed no proteinuria and no urinary protein band differences between DPP9$^{wt/wt}$, DPP9$^{wt/S729A}$ or DPP9$^{S729A/S729A}$ littermates, thus excluding renal damage as a cause of death.

3.2.3.3 DPP9$^{S729A/S729A}$ mouse embryonic fibroblasts express intact DPP9 mRNA and enzyme-inactive DPP9 protein

To verify the expression of DPP9 enzyme-inactive protein, immortalised MEFs and neonate livers of DPP9$^{S729A/S729A}$ and wild-type littermates were characterised for DPP mRNA and protein expression and activity. DPP9 protein and mRNA levels were measured by immunoblot and qPCR respectively.

qPCR results indicated that DPP9$^{S729A/S729A}$ MEFs and neonatal liver expressed similar levels of DPP9 mRNA, as well as FAP, DPP8 and DPP4 mRNA, to wild-type (Figs. 3.3A and 3.3B). When immunoblotting with a DPP9 antibody, DPP9 bands run at different sizes in different cell lines (Yao et al., 2011, Chowdhury et al., 2013). Immunoblotting of MEFs showed similar levels of intact DPP9 protein expression in DPP9$^{S729A/S729A}$ MEFs and wild-type MEFs (110 and 130 kDa) (Figure 3.3C) and was confirmed by densitometry (Figure 3.3D). These results demonstrated that the targeted point mutation did not influence the expression of DPP9 mRNA and protein. In addition, it indicates that there was no detectable compensatory upregulation of the other DPPs due to the lack of DPP9 enzymatic activity.

Enzyme activity derived from DPP9 and DPP8 can be measured in the presence of a DPP4 inhibitor and a substrate that is hydrolysed by all three proteases (Yu et al., 2009). Enzyme activity assays on whole MEFs showed that DPP9$^{S729A/S729A}$ MEFs had significantly less DPP enzymatic activity than wild-type MEFs (Figure 3.3E). Moreover, in neonatal liver lysates (Figure 3.3F), DPP9$^{S729A/S729A}$ neonatal liver contained significantly less DPP8/ 9-derived enzymatic activity than wild-type liver, which is consistent with a lack or large reduction of DPP9 enzymatic activity. Together with the immunoblot and qPCR data, this provides evidence that DPP9-S729A enzyme-inactive protein was expressed at similar levels to DPP9-WT enzyme-active protein in MEF cell lines and neonatal livers.

3.2.3.4 DPP9-S729A and wild-type DPP9 have the same subcellular localisation

A point mutation in rat DPP4 (Erickson et al., 1992) causes mis-localisation and intracellular degradation of DPP4 rather than normal cell surface expression. To examine whether enzyme- inactive DPP9 protein and active DPP9 protein are similarly localised in vitro, DPP9- overexpressing Huh7 cells and endogenous DPP9 in MEFs were examined by immunofluorescence staining and confocal microscopy. DPP9-S729A-EGFP had an intracellular distribution similar to DPP9-WT-EGFP (Figure 3.4A). Similarly, endogenous DPP9 expression in DPP9$^{S729A/S729A}$ MEFs was indistinguishable from DPP9 protein in wild-type MEFs (Figure 3.4B).

Figure 3.3: DPP9 expression in DPP9$^{wt/wt}$ and DPP9$^{S729A/S729A}$ MEFs and neonatal liver is equivalent.

By qPCR, **(A)** DPP9$^{S729A/S729A}$ MEFs (n=3) and **(B)** neonatal liver (n=8) showed similar mRNA expression levels of DPP4, DPP8, DPP9 and FAP compared to DPP9$^{wt/wt}$.

(C) Similar levels of intact DPP9 protein were detected by immunoblotting in DPP9$^{S729A/S729A}$ MEFs compared to DPP9$^{wt/wt}$ littermate MEFs.

(D) Densitometry analysis of this immunoblot; the 110 kDa and 130 kDa bands were combined. DPP8/9 enzyme assays showed less enzymatic activity in **(E)** DPP9$^{S729A/S729A}$ MEFs compared to WT MEFs (n=3), $**p < 0.001$ and **(F)** DPP9$^{S729A/S729A}$ neonatal livers (n=4) compared to WT livers (n=6), $*p < 0.05$.

The DPP enzyme activity contributed by DPP9 and DPP8 is the proportion of non-inhibited control activity which was calculated as the hydrolysis of H-Gly-Pro-AMC observed after inhibition of DPP4 by sitagliptin. dF is change in fluorescence.

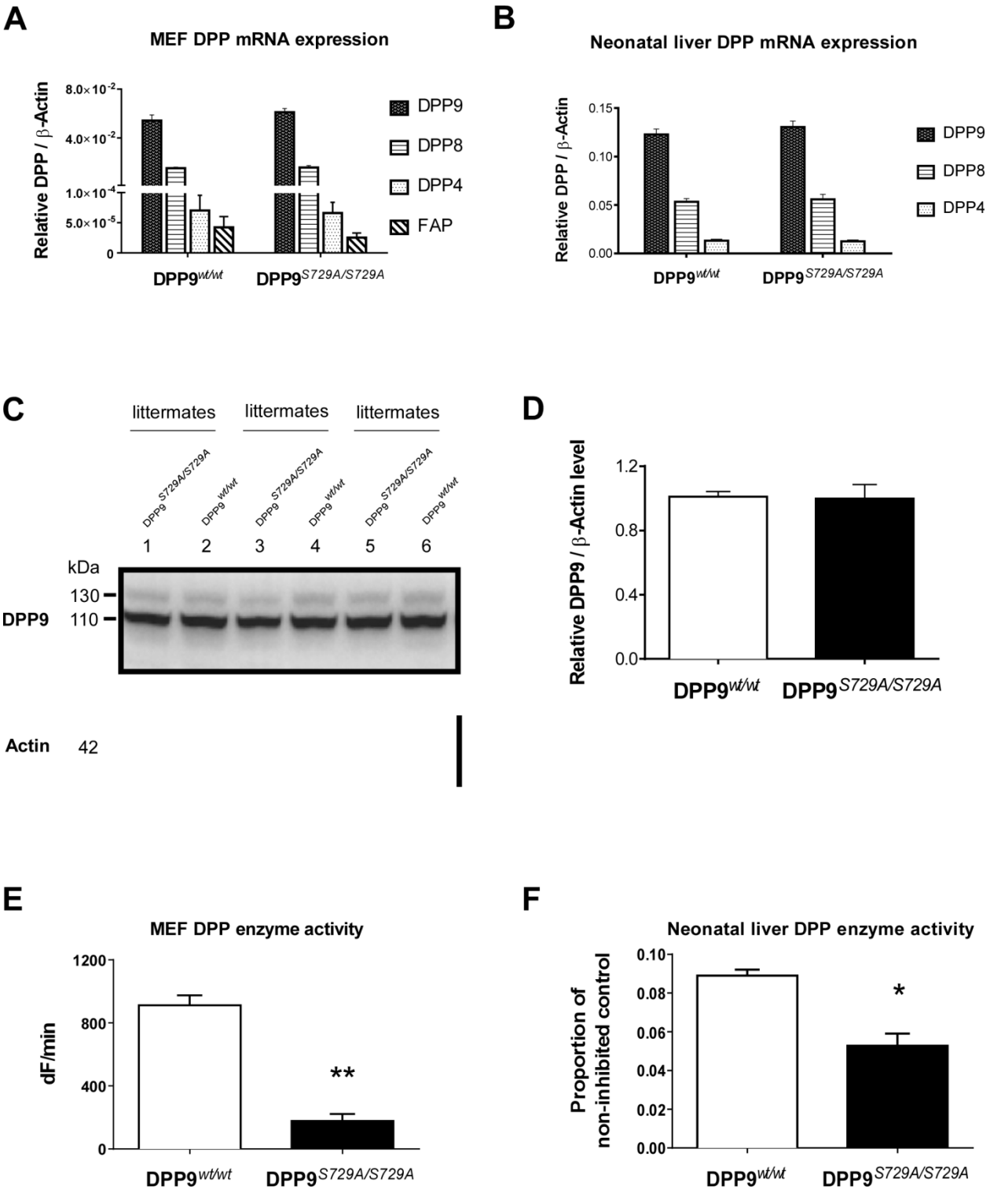
A
MEF DPP mRNA expression
Relative DPP / β-Actin
8.0×10-2
4.0×10-2
1.0×10-4
5.0×10-5
0
DPP9
DPP8
DPP4
FAP
DPP9wt/wt
DPP9S729A/S729A
B
Neonatal liver DPP mRNA expression
Relative DPP / β-Actin
0.15
0.10
0.05
0.00
DPP9
DPP8
DPP4
DPP9wt/wt
DPP9S729A/S729A
C
littermates
littermates
littermates
DPP9 S729A/S729A
DPP9 wt/wt
1 2 3 4 5 6
kDa
130
110
DPP9
Actin 42
D
Relative DPP9 / β-Actin level
1.2
0.8
0.4
0.0
DPP9wt/wt
DPP9S729A/S729A
E
MEF DPP enzyme activity
dF/min
1200
800
400
0
**
DPP9wt/wt
DPP9S729A/S729A
F
Neonatal liver DPP enzyme activity
Proportion of non-inhibited control
0.10
0.08
0.06
0.04
0.02
0.00
*
DPP9wt/wt
DPP9S729A/S729A

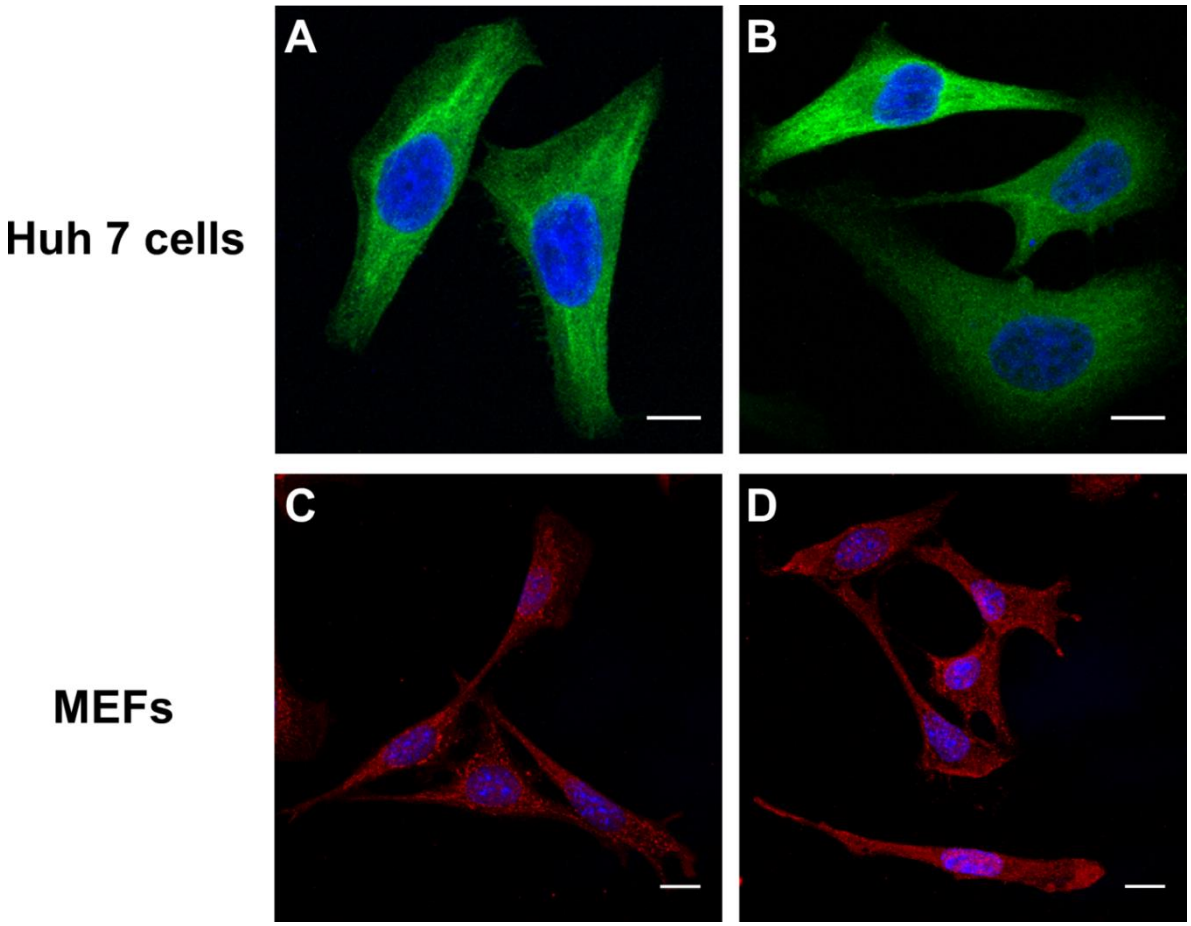

Figure 3.4: Active DPP9-WT and enzyme-inactive DPP9-S729A show the same intracellular localisation.

DPP9-EGFP visualisation in Huh7 cells transfected with **(A)** DPP9-WT-EGFP or **(B)** DPP9-S729A-EGFP showed no localisation difference. Similar expression patterns of antibody-stained DPP9 (red) were observed in **(C)** wild-type MEFs and **(D)** *DPP9*$^{S729A/S729A}$ MEFs. Confocal images were created only from Z-stacks that contained the nuclear region. Scale bar 15 µm.

3.2.4 Discussion

In this study, we found that DPP9 enzymatic activity is essential for neonatal survival in the mouse. The mice express intact DPP9 protein but with the loss of enzymatic activity. This did not alter pre-natal development but resulted in neonatal deaths. Thus, the complete disruption of DPP9 expression was not necessary for early lethality, highlighting the biological importance of the enzyme activity of DPP9 at this stage of development. The lethality of lacking DPP9 activity indicates that DPP9 is unique such that no other enzyme can compensate for this enzyme at this developmental stage. The cause of death was not apparent. All neonates suckled and contained milk spots and males and females of each genotype were of similar body weight. No differences were seen by histological examination and no urinary proteinuria was observed.

The close structural similarity of DPP9 to DPP8 makes the development of selective DPP9 inhibitors challenging (Van Goethem et al., 2011, Rummey and Metz, 2007) and has not been achieved. Thus, the DPP9 enzyme-inactive mouse is a useful and unique model for emulating the biological effects of selective DPP9 inhibition from the embryonic stage and avoids potential off-target effects that chemical compounds may produce in mice. Our genetic targeting approach is the only DPP9-specific model for understanding the biological significance of DPP9 enzymatic activity in vivo. The biology in this model is very different to previous studies that have treated adult animals with inhibitors of both DPP9 and DPP8 or of DPP9, DPP4 and DPP8 together (Wu et al., 2009, Wang et al., 2012, Burkey et al., 2008).

To verify the status of DPP9 protein in our mice, the MEF and neonatal liver data indicate that the S729A mutation produced a full-length DPP9 protein with no enzymatic activity. Comparable sizes and intracellular localisations of DPP9 intact protein and similar DPP mRNA levels were shown in DPP9 enzyme-inactive MEFs compared to MEFs and neonatal liver derived from wildtype littermates. In addition, related dipeptidyl peptidases were not upregulated in the DPP9 enzyme-inactive mouse to compensate for the absence of DPP9 activity. We similarly observed in our enzyme distribution studies on DPP4-GKO mice (Yu et al., 2009) and FAP-GKO MEFs (Hamson, Yu, Gorrell, unpublished data) that DPP4-related dipeptidyl peptidases are not upregulated in those mouse strains.

Like DPP9, DPP8 has intracellular expression (Yu et al., 2006b, Abbott et al., 2000b) and DPP4, FAP and DPP8 all have DPP enzymatic activity (Kirby et al., 2010, Yu et al., 2009, Ajami et al., 2004, Abbott et al., 2000b, Heymann and Mentlein, 1978, Park et al., 1999, Wang et al., 2005, Abbott et al., 1999). Since DPP4-GKO and FAP-GKO mice are phenotypically healthy, DPP9 neonate lethality was unexpected. This lethality shows that DPP4, DPP8 and FAP are unable to fulfill an essential role of DPP9 in early mouse neonate life, thereby highlighting a unique role for DPP9 activity within the DPP4 gene family.

Many factors can contribute to neonate deaths but the time of death can provide clues to the potential causes (Turgeon and Meloche, 2009). While there are numerous examples of neonatal lethality in genetically modified mice (Turgeon and Meloche, 2009), very few die so quickly and without morphological differences from their

heterozygous or wild-type littermates. Having survived the stress of parturition, neonates fulfill new metabolic needs by their own homeostasis, failure of which can result in poorer survival. As the DPP9$^{S729A/S729A}$ pups survived parturition with no obvious gross anatomical and histological differences, it seems the resultant lethality in DPP9$^{S729A/S729A}$ mice is probably attributable to metabolic impairment (Chen et al., 2016). The literature reports dysfunctions in homeostasis due to failures in autophagy (Kuma et al., 2004), kidney filtration (Putaala et al., 2001), transcriptional controls in cell nuclei (Calogero et al., 1999) and *in vivo* glucose homeostasis (Scheuner et al., 2001). The nature of the dysfunction caused by lacking DPP9 enzymatic activity at birth needs to be elucidated by further investigations.

3.3 Supplementary data

This section includes data not shown in Section 3.2 (published paper) but undertaken as part of the neonate mouse studies to identify the lethal phenotype and discussed in the Results (Section 3.2.3) and Discussion (Section 3.2.4).

3.3.1 Embryo studies

Initial investigations of the DPP9 mouse showed that no DPP9$^{S729A/S729A}$ mice were present at weaning. To more accurately observe times of death of DPP9$^{S729A/S729A}$ neonatal mice, litters were first observed and genotyped at embryonic stages. Live homozygote embryos were detected in ED (embryonic day) 12.5, 13.5, 15.5 and 17.5 litters.

Analysis of embryo genotype numbers (n=41) harvested from pregnant females at various embryonic stages confirmed that the DPP9 S729A allele was present in the expected Mendelian frequency as indicated by the high *p* value (Table 3.6). This confirmed that enzyme-active DPP9 is not essential for development of the mouse embryo to parturition (Gall et al., 2013).

	Genotype			
	DPP9$^{S729A/S729A}$	**DPP9$^{wt/S729A}$**	**DPP9$^{wt/wt}$**	**Total**
Observed number	5	24	12	41
Expected number	10.25	20.5	10.25	
Expected ratio	0.25	0.5	0.25	
Actual ratio	0.12	0.59	0.29	
	χ^2 = 3.585 p = 0.167			

Table 3.6: Total embryo genotype numbers compared to expected Mendelian ratios.

3.3.2 Neonate and weaned mouse gender analysis

As discussed in Section 3.2.3.1, no gender bias was observed in total neonate numbers (Table 3.4) or total weaned mouse numbers (Table 3.5). While this finding suggests that a gender bias within genotype groups is unlikely, analysis was undertaken to confirm this. These analyses showed no difference in the expected 1:1 Mendelian ratio between male and female neonates for each genotype group (Table 3.7). Similarly, for the mice which survived to weaning (Table 3.8) , there was a slight bias towards male mice for the WT genotype consistent with with previous studies on mouse sex ratios (Rugh, 1968, Hardy, 1997, Schlager and Roderick, 1968).

Genotype	**DPP9$^{S729A/S729A}$**		**DPP9$^{wt/S729A}$**		**DPP9$^{wt/wt}$**	
Gender	♂	♀	♂	♀	♂	♀
Observed number	56	50	112	119	54	47
Expected number	53	53	115.5	115.5	50.5	50.5
Expected ratio	0.5	0.5	0.5	0.5	0.5	0.5
Actual ratio	0.53	0.47	0.48	0.52	0.53	0.47
χ^2	*0.339*		*0.212*		*0.485*	
p value	***0.560***		***0.645***		***0.486***	

Table 3.7: Neonate mouse gender numbers and ratios for each genotype compared to expected Mendelian ratios.

Genotype	**DPP9$^{wt/S729A}$**		**DPP9$^{wt/wt}$**	
Gender	♂	♀	♂	♀
Observed number	183	163	124	93
Expected number	173	173	108.5	108.5
Expected ratio	0.5	0.5	0.5	0.5
Actual ratio	0.53	0.47	0.57	0.43
χ^2	*1.156*		*4.429*	
p value	***0.282***		***0.035***	

Table 3.8: Neonate mouse gender numbers and ratios for each genotype compared to expected Mendelian ratios.

3.3.3 Neonate urinalysis

3.3.2.1 Introduction

The kidney plays a critical role in regulation of fluid homeostasis and mice which completely lack genitourinary structures die soon after birth (Miyamoto et al., 1997). Most newborn mice with kidney anomalies die in the first 2 days of life, with the timing dependent on the defect severity (Turgeon and Meloche, 2009). The normal gross morphology and histology of the kidneys of DPP9$^{S729A/S729A}$ pups meant that any of the many known developmental renal defects are very unlikely to occur in this mouse strain.

Defects in kidney function that impair production and concentration of urine, however, are more subtle and harder to detect. One such functional impairment causing early neonatal death in mice, while displaying no gross morphological kidney defect, is due to a deficiency in the production of nephrin. This malfunction results in the development of massive proteinuria and oedema (Putaala et al., 2001). Therefore, the DPP9$^{S729A/S729A}$ pups were examined for the possibility of high levels of urinary protein.

3.3.2.2 Methods

SDS-PAGE analysis on mouse neonate urine samples to identify high protein levels was carried out in duplicate as described in Section 3.2.2.6. Further SDS-PAGE analysis of urine samples was also carried out in duplicate using a tricine gel to identify the absence, presence or other difference in abundance of low molecular weight proteins between GKI and WT samples. In this instance, 4 µL of urine from each pup together with 5 µL sample buffer and 1 µL reducing buffer was heated at 85^{0}C for 2 min before

being run on a Novex™ 16% Tris-Glycine gel (Invitrogen) under reducing conditions. An XCell SureLock Mini-cell electrophoresis unit (Invitrogen) was used for gel runs at 175 V for 60 m in in 1× Tricine SDS Running Buffer. Gels were stained with SYPRO® Ruby Protein Gel Stain (Invitrogen). Relative molecular masses were estimated by comparison to an Ultra-low Range Molecular Weight Marker (Sigma).

3.3.2.3 Results

There were no urinary protein band differences seen between DPP9$^{wt/wt}$, DPP9$^{wt/S729A}$ or DPP9$^{S729A/S729A}$ littermates after SDS-PAGE analysis, nor any evidence of proteinuria (Figure 3.5). No gender differences were observed. These findings, in conjunction with the normal histological and gross morphological appearance of the neonate kidneys confirmed that renal damage was very unlikely to have contributed to death in the DPP9$^{S729A/S729A}$ pups.

However, the gel showed the possible absence of a low molecular weight band in DPP9$^{S729A/S729A}$ urine samples as compared to the WT and DPP9$^{wt/S729A}$ samples (Figure 3.5B, red arrows and circles) at the 10 kDa level corresponding to an unknown urinary protein. As gel resolution is poor at this level, the samples were re-run using a tricine gel to gain higher protein band resolution. Close examination of the resultant gel (Figure 3.6) showed no absent protein bands around the 10 kDa region while comparing DPP9$^{S729A/S729A}$ and WT urine samples, nor any absent or extra bands across the range of sizes.

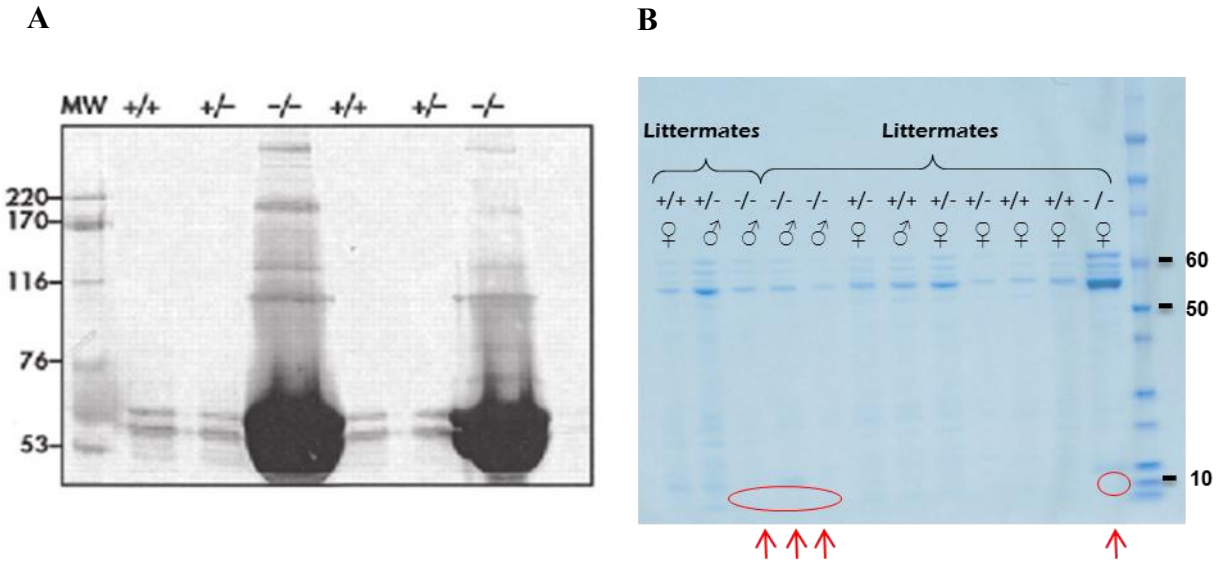

Figure 3.5: Comparative gels indicate the urinary proteins levels in early neonates with and without proteinuria and with comparable gel patterns between genotypes.

SDS-PAGE gels on neonate urine samples showing **(A)** massive proteinuria from nephrin-deficient mice (from (Putaala et al., 2001)), and **(B)** the absence of proteinuria in DPP9$^{S729A/S729A}$ versus WT and DPP9$^{wt/S729A}$ littermate mice. Red arrows and circles indicate the possible absence of an unidentified low molecular weight protein in DPP9$^{S729A/S729A}$ urine samples.

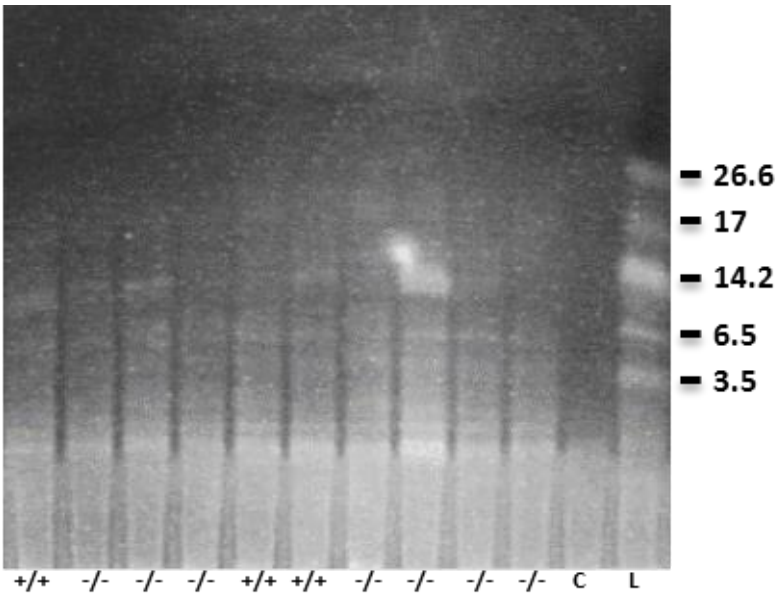

Figure 3. 6: Low molecular weight urinary proteins in early neonates are comparable between genotypes.

Tricine gel using neonate urine samples showing comparable banding between DPP9$^{S729A/S729A}$ and WT littermates with no discernible absence of bands. (**C** buffer only sample; **L** ladder)

CHAPTER 4:

Characterisation of neonate DPP9-GKI mice lacking DPP9 enzymatic activity

4 Characterisation of neonate DPP9-GKI mice lacking DPP9 enzymatic activity

4.1 General introduction

The lethality of the DPP9-GKI mouse was described in Chapter 3 and confirmed as occurring in the early neonatal period with the death of all DPP9$^{S729A/S729A}$ pups, along with a small but significant number of DPP9$^{wt/S729A}$ pups (Gall et al., 2013). At this critical stage, there is a disadvantage in carrying the S729A mutant allele. The post-weaning life expectancy of heterozygous mice, however, did not differ from their wild-type littermates, suggesting that adult mice are no longer reliant on DPP9 enzymatic activity for survival.

With this in mind, further investigation was undertaken on early neonatal mice at Day 1 post birth. As previously described, there are many potential causes for early neonatal lethality but most are associated with gross morphological or behavioural defects that are easily observed (Figure 4.1) (Turgeon and Meloche, 2009). In the case of the DPP9-GKI mice, there were no defects in gross morphology or behaviour, with all neonates having normal appearance and feeding, moving and breathing in a manner consistent with their littermates.

Although initial histological investigations showed no obvious altered tissue histology or pathology, further organ samples were collected from neonate mice to validate previous results. The focus for general histological reassessment of organs was brain,

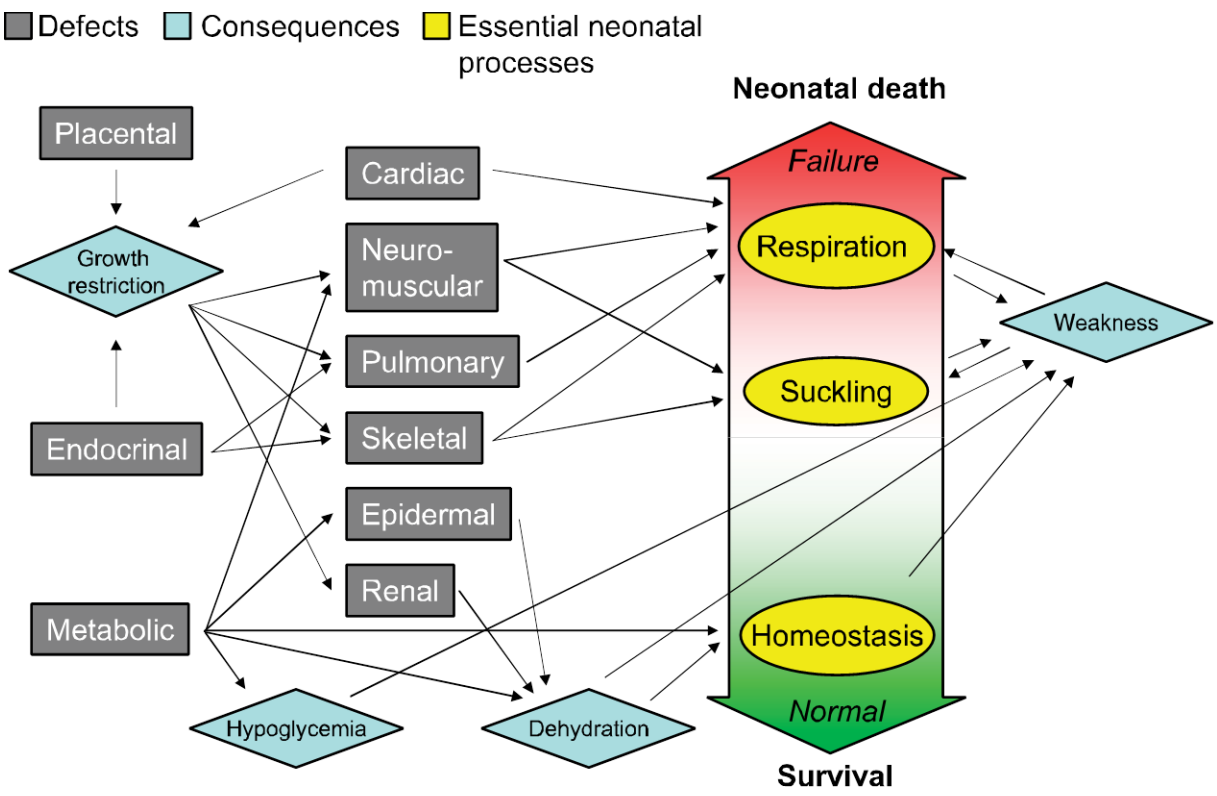

Figure 4.1: Cause-to-effect relationships between defects and physiology causing neonatal death.

Complex biological networks are revealed in the neonatal death of mutant mice. Cause-to-effect relationships are shown in this diagram between organ defects and the affected physiological processes critical for neonatal survival. Modified from (Turgeon and Meloche, 2009).

---

kidney, liver, thymus, pancreas and gut, with a detailed focus on heart.

Consideration was also given to the possibility of an autophagy defect in the early DPP9-GKI neonates as previous studies have found lethality occurring in mutant mice deficient for *Atg5* with autophagy impairment (Kuma et al., 2004) . Autophagy, while low during embryogenesis, is upregulated in a variety of tissues immediately after birth

and maintained for up to 12 hours before returning to basal levels within several days (Kuma et al., 2004).

4.1.1 Aims

The aims of this chapter are:

- to further investigate the possible causes of neonate lethality in DPP9-GKI mice by:
    - considering possible developmental and/or physiological causes of the lethality by analysing organ morphology, histology and function in newborn mice, with specific focus on the heart
    - assessing whether there is a defect in autophagy

4.1.2 Presentation

This chapter is presented in two parts.

- Section 4.2 covers the investigation of organ morphology, histology and function and
- Section 4.3 covers autophagy investigations.

Each section contains its own introduction, materials and methods, results and discussion.

4.2 General neonate histology

While original histological investigations were undertaken on whole body neonate sections and published (Gall et al., 2013), individual organs from Day 1 neonates were later used, in order to undertake a more detailed examination of neonate histology. Organs were isolated, sectioned and stained using methods described in Section 3.2.2.4.

4.2.1 Heart

4.2.1.1 Introduction

The heart is the first organ to form in the developing embryo and embryonic survival depends on the establishment of a normal circulatory function. Many cardiovascular defects are responsible for *in utero* embryonic lethality (Conway et al., 2003). In the post-natal heart, the initiation of breathing at birth and the increased burden associated with newborn activity causes dramatic changes to occur in the circulatory system. Many neonate-lethal mutant mice have heart morphology and functionality defects and the study of these mutants is useful for the understanding of congenital heart diseases in humans (Table 3.7) (Turgeon and Meloche, 2009).

Gene	Gene product	Time of Death	Comments
Heart outflow tract			Models of human CHD
Foxc2	Forkhead transcription factor	10 min after birth	Aortic arch anomalies
Plxnd 1	Plexin	24 h	Truncus arteriosus
Sema3c	Semaphorin	Soon after birth	Various penetrance
Ductus arteriosus			
Hpgd	Prostaglandin dehydrogenase	12-24 h	Model of human disease
Ptger4	Prostaglandin receptor	12-48 h	
Ptgs1/2	Prostaglandin synthase	30 min-12 h	Secondary lung anomalies

Table 4.1: Typical neonatal lethal cardiac mutations in mice associated with respiratory failure

Examples of cardiac defects that compromise mouse neonate survival due to defective circulatory and/or respiratory function. Modified from (Turgeon and Meloche, 2009).

As stated in Section 3.2.3, the DPP9$^{S729A/S729A}$ mice showed no obvious histological or gross morphological difference in the heart compared to WT littermates, and neonate pups appeared to have normal respiratory function and no cyanosis. However, the timing of death after parturition was suggestive of a possible heart defect. Since the heart muscle appeared histologically normal (Figure 3.2A), it was decided to investigate the possibility of less readily observable morphological defects that may impair the survival ability of neonates. Defects in internal heart structure, such as malformation of valve leaflets, heart septa or atrial and ventricular size are not possible to determine by single sections alone. Serial sections and whole heart

dissection are necessary to investigate heart structure.

4.2.1.2 Methods

For further gross morphological studies, neonate hearts were removed from newborn pups as described previously (Section 3.2.2.4). Hearts (n=2 WT and n=2 GKI) were serially sectioned at 5µm and checked microscopically at various planes of section to identify any septal, atrial, or ventricular defects.

For detailed morphological studies, neonate heart/ lung blocks were:

- removed and stored long-term in neutral buffered formalin until dissection or
- removed and treated for 10 min in 60mM KCl solution to arrest the heart muscle at diastole and then stored in neutral buffered formalin until use.

Hearts were dissected by Dr Christine Biben who has a high level of expertise and skill in mouse neonate heart structure and fine dissection (Biben et al., 2000, Sierro et al., 2007), with the assistance of Dr Frederic Sierro.

4.2.1.3 Results

4.2.1.3.1 Gross heart morphology

Neonate whole heart sections of WT and DPP9$^{S729A/S729A}$ mice showed similar histology and gross morphology of major heart structures (Figure 4.2). Slight variations in the transverse plane of section made comparison of valve leaflets between genotypes difficult. However, when valves were present in sections, no

differences in valve leaflet morphology could be confirmed and valves appeared to have comparable histology.

In sections, the presence of an intra-ventricular septal hole or defect in the neonate hearts would be indicated by a discontinuity or unusual morphology in the intra-ventricular septum (Minette and Sahn, 2006). However, serial sections through the ventricular region of neonate hearts from the apex to the base showed no apparent discontinuities (Figure 4.3) in either WT or DPP9$^{S729A/S729A}$ hearts, thus suggesting no intra-ventricular septal defects.

4.2.1.3.2 Detailed heart morphology

Macroscopic assessment of WT and DPP9$^{S729A/S729A}$ neonate hearts by Dr Christine Biben found the major vessels to be grossly normal. Fine dissection of hearts, however, appeared to show a possible abnormality of the aortic valves in two of the three GKI hearts while four WT littermates were normal. Pulmonary valves appeared normal, however mitral and tricuspid valves have yet to be investigated.

At the time of writing this thesis, further dissection of neonate hearts was ongoing.

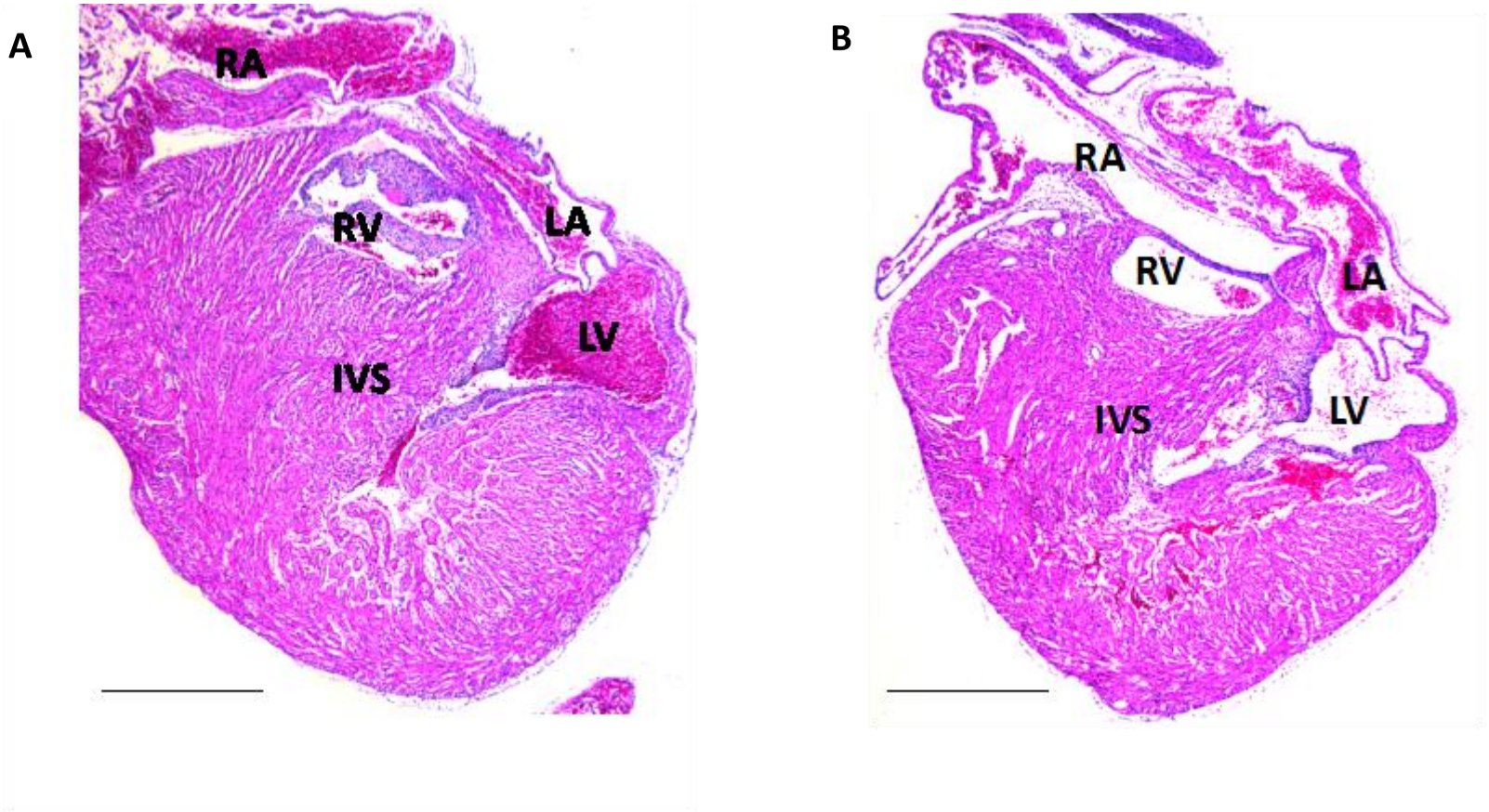

Figure 4.2: Comparative transverse sections at the venous pole of whole neonate heart in WT and DPP9$^{S729A/S729A}$ mice

Neonate heart sections of **(A)** WT and **(B)** GKI mice showed similar histology and gross morphology. Intraventricular septum IVS; left ventricle LV; left atrium LA; right ventricle RV; right atrium RA. Haematoxylin and eosin stained. Scale bar 500 µm.

Figure 4.3: Representative transverse sections through progressive levels of the ventricular region in whole neonate heart of DPP9$^{S729A/S729A}$ mice

Serial transverse sections of neonate hearts from the apex to the base (L to R) showing the intra-ventricular septum (IVS) with no apparent septal discontinuities or defects. Haematoxylin and eosin stained. Scale bar 500 µm.

4.2.1.4 Discussion

This study investigated the possible presence of a heart defect as the cause of neonate lethality in the case of the DPP9$^{S729A/S729A}$ mice. Problems with heart structure and function may certainly cause or contribute to neonate lethality (Turgeon and Meloche, 2009) and can often be detected by histological observation as a starting point. In the case of the DPP9$^{S729A/S729A}$ mice, the heart muscle histology (Section 3.2.3.2 and Figure 3.2) showed no apparent differences with a normal striated appearance of the muscle and nuclei present.

The next step was to investigate aspects of fine morphology and internal heart structure. Cardiovascular abnormalities that bypass embryonic lethality are often associated with cyanosis from poor blood oxygenation and cause respiratory distress. Since no cyanosis or respiratory distress was observed in the DPP9$^{S729A/S729A}$ neonates, further study focused on more subtle heart abnormalities such as septal discontinuities or defects (Biben et al., 2000, Sierro et al., 2007). Serial sections of neonate hearts showed no discontinuity between the left and right ventricles and no evidence of an intra-ventricular septal defect. Attempting to identify atrial septal defects via serial sections was beyond the scope of this current study.

A collaborative study with Dr Christine Biben, to identify defects in hearts valves, atrial and ventricular chamber size and outflow tract and aortic arch vessels, is ongoing. Major vessels and pulmonary valves appeared to be normal which is

consistent with no observed cyanosis or obvious respiratory distress in newborn mice. While the observed possible aortic valve defects could contribute to neonate lethality, it is unlikely to be the sole cause as the current literature suggests an incomplete penetrance of such defects and a delayed onset of problems (Garg et al., 2005, Hinton et al., 2008, Laforest et al., 2011). Future results from our collaborator may clarify this point.

4.2.2 Kidney, liver, thymus, pancreas, muscle and cartilage

4.2.2.1 General introduction

The kidney, liver, thymus, pancreas, muscle and cartilage of the neonatal mouse are the focus of this section as many organs can be implicated in mouse neonate lethality (Turgeon and Meloche, 2009) and observation of the histology of tissue can provide evidence of organ malformation.

4.2.2.1.1 Kidney

The kidney in the neonate mouse plays a crucial role in the regulation of fluid homeostasis and normal development and function is important for survival. Anomalies in kidney development or complete lack of kidneys is due to the inactivation of many genes and results in neonate lethality in mice (Turgeon and Meloche, 2009).

As an example, the transcription factor Brn1 is necessary for normal development of Henle's loop and the distal convoluted tubule (Nakai et al., 2003). Another example is that mutation of the *α3 integrin* gene results in abnormal nephrogenesis with marked abnormalities in renal structure (Kreidberg et al., 1996). Aside from morphological defects, deficiencies in kidney function can cause death in mice and this has been investigated and discussed in Chapter 3 of this thesis. In newborn mice, the kidney stroma is loosely arranged and capillaries have narrow linings with thick endothelium. The tubules and glomeruli are less proximally placed than in adult mice and glomeruli are smaller as dilation of the capillaries associated with normal kidney function has yet to occur (Clark, 1957).

4.2.2.1.2 Liver

In neonatal mice, the characteristic liver architecture takes two to three weeks after birth to establish. The first week is represented histologically by developing hepatocyte chords interspersed with clumps of hematopoietic cells of mixed cell lineages (Crawford et al., 2010, Liu et al., 2014). Functionally, the newborn mouse liver has to cope with a rapidly changing environment in order to provide glucose necessary for energy needs which was previously provided by a maternal source. The glucose is produced via the gluconeogenic pathway and involves many enzymes which are essential for the proper functioning and differentiation of hepatocytes. Mutations that interfere with normal liver development can result in neonatal death (Turgeon and

Meloche, 2009). CCAAT/enhancer-binding protein α – deficient mice die soon after birth from hypoglycemia due to an inability to store hepatic glycogen (Wang et al., 1995). Neonate lethality due to hypoglycemia also occurs in high mobility group 1-deficient mice when abundant glycogen accumulation in the liver results in a glucose metabolism defect which is critically damaging at the time of birth (Calogero et al., 1999). Defective gluconeogenesis resulting in hypoglycemia causes death in mice with a mutation at the eukaryotic translation initiation factor 2 phosphorylation site (Scheuner et al., 2001) and liver dysfunction along with hypoglycemia also causes death when fumarylacetoacetate hydrolase is depleted (Grompe et al., 2011).

4.2.2.1.3 Thymus

The thymus, which is present in most vertebrates, is a primary lymphoid organ of the immune system. It is the major organ involved in T-cell production and, in the mouse, increases its size and upregulates its function during the neonatal period (Shanley et al., 2009). Neonatal mice require the population of the peripheral immune system with T-cells at birth and there is an increased migration of cells out of the thymus during the early neonatal stage (Hess et al., 1967). Hence, the thymus is important for effective immune function during the neonatal period.

4.2.2.1.4 Pancreas

The mouse pancreas is composed of the endocrine and exocrine components which develop in a biphasic manner. The endocrine Islet cells are present at birth and achieve adult form in the first two weeks of neonate life, with the proliferation and growth of the exocrine tissue increasing later (Dore et al., 1981, Kaufman et al., 2010). Mutations in neonate pancreas structure and/or function affect energy balance and glucose homeostasis and pose a serious threat to survival. Some examples include the gene *Arx* involved in endocrine pancreas development and the protein PTF1-p48 which is essential for exocrine pancreatic formation and endocrine pancreatic spatial organisation. *Arx*-deficient mice die two days after birth after developing hypoglycemia, dehydration and lethargy (Collombat et al., 2003) and the null PTF1-p48 mutation leads to a complete absence of exocrine pancreatic tissue resulting in abnormal spatial assembly of the endocrine pancreas (Krapp et al., 1998).

4.2.2.1.5 Muscle

Normal muscular activity, while important for general mobility, is of critical importance directly after birth for the initiation of respiration. An inability to breathe can result from defects in muscle development, muscle function or in the development of a functional neuromuscular junction. Many lethal phenotypes exist which are associated with respiratory failure (Turgeon and Meloche, 2009) and with death occurring very rapidly after birth. Also important for neonate survival is the ability to suckle normally. Morphological abnormalities in skeletal muscle lacking junctophilin type 1 (JP-1) result

in muscle with less contractile force. Mice deficient in JP-1 have impaired contractile activity of the jaw muscles and an inability to suckle effectively (Ito et al., 2001).

4.2.2.1.6 Cartilage

The mouse skeleton consists of both cartilage and bone which is spread throughout the body and abnormal development can result in many neonatal lethal phenotypes (Turgeon and Meloche, 2009). Hyaline cartilage, which is the precursor to bone, is recognized by its homogenous and highly hydrated matrix interspersed with spaces enclosing chondrocytes. As well as imparting structural resilience, cartilage tissue also allows the diffusion of small metabolites through its avascular matrix (Karsenty and Wagner, 2002).

Bone develops by endochondral ossification of cartilage and, because of its structural and developmental importance as a bone precursor, defects in cartilage can have catastrophic impacts on neonate survival. Rib cage cartilage plays a role in protection of body organs but, most importantly, enables proper respiration. Rib cage dysmorphia is associated with respiratory failure and neonatal death in connective tissue growth factor (CTFG)-deficient mice due to impaired matrix remodeling during chondrogenesis (Ivkovic et al., 2003). The proteoglycan perlecan has an important role in matrix structure and cartilage development and disruption of the gene encoding perlecan results in both embryonic and neonatal lethality in mice with varying degrees of abnormality (Arikawa-Hirasawa et al., 1999).

4.2.2.2 Methods

Individual organs were removed from genotyped newborn pups, combined into groups of 3 to 5 organs per genotype and processed as described previously (Section 3.2.2.4) into organ-specific paraffin blocks for sectioning.

4.2.2.3 Results

Consistent with results from Chapter 3, no obvious morphological defects were observed in the DPP9$^{S729A/S729A}$ kidney and both WT and DPP9$^{S729A/S729A}$ kidney (Figure 4.4A and D) histology showed small compact glomeruli and loosely arranged stroma as expected in the cortical region.

Both WT and DPP9$^{S729A/S729A}$ liver (Figure 4.4B and E) display normal neonate liver histology, with large numbers of hematopoietic cells present and evidence of developing hepatocyte chords. No abnormalities were observed.

The cortex of the thymus (Figure 4.4C and F) shows large numbers of intensely staining nuclei of developing T-cells, with the dense accumulation of cells giving a highly basophilic appearance in H & E stained sections. This was consistent with published

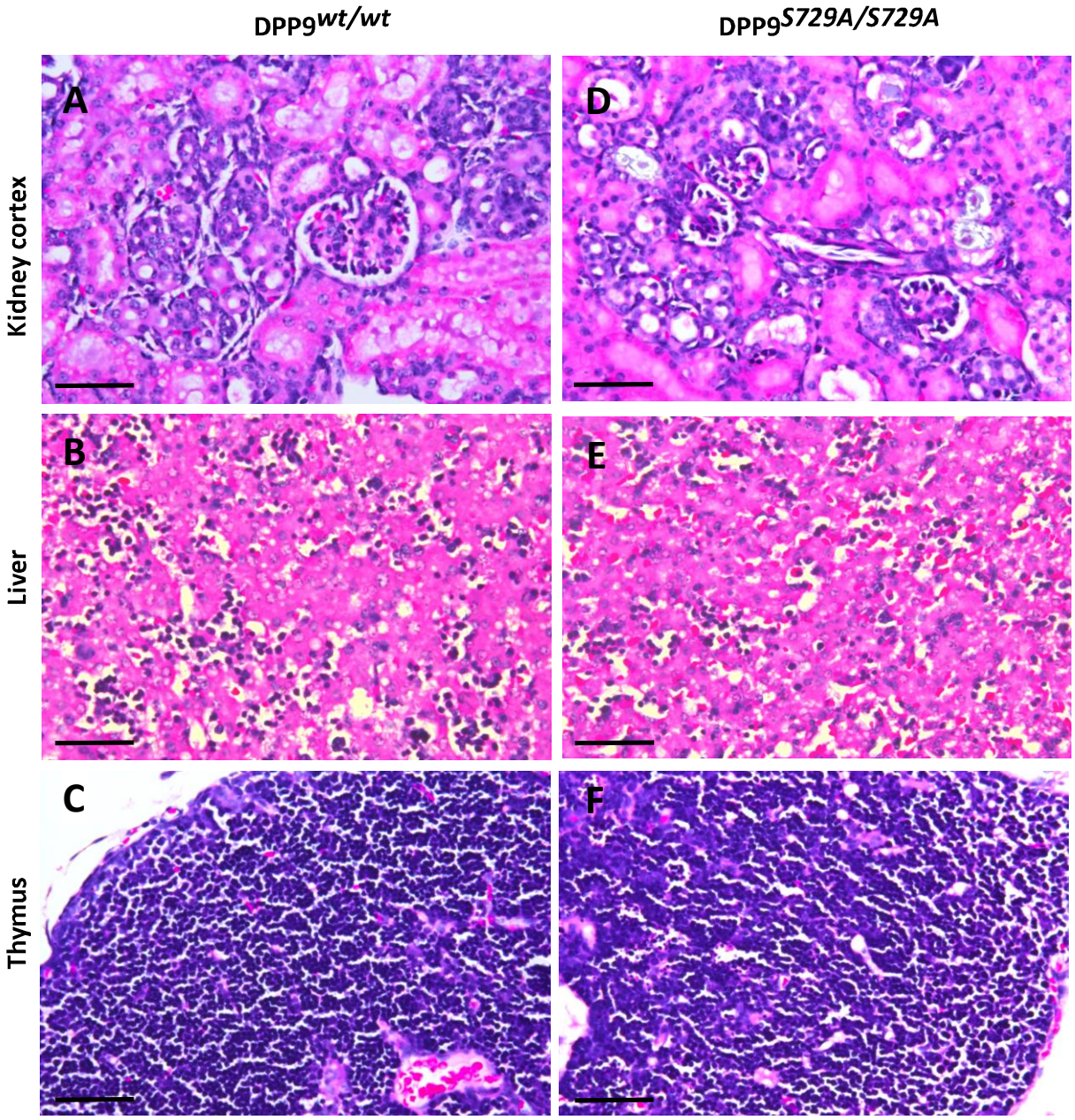

.

Figure 4.4: Histology of early neonate tissues is comparable between genotypes.

Neonate kidney cortex (A and D), liver (B and E) and thymus (C and F) DPP9$^{wt/wt}$ tissue compared to DPP9$^{S729A/S729A}$ tissue show no differences in histological structure. Haematoxylin and eosin stained. Scale bar 50 µm.

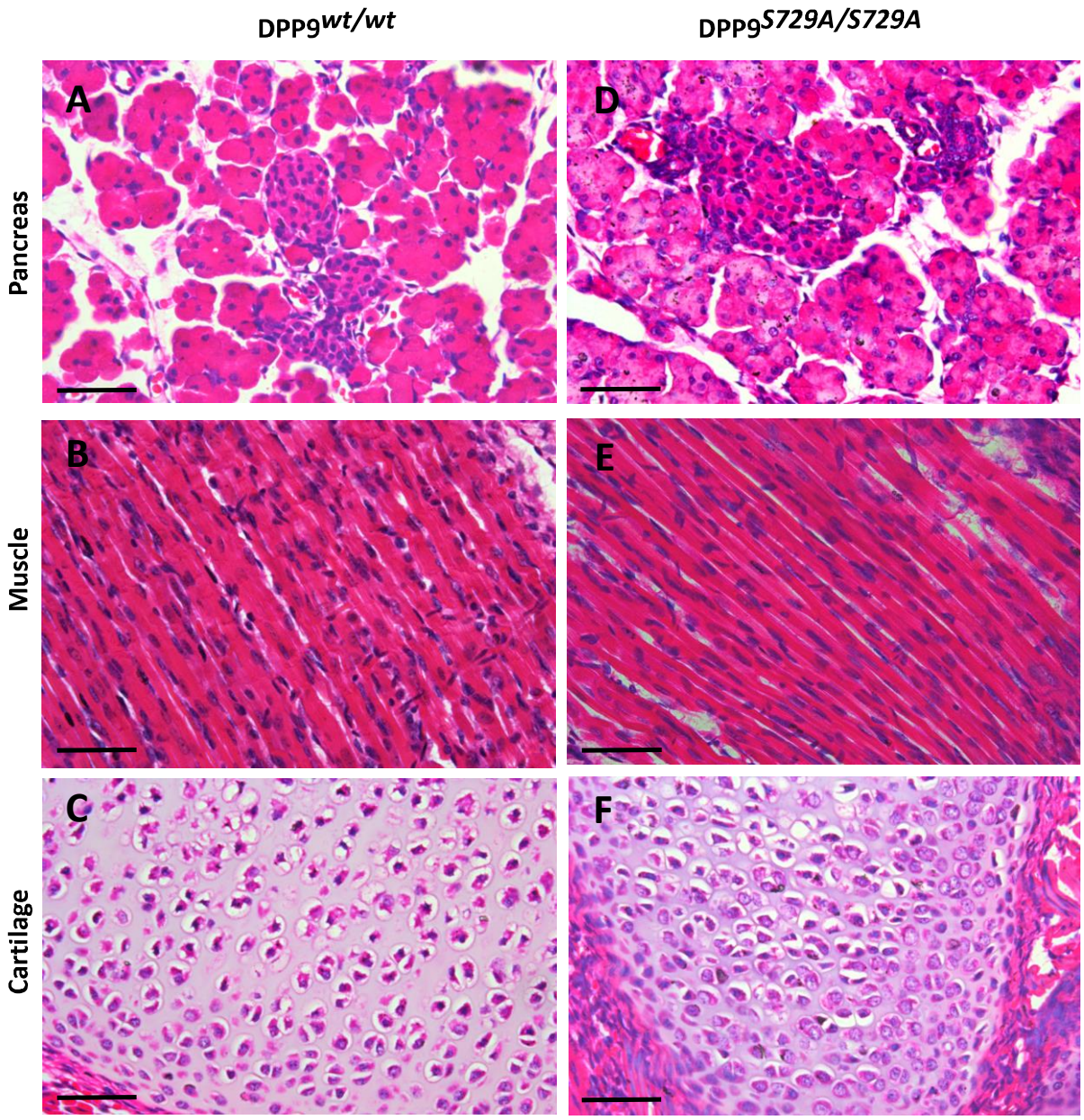

Figure 4.5: Histology of early neonate tissue is comparable between genotypes.

Neonate pancreas (A and D), thigh muscle (B and E) and rib cartilage (C and F) DPP9$^{wt/wt}$ tissue compared to DPP9$^{S729A/S729A}$ tissue show no differences in histological structure. Haematoxylin and eosin stained. Scale bar 50 µm.

data (Theiler, 1989) and no differences can be seen between WT or DPP9$^{S729A/S729A}$ thymus.

Both endocrine and exocrine pancreatic components are visible in WT and DPP9$^{S729A/S729A}$ pancreas (Figure 4.5A and D) with the presence of accumulations of endocrine cells making up the islets of Langerhans and intervening exocrine acinar cells. No differences or abnormalities could be detected in either tissue type.

Skeletal muscle cells in longitudinal section (Figure 4.5B and E) show multiple nuclei within fibres and capillaries and connective tissue of the endomysium between fibres. Both WT and DPP9$^{S729A/S729A}$ muscle fibres show normal histology.

Cartilage (Figure 4.5C and F) of both WT and DPP9$^{S729A/S729A}$ mice display a normal homogeneous amorphous matrix with basophilic staining and chondrocytes are clearly visible in lacunae. The matrix is avascular and associated connective tissue appears normal. There are no observed differences between genotypes in cartilage.

4.2.2.4 Discussion

This study investigated the possibility of histological defects or differences between WT and DPP9$^{S729A/S729A}$ mouse tissues. The presence of defects can be an indicator of organ dysfunction which could contribute to early neonate death. The organs chosen for presentation in this section of the thesis covered those not previously discussed in detail (in Chapter 3 or Chapter 4 Section 4.2.1) which are considered

important for neonate survival in the first 12-24 hours after birth (Turgeon and Meloche, 2009). The timing of death is consistent with this group's DPP9 enzyme inactive mice which died within 12 hours of birth (Chapter 3 of this thesis) (Gall et al., 2013).

In comparing the WT and DPP9$^{S729A/S729A}$ neonate mouse organs of kidney, liver, thymus, pancreas, skeletal muscle and cartilage, no differences could be found. The appearance of all tissue types examined was consistent with published works. This confirmed previous findings (Chapter 3 of this thesis) and suggested that the cause of neonate death in the DPP9 enzyme activity-deficient mice may be due to other factors rather than abnormal organ structure or histology.

4.3 Autophagy

4.3.1 Introduction

Autophagy in mammals is a critical process whereby cytoplasmic elements are broken down to remove damaged proteins and organelles and re-use essential molecules, such as amino acids (Figure 4.6). The mechanism required to achieve this is by the internalisation of these components into autophagosomes which then fuse with lysosomes to enable proteolytic digestion of the contents. It is important for both cell homeostasis and the growth and development of organisms (Levine and Kroemer,

2008). The impairment or activation of autophagy can result in disease state pathogenesis, including inflammatory disorders and neurodegenerative disease such as Crohn's disease and Parkinson's disease respectively (Mizushima and Komatsu, 2011).

Autophagy post-partum is involved in the immediate supply of energy, tissue remodelling and metabolic changes. Directly after birth, neonates face a period of starvation during the transition from maternal nutrient supply until their metabolic requirements can be met through milk nutrients. Since the mechanisms of glucose production via gluconeogenesis are not yet entirely established in the neonate, a transient period of hypoglycemia exists (Kotoulas et al., 2006). Studies in young and adult mice have shown starvation induces autophagy in most organs but this process is regulated differently in different organs (Mizushima et al., 2004, Levine and Klionsky, 2004). The role of autophagy in neonatal tissues, however, is not solely to overcome starvation and, thus, displays different tissue patterns and effects than in older animals (Schiaffino et al., 2008).

The level of autophagy is low during embryogenesis but, after birth, induction is immediate in many tissues and reaches its maximum threshold in three to six hours. This upregulation of autophagy is maintained for up to 12 hours and is critical for early neonate survival. As such, mutations that interfere with normal autophagic processes result in neonate lethal phenotypes (Turgeon and Meloche, 2009).

Autophagy-related (*ATG*) genes, originally identified in yeasts, are conserved in higher eukaryotes and required for autophagosome formation. A study using transgenic mice,

in which autophagosomes were labelled with GFP-microtubule-associated protein light chain 3 (GFP-LC3), has shown that autophagy is extensively induced in neonate mice directly after birth, especially in heart muscle, diaphragm, alveolar cells and skin (Kuma et al., 2004). Mice deficient in Atg5, a protein necessary for autophagosome formation, die within one day of birth. This is believed to be due to the essential role of autophagy for supply of energy during the early starvation period. This result, however, was confounded by the fact that the Atg5 deficient neonates also display a suckling defect (Kuma et al., 2004).

Mice deficient in another ATG family protein, Atg7, also display a neonate lethal phenotype. In Atg7-deficient neonates, plasma amino acid concentrations are lower than in WT neonates, which causes lower nutrient supply (Komatsu et al., 2005). More recently, the RagA-D family GTPases, which enable the mTORC1 pathway to sense amino acids, have been shown to have a key role in nutrient homeostasis and autophagy induction in neonates by signaling glucose and amino acid concentrations to mTORC1 (Efeyan et al., 2013). Mice with constitutive RagA activity prevent mTORC1 inhibition which leads to defective autophagy.

In this study, immunohistochemical and protein analysis of autophagy in mouse neonate tissues was undertaken as represented by autophagosome formation detection. MAP1LC3 (microtubule-associated protein 1 light chain 3) (LC3), a mammalian ortholog of yeast Atg8, is a protein known to contribute to major steps of autophagy and autophagosome formation. Although LC3 functions primarily in the cytoplasm, it is also abundant in the nucleus where it is thought to be the primary

source of membrane-bound LC3 (Huang and Liu, 2015). GFP-tagged LC3 has also been shown to bind to the smooth endoplasmic reticulum independently of autophagy, creating an artefact for consideration in LC3 analysis (Korkhov, 2009). In this study, an antibody against the B isoform of LC3, which detects membrane-bound LC3-II in the

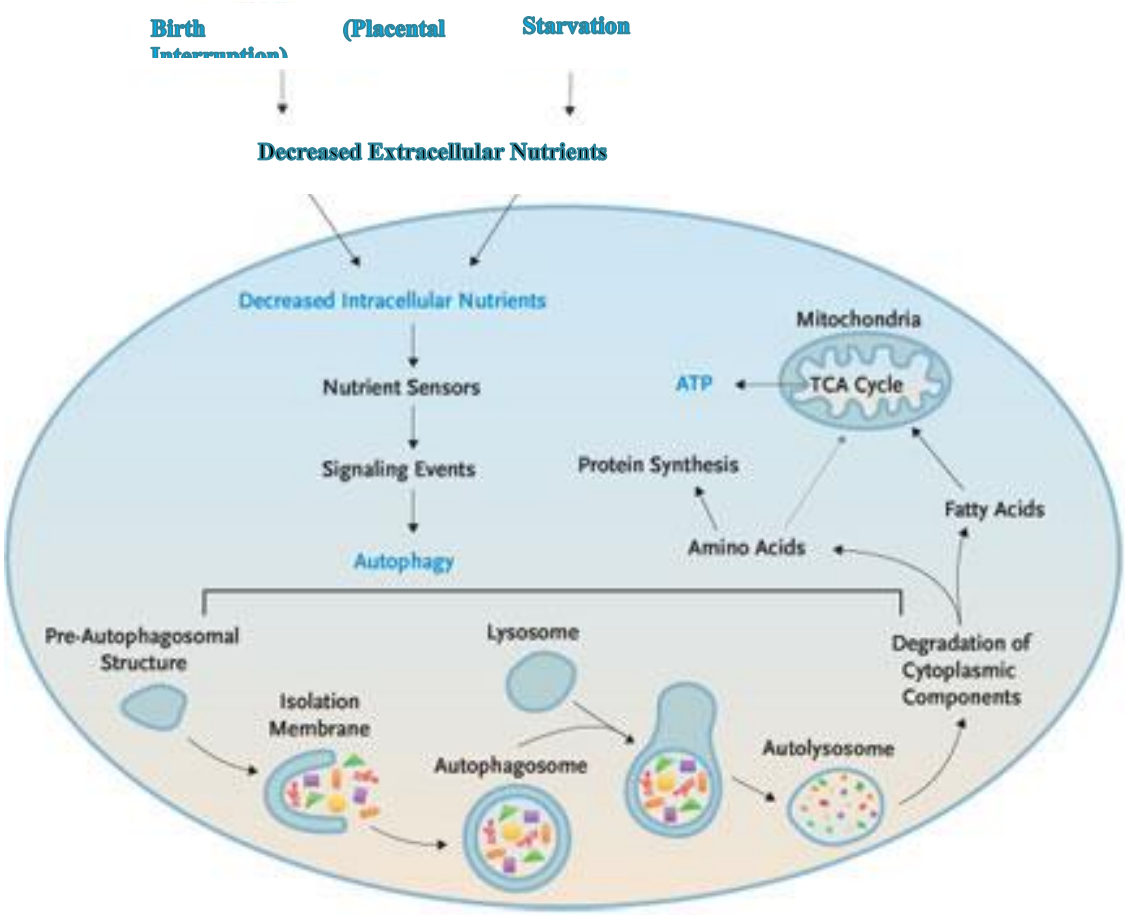

Figure 4.6: Mammalian autophagy is a cellular defence against two forms of nutrient stress, birth and starvation.

Diagrammatic representation of autophagy function in mammals showing the process of nutrient depletion and protein degradation for recycling of amino acids for protein synthesis and energy production. Modified from (Levine, 2005).

autophagic vacuole fraction, was used to identify the LC3 protein localisation. The aim of this study was to determine if autophagy dysfunction occurs and, thus, could contribute to the lethal phenotype of the DPP9-GKI mouse.

4.3.2 Methods

4.3.2.1 Immunohistochemical studies

Neonate mouse organs were isolated and sectioned using methods described in Section 3.2.2.4. To immunolocalise LC3B protein as a marker for autophagy, the polyclonal anti-LC3B antibody (GeneTex; Irvine, CA, #GTX127375, 1:100) was used which bound to the autophagosome membrane proteins. Briefly, 5 µm sections were deparaffinised and rehydrated and then a pressure cooker and Universal Decloaker solution (Biocare Medical, Concord, CA) was used to retrieve antigen. Endogenous peroxidase activity was quenched with 3% H_2O_2 in PBS for 10 mins followed by thorough rinsing in water. Sections were then covered with Background Sniper (Biocare Medical) for 10 mins, rinsed in PBS and incubated at room temperature for 1 h in primary antibody with 1% BSA in PBS and Renaissance Background Reducing Diluent (Biocare Medical). Control sections were treated with rabbit Ig or water in place of primary antbody. After thorough washing in PBS, sections were incubated for 30 mins with goat anti-rabbit conjugated to HRP (Dako, Glostrup, Denmark, #P0448, 1:100), washed and then stained in 3,3-diaminobenzidine (DAB) with H_2O_2. Sections were counterstained in Harris haematoxylin (Sigma-Aldrich, St Louis, MO), rinsed in running water and blued in freshly made Scott's tap water substitute for 2 mins before dehydration through successive increasing percent alcohols to histolene and mounting

with Eukitt (Sigma-Aldrich). Bright-field imaging was performed using a Leica DM6000B microscope.

In all tissues, intensity readings (*r*) of LC3B staining levels were calculated from 25 measurements taken from 5 different tissue sections containing 5 regions of interest of fixed area in ImageJ software (Schindelin et al., 2012). The tissue sections were sourced from 5 WT and 5 DPP9-GKI mice. The WT mouse sections were from two sets of two littermates and one single mouse and the DPP9-GKI tissue sections were from 3 littermate mice from one litter and two from another. Regions of interest (ROI) within each section were from corresponding areas of tissue. ROIs containing high levels of white background space were avoided. For lung, ImageJ thresholding tools were used to avoid staining contributed by red blood cells in alveolar spaces and thereby obtain true measurement of lung tissue staining. In all tissues, measurements were converted to reciprocal intensity (255 – *r*) to focus on areas of low intensity which indicate darker staining (Nguyen et al., 2013). All images used in IHC quantification were analysed after subtraction of background staining and removal of the colour contribution from hematoxylin by colour deconvolution in ImageJ. Data were analysed by unpaired t-test using GraphPad Prism (GraphPad, San Diego, USA) and significance was assigned to *p* values less than 0.05.

4.3.2.2 Immunoblotting studies

Neonate mice were euthanised by decapitation within six hours of birth and brains were harvested in 2 mL screwcap tubes (Astral Scientific, NSW, Australia) for snap freezing in liquid nitrogen and storage at -70˚C. Samples were prepared as detailed in

Section 2.2.4.2 of Materials and Methods. Briefly, for immunoblot sample preparation, frozen neonate mouse brain samples were homogenised in lysis buffer using a bead-based homogeniser (TissueLyser, Qiagen Venlo, Netherlands) at 4^0C. Protein concentration was determined using the Micro BCA Protein Assay Kit (Thermo Scientific, Waltham, Massachusetts, USA) following the manufacturer's protocol.

Brain lysates from DPP9$^{S729A/S729A}$ (n=5) and WT (n=5) littermate mice sourced from three litters were used for immunoblotting. Lysates (30 µg protein per lane) were resolved on 4–12% Bis-Tris SDS-PAGE (Invitrogen) followed by immunoblotting with anti-LC3B antibody (GeneTex; #GTX127375, 1:4000), anti-DPP9 (OriGene, #TA503937, 1:6000) and anti-β-Actin (Sigma-Aldrich, #A2103, 1:6000). Relative band intensities were quantitatively analysed using ImageJ and normalised against control proteins as indicated.

4.3.3 Results

4.3.3.1 Immunohistochemical studies

Immunohistochemistry, where an antibody specific to LC3B was used as an autophagy marker (Lee et al., 2014, Hung et al., 2015), showed strong immune-positivity on both WT and DPP9$^{S729A/S729A}$ samples. Autophagy is upregulated in most tissues directly after birth in the early neonatal period (Kuma et al., 2004).

In heart muscle (Figure 4.7 A and B), LC3B immunoreactivity was observed in the cardiomyocytes with staining of the muscle fibres and intense staining of nuclei in both the WT and DPP9$^{S729A/S729A}$ samples. Staining was significantly stronger, however, in the DPP9$^{S729A/S729A}$ heart muscle nuclei. In lung, staining was most prominent in the

alveolar sacs with alveolar cell nuclei showing strong staining (Figure 4.7 C and D). As with the heart muscle, the DPP9$^{S729A/S729A}$ sample showed significantly more staining than the WT suggesting and upregulation of autophagy in these GKI tissues.

Gut (Figures 4.8 A and B) showed greater staining intensity in the epithelial layer than in the lamina propria for both samples. In the gut epithelium, nuclei of enterocytes and goblet cells stained strongly, with the most intense staining seen in the regions of proliferating cells at the bottom of intestinal crypts. LC3B immunoreactivity was significantly higher and staining more intense in nucleus than cytoplasm in the DPP9$^{S729A/S729A}$ samples than in the WT samples. Liver (Figures 4.8 C and D) showed diffuse low level staining throughout with stronger staining of nuclei in some hepatocytes. While the down-regulation of staining in the DPP9$^{S729A/S729A}$ samples compared to the WT was slight but significant, the pattern of staining appeared different. In the WT samples, nuclear LC3B immunoreactivity encompassed the entire nucleus in positive hepatocytes, whereas the GKI samples showed perinuclear staining of many hepatocyte nuclei.

Figure 4.7: LC3B immunohistochemistry in mouse early neonate heart muscle and lung

Paraffin sections of tissues were stained with anti-LC3B antibody and DAB chromogen and counterstained with hematoxylin. In heart muscle (**A** and **B**), LC3B was detected in cardiomyocytes with strong nuclear staining (arrows). In lung (**C** and **D**), LC3B was detected in alveolar cells (arrows) of the lung parenchyma. Upper right insets show staining for secondary antibody only controls (**A** and **C**) and isotype controls (**B** and **D**). Scale bar 50µm. The reciprocal intensity of positive immunoreactivity was calculated in random tissue section areas from DPP9$^{wt/wt}$ (n=5) and DPP9$^{S729A/S729A}$ (n=5) neonate mice (**E**). Horizontal bars (red) are means and error bars depict SD. Significance was assigned where $p < 0.05$ (*), $p < 0.01$ (**), $p < 0.001$ (***). Abbreviations: a.u., arbitrary units.

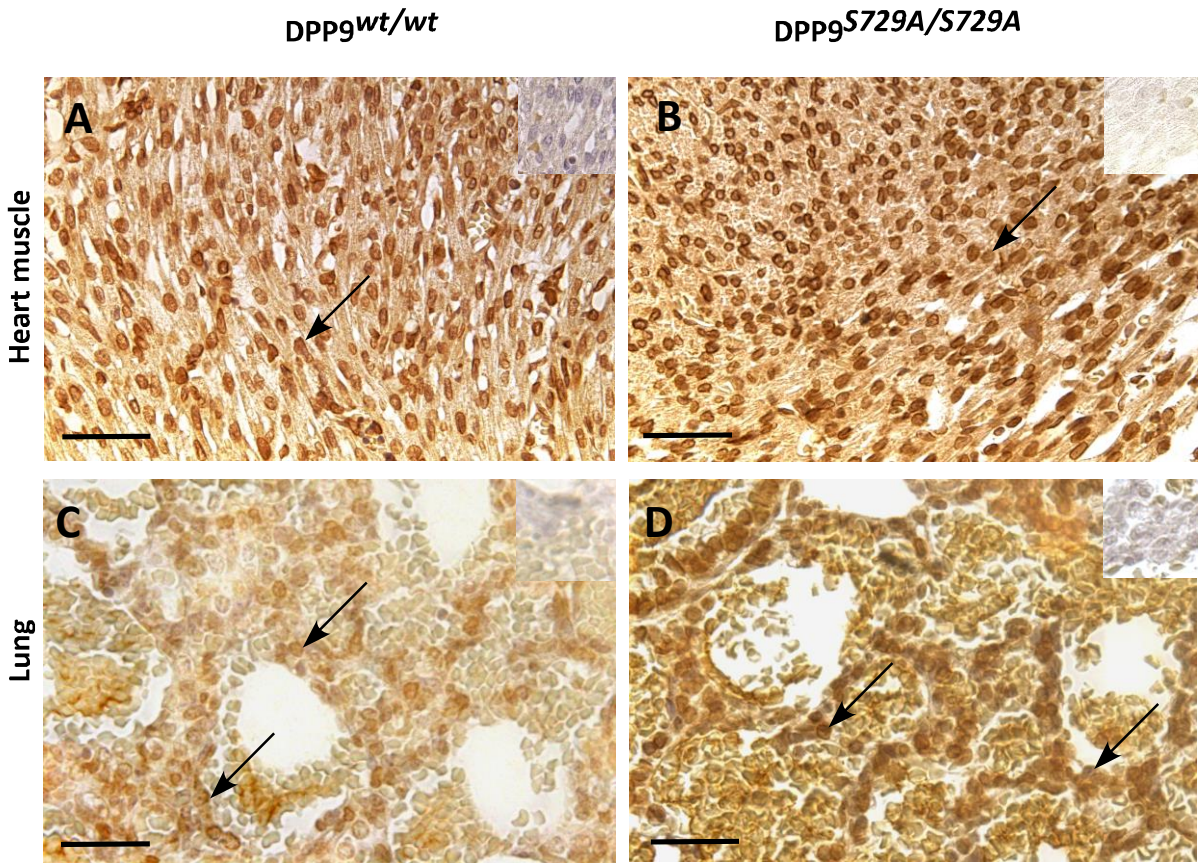
DPP9wt/wt
DPP9S729A/S729A
Heart muscle
Lung
A
B
C
D

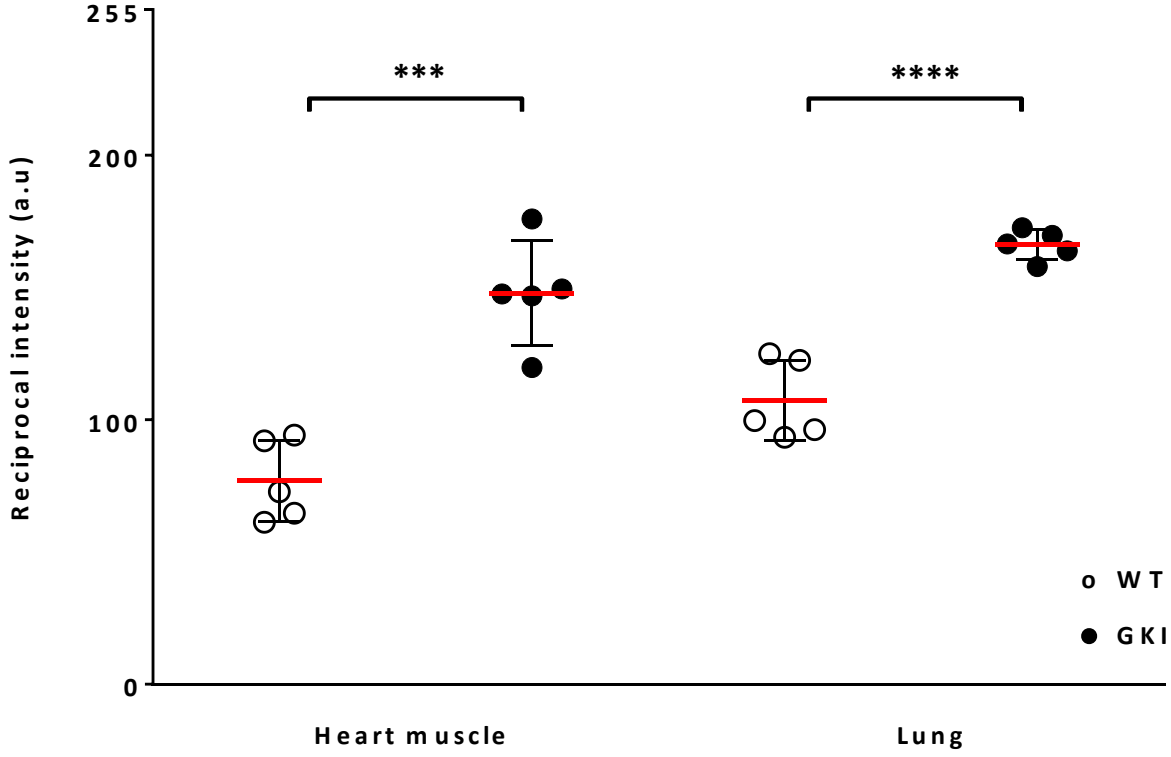
255
200
100
0
Reciprocal intensity (a.u)
***
****
o WT
GKI
Heart muscle
Lung

The area of the brain shown (Figure 4.9 A and B) and used for quantification was the thalamic region of the diencephalon as classified by Lee et al. in mouse neonate brain (Lee et al., 2005). This region was the only area consistently present in all mouse sections and so was used for analysis. Staining was strongest in the nuclei of neurons but also present less intensely in the nuclei of glial cells. There was a significant down-regulation of LC3B immunoreactivity in the DPP9$^{S729A/S729A}$ samples compared to the WT samples. In the spinal cord (Figure 4.9 C and D), however, no significant difference was observed between samples. Staining was observed in the perinuclear region of the glial cell nuclei and also in the dendritic branches of neurons for both tissue samples.

Figure 4.8: LC3B immunohistochemistry in mouse early neonate gut and liver

Paraffin sections of tissues were stained with anti-LC3B antibody and DAB chromogen and counterstained with hematoxylin. In gut (**A** and **B**), LC3B was detected in epithelium with strong staining of the nuclei of enterocytes and goblet cells (arrows). In liver (**C** and **D**), LC3B was diffuse with strong staining of the nuclei of some hepatocytes (arrows). Upper right insets show staining for secondary antibody only controls (**A** and **C**) and isotype controls (**B** and **D**). Scale bar 50µm. The reciprocal intensity of positive immunoreactivity was calculated in random tissue section areas from DPP9$^{wt/wt}$ (n=5) and DPP9$^{S729A/S729A}$ (n=5) neonate mice (**E**). Horizontal bars (red) are means and error bars depict SD. Significance was assigned where $p < 0.05$ (*), $p < 0.01$ (**), $p < 0.001$ (***). Abbreviations: a.u., arbitrary units.

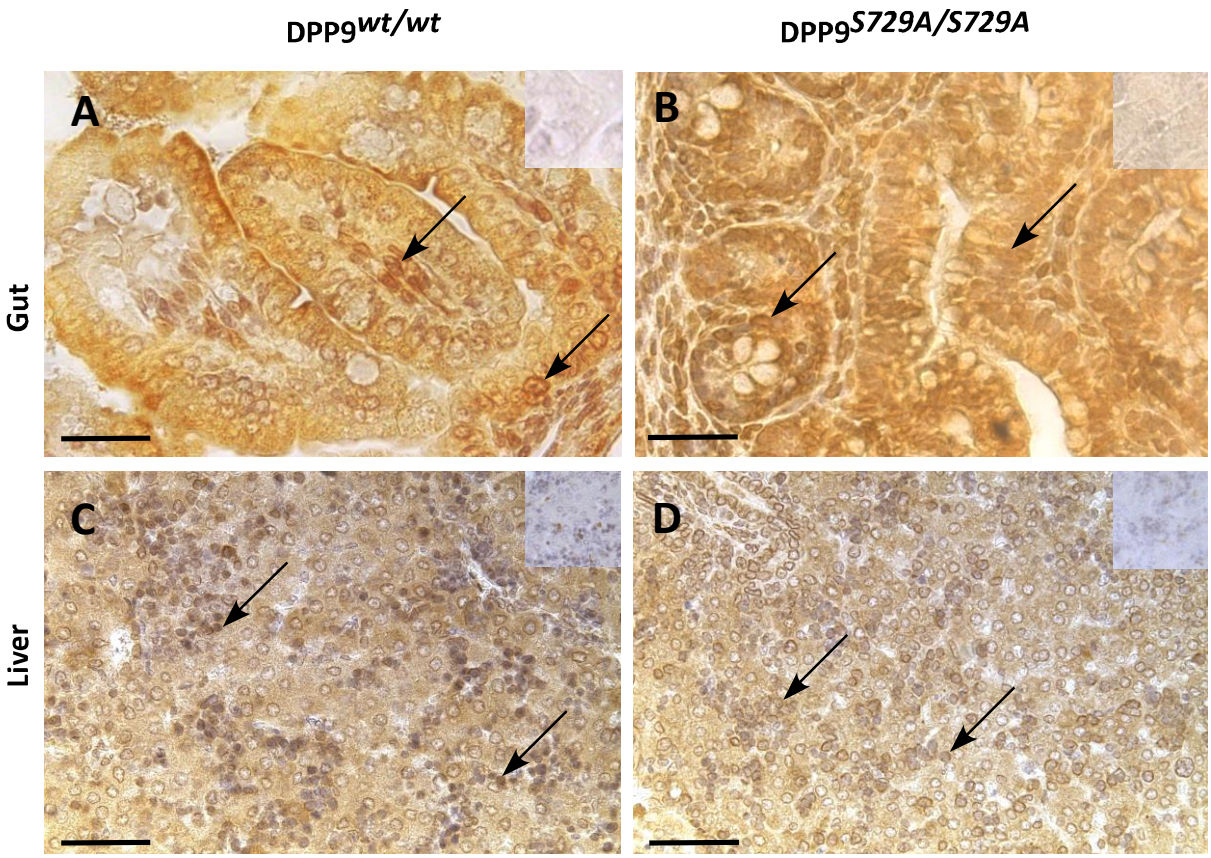
DPP9wt/wt
DPP9S729A/S729A
A
B
C
D
Gut
Liver

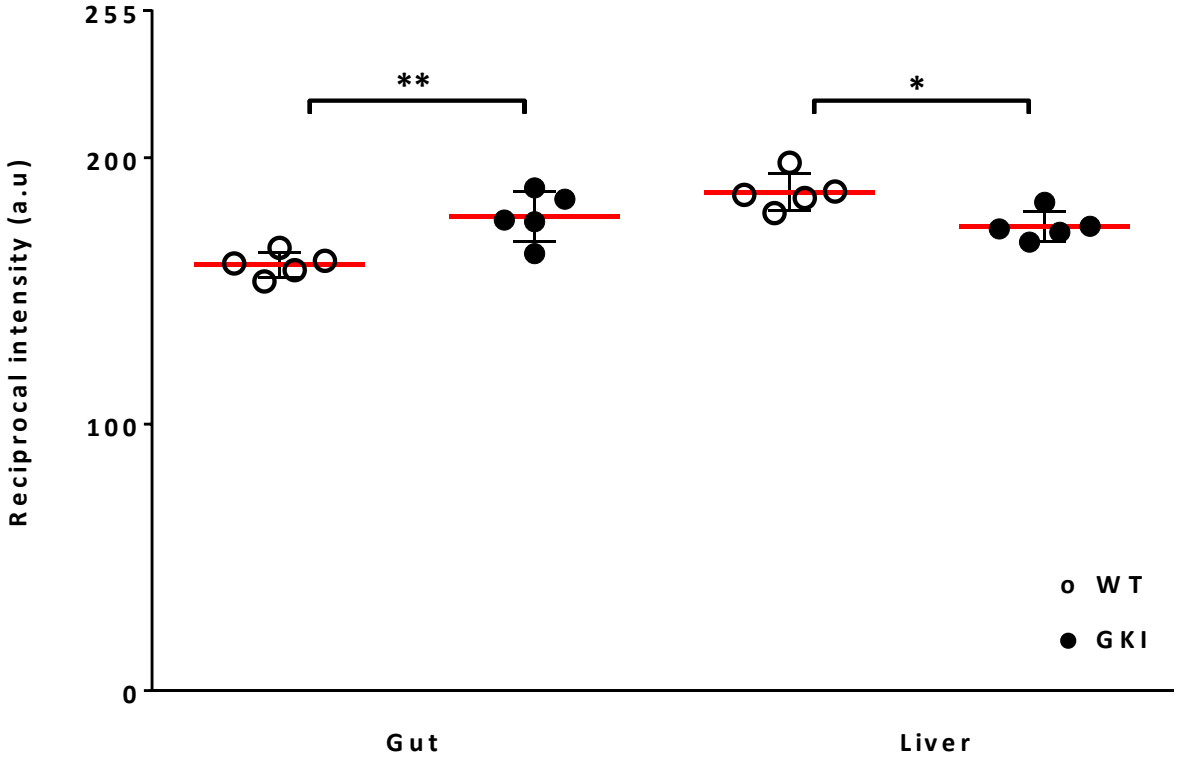
255
200
100
0
Reciprocal intensity (a.u)
**
*
WT
GKI
Gut
Liver

Neonate kidney (Figure 4.10 A and B) of both the DPP9$^{S729A/S729A}$ and WT mice showed diffuse staining in the distal tubules with more intense staining in the connecting tubules and glomeruli and no significant difference in overall staining intensity observed. The adrenal gland (Figure 4.10 C and D) had diffuse staining throughout with the presence of many dark granules in the DPP9$^{S729A/S729A}$ samples and very few visible in the WT. As the adrenal gland is the organ where catecholamine production is undertaken, these are probably storage granules of secretory cells.

Very low levels of LC3B immunoreactivity were observed in all samples in skeletal muscle (Figure 4.11 A and B) and skin (Figure 4.11 C and D) although some staining of the hair follicle was apparent. Both pancreas (Figure 4.12 A and B) and thymus (Figure 4.12 C and D) showed strong overall staining in both the WT and DPP9$^{S729A/S729A}$ samples. The pancreas showed stronger staining of acinar cell nuclei than cytoplasm. The islet cell cytoplasm stained less intensely than the acinar cell cytoplasm, however, their nuclei were as immunoreactive as the acinar cell nuclei. The thymus showed strong staining in both neonate genotypes, which was apparent in the reticulocytes and lymphocytes.

With respect to the quantification of staining intensity in tissue samples, heart muscle, lung, brain, gut and liver showed significant differences in LC3B staining between WT and DPP9$^{S729A/S729A}$ samples. Staining of LC3B in heart muscle, lung and gut was more intense in DPP9$^{S729A/S729A}$ samples compared to WT (Figures 4.7 E and 4.8 E) suggesting increased levels of autophagy in those organs in DPP9$^{S729A/S729A}$ neonates, whereas liver and brain showed less staining in the DPP9$^{S729A/S729A}$ samples (Figures 4.8 E and

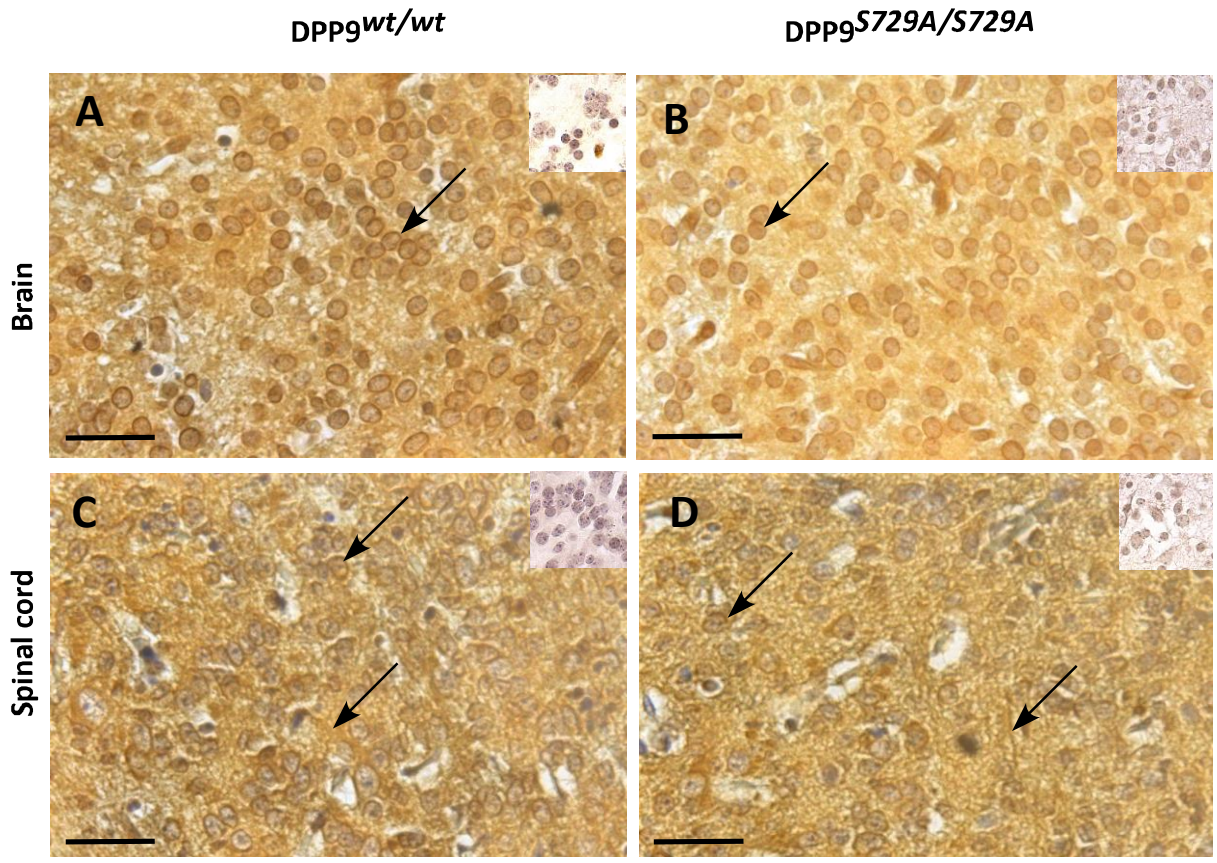
DPP9wt/wt
DPP9S729A/S729A
A
B
C
D
Brain
Spinal cord

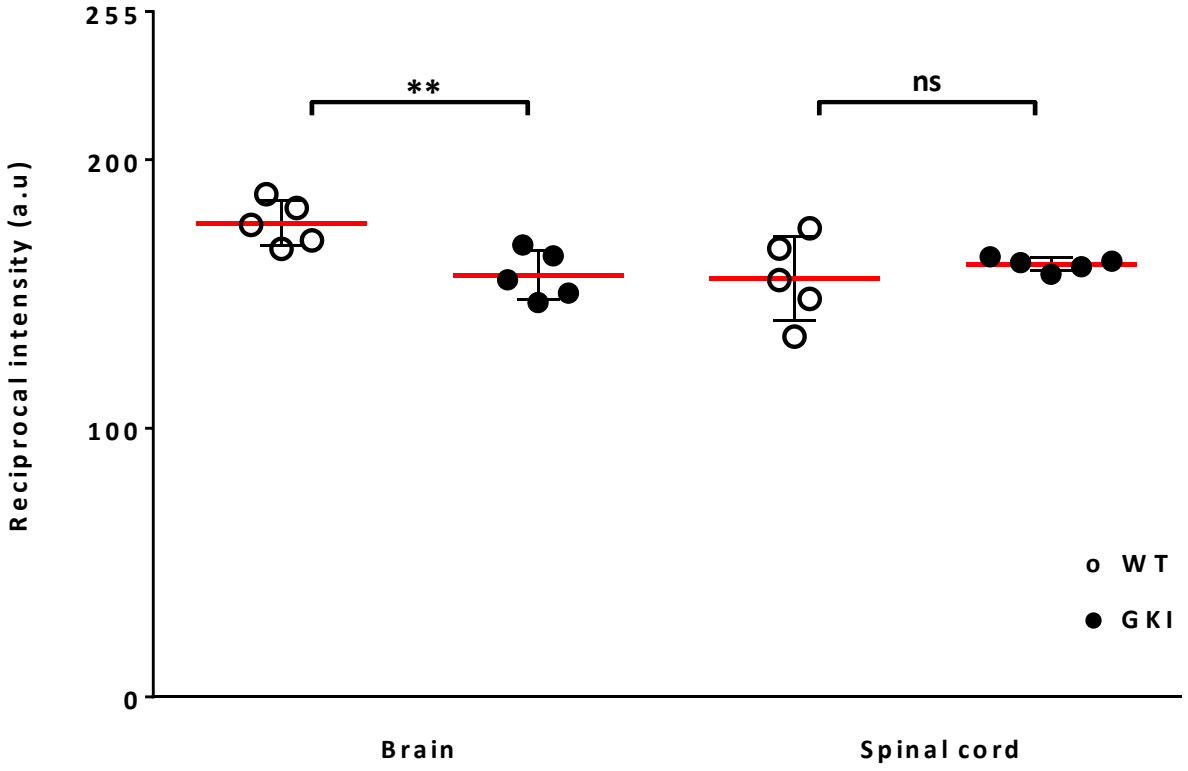
255
200
100
0
Reciprocal intensity (a.u)
**
ns
o WT
GKI
Brain
Spinal cord

Figure 4.9: LC3B immunohistochemistry in mouse early neonate brain and spinal cord

Paraffin sections of tissues were stained with anti-LC3B antibody and DAB chromogen and counterstained with hematoxylin. In brain (**A** and **B**), LC3B was strongly detected in the nuclei of neurons (arrows). In spinal cord (**C** and **D**), LC3B was present in the dendritic branches of neurons and glial cells (arrows). Upper right insets show staining for secondary antibody only controls (**A** and **C**) and isotype controls (**B** and **D**). Scale bar 50µm. The reciprocal intensity of positive immunoreactivity was calculated in random tissue section areas from DPP9$^{wt/wt}$ (n=5) and DPP9$^{S729A/S729A}$ (n=5) neonate mice (**E**). Horizontal bars (red) are means and error bars depict SD. Significance was assigned where $p < 0.05$ (*), $p < 0.01$ (**), $p < 0.001$ (***). Abbreviations: a.u., arbitrary units; ns, no significance.

Figure 4.10: LC3B immunohistochemistry in mouse early neonate kidney and adrenal gland

Paraffin sections of tissues were stained with anti-LC3B antibody and DAB chromogen and counterstained with hematoxylin. In kidney (**A** and **B**), LC3B was detected at low levels in the distal tubules (red arrows) and more intensely in the connecting tubules and glomeruli (blue arrows). In adrenal gland (**C** and **D**), LC3B was present in secretory cell nuclei (black arrows) and structures that are probably storage granules (green arrows). Upper right insets show staining for secondary antibody only controls (**A** and **C**) and isotype controls (**B** and **D**). Scale bar 50µm. The reciprocal intensity of positive immunoreactivity was calculated in random tissue section areas from DPP9$^{wt/wt}$ (n=5) and DPP9$^{S729A/S729A}$ (n=5) neonate mice (**E**). Horizontal bars (red) are means and error bars depict SD. Abbreviations: a.u., arbitrary units; ns, no significance.

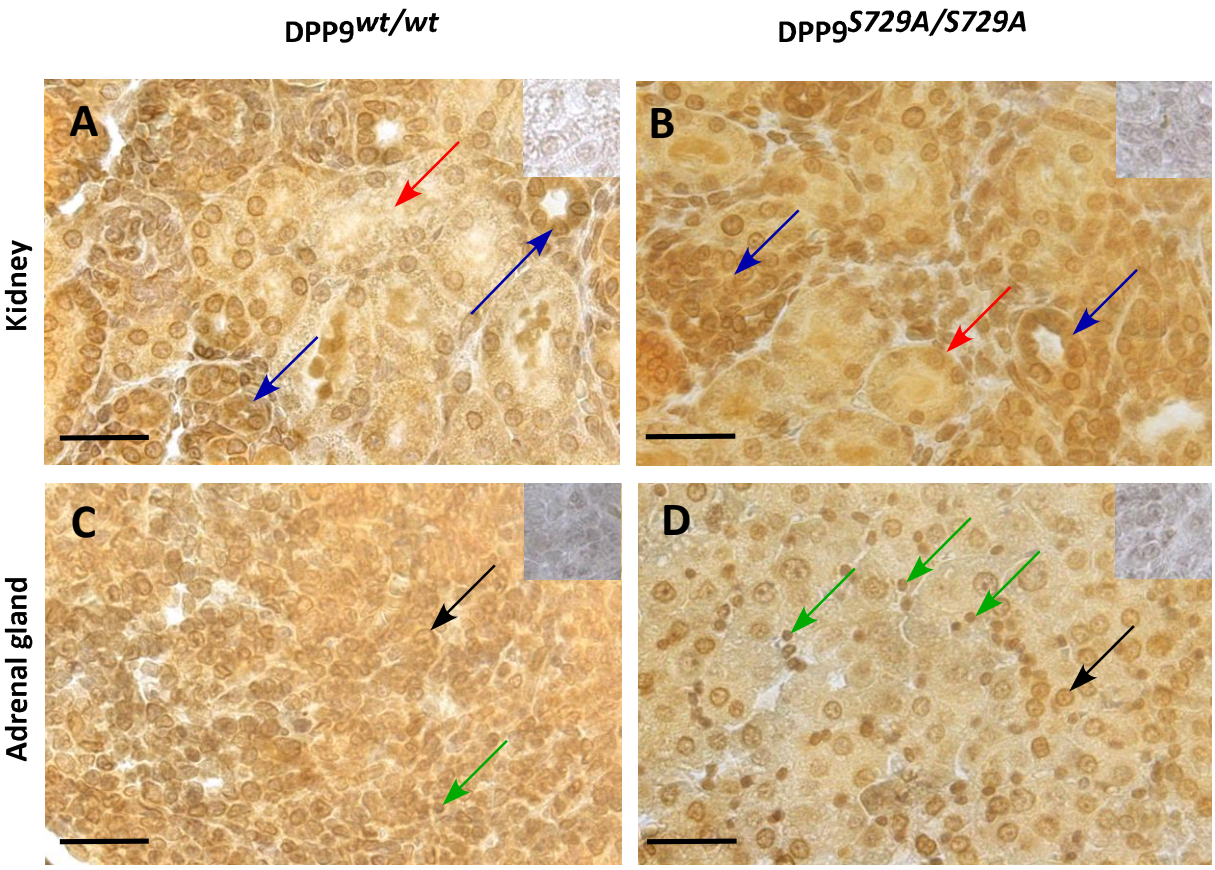
DPP9wt/wt
DPP9S729A/S729A
A
B
C
D
Kidney
Adrenal gland

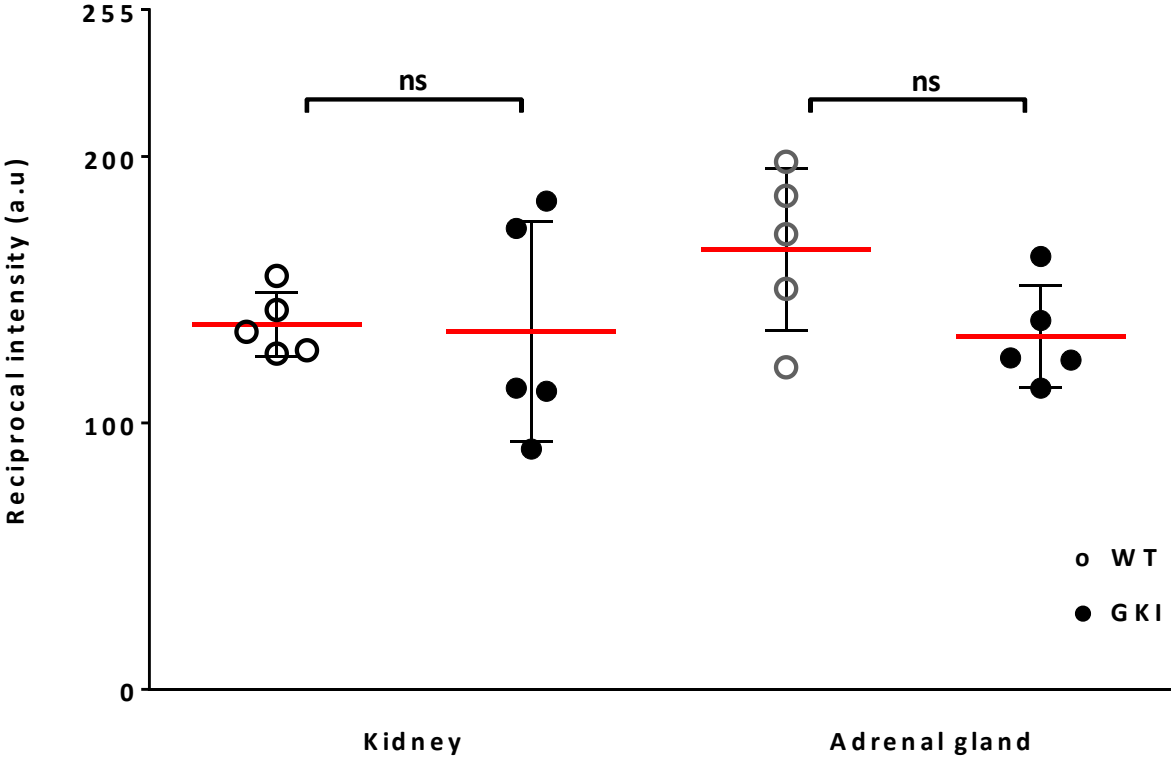
255
200
100
0
Reciprocal intensity (a.u)
ns
ns
o WT
GKI
Kidney
Adrenal gland

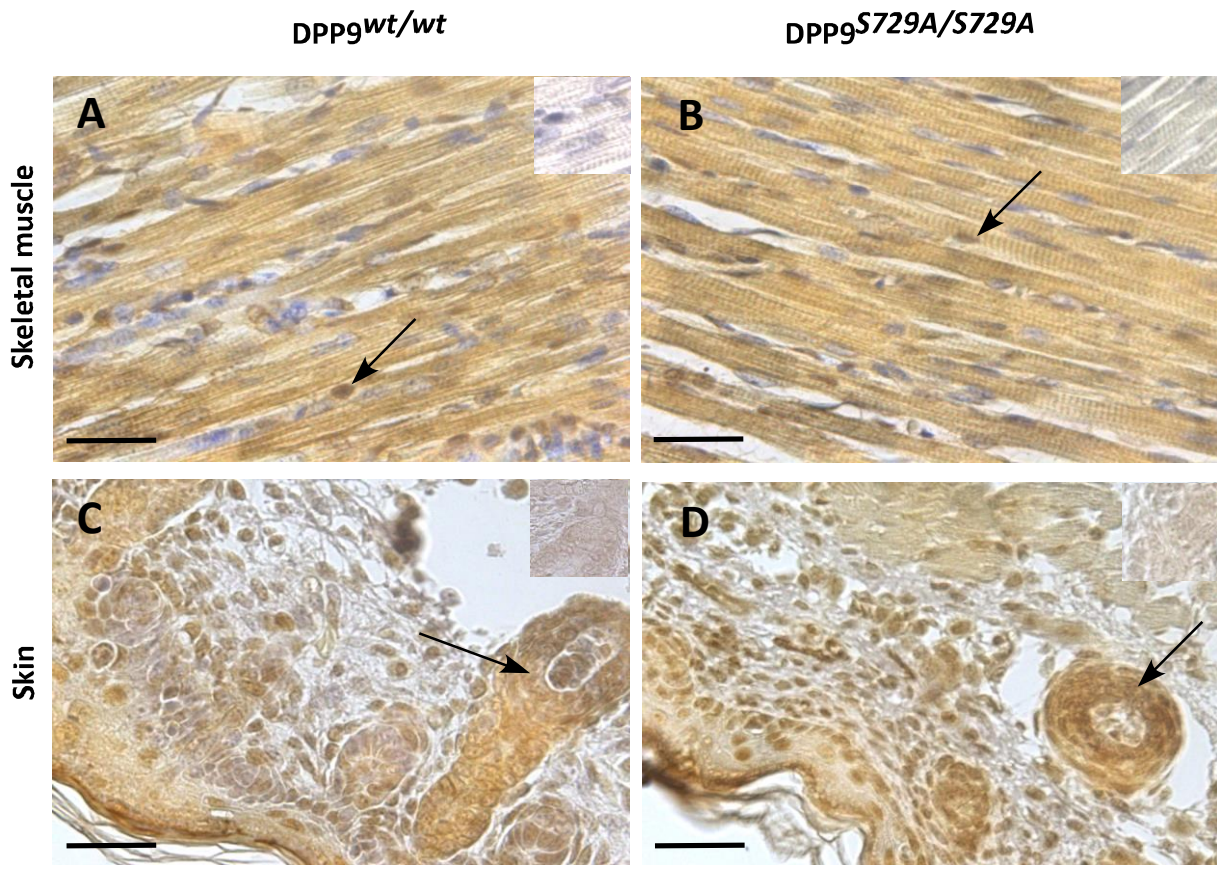
DPP9wt/wt
DPP9S729A/S729A
Skeletal muscle
Skin
A
B
C
D

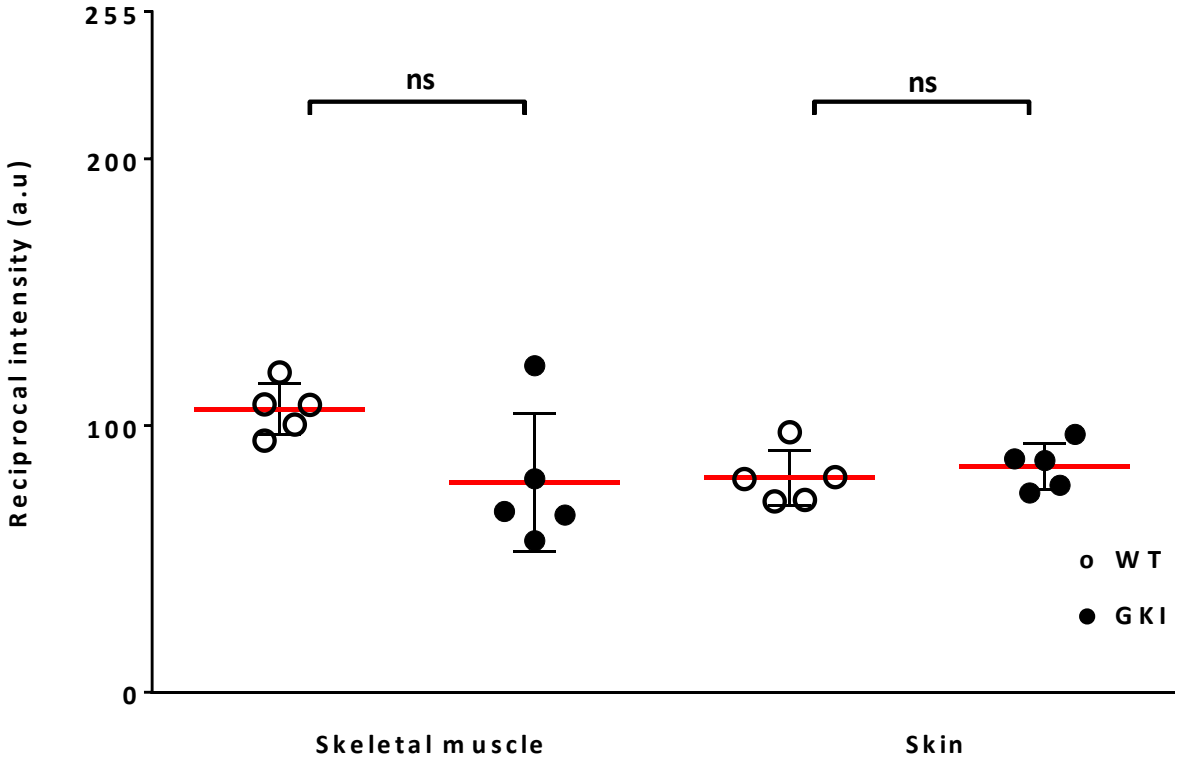
255
200
100
0
Reciprocal intensity (a.u)
ns
ns
o WT
GKI
Skeletal muscle
Skin

Figure 4.11: LC3B immunohistochemistry in mouse early neonate skeletal muscle and skin

Paraffin sections of tissues were stained with anti-LC3B antibody and DAB chromogen and counterstained with hematoxylin. In skeletal muscle (**A** and **B**), LC3B was detected at low levels with some stronger staining in muscle cell nuclei visible (arrows). In skin (**C** and **D**), LC3B was most intense in the hair follicles (arrows). Upper right insets show staining for secondary antibody only controls (**A** and **C**) and isotype controls (**B** and **D**). Scale bar 50µm. The reciprocal intensity of positive immunoreactivity was calculated in random tissue section areas from DPP9$^{wt/wt}$ (n=5) and DPP9$^{S729A/S729A}$ (n=5) neonate mice (**E**). Horizontal bars (red) are means and error bars depict SD. Abbreviations: a.u., arbitrary units; ns, no

---

Figure 4.12: LC3B immunohistochemistry in mouse early neonate pancreas and thymus

Paraffin sections of tissues were stained with anti-LC3B antibody and DAB chromogen and counterstained with hematoxylin. In pancreas (**A** and **B**), LC3B was detected with strong staining in acinar cells (red arrows) and less intensity in islet cells (blue arrows). In thymus (**C** and **D**), LC3B was most intense in lymphocytes (black arrows) and reticulocytes (green arrows). Upper right insets show staining for secondary antibody only controls (**A** and **C**) and isotype controls (**B** and **D**). Scale bar 50µm. The reciprocal intensity of positive immunoreactivity was calculated in random tissue section areas from DPP9$^{wt/wt}$ (n=5) and DPP9$^{S729A/S729A}$ (n=5) neonate mice (**E**). Horizontal bars (red) are means and error bars depict SD. Abbreviations: a.u., arbitrary units; ns, no significance.

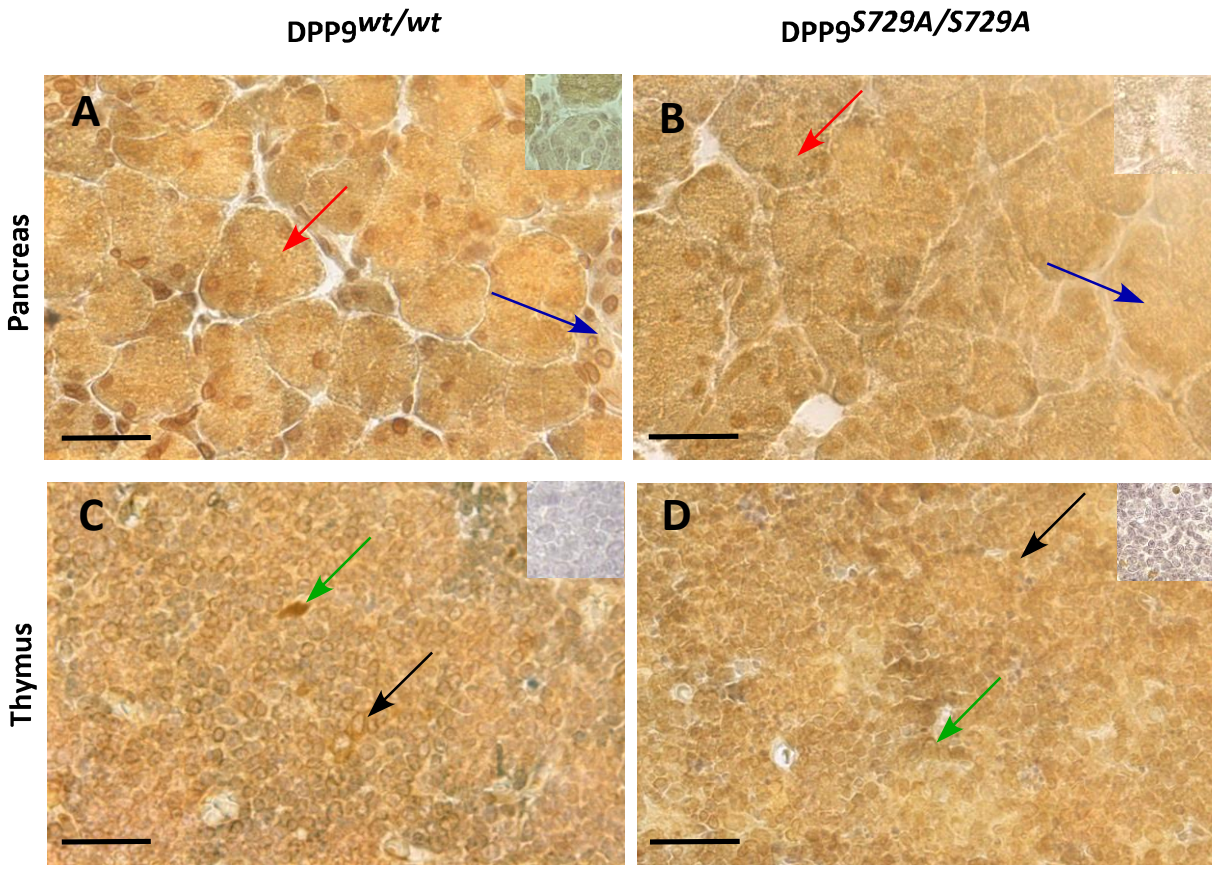
DPP9wt/wt
DPP9S729A/S729A
Pancreas
Thymus
A
B
C
D

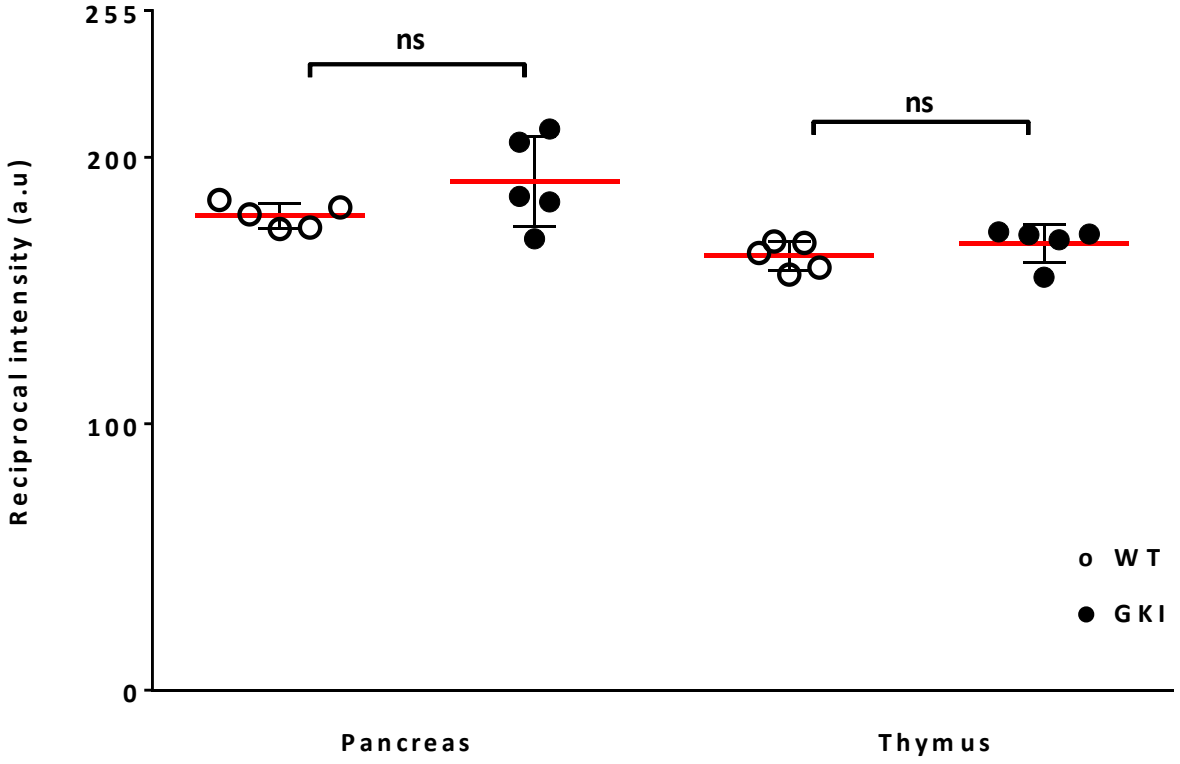
255
200
100
0
Reciprocal intensity (a.u)
ns
ns
o WT
GKI
Pancreas
Thymus

4.9 E) suggesting decreased levels of autophagy. All other tissue types, namely spinal cord (Figure 4.9 E), kidney and adrenal gland (Figure 4.10 E), skeletal muscle and skin (Figure 4.11 E) and pancreas and thymus (Figure 4.12 E) showed no significant difference between the levels of staining of WT and DPP9$^{S729A/S729A}$ tissue sections. Quantification results are summarised in Table 4.2.

Tissue type	LC3B staining levels in DPP9$^{S729A/S729A}$ tissue compared to WT	*p* value < 0.05
Heart muscle	↑	***
Lung	↑	****
Gut	↑	**
Liver	↓	*
Brain	↓	**
Spinal cord	O	ns
Kidney	O	ns
Adrenal	O	ns
Skeletal muscle	O	ns
Skin	O	ns
Pancreas	O	ns
Thymus	O	ns

Table 4.2: Summary list of staining reciprocal intensity difference with LC3B autophagy marker in DPP9$^{S729A/S729A}$ neonate tissues compared to WT.

Symbols represent:

Up-regulation of autophagy in DPP9$^{S729A/S729A}$ tissue compared to WT (↑)

Down-regulation of autophagy in DPP9$^{S729A/S729A}$ tissue compared to WT (↓)

No change of autophagy in DPP9$^{S729A/S729A}$ tissue compared to WT (O)

Abbreviation: ns, not significant

4.3.3.2 Immunoblotting studies

To verify the presence of autophagy as indicated by LC3B protein expression, neonate brain lysates of WT and DPP9$^{S729A/S729A}$ littermates were characterised for protein expression by immunoblot. Using the LC3B antibody with neonatal brain showed less

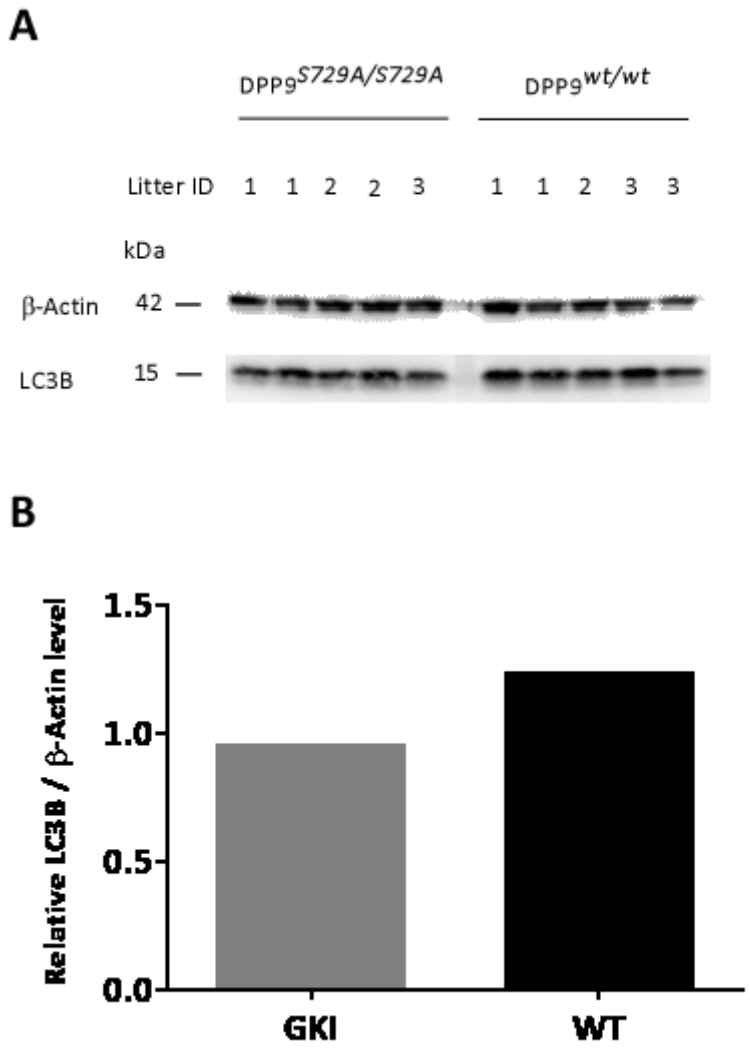

Figure 4.13: LC3B protein expression in neonate brain tissue lysates

Brain tissue lysates of littermate neonate mice (GKI n=5, WT n=5) were analysed by immunoblot (A) and densitometry analyses of LC3B normalised against β-Actin (B).

LC3B protein in the DPP9$^{S729A/S729A}$ brain lysate than the WT (Figure 4.13A). However, densitometry (Figure 4.13B) showed that this difference was not significant.

4.3.4 Discussion

The purpose of this study was to assess whether a defect in autophagy may contribute directly or indirectly to death of DPP9-GKI mice. An anti-LC3B antibody, which binds to the autophagosome membrane proteins, was used as a marker for autophagy. High levels of autophagy are expected in most neonate tissues directly after birth as the post-partum period is a time of extensive energy consumption and metabolic change. The strong immunoreactivity of LC3B detected in all neonate tissues studied supported this for both WT and DPP9$^{S729A/S729A}$ samples.

Ideally, LC3B immunohistochemical staining should clearly define autophagic vacuoles as a marker for autophagy. However, it has been suggested in a published work that there are low levels of this protein in paraffin-embedded tissue when using routine preparation techniques which may impair unambiguous detection (Martinet et al., 2013). Also problematic is the use of DAB as the chromogen for visualisation of LC3B immunoreactivity, as its macromolecular structure causes light scattering and the production of non-stoichiometric signals which can introduce errors in quantification of intensity readings (Haub and Meckel, 2015).

To overcome these problems, the observation and quantification in this chapter was done as a comparative assessment of autophagy with WT levels assumed as normal for early neonate tissue types. Although LC3 function in autophagy happens in the

cytoplasm, it is known to be abundantly distributed in the nucleus where it is the main source of membrane-conjugated LC3 on autophagosomes (Huang and Liu, 2015). In many tissue types investigated in this chapter, where strong staining was observed, the staining localisation occurred in the nuclear or perinuclear regions of cells in both WT and DPP9$^{S729A/S729A}$ samples which is consistent with published work.

Whereas significant differences in overall staining intensity were seen in heart muscle, lung, gut, liver and brain, in most cases the localisation patterns were identical. One exception was the liver, where positive perinuclear staining was seen in the DPP9$^{S729A/S729A}$ samples but throughout the entire nucleus in the positive WT nuclei. This may suggest a different interplay between the nuclear and cytoplasmic autophagy processes in the GKI neonate liver.

Also displaying staining pattern variations was the adrenal gland, where dark secretory granules could be seen prominently in the DPP9$^{S729A/S729A}$ samples but were far less evident in the WT tissue. The increased number of these granules in the DPP9$^{S729A/S729A}$ samples compared to the WT samples suggests that there might be abnormal retention of catecholamines in adrenal cells, which may have an impact on critical metabolic processes in these neonates. To elucidate whether this issue exists in the neonates would require specific focus on neonate adrenal histology and function. While this was beyond the scope of the current study, it would be interesting to investigate in the future as a potential contributor to neonate lethality in the DPP9$^{S729A/S729A}$ and DPP9$^{wt/S729A}$ mice.

As well as nuclear staining, notable cytoplasmic staining was observed in alveolar cells of the lung, gut epithelial cells, dendritic branches of neurons in spinal cord, myosin fibrils of skeletal muscle, hair follicle cells in skin, acinar cells of the pancreas and lymphocytes in the thymus. This finding is consistent with increased autophagic activity in tissues undergoing development and metabolic change.

In the early neonate, autophagy is at high levels in brain tissue and normal brain function is imperative for survival. As reduced autophagy was indicated in DPP9$^{S729A/S729A}$ brain tissue in this study, LC3B protein levels were measured by immunoblotting to confirm the down-regulation. The results indicated a trend towards less autophagy occurring in DPP9$^{S729A/S729A}$ brain but analysis showed no significant difference between samples. This may be due to variable localisation of LC3B protein to the various cell types or regions of the brain, and immunoblotting of whole brain lysates is necessarily an average of the whole. Microscopic observation of immunoreactivity to LC3B in various brain tissue samples suggested that different regions displayed different levels of staining intensity, however, the small number of brain samples and varied orientation of tissues in blocks meant that there were insufficient replicates of most brain areas to verify such ideas in the current study.

Of interest is the quantitative analysis which showed an up-regulation of autophagy in heart muscle, lung and gut in DPP9$^{S729A/S729A}$ tissue and a down-regulation in DPP9$^{S729A/S729A}$ liver and brain compared to WT. Either an overall up-regulation or an overall down-regulation of autophagy in affected tissue types may be expected to result in neonate lethality but these findings are more indicative of a systemic

dysregulation, which suggests that autophagy may only be a contributing factor or a flow-on effect of the event(s) that result in the death of all DPP9$^{S729A/S729A}$ and some heterozygous neonates. Alternatively, the mechanisms of DPP9-driven altered autophagy intensity might be direct in some organs but indirect in others.

Consideration of technical aspects of immunostaining such as sample preparation, antibody specifity and sensitivity of staining are important. While the quantification of immunostaining presented in the literature needs to be interpreted with caution due to the shortcomings of immuneperoxidase-based staining methods, the data do provide a useful starting point for future investigations. Further quantitative analysis of additional mouse sections using this and other staining methods would provide greater knowledge of the role of autophagy in the DPP9-enzyme deficient mouse.

CHAPTER 5:

Comparative analysis of adult DPP9$^{wt/S729A}$ and WT mouse skin

5 Comparative analysis of adult DPP9$^{wt/S729A}$ and WT mouse skin

5.1 Introduction

In both neonatal and adult mice, any major defect and damage to the skin is life threatening. Tissue regeneration and restoration of structural integrity relies on redundant reservoirs of stem cells in both the epidermis and dermis (Kimlin and Virador, 2013). For murine skin, these stem cells are found in the hair follicle bulge and dermal papilla and the dermis, the same regions where DPP9 is present. Many studies have shown defects in wound healing and skin integrity resulting from protease impairments or deficiencies (Basu et al., 2001, Drew et al., 2001, Bradshaw et al., 2003, Leitch et al., 2008).

The role of other DPPs has been reported in wound healing and skin repair. DPP4-positive T cells are involved in regulating granulation tissue formation (Kohl et al., 1991). DPP4-like activity mediates anti-fibrotic effects in fibroblasts and may regulate fibroblast functions (Thielitz et al., 2008). Inhibition of DPP4 in keratinocytes of skin can enhance healing (Schürmann et al., 2012, Sinagra et al., 2015). Also, FAP has long be reported as being expressed in the granulation tissue of healing wounds and FAP expression is strongly induced during scar formation (Garin-Chesa et al., 1990).

Recent work *in vitro* has shown that inhibition of DPP9 results in less cell mobility and adhesion compared to control cells (Zhang et al., 2015a), indicating DPP9 enzymatic

function may have a role in skin repair. No enzyme activity assay exists that detects DPP9 alone (Yu et al., 2009) which makes accurate assessment of activity levels in DPP9-GKI heterozygous mouse skin difficult. Thus, the level of specific DPP9 enzymatic activity in skin has not been examined. Others have previously evaluated DPP9 enzyme activity using whole MEFs in the absence or presence of a DPP8/9 inhibitor (Yu et al., 2009, Yao et al., 2011, Chen, 2013) which showed activity present at similar low levels in both WT and heterozygous MEFs. However, the role of DPP9 in wound healing *in vivo* has not been investigated.

The early focus of the work in this thesis was placed on identifying the developmental stage and cause of DPP9-GKI mouse lethality. It has been shown that death occurs in the neonatal stage, however, the cause of lethality remains elusive. Working with neonate pups is technically challenging and time intensive and the early timing of death limits the scope of experimentation. Neonatal mice possess a very small total skin area and their collagen levels are less than 10% of adult mice (Mao et al., 2002). Therefore, in-depth analysis of neonatal skin for tensile strength and collagen content was beyond the scope of this work.

Because of this, and the increased logistical and technical ease of working with larger mice, further investigation was undertaken on adult DPP9-GKI heterozygous mice. While heterozygous mice appear normal and healthy, it has been shown previously that carrying the DPP9 S729A mutant allele affects survival to weaning in neonate mice (Gall et al., 2013). Since most heterozygous neonates survive to weaning, this suggests that variability in the levels of DPP9 enzymatic activity expression at the neonatal stage

may influence the post-weaning structure or function of organs without causing lethality or serious impairments. Once weaned, the long term survival of adult DPP9 heterozygous mice does not differ from their wild-type littermates. Nevertheless, there is a possibility that the neonatal differences of DPP9 enzyme activity in these mice result in adult biological functions which are altered, impaired or even enhanced.

In chapter 3 of this thesis, the presence of positive DPP9 immunoreactivity in skin of WT, DPP9-GKI heterozygous and DPP9$^{S729A/S729A}$ neonates was shown. This was expected as the anti-DPP9 antibody binds with DPP9 protein and, thus, detects both enzyme-active and enzyme-inactive DPP9. Positive immunostaining was seen in the cytoplasm of epidermal basal keratinocytes and dermal lymphoid cells. There was also strong staining of hair follicles. While displaying similar localisation, the levels in adult skin are much lower than in embryonic and neonatal skin. This localisation of staining was consistent with other published works where DPP9 in skin has been assessed by *in situ* hybridisation and immunohistochemistry (Yu et al., 2009, Harstad et al., 2013, Pantano et al., 2013).

In this chapter, the novel characterisation of adult DPP9-GKI heterozygous and WT mouse skin was undertaken to investigate a potential role of DPP9 in cutaneous wound healing and skin structure, integrity and strength. As well as wound repair, other changes in skin could relate to its tensile strength and collagen content. With consideration of this along with the known role of other DPPs in skin function and the lack of information available in relation to skin functions of DPP9, various aspects of

skin structure and function were investigated for DPP9-GKI heterozygous and WT adult mouse skin.

5.1.1 Aims

The aims of the work in this chapter are:

- to determine whether carrying the S729A mutant allele in DPP9 heterozygous adult mice affects wound healing by causing a delay in wound closure
- to measure tensile strength of wounded and healthy steady-state mouse skin in DPP9$^{wt/S729A}$ mice compared to WT littermates and WT C57BL/6J mice
- to investigate collagen levels in skin of DPP9$^{wt/S729A}$ mice and wild-type littermates

5.2 Methods

5.2.1 Cutaneous model of wound healing

DPP9$^{wt/S729A}$ mice, DPP9$^{wt/wt}$ mice and C57BL/6J mice aged 8 weeks were used in this study. Mice were anaesthetised using isoflurane (flow rate of 0.4X0.8 L/min) (I.S.O.,

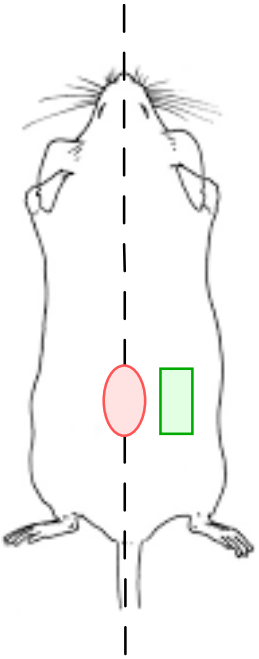

Figure 5.1: Schematic representation of mouse wound location

In this experiment a full thickness wound (red oval) was created on the dorsal midline of the mouse using an 8 mm biopsy punch. During skin harvesting for analysis, a size-matched section of non-wounded steady-state skin adjacent to the wound area (green rectangle) was collected for comparison purposes.

VCA) and the surface of the dorsum was shaved, washed with warm water and then excess hair removed using Nair sensitive hair removal cream (Nair®, Church & Dwight Co Inc., Ewing, NJ, USA). Prior to wounding, the skin was cleaned with Povidone-iodine (Betadine, Stamford, CT, USA). An 8 mm biopsy punch (Kays Medical, Liverpool, UK) was used to make an incision wound on the dorsal midline of the mice. Post-wounding, mice were given a subcutaneous injection of ampicillin [50 mg/kg] (Austrapen) and temgesic [0.03 mg/kg] (Reckitt Benckiser) and recovered on a heating pad. The wound was covered for 12 h with Tegaderm (Tegaderm™, 3M Company, Maplewood, MN, USA). After removal of the Tegaderm, a second subcutaneous dose of ampicillin/temgesic was given to the mice.

Daily measurements of wound closure rates were undertaken for 5 or 10 days by photographing wounds then analysing the wound image using ImageJ software. Data were analysed by unpaired t-test using GraphPad Prism and significance was assigned to *P* values less than 0.05.

5.2.2 Tissue harvest and staining

Wound and non-wound steady-state tissue for histological analysis was harvested 5 days post-wounding, flattened onto biopsy pads in histosettes, incubated overnight in 10% formalin and then processed routinely through to paraffin blocks. To undertake histological observations, paraffin-embedded skin samples were sectioned at 5 µm and hematoxylin and eosin (H and E) stained. For localisation and assessment of collagen, sections were stained with Sirius Red. H and E and Sirius red staining were

performed by the Histopathology Department, Discipline of Pathology, Blackburn Building, University of Sydney.

Microscopic analysis of sections was performed using a Leica DM6000 B microscope and ImageJ software was used to quantify levels of collagen as represented by positive Sirius red staining (Hadi et al., 2011). Data were analysed by unpaired Mann-Whitney t test using GraphPad Prism and significance was assigned to *P* values less than 0.05.

5.2.3 Hydroxyproline assay

Wound and non-wound steady-state tissue was harvested at Day 5 post-wounding, weighed (ranging between 100-250 mg) and then placed in a 2 ml screw cap tube. 150 µl of concentrated HCl (Sigma) was added to each tube and samples were hydrolysed on a heat block at 110˚C for 3 h. After samples had liquefied they were vortexed then quickly spun in a centrifuge (30 sec). Standards were prepared by diluting 1 mg/ml hydroxyproline (Sigma #MAK008) in TDW to make a standard curve ranging from 0-20 µg/ml. After samples had cooled they were transferred to wells of a 96-well clear, flat-bottomed plate in triplicate along with standards samples. The plate was placed in a dry oven at 60˚C until samples had completely dried. 100 µl of solution A (chloramine T/citrate-acetate buffer) was added to each well and left for 5 min at RT. 100 µl of solution B (Erhlich's solution) was then added and the plate was incubated at 60˚C for 90 min. Absorbance was read at 560 nm using a BMG plate reader (BMG Labtech, Germany). Using the BMG plate reader software (Omega Mars, BMG Labtech,

Germany), the values for each well were corrected for background and triplicates were averaged.

5.2.4 Biomechanical analysis of tissue

Skin tensile strength was measured using an Instron 5567 tensiometer (Instron Corporation, Buckinghamshire, UK) after training by Mr Trevor Shearing at the School of Aerospace, Mechanical and Mechatronic Engineering, University of Sydney. Dorsal skin samples from the wound area and adjacent non-wound steady-state skin were harvested 14 days post-wounding. At this stage, wounds from all the groups (n = 3-8) had closed completely. Skin samples were trimmed to approximately 3 cm x 1 cm and attached to paddle pop sticks using super glue to clamp them firmly (Figure 5.2). The glue was applied with care to avoid contamination of the 1 cm x 1 cm analysis area.

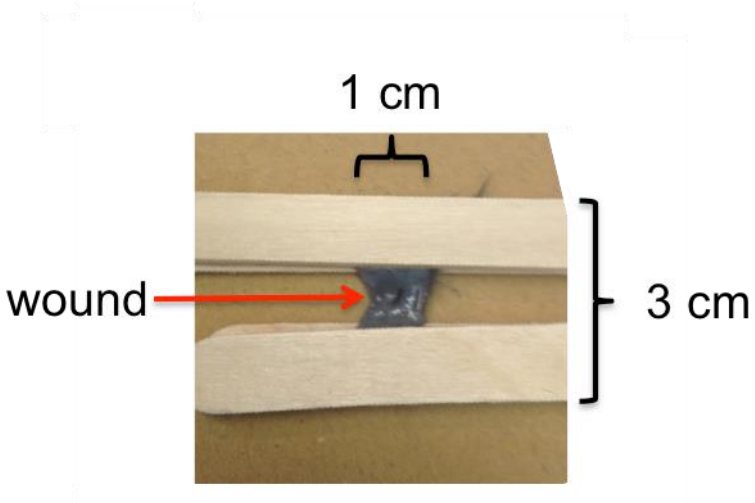

Figure 5.2: Preparation of samples for tensile strength measurements.

A strip of wounded or steady-state skin was cut to approximately 3 cm x 1 cm and the two ends were glued between two paddle pop sticks using super glue. The sticks were used to attach samples to the upper and lower clamps of the Instron tensiometer. Samples were then stretched until breaking point to measure tensile strength.

Samples were flattened onto cardboard, wrapped in tissue then foil, snap frozen in liquid nitrogen and stored at -80˚C until they were ready for analysis. Upon thawing, samples were prevented from drying out by dampening them with PBS. Advice for the preparation and tensile strength measurement of skin samples was given by Dr Philip Boughton (Biomedical Engineering, School of Aerospace, Mechanical and Mechatronic Engineering, University of Sydney).

Tensile force was applied using a 100 N load cell and motor drive speed was controlled by Instron Merlin software (version 5.52). The output force was 4 g and the sample cycle was 0.2 sec. The paddle pop sticks were placed between two clamps and stretched at 5 mm/min until breaking. Data were analysed for toe region, linear region and maximum load (Figure 5.4) using GraphPad Prism and significance using t test was assigned to *p* values less than 0.05.

5.3 Results

5.3.1 Wound closure and healing

In the first 24 hours post-wounding, wound sizes increase in all mice due to skin flexibility and stretchiness. Hence, all analysis was determined from Day 1 onwards with subsequent measurements being normalised against Day 1 percentage wound areas. Since no percent-wound-area difference was seen between DPP9$^{wt/wt}$ mice, which are raised on a C57BL/6J background, and C57BL/6J mice (data not shown), the means of all WT mice (DPP9WT + C57BL/6J) from both sources were combined for wound closure analysis and graphing. Macroscopic analysis of wounds from daily

measurements revealed no significant delay in wound closure in DPP9$^{wt/S729A}$ mice compared to either DPP9$^{wt/wt}$ mice or C57BL/6J (Figure5.3). All wounds had completely closed by Day 10-11 in all groups.

5.3.2 Skin tensile strength

To give an indication of skin strength and elasticity after the closure of wounds, tensile strength was investigated on wounded and adjacent steady-state tissue harvested 14 days post-wounding. Because the mechanical behaviour of skin is not the same in every direction (Funk, 2007, Annaidh et al., 2010, Yang et al., 2015), several different methods of analysis were employed to overcome the variability in data. The physical behaviour of skin, when subjected to stretching, differs from properties observed with non-biological materials. Figure 5.4 represents a simplified diagram of the behaviour of the collagen fibres in skin when subjected to a load. In the toe region of stress-strain graphs the collagen fibres are pulled into alignment reflecting skin stretchiness, while the linear region reflects the stiffness, density and cross-linking of the fibres after alignment (Mao et al., 2002). Once the stretch of the skin is beyond the physiological range, collagen fibrillar failure results in rupture of the skin at maximum load.

Raw tensiometer data was used to create stress-strain curves (data not shown) which were used to extrapolate the toe region length, linear region slope and maximum load

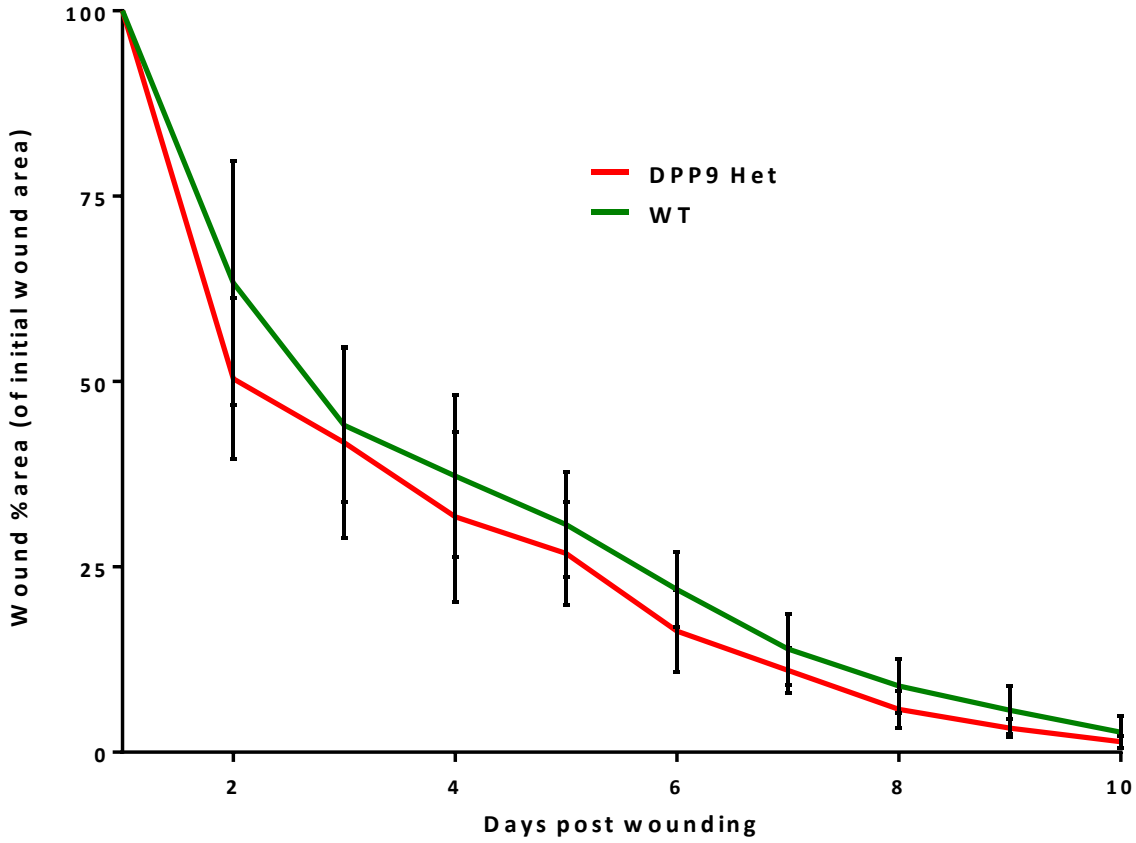

Figure 5.3: Wound closure rate of WT and DPP9$^{wt/S729A}$ adult mouse skin

No difference was seen in wound closure rates between WT and DPP9$^{wt/S729A}$ adult mouse skin. Wound area change during healing is represented as a percentage of the initial wound size at Day 1. Wounds were measured daily using ImageJ software to determine area by analysis of wound images. n = 8 (DPP9het) and 11 (DPP9WT + C57BL/6 WT). The error bars depict standard deviation.

point. Most stress-strain curves generated for the skin samples measured displayed the expected format of initial stretch, extension and finally skin breakage (Figure 5.4). However, from sample to sample, the points where extension and breakage occurred was reasonably variable. In a small number of samples the curve was skewed away from the expected format which is most likely due to the mechanical nature of skin and microscopic differences between skin samples.

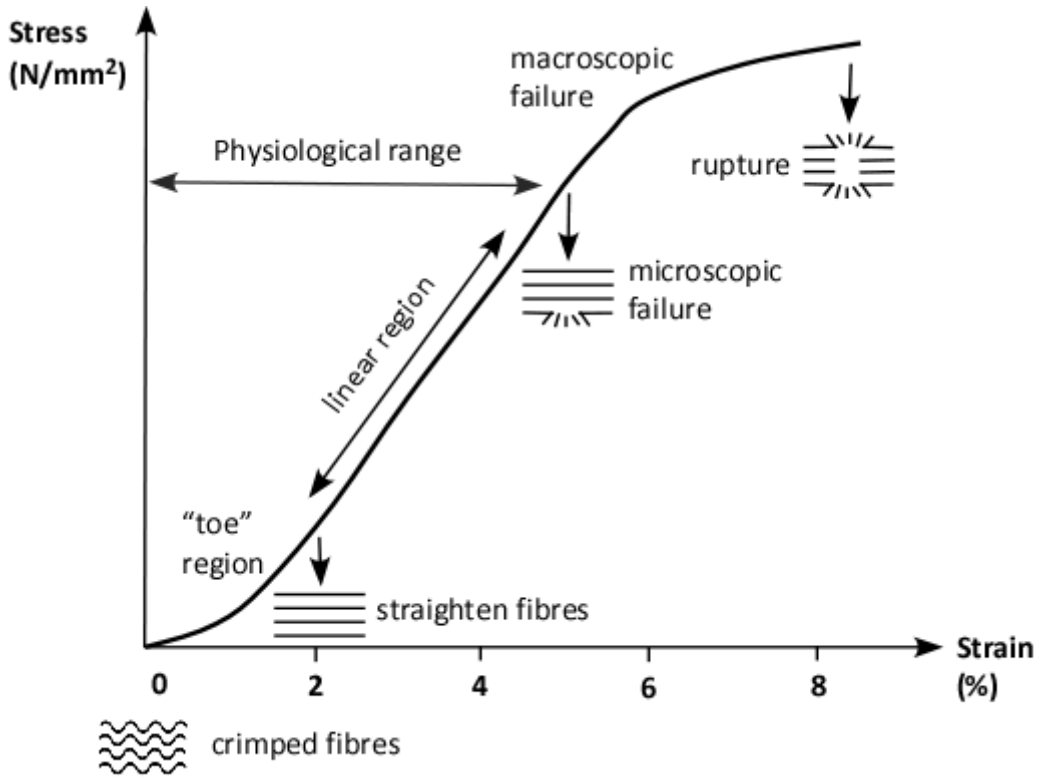

Figure 5.4: Diagrammatic representation of the stress-strain curve for skin

When a load is applied to a skin sample the crimped collagen fibres first straighten and align, then stretch and eventually fracture. The toe region is an indicator of skin stretchiness. The linear region indicates the ability of the collagen fibres to slide past each other. The skin ruptures when the collagen fibres fracture. Modified from (Funk, 2007)

The toe region of the curve gives an indication of the normal range of skin deformation and, hence, the elasticity of skin when first subjected to a load. Not surprisingly, there was a significant difference in the toe region of the stress-strain curves for both DPP9$^{wt/S729A}$ and WT mouse skin when comparing wounded skin with normal steady-state skin (Figure 5.5). At Day 14 post-wounding, re-epithelialisation is complete but the resultant scar has reduced tensile strength (Schafer and Werner, 2008). Therefore, the stretchiness of wounded skin will be reduced. However, when considering the difference in elasticity of skin from heterozygous and WT mice, there was no statistical difference in toe length between them for either wounded or adjacent steady-state skin (Figure 5.6).

The linear region of the stress-strain curve sits within the physiological range where skin has not yet undergone any microscopic failure and this region gives an indication of the ability of the collagen fibres to move past each other once straightened. This is a measure of skin stiffness (Mao et al., 2002). In order to avoid the toe region and any potential microscopic failure, the slope was measured using the central half of the linear region. Wounded skin (Figure 5.7) showed no statistical difference in the slope of the linear region for DPP9 heterozygous skin as compared to WT. Similarly, no statistical difference was seen in the slope of the linear region between heterozygous and WT skin for steady-state skin (Figure 5.8).

The final consideration of skin properties between samples is ultimate tensile strength which is the point at which macroscopic failure and rupture of the skin occurs. This

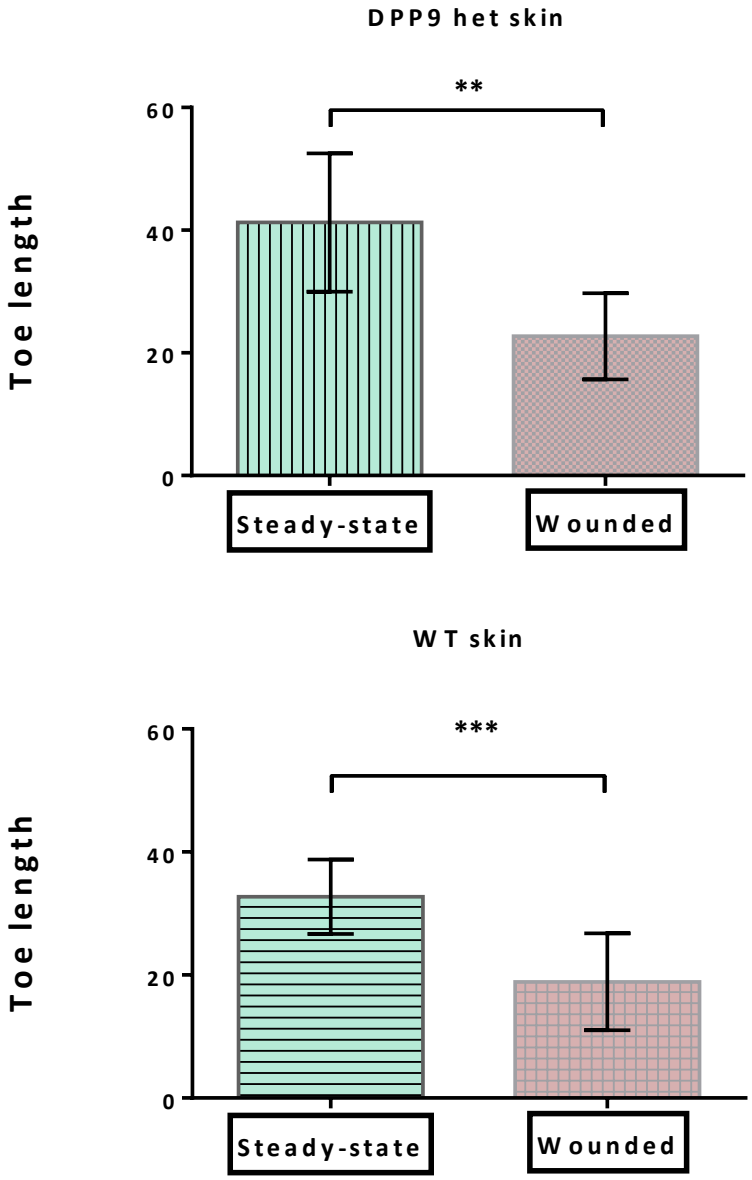

Figure 5.5: Estimated length of the toe region of the stress-strain curve for DPP9$^{wt/S729A}$ and WT mice from steady-state and wounded skin

The toe region of the stress-strain curve of Day 14 mouse skin showed significant differences between the wounded and adjacent steady-state skin for both DPP9$^{wt/S729A}$ and WT mice. The analysis of the toe region was determined with GraphPad Prism software. n = 7-8 (DPP9het) and 10-11 (DPP9WT + C57BL/6 WT). Error bars denote SD and significance was assigned where $p < 0.05$ (*), $p < 0.01$ (**), $p < 0.001$ (***).

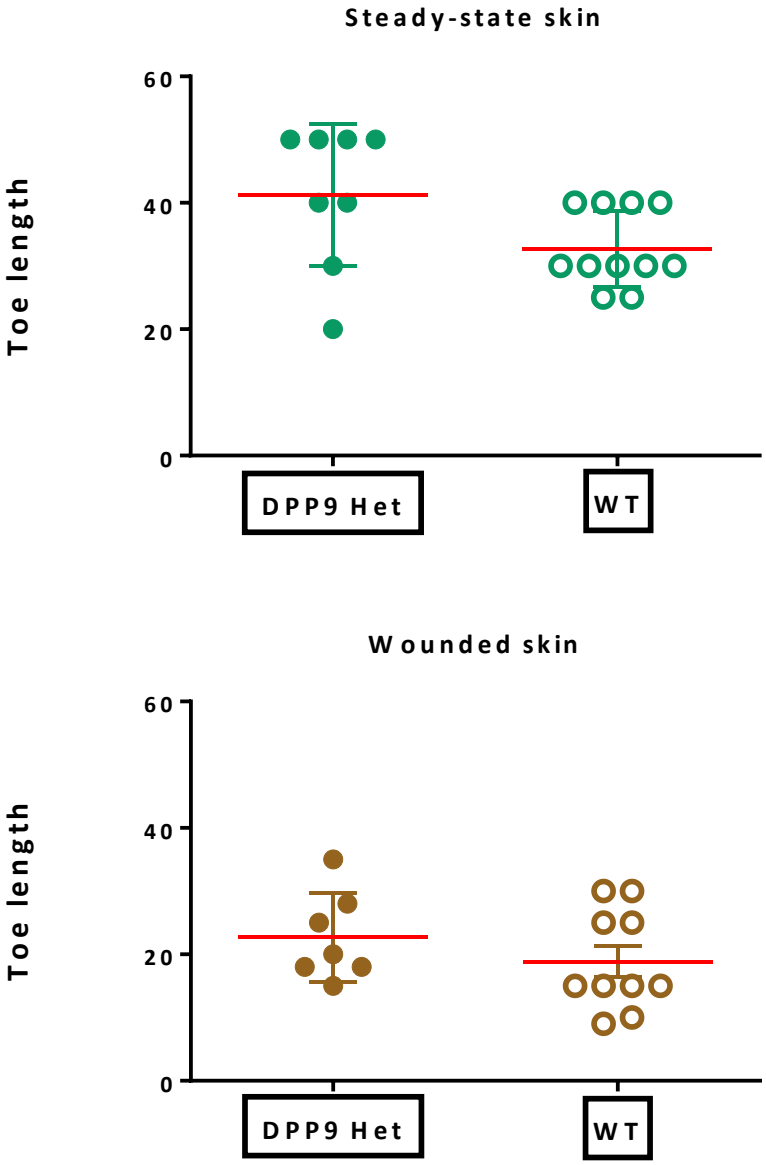

Figure 5.6: Estimated length of the toe region of the stress-strain curve for wounded and steady-state skin from DPP9$^{wt/S729A}$ and WT mice

The toe region of the stress-strain curve of Day 14 mouse skin showed no significant differences between DPP9$^{wt/S729A}$ and WT mice for either the wounded or the adjacent steady-state skin. The analysis of the toe region was determined with GraphPad Prism software. n = 7-8 (DPP9het) and 10-11 (DPP9WT + C57BL/6 WT). Horizontal bars (red) are means and error bars depict SD.

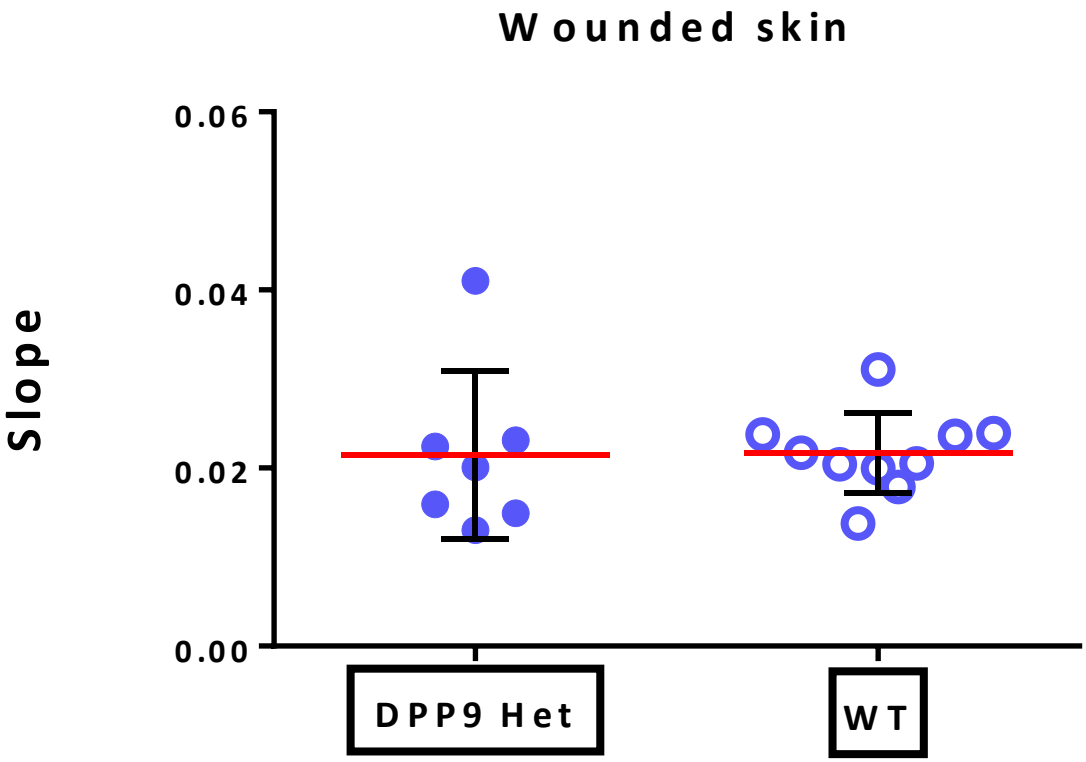

Figure 5.7: Analysis of the slope of the linear region of the stress-strain curve for wounded mouse skin

The slope of the linear region of the stress-strain curve from Day 14 wounded mouse skin from DPP9$^{wt/S729A}$ and WT mice showed no significant difference between genotypes. Stress-strain curves were measured using an Instron tensiometer and the analysis of the linear region was determined with GraphPad Prism software. n = 7 (DPP9het) and 10 (DPP9WT + C57BL/6 WT). Horizontal bars (red) are means and error bars depict SD.

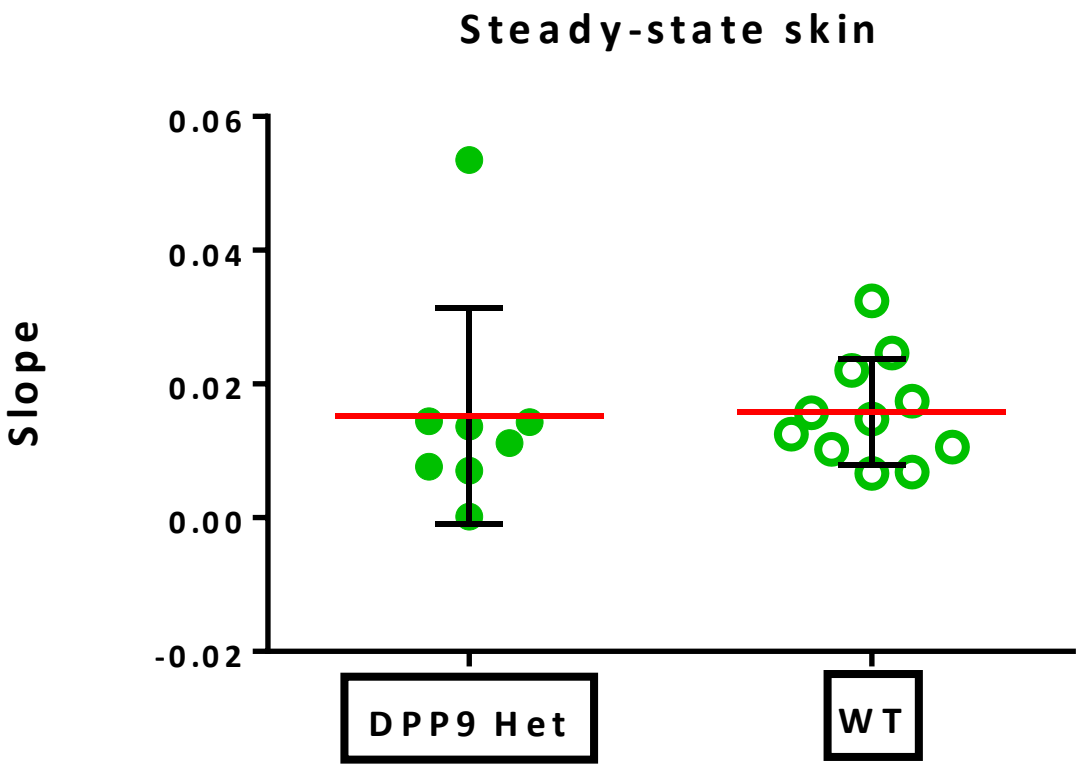

Figure 5.8: Analysis of the slope of the linear region of the stress-strain curve for steady-state skin adjacent to the wound area in mouse skin

The slope of the linear region of the stress-strain curve from Day 14 steady-state mouse skin from DPP9$^{wt/S729A}$ and WT mice showed no significant difference between genotypes. Stress-strain curves were measured using an Instron tensiometer and the analysis of the linear region was determined with GraphPad Prism software. n = 8 (DPP9het) and 11 (DPP9WT + C57BL/6 WT). Horizontal bars (red) are means and error bars depict SD.

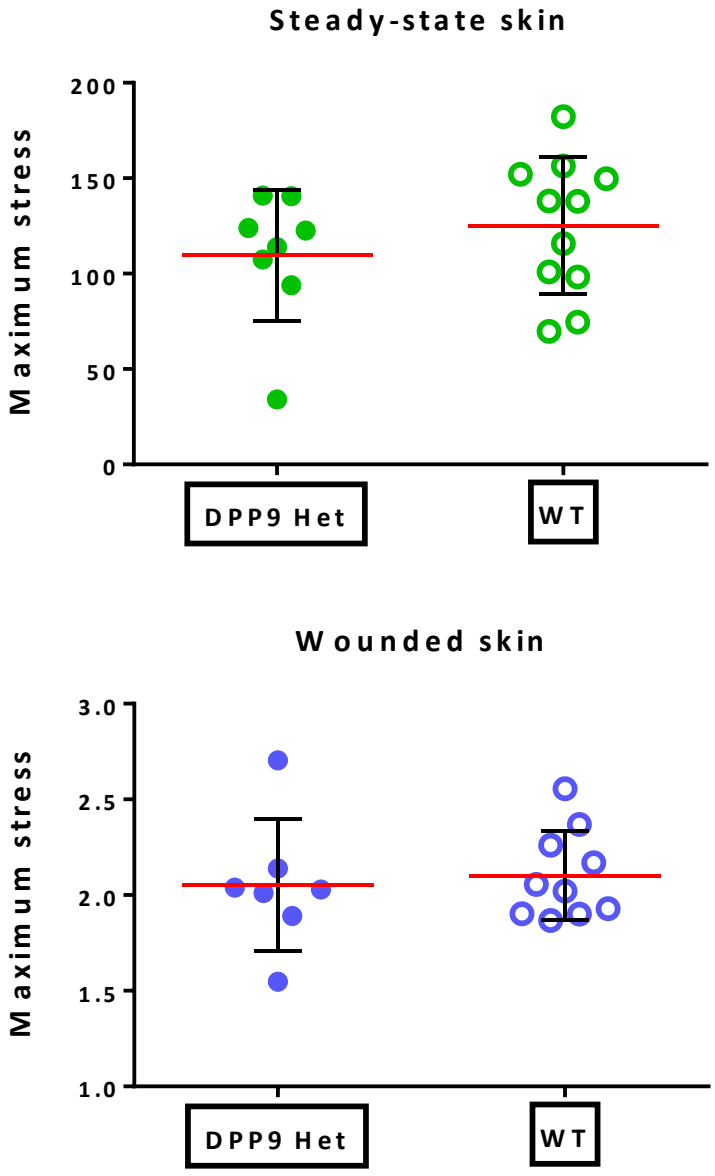

Figure 5.9: Maximum stress of the stress-strain curve for steady-state and wounded mouse skin

The maximum stress measurements of Day 14 mouse skin showed no significant differences between DPP9$^{wt/S729A}$ and WT mice for either the wounded or the adjacent steady-state skin. The analysis maximum was determined with GraphPad Prism software. n = 7-8 (DPP9het) and 10-11 (DPP9WT + C57BL/6 WT). Horizontal

failure force was measured as the point of maximum stress which corresponds directly with the maximum load applied for skin breakage. No statistical difference was found for the ultimate tensile strength of DPP9$^{wt/S729A}$ and WT mouse skin in the wounded skin and adjacent steady-state skin (Figure 5.9). The maximum stress needed to cause skin breakage was, however, fifty fold greater in steady-state skin compared to wounded skin which is consistent with the presence of scar tissue and reduced tensile strength as mentioned previously.

5.3.3 Skin collagen levels

Collagen levels were estimated by two methods: Sirius red staining and skin hydroxyproline content. The Sirius red staining and hydroxyproline assays were performed on wound tissue and adjacent steady-state tissue harvested 5 days post wounding.

5.3.3.1 Sirius Red staining

Skin tissue from wounded or the adjacent steady-state skin in DPP9$^{wt/S729A}$ and WT mice was harvested at Day 5 post-wounding and sections were stained with Sirius Red. In these sections, the presence of cross-linked collagen was indicated by positive red staining. All measurements for wounded tissue were taken in the areas of granulation tissue formation at the edges of the wound. All measurements for steady-state tissue were taken from random areas along the skin section length. In steady-state skin

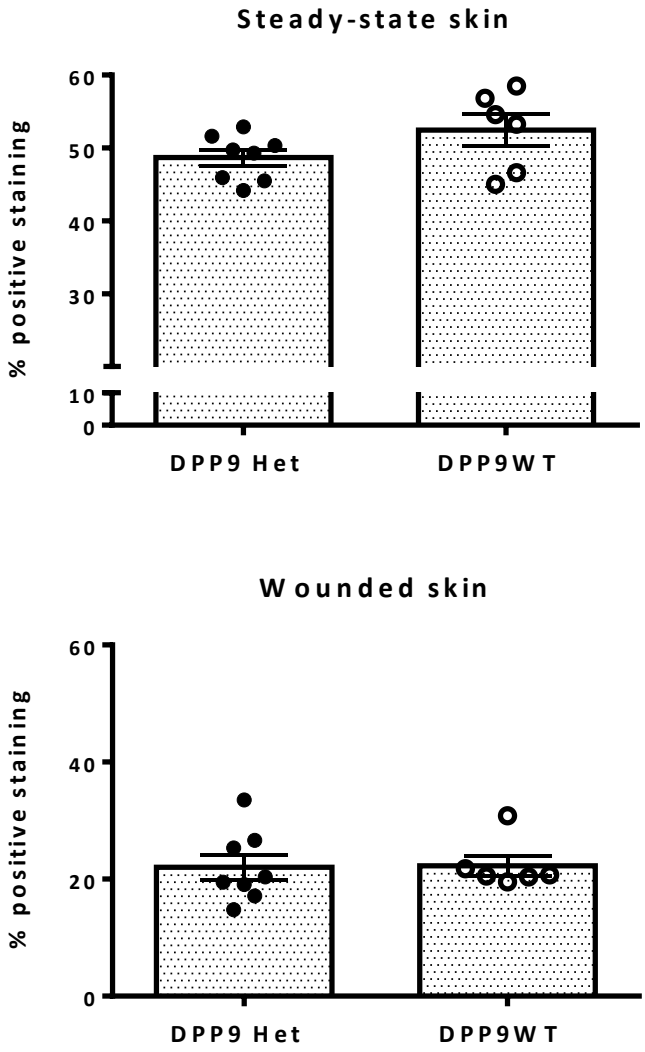

Figure 5.10: Collagen levels indicated by positive Sirius Red staining of steady-state and wounded mouse skin

Skin tissue from wounded and adjacent steady-state skin in DPP9$^{wt/S729A}$ and WT mice was harvested at Day 5 post-wounding and sections were stained with Sirius Red. Positive staining corresponded to the presence of cross-linked collagen. No significant differences between DPP9$^{wt/S729A}$ and WT mice for either the wounded or the adjacent steady-state skin were detected. Each value represents the average of 5 separate ROIs in 5 separate areas analysed from the same slide. The percentage positive staining was determined with GraphPad Prism software. n = 8 (DPP9het) and 6 (DPP9WT). Horizontal bars (red) are means and error bars depict standard error of the mean.

(Figure 5.10), positive staining was lower in DPP9$^{wt/S729A}$ mouse skin compared to DPP9WT skin but this difference was not statistically significant. In wounded skin (Figure 5.10), no differences in collagen levels between DPP9$^{wt/S729A}$ and WT mice were detected. This finding is consistent with the wound healing data (Figure 5.3) where wound closure rates were not significantly different between genotypes at Day 5 post-wounding. Across all data, however, collagen levels were at least two times higher overall in steady-state skin compared to wounded skin. This result is expected as the early stage of wound healing has depleted levels of collagen where only small amounts of newly synthesised collagen exist (Sabol et al., 2012).

5.3.3.2 Hydroxyproline assays

Since hydroxyproline is a major component of cross-linked collagen, total collagen can be estimated from skin samples by acid hydrolisation of proteins and measurement of hydroxyproline content by colorimetric assay. As with Sirius Red staining, hydroxyproline levels were also measured in Day 5 post-wounding skin tissue.

In line with the collagen levels measured in Sirius Red-stained skin wound tissue, the hydroxyproline content measured by assay in wound samples (Figure 5.11) showed no significant difference between DPP9$^{wt/S729A}$ mouse skin compared to DPP9WT skin. Interestingly, the adjacent steady-state tissue shows significantly reduced levels of hydroxyproline (p = 0.0082) in the DPP9$^{wt/S729A}$ mouse skin compared to DPP9WT skin. This is consistent with the trend towards reduced positive staining in steady-state Sirius Red-stained skin (Figure 5.10), although no statistical significance was shown there.

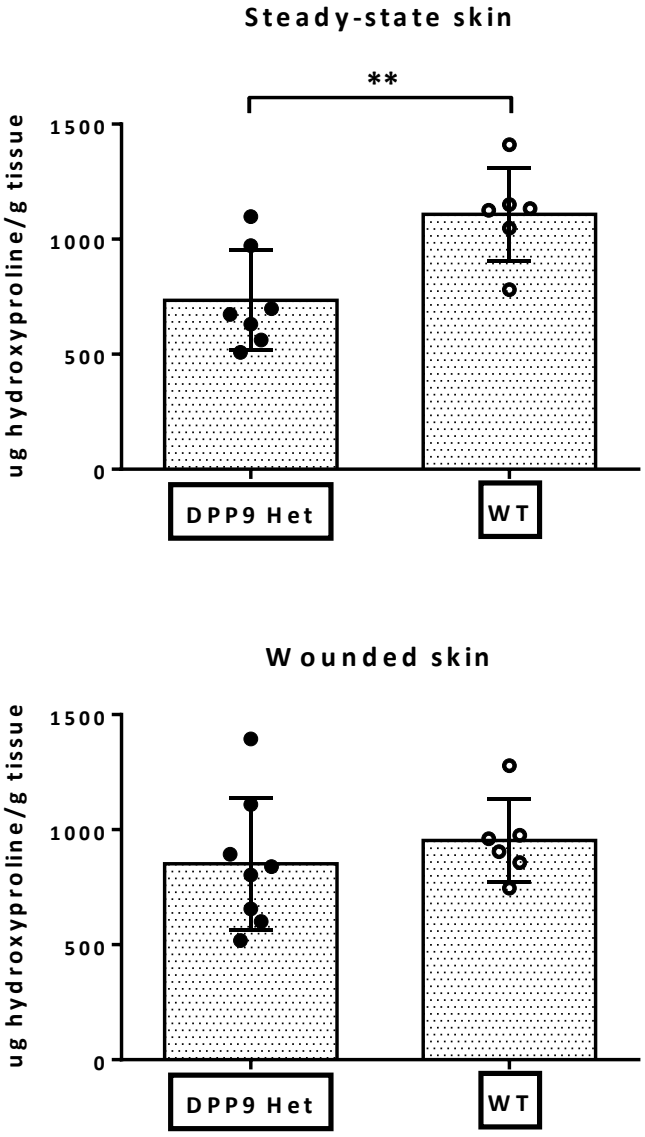

Figure 5.11: Collagen indicated by hydroxyproline levels in steady-state and wounded mouse skin

Skin tissue from wounded and adjacent steady-state skin in DPP9$^{wt/S729A}$ and WT mice was harvested at Day 5 post-wounding and tissue was assayed for hydroxyproline. No significant difference between DPP9$^{wt/S729A}$ and WT mice for wounded skin was detected. Steady-state skin showed a significantly lower level of hydroxyproline in DPP9$^{wt/S729A}$ mice compared to WT mice (P=0.0082). n = 7-8 (DPP9het) and 6 (DPP9WT). Column heights are means and error bars depict SD. Data were analysed by unpaired Mann-Whitney t test using GraphPad Prism and significance was assigned where $p < 0.05$ (*), $p < 0.01$ (**), $p < 0.001$ (***).

5.4 Discussion

In this chapter, the aim was to characterise adult DPP9-GKI mouse skin and determine differences, if any, between DPP9-GKI heterozygous skin and that of their WT littermates and WT C57BL/6J mice. This was undertaken by sampling mouse skin subjected to a full thickness wound or adjacent skin in a non-wounded steady state. Other members of the DPP4 protein family are known to be involved in wound healing, fibroblast regulation and skin function, but no *in vivo* studies have been undertaken in relation to DPP9. Also, no published works have addressed the structural integrity of adult mouse skin partially deficient in DPP9.

In this study, macroscopic monitoring of wound closure rates were investigated comparatively in WT and DPP9-GKI heterozygous mice. It has been shown that the skin of loose-skinned animals, such as mice, can move and retract over subcutaneous fascia enabling relatively rapid bridging of the wounded edges by granulation tissue and new epithelium. (Davidson, 2001). All wounds in the mice in this study had closed by 11 days after wounding and no difference was seen between C57BL/6J WT, DPP9$^{wt/wt}$ and DPP9$^{wt/S729A}$ adult mouse skin in relation to the rate of wound closure. Since the ability of skin to heal after wounding is essential to survival, there are almost certainly redundant pathways that ensure healing occurs when regular processes are slow or non-functional. With this in mind, it may be surmised that, if DPP9 plays a part in the healing process, its role is non-essential.

Consideration of steady-state skin provides a benchmark with which to compare the effect of wounding on skin structure and function. Most importantly, however, it

provides a comparison between DPP9-GKI heterozygous and WT skin which directly relates to the possible role of DPP9 in skin of the adult DPP9-GKI mouse. Biomechanical analyses were used to assess the overall tensile strength, with stress-strain curves providing data on skin elasticity, skin stiffness and ultimate tensile strength before rupture. For skin elasticity, as shown by the toe region of stress-strain curves, no statistical difference was seen between WT and DPP9-GKI heterozygous steady-state skin, although there was a trend towards increased elasticity in the DPP9 heterozygous skin over the WT skin suggesting a possible variation from the normal range of skin deformation.

When a load is applied, collagen fibres in the skin straighten and slide past each other within the physiological range of normal steady-state skin extension and stiffness. This is displayed by the linear region of the stress-strain curve. While most steady-state skin samples measured on the tensiometer displayed a smooth linear region, the levels of variability amongst samples was fairly high. Because the mechanical nature of skin is multi-directional, some samples showed abnormal curves in the linear region which most likely corresponded to microscopic fracture of collagen fibres preceding macroscopic skin rupture. Despite this variability, analysis of the slope measurements resulted in fairly close grouping of data points, with few outliers, in steady-state heterozygous and WT skin and no statistically significant difference was observed between these groups for linear region slope.

The point of macroscopic failure of skin is generally considered to be its ultimate tensile strength. While no significant difference was seen between WT and DPP9-GKI

heterozygous samples in the steady-state skin, there was a trend towards earlier breakage in DPP9-GKI heterozygous skin compared to WT. However, the data for the steady-state skin encompassed a large range of maximum stress readings and this variability conferred some uncertainty about the strength of heterozygous compared to WT skin.

Both collagen and elastin fibres are components of skin. Elastin makes tissues elastic and allows recoil after deformation and a mixture of collagen and elastin prevents skin from overstretching (Starcher et al., 2005). Collagen, however, is the most common fibrous protein in the extra-cellular matrix of skin and has an important role in the structural integrity of skin and in wound healing. It was, therefore, the focus of this study.

To better compare whether changed collagen accumulation existed between healing and/or steady-state DPP9 heterozygous skin and WT skin, collagen content was assessed in Day 5 post-wounding skin by two methods. Firstly, Sirius Red staining of skin sections was undertaken to assess *in situ* collagen and, secondly, hydroxyproline assay of digested skin samples was used to estimate total collagen.

With Sirius Red staining analysis, the steady-state tissue was of interest since the collagen levels were less in the DPP9-GKI heterozygous skin compared to WT skin. While this result was not statistically significant, it was consistent with the trends observed previously for tensiometer data of steady-state skin and possibly suggested reduced collagen present in heterozygous adult mouse skin. Tissue collagen level of steady-state skin at Day 5 post-wounding was also assessed using a hydroxyproline

assay as a measurement of cross-linked collagen. Interestingly, for this analysis, there was a statistically significant decrease in hydroxyproline levels in the DPP9-GKI heterozygous skin compared to WT skin. As DPP9 is able to hydrolyse the post-proline bond of a hydroxylated proline (Zhang et al., 2015b), it is very likely that this hydroxyproline measurement was an accurate reflection of total collagen.

This result supports the trends shown in the tensile strength and Sirius Red staining data towards reduced collagen levels in steady state heterozygous skin. This is a novel finding for the DPP9-GKI heterozygous mouse and raises the question as to whether this low level of collagen in skin is confined to that organ. It would be interesting to measure collagen in other organs throughout the DPP9-GKI heterozygous mouse in future studies to assess whether any of these also display reduced collagen levels.

Two weeks post-wounding, when the healing was complete, the wounded skin was analysed biomechanically in the same manner as steady-state skin for skin elasticity, skin stiffness and ultimate tensile strength. Assessment of skin elasticity also showed no statistical difference between WT and DPP9-GKI heterozygous wounded skin, but a similar trend towards increased elasticity in the DPP9-GKI heterozygous skin was seen.

When comparing steady-state and wounded skin, however, significantly shorter toe regions were seen between wounded and steady-state skin reflecting the decreased integrity of wounded skin. This is not surprising as it has been previously reported that skin never regains its full tensile strength after wounding (Broughton et al., 2006) or at least has reduced tensile strength in the scar region (Schafer and Werner, 2008). However, unlike other organs such as liver where scarring is detrimental to normal

function (Chowdhury et al., 2013), scarring in skin is well tolerated, possibly due to the looseness of mouse skin.

Analysis of the linear region in stress-strain curves of wounded skin showed no significant difference between WT and DPP9-GKI heterozygous skin suggesting that, like the steady-state skin, these samples displayed a similar level of stiffness and skin extension ability. While the ultimate tensile strength of wounded skin did not vary between heterozygous and WT groups, the maximum stress needed to cause wounded skin to break was only around 2% of that needed than for steady-state skin. This finding is consistent with the reduced strength of scar tissue mentioned previously.

Analysis of collagen content in wounded skin, as with steady-state skin, was undertaken by Sirius Red staining and hydroxyproline assays. For Sirius Red staining of the skin wound regions, measurements and analysis was confined to the granulation region. In this region, remodelling of the extra-cellular matrix enables the body to replace damaged tissue. The secretion of collagen by fibroblasts after wounding acts as a framework for the migration of cells involved in replenishing the extra-cellular matrix and is an essential process in wound healing (Broughton et al., 2006). In wound tissue, there was no significant reduction in cross-linked collagen levels, as represented by Sirius red staining, between WT and DPP9-GKI heterozygous skin which is consistent with the wound closure rate data at Day 5. The percentage of positive staining of collagen was around 25% of total tissue area and reflects the lessened levels of collagen in early stages of wound repair.

Wounded skin also showed no significant difference in hydroxyproline content between WT and DPP9-GKI heterozygous skin. The amounts of hydroxyproline observed in wounded skin were only slightly reduced compared to those seen in steady-state skin which is contrary to the expected reduced level of collagen present in early wound healing. However, the harvest of wound tissue for assay included some surrounding healthy tissue, as well as wound tissue, and this may have increased the overall hydroxyproline levels. Careful excision of wound tissue to avoid surrounding steady-state tissue may overcome this and provide more accurate levels of hydroxyproline content.

In summary, detailed analyses of wounded skin showed no significant differences in skin strength or collagen content between DPP9-GKI heterozygous and wild-type controls. For wounded skin, clear conclusions cannot be made about skin tensile strength or collagen content differences between DPP9-GKI heterozygous skin and WT skin because of the confounding factor of scar formation and some inclusion of steady-state skin in harvest tissue. Future experiments should focus on examining greater numbers of wounds which will increase the statistical power of data and help to overcome the high variability between samples.

The overall analyses of adult mouse skin showed that skin in the steady state contains less collagen in DPP9-GKI heterozygous mice than in their WT littermates and WT C57BL/6J mice. When DPP9 is genetically altered, this may cause a reduction in early collagen deposition in developing skin, which results in reduced tensile strength and

collagen levels. This effect is likely via its enzymatic activity, as DPP9 intact protein is still present in heterozygous mouse skin, although some may be inactive.

Future studies could include investigation of collagen levels in DPP9-GKI embryos and/or neonates in skin and other organs. Also, if a specific DPP9 inhibitor becomes available, it may be possible to assess collagen levels in WT C57BL/6J mouse skin, with and without inhibitor administration to ascertain if the DPP9-GKI results can be emulated. Nevertheless, the suggestion of reduced collagen levels in DPP9-GKI heterozygous skin compared to WT skin in the steady-state condition is intriguing and the possibility that carrying the DPP9 S729A mutant allele affects the collagen content and integrity of DPP9-GKI heterozygous skin is worthy of further investigation

CHAPTER 6:

The role of DPP9 enzymatic activity in immune regeneration and function

6 *The role of DPP9 enzymatic activity in immune regeneration and function*

6.1 Introduction

DPP9 has been shown to have roles in both innate and adaptive immunity. DPP9 has extensive *in vivo* expression in immunological tissues (Yu et al., 2009) and leukocyte populations (Abbott et al., 2000b, Lankas et al., 2005, Maes et al., 2007, Bank et al., 2011, Chowdhury et al., 2013). DPP9 mRNA and protein is up-regulated *in vitro* in some cell lines upon B and T cell activation (Heimburg et al., 2008, Chowdhury et al., 2013). DPP9 has been shown to be involved in antigen presentation (Geiss-Friedlander et al., 2009) and activation and proliferation of immune cells may be affected by DPP9 enzymatic activity (Lankas et al., 2005, Reinhold et al., 2009, Waumans et al., 2015, Waumans et al., 2016) suggesting a role for DPP9 in the regulation of immune function.

The role of other dipeptidyl peptidases in recovery from irradiation and subsequent hematopoiesis have been studied and shown to have potential for therapeutic utility. Using irradiated DPP4-deficient mice or mice treated with an oral DPP4 inhibitor, hematopoiesis and engraftment can be enhanced while maintaining normal hematopoietic stem cell (HSC) function (Broxmeyer et al., 2012). The dipeptidyl peptidase inhibitor Val-boro-Pro, which inhibits DPP4, DPP8, DPP9 and FAP (Okondo et al., 2016), resulted in increased hematopoietic progenitor cell growth *in vivo* and up-regulation of erythrocyte and neutrophil regeneration in mouse models of acute

anemia (Jones et al., 2003). DPP4 has also been shown to be expressed on immune cells of both the myeloid and lymphoid lineages including activated NK cells, activated B cells, T cells and myeloid cells and the current knowledge of its interactions has been recently reviewed (Klemann et al., 2016).

Of possible clinical significance, FAP-positive mesenchymal stromal cells have been shown to be resistant to lethal levels of irradiation. While host HSCs are destroyed, the stromal cells survive, leaving them to support hematopoietic reconstitution along with donor HSCs (Sugrue et al., 2013). Despite these findings, there have been no studies examining the role of DPP9 in the regenerating immune system and/or whether the absence of DPP9 enzymatic activity can affect short term and long term repopulation of immune cells of the lymphoid or myeloid lineages.

This study aims to expand the current knowledge of DPP9 in immune regeneration by the creation of mouse chimeras using donor fetal liver cells or adult bone marrow cells injected into irradiated myelo-ablated recipient mice. As the DPP9$^{S729A/S729A}$ mice are neonate lethal but embryonically stable, it was necessary to use fetal liver tissue for the primary chimera creation to bypass this lethality.

In the mouse, HSCs migrate into the fetal liver between ED 11 and 12 where their numbers expand massively and the fetal liver becomes the main hematopoietic organ until birth (Ema and Nakauchi, 2000, Mikkola and Orkin, 2006). Although hematopoiesis in the liver is sustained throughout the first week after parturition, it is no longer a prime hematopoietic site, instead becoming the functional hub of metabolism. Between ED 13.5 and 14.5, the fetal liver contains a large number of

hematopoietic foci with erythropoiesis constituting a major part of their activity (Takeuchi and Miyajima, 2004) but myelopoiesis and lymphopoiesis are also occurring (Traver et al., 2001).

While it is technically challenging using fetal liver cells for transplantation, there is an advantage in that the regenerative capacity of fetal liver is much more effective than bone marrow for long term repopulation as the fetal liver HSCs are actively cycling (Harrison et al., 1997, Mikkola and Orkin, 2006). Additional to the increased effectiveness of fetal liver cells, the long-term reconstituting HSCs are up to seven fold more frequent in fetal liver than in adult bone marrow (Morrison et al., 1995). This can be important for the creation of a primary chimera as it reduces the chances of failure of hematopoietic cell reconstitution.

After transplant, the identification of the progeny of the transplanted HSCs is important to ascertain the effectiveness of the original graft and the properties of the regenerating immune system. The most common method used to achieve this is by the CD45 allelic model where the genetic differences between donor and recipient mouse strains of the pan-leukocyte antigen CD45 can be traced using specific markers and flow cytometry analysis (Spangrude, 2001, Gudmundsson et al., 2012, Wognum and Szilvassy, 2015). The DPP9 mouse strain has been raised on a C57BL/6 background which has the CD 45.2 allelic variant, therefore donor cells were transplanted into a congenic mouse strain expressing the CD 45.1 allele (Shen et al., 1985), thus enabling identification of donor and recipient cells for this experiment.

The establishment of a long-term detectable graft is dependent on the self-renewal activity of the original HSCs. Mouse HSCs have been shown to include at least three multipotent populations consisting of long-term (LT)-HSC, short-term (ST)-HSC and multipotent progenitor (MPP) cells. However, the MPP cell population has lost the self-renewal capacity of HSC and, therefore, engraftment can only be achieved with HSCs (Morrison and Weissman, 1994, Seita and Weissman, 2010). The mechanisms that determine whether self-renewal is stable or transient are under continuing investigation and refinement (Benveniste et al., 2010). While LT-HSCs are capable of

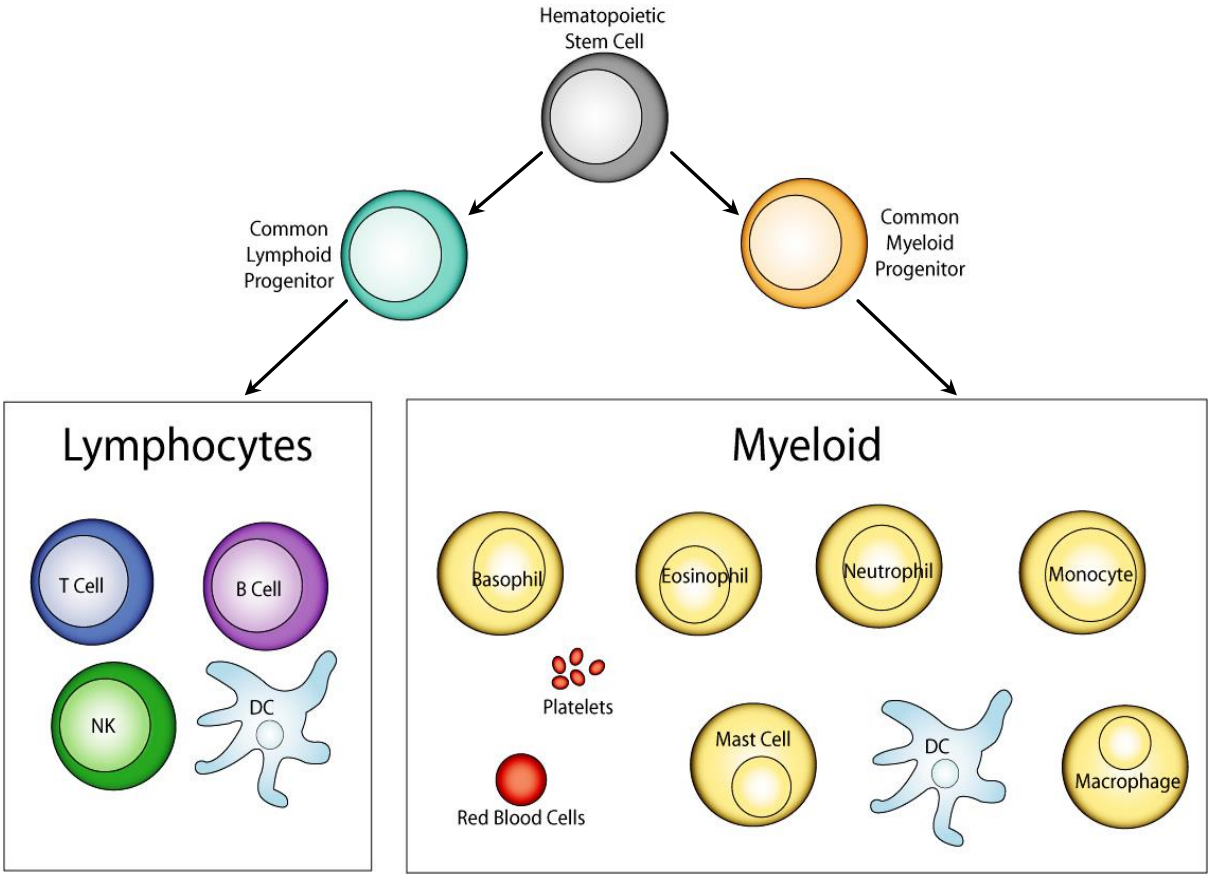

Figure 6.1: Diagram of the fate of hematopoietic stem cells in immune regeneration

Hematopoietic stem cells derived from fetal liver or adult bone marrow differentiate through lymphoid and myeloid cell lineages into a variety of cell types. Modified from (Tai et al., 2012)

self-renewal for life, ST-HSCs can self-renew for six to eight weeks and are known to give rise to the MPP population consisting of the common lymphoid (Kondo et al., 1997) and myeloid (Akashi et al., 2000) progenitors which subsequently result in the production of all cell types existing in the regenerated bone marrow and peripheral blood of the recipient mice (Figure 6.1) (Shizuru et al., 2005, Tai et al., 2012).

Donor-derived cells are detected in very low numbers at approximately two weeks after transplantation when chimerism is being established and are easily detectable by the 4 week time-point (Spangrude, 2001). The neutrophils and macrophages are the first cell types to recover after combined myelo-ablative irradiation and fetal liver or adult bone marrow cell transplant. They appear in the first few days after transplant followed closely by B cells. Platelets and red blood cell lineages then occur in the peripheral circulation at one to two weeks (Duran-Struuck and Dysko, 2009). As T cells are resistant to irradiation, surviving residual host T cells can be found within three weeks of transplant, while donor T cells do not usually appear in high numbers until 4 to 5 weeks after irradiation (Spangrude, 2001). Interestingly, at 4 to 6 weeks post-transplant, HSCs undergo a reprogramming 'switch' of many characteristics which results in a change in the gene expression pattern of the cells from fetal to adult genes (Bowie et al., 2007). The HSCs show less self-renewal and become more quiescent and this is similar to the situation that exists for endogenous HSCs in non-chimeric mice between birth and six weeks of age (Figure 6.2).

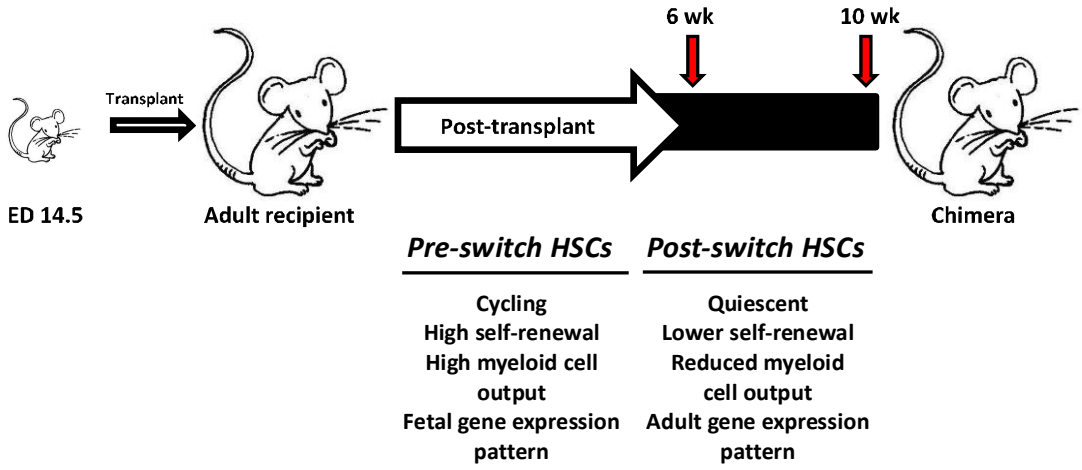

Figure 6.2: Diagram of programming of hematopoietic stem cells in immune regeneration

Hematopoietic stem cells, after the time-point at 4 to 6 weeks post irradiation, show a coordinated reprogramming of multiple key properties which mimic the endogenous HSC changes in non-chimeric mice at a similar time-point. These include a reduction in cell cycling, a lower self-renewal potential, a decrease in myeloid cell output and a transition from a fetal to adult gene expression profile. Modified from (Bowie et al., 2007)

Transplants carried out using adult bone marrow are not as effective as fetal liver for long-term cell repopulation since BM cells need to first overcome their quiescent status. Once they have entered the cell cycle, however, BM cells undergo the same cell cycle transit time as fetal liver cells (Bowie et al., 2007). In a comparable manner to fetal liver cell transplant, donor-derived cells from bone marrow transplant, such as monocytes and neutrophils, can be found in recipient mice in the first week and by the third week after transplant the peripheral reconstitution of all cell lineages may be

complete (Duran-Struuck and Dysko, 2009). However, as with fetal liver cell transplant, the functionality of the regenerated immune system at this early stage is not yet assured.

As previously stated, it was necessary for the primary chimera to use fetal liver cells for transplant to overcome the neonate lethality of DPP9-GKI mice. The secondary chimera could then be created using adult bone marrow from primary chimeric mice. Fetal liver or adult bone marrow cells carrying the DPP9 mutant allele that have been transplanted into wild-type mice would enable detection of the intrinsic effect of DPP9 deficiency on lymphoid and myeloid differentiation in a cell autonomous manner. Short term (30 to 60 days) and long-term (4 months) engraftment analysis would be expected to reveal whether DPP9 deficiency leads to defects in HSCs and/or hematopoietic progenitor cells.

A successful short- term primary engraftment can provide confirmation that the progenitor cell pool is intact and that all myeloid and lymphoid cell types are present and, in the long term, whether the reconstituted HSCs are functional (Auletta et al., 2004, Duran-Struuck and Dysko, 2009, Gudmundsson et al., 2012). However, even successful long-term engraftment in a primary transplant recipient may still have defects in self-renewal capability or the capacity for proliferation. It was therefore necessary to serially transplant the HSCs to overcome those issues. Hence, for this study, a secondary chimera was undertaken. Tertiary or even further serial transplants are often undertaken in chimera studies, however, any transplants after the secondary one undertaken were beyond the scope of the current work.

6.1.1 Aims

The aims of the work in this chapter are to explore the role of DPP9 in the regeneration and function of the mouse immune system by:

- creating chimeric mice via inoculation of irradiated PTPRC^{A} mice with either fetal liver cells or adult bone marrow cells of DPP9$^{S729A/S729A}$ and DPP9$^{wt/wt}$ genotype origin
- assessing the immune regeneration of irradiated chimeric mice by weight monitoring data and body scoring as an indicator of ongoing health and recovery
- assessing donor engraftment and the degree of chimerism of resultant chimeric mice by flow cytometry of peripheral blood samples at two time-points
- comparing cell types and percentages of regenerated immune cells in both primary and secondary chimeric mice to detect possible dysregulation of immune function in DPP9$^{S729A/S729A}$–origin chimeras.

6.2 Methods

Immune regeneration was studied using irradiated recipient mice inoculated to produce either primary or secondary chimeras. DPP9$^{S729A/S729A}$ pups die in the early neonatal period and cannot be used for the harvest of bone marrow cells. Therefore, primary chimeras were produced by inoculating irradiated mice with donor fetal liver cells retrieved from embryonic mouse livers at embryonic day (ED) 13.5 – ED 14.5. Secondary chimeras were produced by using regenerated donor bone marrow cells

from adult primary chimeric mice as the inoculum for a new batch of recipient mice. After the completion of the flow analysis of peripheral blood, the remaining mice were subjected to an immune challenge. The experimental plan is detailed in Figure 6.3.

6.2.1 Primary chimera methods

6.2.1.1 Timed mates for embryo production

Embryos required for fetal liver cells were obtained from pregnant females where pregnancy resulted from timed mating of DPP9$^{wt/S729A}$ intercrosses. Two days prior to mating, soiled male bedding was placed in female cages to stimulate ovulation (Whitten, 1956). For mating, single females were placed in the male home cage for a period of 12 h then checked for the presence of a vaginal plug as an indicator of mating prior to removal from the male cage. For the purposes of estimation of developing embryos, the time at which the female was separated from the male was assumed to be embryonic day (ED 0.5). Females were weighed at ED 0.5 to establish a baseline weight, then weighed daily from ED 4.5 until ED 13. Although most female mice increased their weight over this period, pregnancy was indicated if females displayed a noticeable increase in weight gain between ED 7.5 to ED 13.5 (Figure 6.4) (Mader et al., 2009).

This method was found to be very accurate at estimating pregnancy and often gave an indication of the number of embryos being carried.

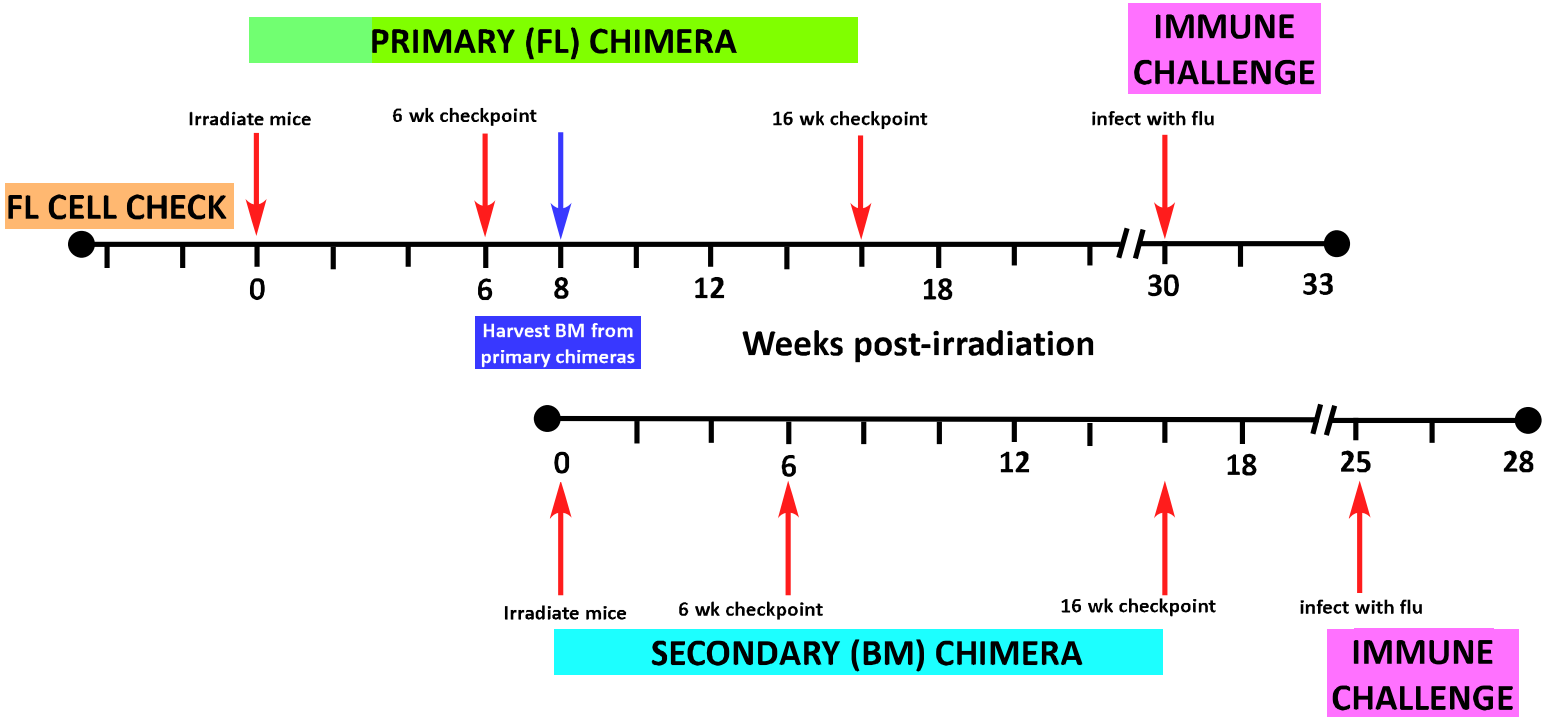

Figure 6.3: Experimental plan for investigating the role of DPP9 in immune regeneration.

Prior to irradiation of mice, fetal liver cells were accumulated for inoculation, genotyped and assessed for differences by flow cytometry analysis. Primary chimeras were created by tail vein injection of FL cells into irradiated mice. Flow cytometry analysis of peripheral blood was performed at 6and 16 weeks post-irradiation. At 8 weeks post-irradiation, bone marrow cells were harvested from four primary chimeric mice and used to create a secondary chimera. Both primary and secondary chimeric mice were subjected to an immune challenge by being infected with influenza for 21 days.

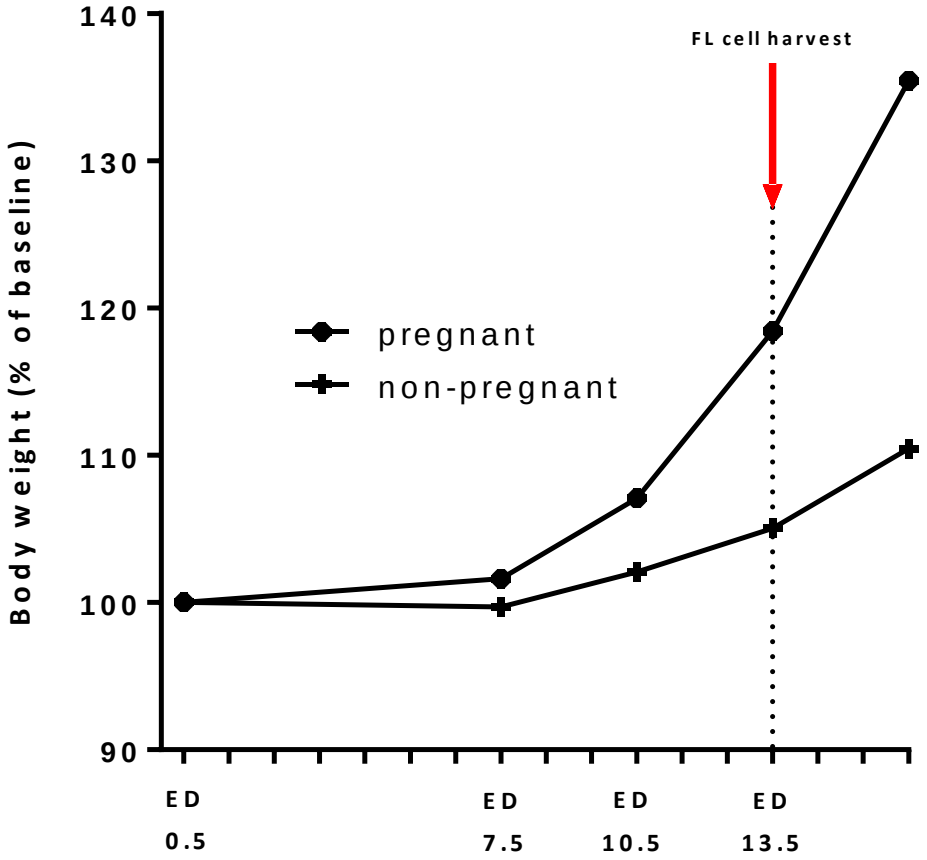

Figure 6.4: Graphical representation of body weight changes in female mice after 12 h timed exposure to males

Baseline body weight of female mice was measured immediately after separation from male mice in a 12 h timed mate and daily thereafter. An increase in body weight, as compared to the baseline weight, between day 7 and day 13 after timed mating was used to indicate pregnancy of female mice. This graph is a representation of the pattern of observed differences in weight gain (as a percentage of baseline weight) between pregnant and non-pregnant female mice.

6.2.1.2 Fetal liver cell harvest and storage

Only DPP9$^{S729A/S729A}$ or DPP9$^{wt/wt}$ fetal liver cells were used as donor cells for inoculation of irradiated mice, therefore it was necessary to isolate the liver cells and store them by freezing until genotyping results confirmed which samples were suitable for use in inoculation.

6.2.1.2.1 Isolation of fetal liver cells

Pregnant female DPP9$^{wt/S729A}$ were sacrificed at ED 13.5-14.5, uterine horns removed and individual embryos isolated under sterile conditions into 6-well plates containing liver cell (LC) buffer. The embryonic liver was carefully excised and placed on ice in a 1.5 ml Eppendorf tube containing LC buffer until processing. A small piece of embryonic tissue was retained separately for genotyping. Each liver was mashed through a 70 µm sieve using a rubber stopper and rinsed into a 50 ml Falcon tube containing 5-10 ml LC buffer. A 20 µl aliquot of cell suspension was retained for cell count and viability checks.

6.2.1.2.2 Freezing of fetal liver cells

The cell suspension was centrifuged at 2000 rpm for 5 min, supernatant removed and the pellet resuspended by gentle pipetting in 500 µl of RT freezing solution. A 100 µl aliquot of this suspension was transferred to a cryotube for flow cytometry analysis and the remaining cell suspension to a separate cryotube for injection of irradiated

mice. Both tubes were placed in an isopentane-cooled container at -80^{o} C overnight and then transferred into liquid nitrogen for deep storage until needed.

6.2.1.2.3 Thawing of fetal liver cells

Frozen aliquots of fetal liver cells were thawed for flow cytometry analysis or injection into irradiated mice. Each cryotube was swirled in lukewarm water to defrost the frozen pellet and the cell suspension transferred to a 15 ml Falcon tube containing 10 ml RT LC buffer. The cell suspension was centrifuged at 2000 rpm RT for 7 min, supernatant removed and the pellet resuspended in 10 ml RT LC buffer. After standing at RT for 30 min to release the maximum amount of DMSO, the cell suspension was centrifuged at 4^{o}C at 2000 rpm for 7 min.

For injection, the pellet was resuspended in 400 µl of Hank's balance salt solution (HBSS) and placed on ice. Cell suspensions were used to tail-vein inject two mice per sample at 200 µl per injection volume.

For flow cytometry analysis, the pellet was resuspended in 1 ml ACK/ RBC lysis solution, transferred to an Eppendorf tube, vortexed briefly and left on ice for 5 min. The cell suspension was then processed as described in Section 6.2.1.2.4 below.

6.2.1.3 Irradiation of recipient mice

In order to later identify the origin of immune cells and the degree of donor engraftment in peripheral blood cells, PTPRC^{A} mice were used as recipient mice for

immune regeneration studies. This C57BL/6 congenic strain is used widely in transplant studies because it carries the differential *Ptprc*^{a} pan leukocyte marker commonly known as CD45.1 or Ly5.1 (Shen et al., 1985), while DPP9-GKI mice have been bred on a C57BL/6 background and express the CD45.2 allele. Male mice were used as they are known to show enhanced recovery of platelets in response to irradiation (Billings et al., 2014) and their generally larger body weight also improves their ability to recover. Male mice can also be used as universal recipients in relation to possible immune responses due to the donor Y-chromosome and will accept either female or male donor grafts (Wang and Bunting, 2008). Before irradiation, all mice were weighed to provide a baseline weight.

Eighteen 10 week old male PTPRC^{A} mice received a myeloablative radiation using a Gammacell® 40 Exactor Low Dose-Rate Research Irradiator (MDS Nordion Inc.,Ontario, Canada). Two doses with a 600 rad exposure (at a dose rate of 110 rad per minute) were administered 4 h apart. After each dose, mice were returned to their home cage and provided water containing the antibiotic Amphoprim (Virbac, New Zealand) at a dose of 1ml per 50 ml water bottle. Antibiotic water was provided for 14 days post-irradiation and changed weekly.

6.2.1.4 Inoculation of recipient mice

After irradiation, mice were rested for 24 h before inoculation with fetal liver cells which were prepared as detailed in Section 6.2.1.2. The minimum number of cells required for fetal liver cell transplantation is 2 x 10^{5} (Gudmundsson et al., 2012) and

each fetal liver yields 6 -8 x 10^6 cells. For this experiment, cells from each fetal liver were used to inoculate two mice only with a non-competitive strategy (Figure 6.5), ensuring cell numbers greatly in excess of those needed. Nine mice were injected with DPP9$^{S729A/S729A}$-origin fetal liver cells which included four sets of replicate recipient mice (one donor liver per set) and one single recipient mouse. Similarly, nine mice were injected with DPP9$^{wt/wt}$-origin cells.

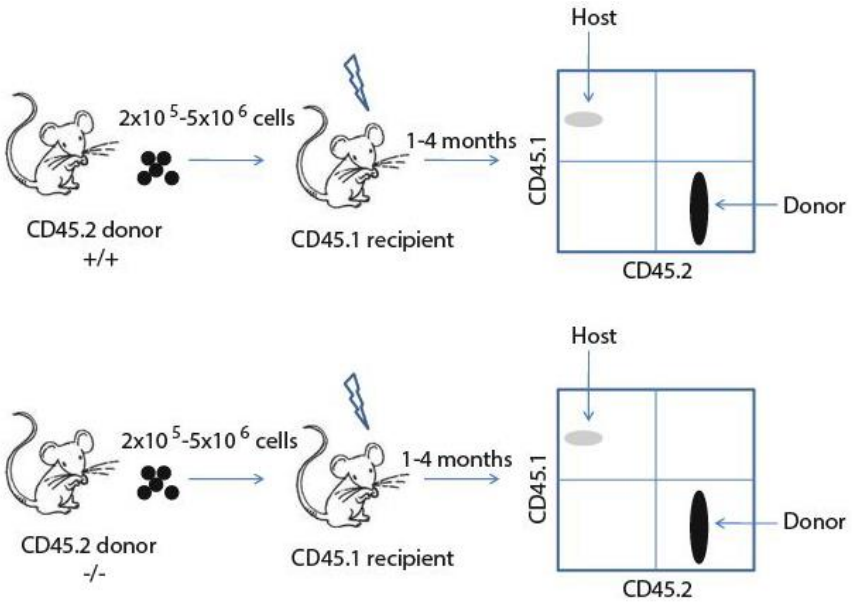

Figure 6.5: An example of a non-competitive strategy for transplanting fetal liver cells from a DPP9$^{wt/wt}$ (+/+) and a DPP9$^{S729A/S729A}$ (-/-) CD45.2 donor

Fetal liver cells can be transplanted into a lethally irradiated PTPRC^{A} (CD45.1) recipient and analysed for donor reconstitution 1-4 months post-transplantation. A CD45.1 x CD45.2 staining usually shows some CD45.1-positive cells (5-10%) due to residual HSC and progenitor cells contributing to hematopoiesis. Modified from (Gudmundsson et al., 2012).

After warming for several minutes under a heat lamp, mice were placed in a mouse restrainer and injected with a 200 µl volume of fetal liver cells in HBSS via the tail vein using a 25-gauge needle. All tail vein injections were carried out by Dr Adam Cook who has extensive experience in mouse handling and tail vein injection. Mice were observed for signs of distress or adverse reaction to injection for 10 min before being returned to their home cage.

6.2.1.5 Monitoring of irradiated mice

All mice were checked 2 – 3 h after inoculation for adverse effects. Mice were then weighed and monitored daily for 14 days post-irradiation. A body scoring system was used recording details for each mouse of posture, activity and gait, breathing, hydration, the presence of abnormal excreta, body condition and body weight as compared to the baseline weight. A weight loss of greater than 15 % compared to original weight was considered as necessary for euthanasia of the mouse.

After 2 weeks, antibiotic water was replaced with normal water. Mouse monitoring and weighing was reduced to twice weekly using the same scoring system as previously and continued until 6 weeks post-irradiation. At this point, it was undertaken weekly up until 16 weeks and termination of the experiment.

6.2.1.6 Flow cytometry of fetal liver cells

Flow cytometry analysis of aliquots of fetal liver cells was carried out to investigate

whether there was any difference between DPP9$^{S729A/S729A}$ and DPP9$^{wt/wt}$ fetal liver cells to be used for inoculation of irradiated mice to produce chimeras. Cell aliquots were thawed as described in Section 6.2.2.3 above. After initial RBC lysis, the cell suspension was centrifuged at 4^{o}C at 2000 rpm for 5 min, the supernatant aspirated off and the pellet resuspended in ACK/ RBC lysis solution as previously. Centrifugation and washing of the cell suspension was repeated twice as above and the cell pellet was resuspended in 200 µl of FACS wash each time. During the wash/spin steps, the stain cocktail was prepared as described in Section 6.2.2.5. After the final washing step, 100 µl of stain cocktail was added to each tube, the pellet resuspended by gentle pipetting and the tubes placed on ice in a covered container for 1 hr. Staining was followed by two repeats of centrifugation and resuspension of cells in 200 µl of FACS wash, then the cell suspensions were placed on ice until flow cytometry was carried out. Just prior to analysis, cells were filtered and DAPI was added [100 ng/ml]. Flow cytometry data were acquired using a BD LSRFortessa cytometer (BD Pharmingen) and subsequently analysed with FlowJo software (Treestar Inc., Ashland, OR, USA).

6.2.1.6.1 Preparation of stain cocktail

For the staining of fetal liver cells for flow analysis, the required fluorophore-conjugated antibodies were added to an appropriate volume of FACS wash in a non-transparent Eppendorf tube according to the number of samples and the chosen dilution, as detailed in Table 6.1. The stain cocktail was then centrifuged at maximum speed in a benchtop centrifuge at 4^{o}C for 30 min to remove aggregates of non-specific fluorophores that can contaminate the stain.

Table 6.1: Antibodies used in the fetal liver stain and their target cells.

Antibody	Synonym/clone	Target cell	Dilution used	Source: catalog #
FITC CD11b	M1/70	Myeloid cells	1:250	BD Biosciences #557396
APC TER-119	TER-119	Erythroid cells	1:250	BD Biosciences #557909

6.2.1.6.2 Gating strategy for flow analysis

Beginning at ED 10.5 and through until the end of gestation, the mouse fetal liver acts as the main hematopoietic organ (Chagraoui et al., 2003). The production of hematopoietic stem cells (HSC) peaks between ED 13 and 15 (Morrison et al., 1995). During this phase, the fetal liver predominantly reflects active erythropoiesis and myeloid and lymphoid progenitors increase at a later stage (Mikkola and Orkin, 2006). The antibody TER-119 is reactive with mouse hematopoietic cells with a high specificity for erythroid cells at all developmental stages and, between ED 13.5 – 14.5, the majority of HSC are TER-119 positive (Kina et al., 2000, Kim et al., 2006). CD11b is a non-erythroid lineage marker and positive HSC usually only occur in small numbers in mid-gestation in the mouse (Babovic and Eaves, 2014).

To compare whether the proportion of HSC present differed between DPP9$^{S729A/S729A}$ and DPP9$^{wt/wt}$ fetal liver cells to be used for inoculation, cells were stained with a simple stain panel using the markers TER-119 along with CD11b to define erythroid and myeloid cells respectively. Cells were gated to exclude RBC remaining after lysis and then gated to remove the contribution of cell doublets and dead cells. After this, the live cells were gated to identify the percentage of TER-119 positive and CD11b positive cells (Figure 6.6).

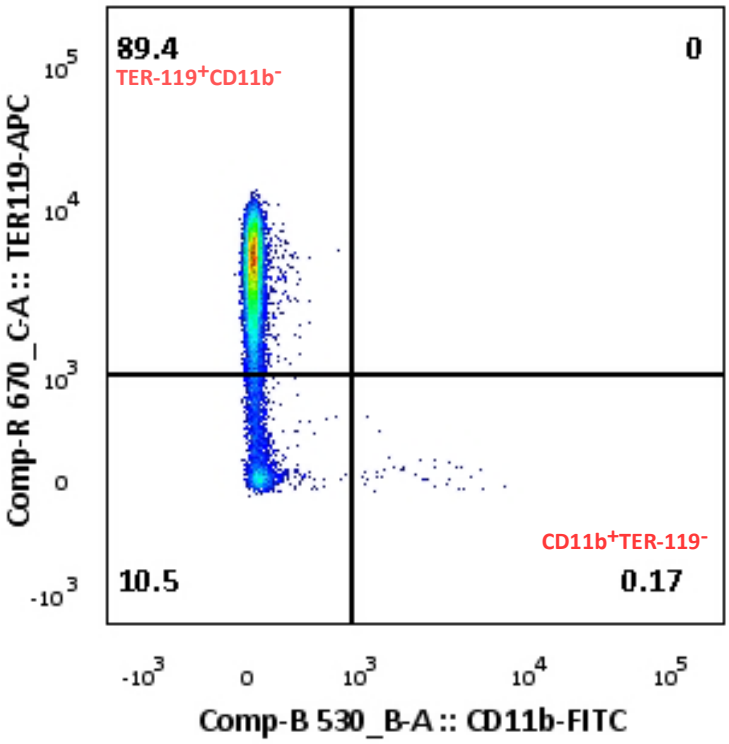

Figure 6.6: FACS plot showing a representative final gate for fetal liver cell percentage comparisons of data from DPP9$^{S729A/S729A}$ and DPP9$^{wt/wt}$ aliquots.

Panel shows the proportions of TER-119 and CD11b reactive cells after gating which excluded non-lysed RBC and isolated single cells and live cells. TER-119 positive cells indicate cells of the erythroid lineage while CD11b positive cells indicate cells of the myeloid lineage. This FACS plot is showing data from a WT aliquot.

6.2.2 Secondary chimera methods

Prior to the harvest of bone marrow cells, all primary chimeric mice were genotype checked using a sample of peripheral blood. This confirmed that all chimeric mice displayed a peripheral blood genotype consistent with that of the fetal liver cells used in their original inoculation. Two healthy DPP9$^{S729A/S729A}$ –origin chimeric mice were then selected who had shared a cage but whose chimeric state was produced with different original fetal liver cell batches. Similarly, two DPP9$^{wt/wt}$ –origin chimeric mice were chosen. These four mice were used to provide bone marrow for the secondary chimera, along with two control PTPRC^{A} mice used for competitor cells.

6.2.2.1 Isolation of bone marrow cells

Four PTPRC^{A} primary chimeric male mice (8 weeks post-irradiation) and two PTPRC^{A} non-chimeric male mice were used to harvest bone marrow cells for donor and competitor cells, respectively. Mice were sacrificed, pinned out belly up and swabbed with ethanol. After dissecting off the skin, the hind legs were removed and the femur, tibia and fibula separated and the muscle removed. The bones were then placed in a 5 ml yellow-cap tube containing 3-4 ml of clean 2% FCS in PBS on ice.

The tube contents were emptied into mortar and each bone was depressed with a pestle to crack and release bone marrow until the bones had no visible bone marrow and the buffer solution was pink. The supernatant was pipetted off and filtered through a 70 µm filter on top of 50 ml Falcon tube and several rinses carried out of the

mortar and filter to maximise the bone marrow cell yield. Tubes were centrifuged at 300 x g for 5 min at 4^{o}C and the supernatant carefully removed. The pellet was re-suspended in 10-20 ml buffer then refiltered through a 40 µm filter into a clean 50 ml Falcon tube with rinsing as before. Tubes were centrifuged at 300 x g for 5 min at 4^{o}C and the pellet re-suspended in 10 ml FCS buffer.

10 µl of cell suspension was removed from each tube, treated with 2% acetic acid in PBS to lyse RBC and Trypan Blue to identify dead cells. Leukocytes were then counted in triplicate using a haemocytometer. For bone marrow transplant, 10 x 10^6 cells per recipient mouse are needed and the yield of bone marrow cells from mouse hind leg bones is approximately 125-150 x 10^6 cells per mouse. Once the count was determined, the volume of cell suspension needed to provide enough cells for each inoculation was calculated and master mixes made up in 15 ml Falcon tubes. Tubes were centrifuged at 300 x g for 5 min at 4^{o}C and the each pellet was re-suspended in HBSS in a 1.5 ml Eppendorf tube at a volume of 200 µl per mouse for tail vein injection. Tubes were stored on ice until needed.

6.2.2.2 Irradiation of recipient mice

Mice were weighed to provide a baseline weight for monitoring before irradiation. Nineteen 10 week old male mice received a myeloablative radiation using a Gammacell® 40 Exactor Low Dose-Rate Research Irradiator (MDS Nordion Inc.,Ontario, Canada). One dose with a 750 rad exposure (at a dose rate of 110 rad per minute) was administered. Mice were then returned to their home cage and provided water

containing the antibiotic Amphoprim (Virbac, New Zealand) at a dose of 1ml per 50 ml water bottle. Antibiotic water was provided for 14 days post-irradiation and changed weekly.

6.2.2.3 Inoculation of recipient mice

For the secondary chimera studies, a competitive strategy of bone marrow cell transplant was used with primary chimera bone marrow cells (carrying the CD45.2 allele) as the donor cells and non-chimeric bone marrow cells from $PTPRC^{A}$ mice (carrying the CD45.1 allele) used as the competitor cells (Figure 6.7).

The ratio of donor to competitor cells was 2:3 respectively for this study, with cell numbers of 6.7 x 10^6 donor cells combined with 10 x 10^6 competitor cells per inoculation. For bone marrow cells, a minimum of 10 x 10^6 cells are suggested for transplant and, therefore, an excess of cells was injected into each mouse increasing the chance of successful reconstitution of the immune system of recipient mice.

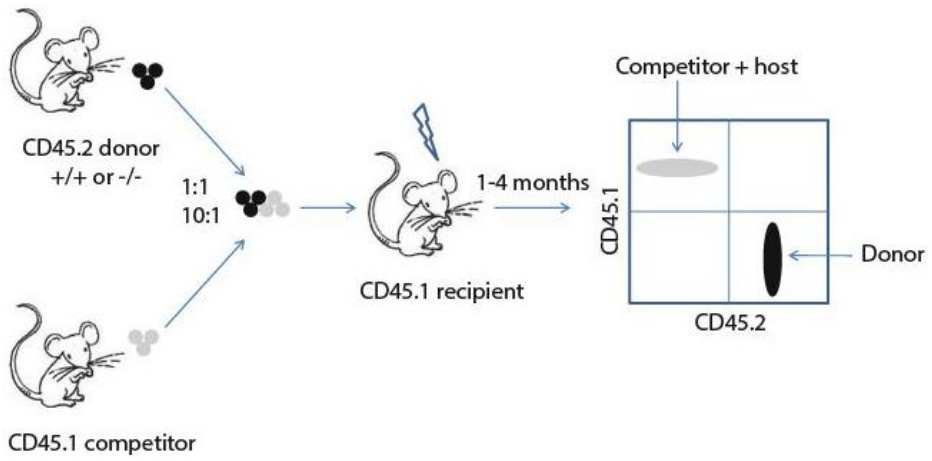

Figure 6.7: An example of a competitive strategy for transplanting adult bone marrow cells from DPP9$^{wt/wt}$ (+/+) and DPP9$^{S729A/S729A}$ (-/-) (CD45.2) donors with PTPRC^{A} (CD45.1) competitors

Bone marrow cells can be transplanted into a lethally irradiated PTPRC^{A} (CD45.1) recipient and analysed for donor reconstitution 1-4 months post-transplantation. Different combinations of donor and competitor cells can be mixed to test the function of CD45.2 HSC and progenitor cells. Modified from (Gudmundsson et al., 2012).

Four master mix tubes of donor plus competitor cells were used to inoculate the irradiated mice. Two tubes contained DPP9$^{S729A/S729A}$ –origin primary chimera BM cells sourced from two different mice and two contained DPP9$^{wt/wt}$-origin BM cells, also sourced from two different mice (as per Section 6.2.2.1). Each tube was used to inject five mice. Individual mice were injected with a 200 µl volume of bone marrow cells in HBSS as detailed in Section 6.2.1.3 by Dr Adam Cook and checked for adverse reactions as previously. Mice were monitored as described in Section 6.2.1.5.

6.2.3 Flow cytometry of peripheral blood from primary and secondary chimeras

At 6 weeks and 16 weeks post-irradiation, flow cytometry analysis of peripheral blood of both primary and secondary chimeric mice was carried out to assess the level of reconstitution of the immune system of irradiated mice and to obtain information on the development of the different hematopoietic lineages.

After warming for several minutes under a heat lamp, each mouse was placed in a mouse restrainer. 5-6 drops of blood was taken via the tail vein into an Eppendorf containing 50 µl 0.1M EDTA and the tubes were placed on ice. 1.2 ml ACK/RBC lysis solution was added and each tube vortexed vigorously for 5 s and left for 5 min for lysis to occur. After centrifuging at 1500 rpm at 4^0 C for 5 min, the pellet was re-suspended in 1 ml ACK/RBC lysis solution for 5 min for further lysis as before. Centrifugation was repeated and the pellet re-suspended in 200 µl FACS wash.

Further washing and staining of cells was carried out as described in Section 6.2.1.6 and using a stain cocktail prepared according to Section 6.2.1.6.1. with fluorophore-conjugated antibodies in Table 6.3.

6.2.3.1 Immune stain for flow cytometry of peripheral blood

For flow analysis of immune cells, a number of antibodies were used to broadly identify and compare different immune cell populations represented in a reconstituted immune system after irradiation (Table 6.2).

6.2.3.2 Gating strategies for peripheral blood flow analysis

For all flow cytometry analysis of peripheral blood from DPP9$^{S729A/S729A}$ –origin and DPP9$^{wt/wt}$-origin chimeric mice for both the primary and secondary chimera

Table 6.2: Antibodies used in the primary and secondary chimera peripheral blood cell stain and their target cells.

Antibody	Synonym/ clone	Target cell	Dilution used	Source: catalog #
BUV395 CD19	1D3	B cells	1:200	BD Biosciences #563557
BV421 CD3e	145-2C11	T cells, NK cells	1:250	BD Biosciences #562600
V500 CD45.2	104	Leukocytes	1:250	BD Biosciences #562129
FITC CD11b	M1/70	Myeloid cells	1:250	BD Biosciences #557396
PerCP-Cy5.5 CD45.1	A20	Leukocytes	1:250	eBioscience #45-0453
PE NK1.1	PK136	NK cells	1:250	BD Biosciences #557391
AF647 Ly6G	1A8	Myeloid cells, peripheral neutrophils	1:250	Biolegend #127610
APC.Cy7 CD8a	53-6.7	T cells	1:250	BD Biosciences #557654

experiment, the gating strategy to identify different cell types was the same. All samples were initially gated to exclude residual RBC remaining after RBC lysis was undertaken (Figure 6.8 A). Doublet cells, which result from cells adhering to each other or two cells passing through the laser in very close proximity, were excluded to leave single cells (Figure 6.8 B). The addition of DAPI to each sample before flow analysis was undertaken to exclude dead cells (Figure 6.8 C). The staining regime used here for peripheral blood flow analysis relied on the inclusion of the fluorophore BUV395 which bleeds into the DAPI channel. Therefore, a gating comparison between BUV395 and DAPI was used to identify live cells. While the contribution of autofluorescence in blood leukocytes is low, gating in empty channels, where there is no contribution from fluorophores in the stain cocktail, was used to exclude autofluoresence signals (Figure 6.8 D). Once preliminary gating steps A to D were completed, further analysis was undertaken to identify different cell populations.

Leukocyte cell populations were identified by gating for CD45 with donor cells carrying the CD45.2 allele and recipient cells the CD45.1 allele (Figure 6.8 E). Using only the donor leukocytes, myeloid cells were identified by their CD11b expression and T cells were included in the analysis by gating for $CD3e^{+}$ cells (Figure 6.9 A). Next, B cells which have a lymphoid lineage and are $CD19^{+}$ were gated along with neutrophils which have a myeloid lineage and high levels of Ly6G expression (Figure 6.9 B). Finally, natural killer (NK) cells were identified by first gating for CD3e and CD19 subsets and choosing the double negative population as NK cells are both CD3e and CD19 negative (Figure 6.10).

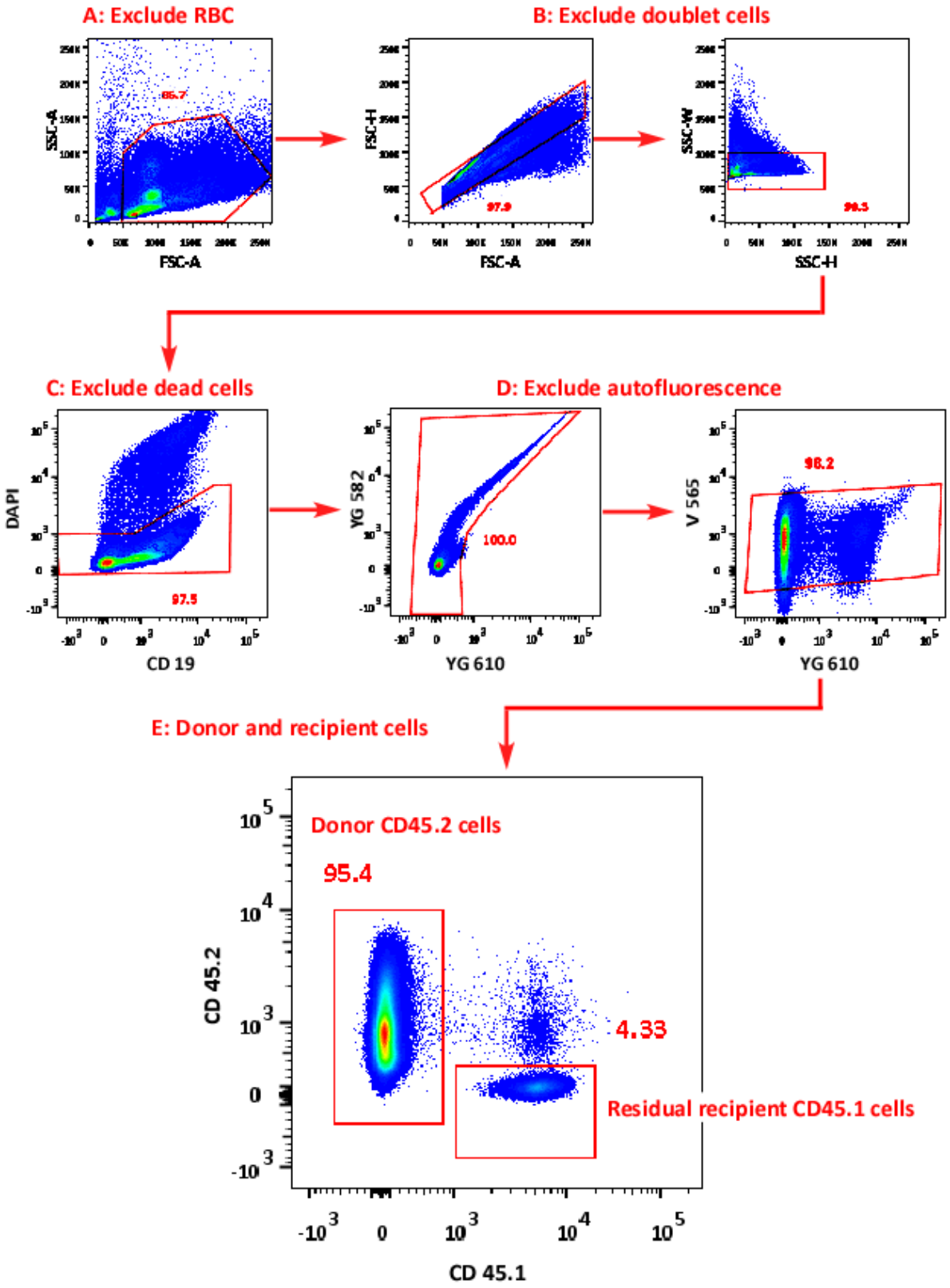
A: Exclude RBC
SSC-A
FSC-A
85.7
B: Exclude doublet cells
FSC-H
FSC-A
97.9
SSC-W
SSC-H
99.5
C: Exclude dead cells
DAPI
CD 19
97.5
D: Exclude autofluorescence
YG 582
YG 610
100.0
V 565
YG 610
98.2
E: Donor and recipient cells
Donor CD45.2 cells
95.4
4.33
Residual recipient CD45.1 cells
CD 45.2
CD 45.1

Figure 6.8: FACS plots showing the gating strategy for donor and recipient cell identification.

Panel A shows exclusion of residual red blood cells remaining after RBC lysis; panels B show the isolation of single cells. Live/dead cell gating is shown in panel C through DAPI staining and panels D shows gating to exclude non-specific staining due to autofluorescence. In panel E, CD45.2 positive donor cells are identified for further gating of immune cells. These are representative plots from DPP9$^{wt/wt}$-origin chimeric mouse peripheral blood harvested 6 weeks post irradiation.

Figure 6.9: FACS plots showing the gating strategy for immune cell identification of T cells and B cells along with neutrophils and other myeloid cells .

Following on from Figure 6.8, panel E, CD45.2 positive donor cells were identified for further gating of immune cells. The markers CD3e and CD11b were used to identify the general myeloid cell population and T cells. The markers Ly6G and CD19 were used to identify B cells and neutrophils. These are representative plots from DPP9$^{wt/wt}$-origin chimeric mouse peripheral blood harvested 6 weeks post irradiation.

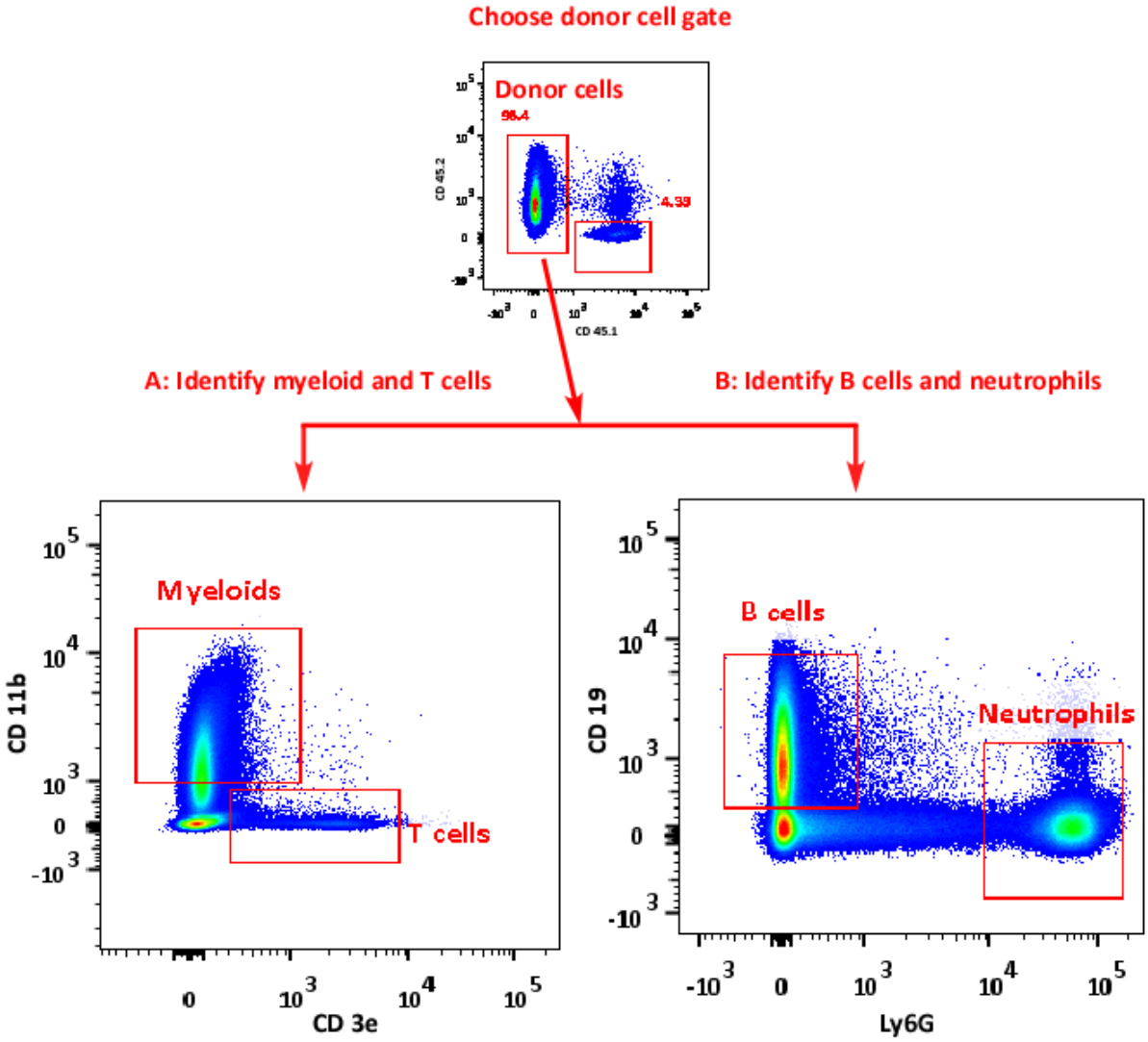

6.2.3.3 Data analysis

Flow cytometry data were analysed with FlowJo software and preliminary analysis carried out in Excel. Data were then graphed and analysed by unpaired t-test using GraphPad Prism and significance was assigned to *P* values less than 0.05.

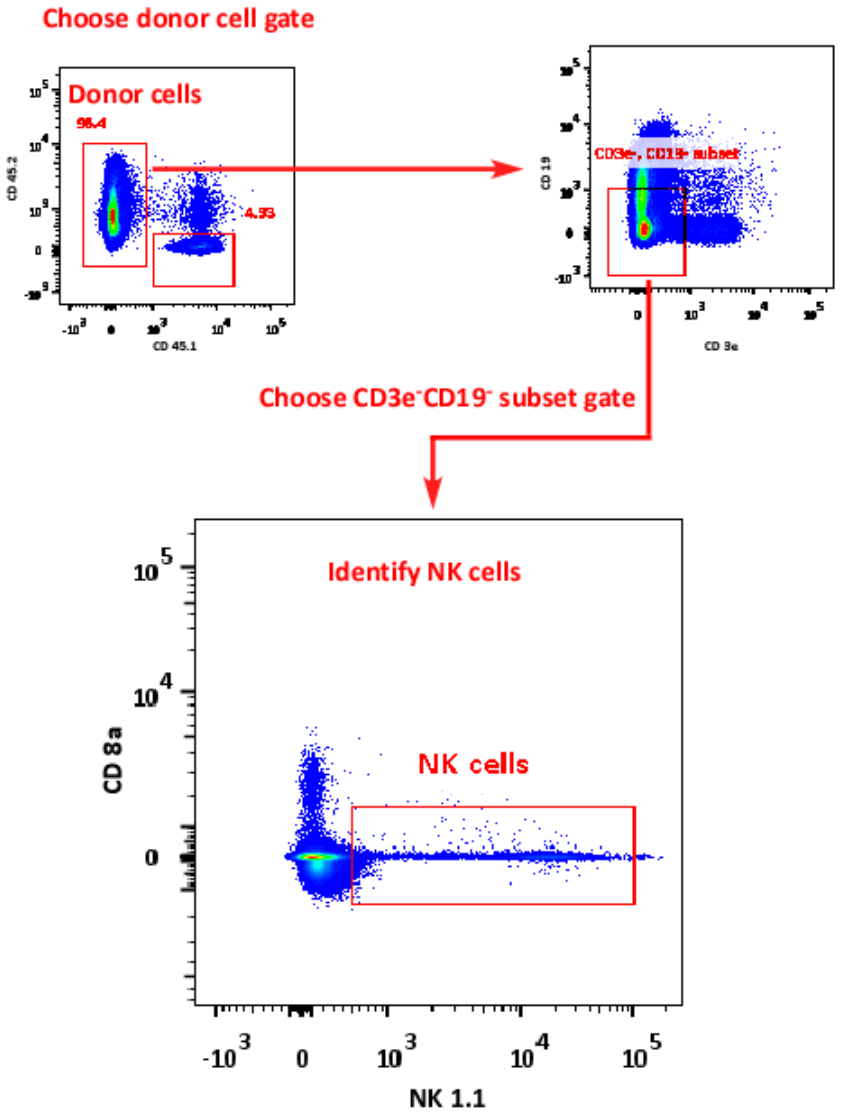

Figure 6.10: FACS plots showing the gating strategy for immune cell identification of NK cells .

Following on from Figure 6.8, panel E, CD45.2 positive donor cells were identified for further gating of immune cells. The markers CD3e and CD19 were used gate for the $CD3e^{-}CD19^{-}$ subset of cells which includes NK cells. The markers CD8a and NK1.1 were used to isolate the NK cell population. These are representative plots from $DPP9^{wt/wt}$-origin chimeric mouse peripheral blood harvested 6 weeks post irradiation.

6.2.4 Immune challenge flu study

In order to understand whether the reconstituted immune system has any functional alteration, mice from both primary and secondary chimera experiments were subjected to an immune challenge by infection with influenza. All influenza experiments were undertaken in collaboration with the Immune Imaging Lab of Centenary Institute by Dr Sioh-Yang Tan and Dr Lois Cavanagh with the assistance of Ms Lisa Shaw.

The first influenza experiment was carried out on primary chimera mice (14 male mice at 40 weeks of age) and the second on the secondary chimera mice (19 male mice at 35 weeks of age). Both experiments followed a similar experimental plan (Figure 6.11). Mice were anaesthetised by intraperitoneal injection of ketamine/xylazine (80/10 mg/kg) and inoculated intra-nasally with a sub-lethal dose of A/Puerto Rico/8/1934 (H1N1) [PR8] influenza virus. The doses were 50 pfu and 25 pfu in 30µl of sterile saline for the first and second experiment respectively. The virus suspension was placed drop-wise onto the nares using a sterile pipette tip.

Mice were then replaced in their home cages and kept warm by placing the cage on a heating pad. All mice were observed to ensure normal breathing patterns until they recovered from anaesthesia and resumed normal behavioural patterns. Infected mice were then weighed daily for 21 days commencing from day 2 after infection.

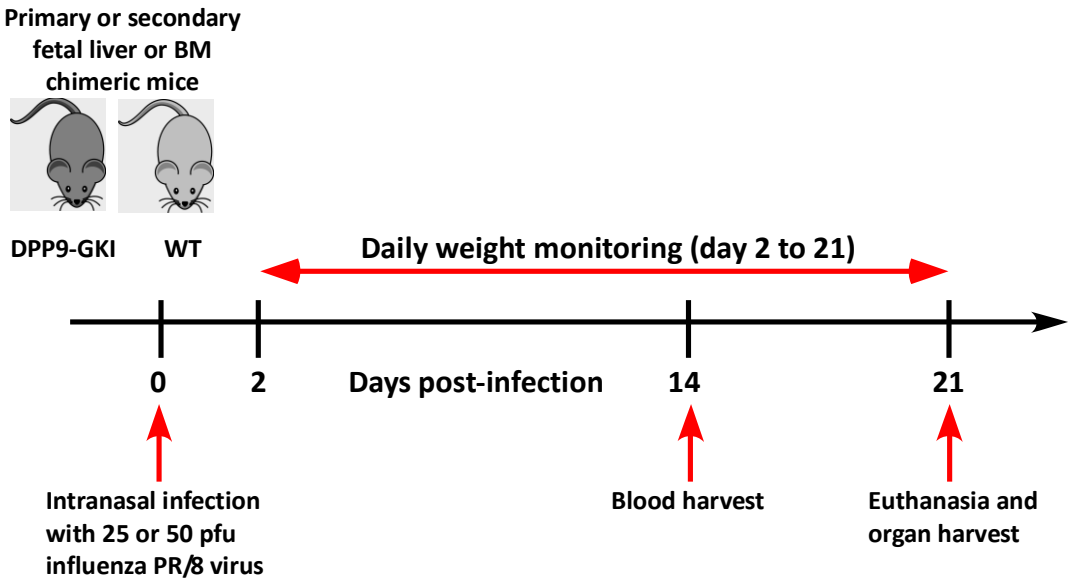

Figure 6.11: Experimental plan for the immune challenge of primary and secondary chimera mice

Two immune challenge experiments were undertaken with mice from the primary and secondary chimera experiments. Primary chimeric mice were infected with 50 pfu of [PR8] influenza virus and secondary mice with 25 pfu of [PR8] influenza virus. Daily weight data was collected to monitor the effect of flu infection on DPP9$^{S729A/S729A}$ –origin and DPP9$^{wt/wt}$-origin chimeras.

6.3 Results

6.3.1 Fetal liver cell flow analysis

As the survival of irradiated mice with ablated immune systems is usually dependent on the reconstitution of immune cells, it is an important consideration whether the initial cell inoculum is viable and contains the hematopoietic stem cells necessary for immune regeneration. The fetal liver cells harvested from DPP9$^{S729A/S729A}$ and DPP9$^{wt/wt}$ embryos at ED 13.5 – 14.5 were stained using markers for erythroid and myeloid lineage HSCs. At this developmental stage the majority of HSCs are of the erythroid lineage as indicated by TER-119 reactivity (Kina et al., 2000, Kim et al., 2006) and only a very small proportion show the CD11b positivity of non-erythroid lineage cells (Babovic and Eaves, 2014). The predominance of TER-119 positive cells was confirmed in the flow analysis of DPP9 fetal liver cells and no statistical difference was noted between DPP9$^{S729A/S729A}$ and DPP9$^{wt/wt}$ cells for either cell lineage (Figure 6.12), thus suggesting that the inoculum used for creation of the primary chimeras was potentially equally viable for both DPP9$^{S729A/S729A}$ and DPP9$^{wt/wt}$ test groups.

6.3.2 Primary chimera results

As stated previously, the creation of chimeras enables detection of dysregulation of hematopoietic and/or immune function in irradiated mice by consideration of weight monitoring and body scoring. It also shows the short-term and long-term engraftment success of immune regeneration by the use of peripheral blood flow cytometry analysis.

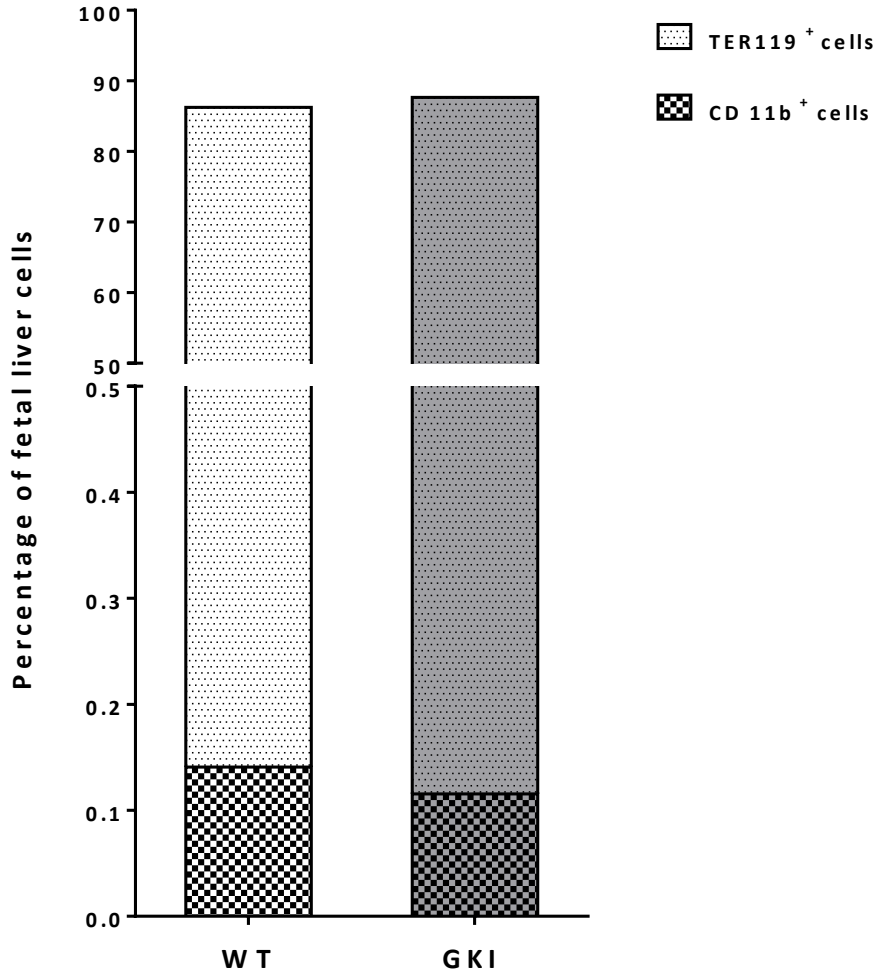

Figure 6.12: Percentage of TER119^{+} and CD 11b^{+} fetal liver cells prepared for inoculation of irradiated mice

DPP9$^{S729A/S729A}$ and DPP9$^{wt/wt}$ fetal liver cells were used to inoculate irradiated mice via tail vein injection in order to reconstitute the immune system after ablation. Flow cytometry analysis of the markers TER-119 and CD 11b were used to indicate fetal liver cells of the erythroid lineage and the myeloid lineage respectively. No statistically significant difference was observed between the percentages of DPP9-GKI and WT cells in the inoculum aliquots for either cell lineage.

6.3.2.1 Weight change data

Mice were monitored as described in Section 6.2.1.5 daily for 2 weeks post-irradiation and then twice weekly for the remaining weeks for signs of failure of immune regeneration. This was achieved by body scoring and weight monitoring. An initial weight loss is a normal consequence of total body irradiation (Duran-Struuck and Dysko, 2009), however losses of 20% or greater are usually an indicator of graft failure. Both the group inoculated with DPP9$^{S729A/S729A}$ fetal liver cells and the group inoculated with and DPP9$^{wt/wt}$ FL cells followed a similar pattern of weight loss and gain (Figure 6.13) and no significant difference was observed for either mean weight of each group (Figure 6.13A) or mean percentage weight change per group (Figure 6.13B) throughout the experimental period. This indicated that the fetal liver cell grafts were successful at establishing immune reconstitution and no apparent functional difference existed between the HSCs from either fetal liver DPP9 genotype.

6.3.2.2 Immune regeneration of primary chimeric mice

The use of congenic PTPC^{A} mice as irradiated recipients for the graft of fetal liver cells enabled later identification of the proportion of donor cells which survived engraftment using flow cytometry of peripheral blood samples. For this experiment, a lethal myeloablative dose of irradiation was received by the recipient mice which results in the presence of very small numbers of residual recipient immune cells after immune regeneration.

6.3.2.2.1 Donor cell survival and degree of chimerism in primary chimeric mice

The proportion of residual recipient (CD 45.1^{+}) cells present at 6 weeks post-irradiation for this experiment was less than 7% of total peripheral blood leukocytes (Figure 6.14), which is consistent with previous studies by others for successful HSC grafts. This result suggests that the donor cells survived the engraftment procedure and that the inoculum had a sufficient donor graft to ensure hematopoietic cell reconstitution.

At 16 weeks post-irradiation, the residual recipient cells had dropped to ~2% showing a strong long term engraftment by the donor (CD 45.2^{+}) cells and confirming their initial viability. This result was the same for both DPP9$^{S729A/S729A}$ and DPP9$^{wt/wt}$ donor cells with no statistical difference seen between the two groups at either time-point. Thus, fetal liver cells carrying the DPP9-GKI mutant allele were not impaired in their ability to engraft.

Figure 6.13: Weight monitoring post-irradiation of primary chimeric mice

Irradiated mice inoculated with DPP9$^{S729A/S729A}$ and DPP9$^{wt/wt}$ fetal liver cells were monitored for weight loss as a gross indicator of dysfunctional or failed immune regeneration. Both GKI and WT cell-origin groups displayed an initial weight loss for several days before gradual weight increase back to the original start weight at around 4 – 5 weeks post-irradiation. Graphs are represented as (**A**) the mean actual weights per mouse group and (**B**) the mean percentage weight change per group where 0 (red dotted line) represents the start weight just prior to irradiation. Each mean value consists of weights measurements of 7 mice for both groups.

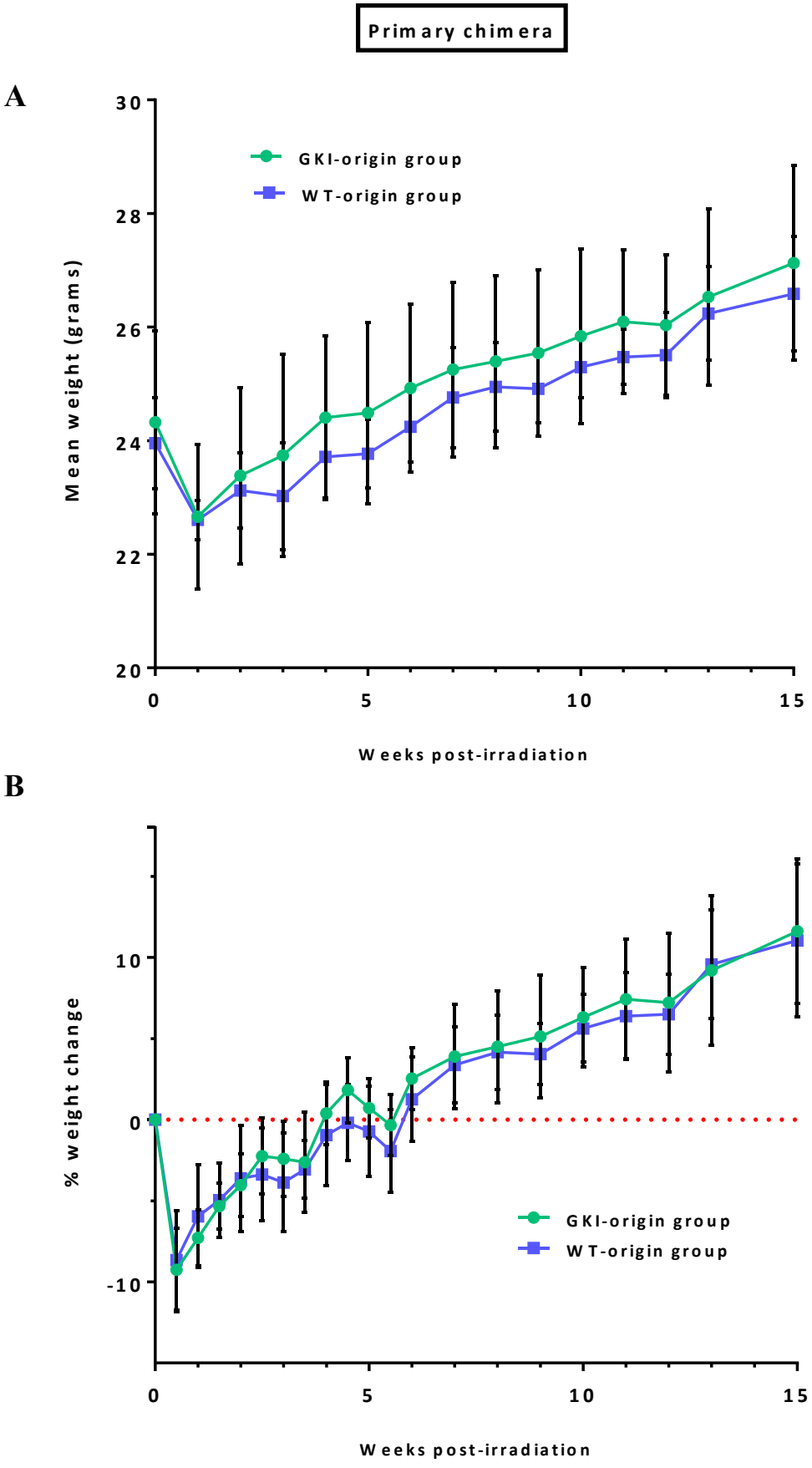
Primary chimera
A
30
28
26
24
22
20
Mean weight (grams)
GKI-origin group
WT-origin group
0
5
10
15
Weeks post-irradiation
B
10
0
-10
% weight change
GKI-origin group
WT-origin group
0
5
10
15
Weeks post-irradiation

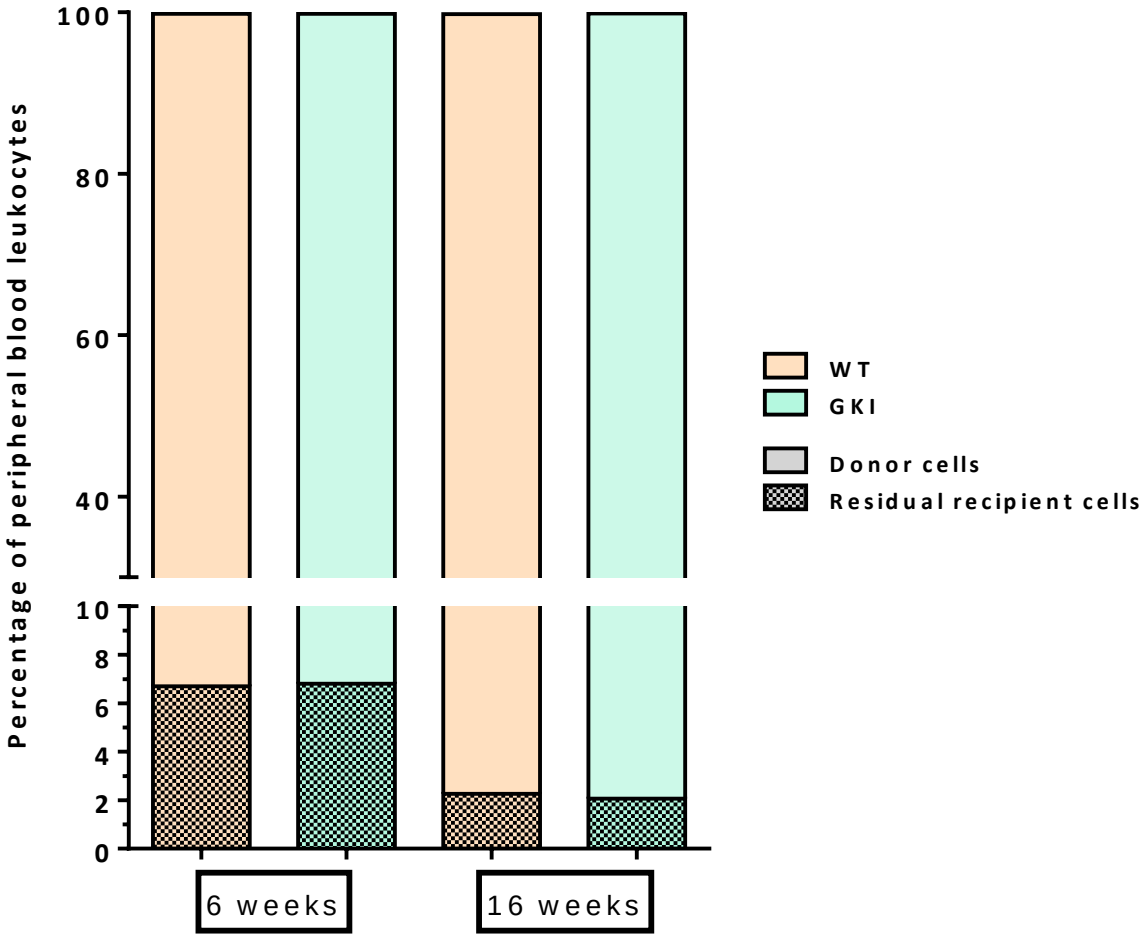

Figure 6.14: Proportion of donor and residual recipient cells of primary chimeric mice

Irradiated mice inoculated with DPP9$^{S729A/S729A}$ and DPP9$^{wt/wt}$ fetal liver cells were assessed for the percentage of donor cell-origin and residual recipient cell-origin leukocytes at six and 16 weeks after irradiation of the recipient mice. Both GKI and WT cell-origin groups displayed a small percentage of residual recipient cells at six weeks post-irradiation which decreased at 16 weeks post-irradiation. Graphs are represented as mean percentages where n = 9 at the 6 week time-point and n = 7 at the 16 week time-point.

6.3.2.2.2 Identification of myeloid and lymphoid cell types in primary chimeric mice

To determine the development and repopulation of the different hematopoietic lineages, peripheral blood was taken at two different time-points of 6 weeks and 16 weeks as representative analysis of short term and long term immune regeneration respectively. Comparison of the major cell types of innate immunity including neutrophils and other myeloid cells of the myeloid lineage and B cells, T cells and NK cells of the lymphoid lineage, provide insight into the effectiveness of the chimera and identify any dysregulation of specific cell types and lineages. For this analysis, the assumption was made that the WT-origin chimeras have a normal reconstitution after irradiation and, thus, these data can be used as a benchmark to detect any differences in the GKI-origin chimeras. Comparisons can also be made with normal peripheral blood leukocyte data for C57BL/6 mice (Chen and Harrison, 2002). In this way, the impact of the absence of DPP9 enzymatic activity on the immune system can be gauged.

Cells of the myeloid lineage include basophils, eosinophils, monocytes, macrophages and neutrophils. At 6 weeks post-transplant, the total myeloid cells present are elevated (Figure 6.15) consistent with an initial inflammatory response to irradiation (van der Meeren et al., 2001, Duran-Struuck and Dysko, 2009). Neutrophils normally represent the largest percentage of myeloid cells, making up at least 50 – 60 %. This is also the case for the primary chimera where the proportion of total myeloid cells which are neutrophils is in this range for both the 6 week and 16 week time-point (Figure 6.15). There was no significant difference observed between the GKI and WT

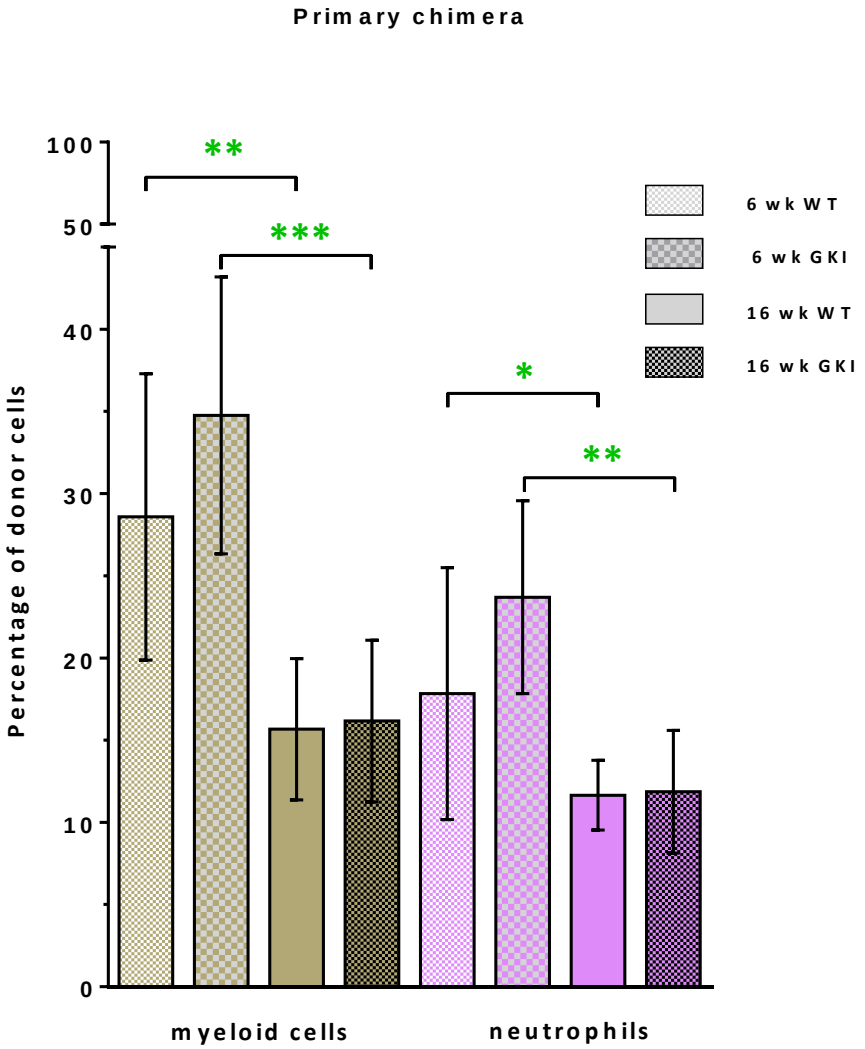

Figure 6.15: Percentage of myeloid cell types in peripheral blood of primary chimeric mice

Mice from the primary chimera were assessed by flow cytometry of peripheral blood for the percentage of total myeloid and neutrophil leukocytes at six and 16 weeks after irradiation. There was no difference observed between GKI-origin groups compared to WT-origin groups. There were significant differences between the 6 and 16 week time-points (green asterisks) for cell types from this lineage with a decrease in myeloid and neutrophils cells at the 16 week time-point. Graphs are represented as mean percentages where n = 9 at the 6 week time-point and n = 7 at the 16 week time-point. Error bars denote SD and significance was assigned where $p < 0.05$ (*), $p < 0.01$ (**), $p < 0.001$ (***).

cell-origin groups in the peripheral blood analysis for either time-point for both total myeloid cells or neutrophils suggesting that carrying the mutant DPP9 allele does not affect hematopoietic regeneration in the primary chimeric mice.

There is, however, a highly significant decrease in myeloid cells for both genotype-origin groups between the six week and the 16 week time-points (Figure 6.15, green asterisks). As this decrease is similarly represented in the groups of both genotype-origin cells, it is consistent with this being a normal change which occurs from short-term to long-term regeneration after irradiation and donor engraftment. This finding is supported by studies undertaken by others where myeloid cells, especially neutrophils and macrophages, are found to dominate early after engraftment (Spangrude, 2001, Bowie et al., 2007). Also, after 5 to 6 weeks post-irradiation, a change in HSC programming results in a reduced myeloid cell output (Figure 6.2)(Bowie et al., 2007). By 16 weeks, myeloid cell levels are comparable to those found in normal mouse peripheral blood (Chen and Harrison, 2002).

Lymphoid lineage cells are represented in this analysis by B, T and NK cells. After engraftment, these cells arise via a common lymphoid progenitor that can only give rise to B, T and NK cells while lacking myeloid differentiation capability (Kondo et al., 1997). NK cells, which contribute to the early detection of virus-infected and cancer cells, are important for defense against pathogens and regain normal cell numbers and function within a month of transplantation (Awwad, 1990, Auletta et al., 2004, Sungur and Murphy, 2014). In the primary chimera, no significant difference was observed between the different genotype-origin groups or between different regeneration time-

points (Figure 6.16), suggesting that, once re-established in the peripheral blood, NK cell numbers remain stable.

B cells exist as two main populations of B lymphocytes known as B-1 and B-2 B cells and are part of the innate and adaptive immune systems respectively (Montecino-Rodriguez and Dorshkind, 2012). These two populations display different functional roles and show variable levels of activity and regenerative capacity depending on the mouse developmental stage from which the cells are sourced (Ghosn et al., 2016). For the purpose of this study, total B cell populations were observed without individual identification of B cell subpopulations or subsets. As B cell reappearance after irradiation is an early event occurring in the first few days after engraftment, the percentage of B cells amongst the total lymphoid donor cells was expected to have reached a stable level by 6 weeks post irradiation. This was the case for peripheral blood of the primary chimeric mice, although there was a small but statistically significant reduction observed in the B cells present in the GKI-origin groups compared to WT-origin groups at the six week time-point (Figure 6.16). This may represent a small delay in the re-establishment of B cells in the GKI-origin chimeric mice or, as the deficit was only small, perhaps arise as a result of the range of variation in B cell numbers between mice in the flow cytometry analysis. By 16 weeks post-irradiation, however, the B cell numbers for both genotype-origin groups of mice are matched, with the GKI-origin B cell numbers recovering to the WT level (Figure 6.15) and consistent with normal peripheral blood B cell percentages (Chen and Harrison, 2002).

T cells, which augment the adaptive immune response, do not recover after irradiation and transplant by replication of the usual cellular developmental pathways. T cell subset ratios are skewed in the early period after engraftment (Auletta and Lazarus, 2005). Residual T cells of host origin, which are the most resistant to irradiation, may be apparent within the first three weeks but donor-derived T cells take 4 to 5 weeks after transplant to appear (Spangrude, 2001). Since the primary chimeric mice received a lethal level of myelo-ablative radiation, residual host T cells would be expected to be at minimum levels and, hence, contribute very little to total T cell numbers. This is supported by the low percentages of donor T cells at the 6 week time-point (Figure 6.16). While no significant differences are seen between WT-origin and GKI-origin groups, there is a significant increase in T cell numbers between the 6 week and 16 week time-points consistent with the recovery of T cell numbers after initial depletion. As T cells comprise roughly 20% of blood leukocytes in normal peripheral blood (Chen and Harrison, 2002), it appears that full reconstitution of the T cell complement has not yet been attained at this time-point.

Considering the overall peripheral blood leukocytes of both myeloid and lymphoid lineages (Figure 6.17), the trend in the primary chimeric mice from the 6 week to the 16 week time-points seems to be from a lower to a higher lymphoid-biased output. This is consistent with a move from unlimited self-renewal ability of HSCs towards limited self-renewal ability as the regenerated immune system moves from short term to long term reconstitution (Kent et al., 2009). Also of note in Figure 6.17, the total percentage of donor blood leukocytes for all cell types sits at approximately 93%. The appearance of a shortfall below 100% is most likely due to the method of analysing the

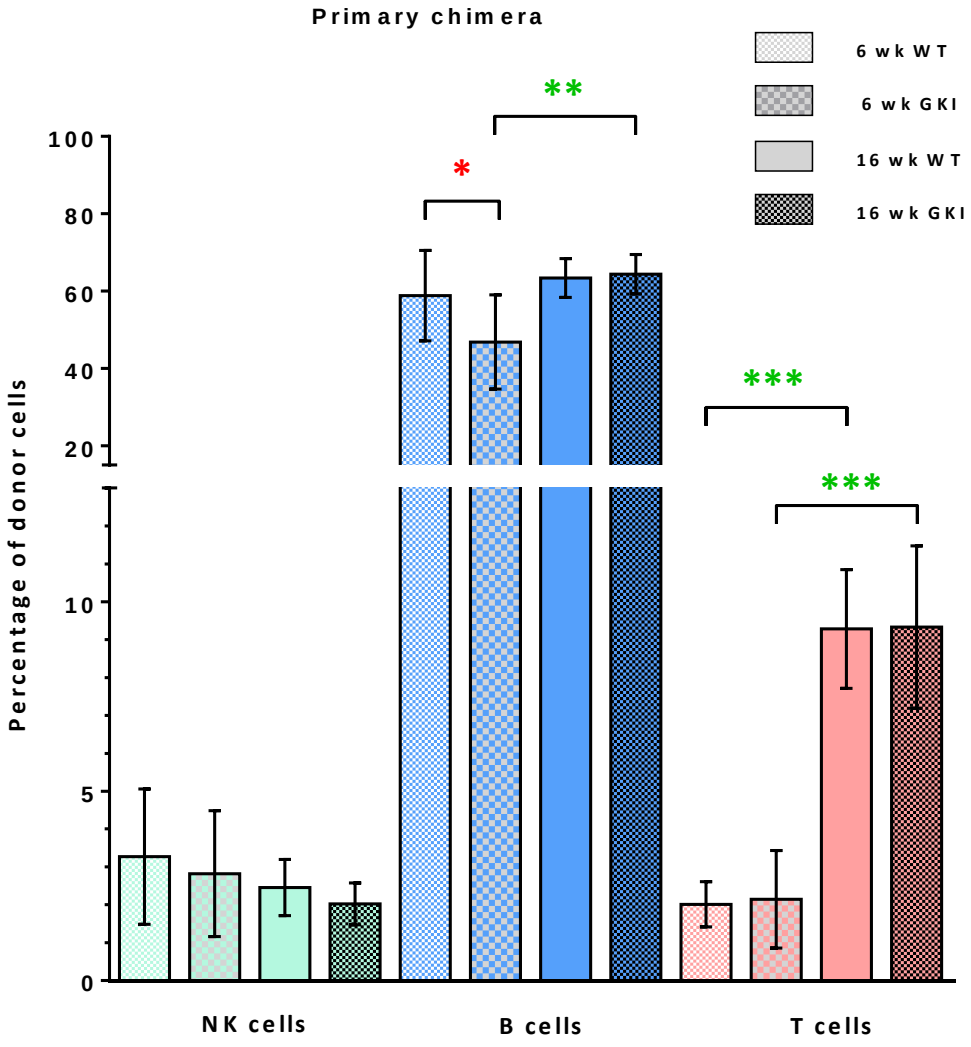

Figure 6.16: Percentage of lymphoid cell types in peripheral blood of primary chimeric mice

Mice from the primary chimera were assessed by flow cytometry of peripheral blood for the percentage of lymphoid lineage leukocytes at six and 16 weeks after irradiation. There was a significant decrease of B cells (red asterisk) at six weeks post-irradiation in GKI-origin groups compared to WT-origin groups. However, no difference was observed for any other cell type between genotype-origin groups. There were significant differences between the 6 and 16 week time-points with an increase in B cells for the GKI-origin cells and T cells for both groups at the 16 week time-point (green asterisks). Graphs are represented as mean percentages where n = 9 at the 6 week time-point and n = 7 at the 16 week time-point. Error bars denote SD and significance was assigned where $p < 0.05$ (*), $p < 0.01$ (**), $p < 0.001$ (***).

donor cells, in which only major myeloid and lymphoid cell markers were included. The placement of gates for analysis and the univariate analysis used in the FlowJo software may also have contributed to that shortfall.

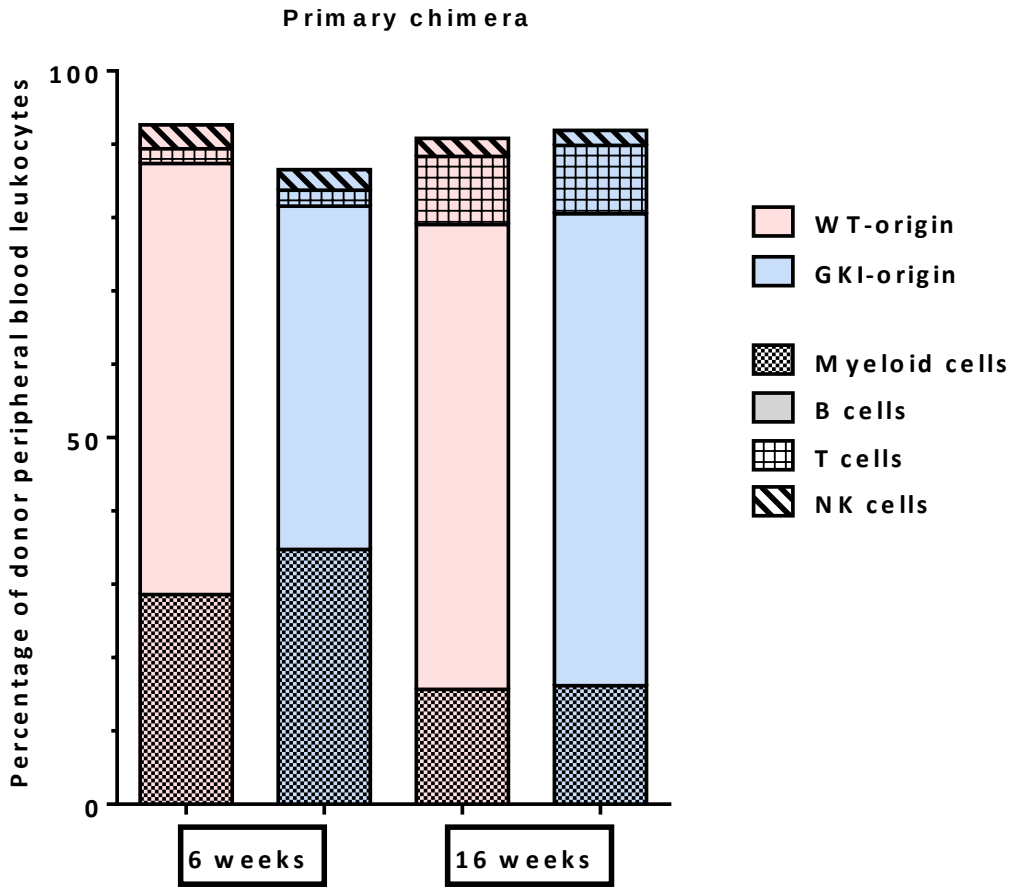

Figure 6.17: Total donor peripheral blood leukocytes of primary chimeric mice

This graph represents the cell type analysis of total peripheral blood leukocytes of donor-origin at six and 16 weeks after irradiation and fetal liver transplant. From six weeks to 16 weeks, both WT-origin and GKI-origin groups show an increased bias towards lymphoid lineage cells which is suggestive of increased limits in self-renewal capacity of HSCs as the new immune system establishes itself.

6.3.3 Secondary chimera results

The secondary chimera experiment was carried out using bone marrow cells from primary chimeric mice as donor cells along with BM cells from congenic $PTPRC^{A}$ mice as competitor cells. These were transplanted into irradiated congenic $PTPRC^{A}$ mice. As the result of the secondary engraftment was unknown before commencement of the experiment, competitor cells were used in the transplant to ensure successful cellular engraftment, immune regeneration and survival of the recipient mice (Duran-Struuck and Dysko, 2009). While the primary chimera can provide information on the integrity of the progenitor pool and the functionality of HSC, serial transplantation into secondary recipients can help identify potential defects in HSC self-renewal capacity and their potential for expansion (Gudmundsson et al., 2012).

6.3.3.1 Weight change data

Mice were monitored throughout the period of the experiment as described for the primary chimera study. While both mouse groups receiving the $DPP9^{S729A/S729A}$-origin and $DPP9^{wt/wt}$-origin primary chimeric mouse BM cells showed a similar pattern of weight loss and gain throughout 13 weeks of weight monitoring (Figure 6.18A), there was a noticeable difference in start weight between the two groups with heavier recipient mice inoculated with GKI-origin BM cells. Unfortunately, these mice were used for the study in the cage groups provided by the supplier and this discrepancy was not detected until the study was underway.

Despite the difference in mean start weight, both the mouse groups receiving the DPP9$^{S729A/S729A}$-origin and DPP9$^{wt/wt}$-origin primary chimeric mouse BM cells showed no significant difference in mean percentage weight change for the study period (Figure 6.18B). As with the primary chimera, this was indicative of a successful immune reconstitution in

the secondary recipient mice. Return to start weight after initial weight loss was achieved in a much shorter time frame (around 2 weeks post irradiation) than for the primary chimeric mice (4 -5 weeks post irradiation). This is consistent with the sub-lethal irradiation dose administered to the secondary mice whereas the primary mice received a higher lethal myelo-ablative treatment.

Figure 6.18: Weight monitoring post-irradiation of secondary chimeric mice

Irradiated mice inoculated with DPP9$^{S729A/S729A}$ or DPP9$^{wt/wt}$ bone marrow cells along with PTPRC^{A} WT BM cells were monitored for weight loss as a gross indicator of dysfunctional or failed immune regeneration. Both GKI and WT cell-origin groups displayed an initial weight loss for several days before gradual weight increase back to the original start weight at around 2 weeks post-irradiation. Graphs are represented as (**A**) the mean actual weights per mouse group and (**B**) the mean percentage weight change per group where 0 (red dotted line) represents the start weight just prior to irradiation. Each mean value consists of weights measurements of 9 mice for the WT-origin group and 10 mice for the GKI-origin group.

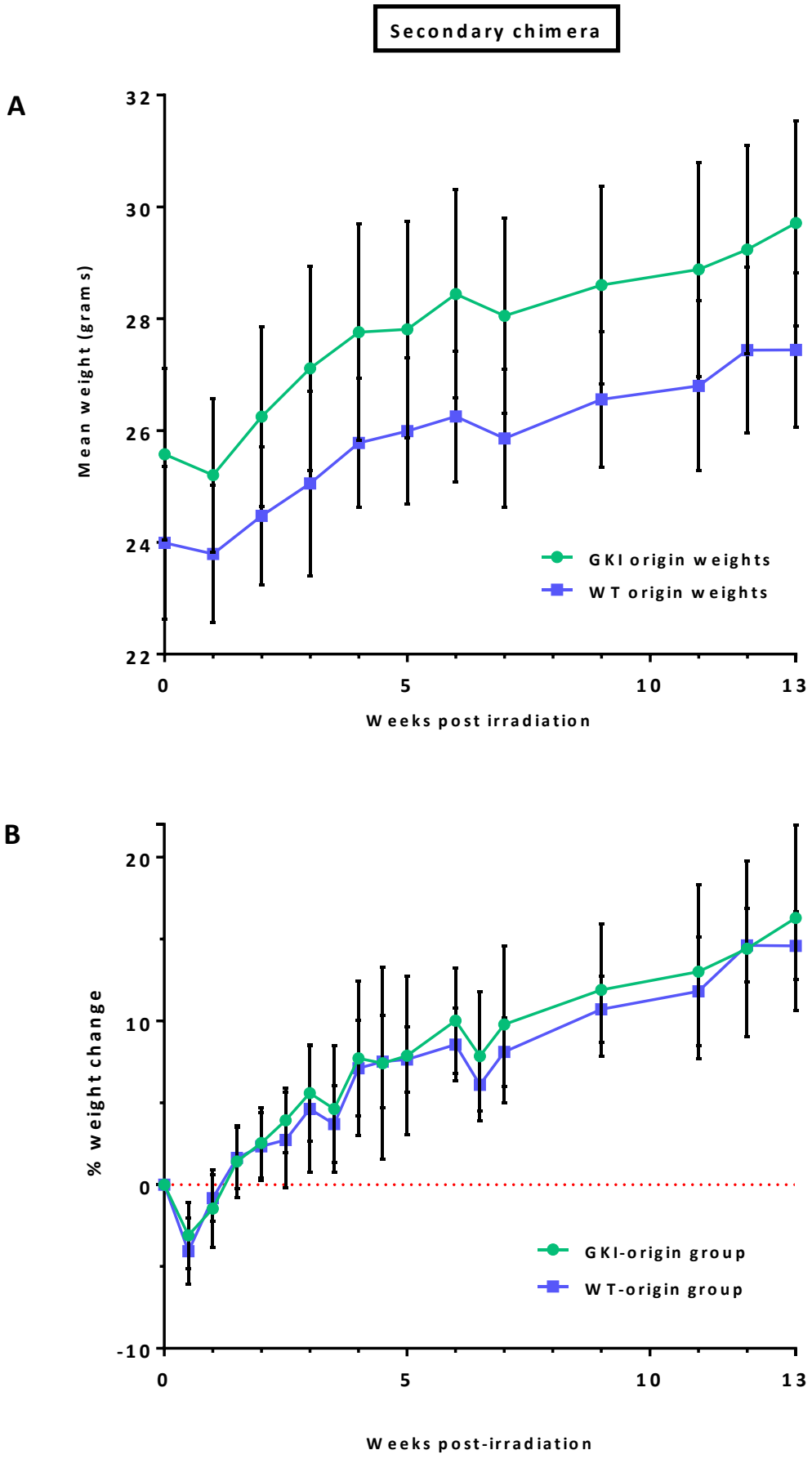
Secondary chimera
A
Mean weight (grams)
32
30
28
26
24
22
0
5
10
13
Weeks post irradiation
GKI origin weights
WT origin weights
B
% weight change
20
10
0
-10
0
5
10
13
Weeks post-irradiation
GKI-origin group
WT-origin group

6.3.3.2 Immune regeneration of secondary chimeric mice

Fetal liver cells have been shown to possess greater repopulation potential than adult bone marrow cells (Rebel et al., 1996, Harrison et al., 1997, Taylor et al., 2002). While the commitment of HSCs to either the myeloid or lymphoid lineages is stricter in bone marrow transplants, the general framework of regeneration with regard to the reappearance of cell types is conserved between fetal liver and adult bone marrow (Takeuchi and Miyajima, 2004, Duran-Struuck and Dysko, 2009). As previously mentioned, for this experiment, both sub-lethal irradiation and the addition of extra bone marrow cells from WT $PTPRC^{A}$ mice were used to ensure successful engraftment.

6.3.3.2.1 Donor cell survival and degree of chimerism in secondary chimeric mice

This study was carried out as a competitive strategy for transplanting adult donor bone marrow cells along with congenic mouse BM cells where the ratio of donor to competitor was 40: 60 respectively (Figure 6.7). As both the competitor cells in the original graft and the recipient mice carried the CD 45.1 allele, then it was not possible for this strategy to differentiate between residual recipient cells after irradiation and competitor cells. Donor cells, however, all carry the CD 45.2 allele and can be clearly differentiated from the competitor and residual recipient cells.

At both 6 and 16 weeks post-irradiation, the ratio of donor cells to competitor cells for WT-origin groups is roughly 20:80 where the 80 % includes residual recipient cells that survived irradiation (Figure 6.19). This shows a dominance of competitor and residual recipient cells over donor cells, which may be due to increased numbers of residual

recipient cells remaining after sub-lethal irradiation. Such a process would result in only partial myelo-ablation of the recipient mice. Alternatively, that 20:80 ratio may suggest an enhanced regenerative ability in the competitor cells over the donor cells, which would result in their more effective engraftment. As both donor and competitor are of WT-origin, this alternative explanation is less likely to be the case. There are, however, studies which have shown that the CD 45.1 and CD 45.2 alleles demonstrate mild alloreactivity between them (Chen et al., 1998, Xu et al., 2004) and variations in the immune cell subpopulations (Basu et al., 2013) in bone marrow chimeras and this action may affect donor versus competitor cell ratios.

Interestingly, for the GKI-origin groups for both time-points, the ratio of donor to competitor (+ residual recipient) cells more closely aligns to the original inoculum ratio (Figure 6.19). This provides evidence for the residual recipient cells contributing around 5% of the total peripheral blood leukocyte numbers which is well within the normal range for murine BM transplants. This also suggests that the GKI-origin donor cells are not impaired in their ability to engraft compared to the WT-origin donor cells and may even display and enhanced engraftment ability.

For all cell-origin groups, the ratios between donor and competitor cells did not alter from 6 to 16 weeks post-irradiation. With the reduced repopulation potential of BM compared to fetal liver along with less enhancement of marrow chimerism in early transplantation after sub-lethal irradiation (Andrade et al., 2011), the donor cells may take longer to establish a dominant chimera than for the primary chimera. Or possibly, the ratios may remain at this level of mixed chimerism in the long term. As no later

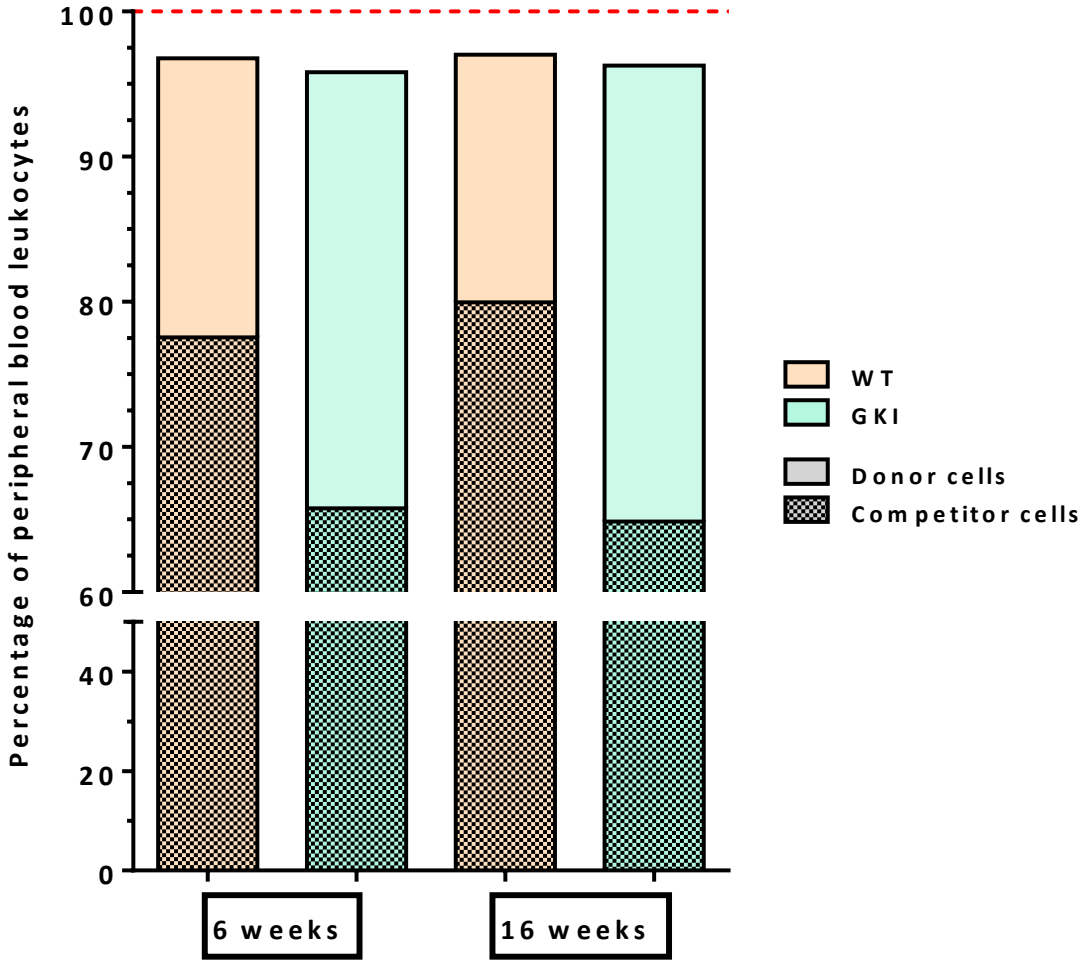

Figure 6.19: Proportion of donor and residual recipient cells of secondary chimeric mice

Irradiated mice were inoculated with DPP9$^{S729A/S729A}$ or DPP9$^{wt/wt}$ adult bone marrow cells along with PTPRC^{A} adult BM cells in the ratio of 60 (donor):40 (competitor). They were assessed for the percentage of donor and competitor cell-origin leukocytes at six and 16 weeks after irradiation of the recipient mice. The WT-origin group displayed a bias towards competitor cells over donor cells for both time-points whereas the GKI-origin group roughly maintained the original ratio of donor to competitor cells for both time-points. All groups displayed a shortfall below 100 % (red dotted line) which represented outlier competitor cells and residual recipient cells gated out during analysis. Graphs are represented as mean percentages where n = 9 for the WT-origin group and n = 10 for the GKI-origin group for both time-points.

time-points were taken, the answer to this question will need to be elucidated by future experiments.

6.3.3.2.2 Identification of myeloid and lymphoid cell types in secondary chimeric mice

The addition of competitor cells to the original BM cell inocula resulted in the creation of viable secondary chimeric mice but with a reduced donor cell level. Despite this, analysis of peripheral blood leukocytes of donor cell origin in these chimeric mice showed the presence of myeloid and lymphoid lineage cells consistent with successful engraftment.

In a similar pattern to the primary chimera, myeloid cell percentages showed a significant reduction from 6 weeks to 16 weeks post-irradiation with no differences observed between WT-origin and GKI-origin groups for either individual time-point (Figure 6.20). The percentages at 6 weeks were lower in the secondary chimera compared to the primary which is consistent with a reduction in the inflammatory response that would have been caused by the sub-lethal irradiation dose applied to recipient mice in that instance. Although the myeloid cell percentages decreased for both genotype groups by 16 weeks, the change was less pronounced than in the primary chimera suggesting that resolution of the inflammation caused by irradiation was slower in the secondary chimera.

As with the primary chimera, around 60% of myeloid cells for both genotype groups were shown to be neutrophils at the 6 week time-point (Figure 6.20). At 16 weeks, however, the proportion of myeloid cells identified as neutrophils reduced to around 50% for both genotype groups and this difference was significant for GKI-origin samples (green asterisks). This data is consistent with a reduction of the irradiation-induced inflammatory response and suggests that the myeloid cell compartment may be normalising from a neutrophil-biased state to encompass other granulocyte cell types.

The main lymphoid lineage cell subsets (Figure 6.21) were all present and showed very little variability across all genotype-origin groups and time-points. No statistically significant differences were seen. NK cells were present in the secondary chimera at similar levels to the primary chimera and did not change between 6 weeks and 16 weeks. B cell percentages were also stable between the two time-points with no differences existing for different genotype-origin groups. As with the primary chimera, the B cell percentages were consistent with those normally observed in peripheral blood (Chen and Harrison, 2002).

T cells did not show any differences between WT-origin and GKI-origin groups which matched the primary chimera results. In contrast to the primary chimera, however, there was also no difference between the time-point data for the groups. All groups had mean percentages of approximately 11% with very little variation in standard deviation. As mentioned previously, T cells are the most resistant to radiation and a sub-lethal dose would leave many viable T cells to bolster the early time-point

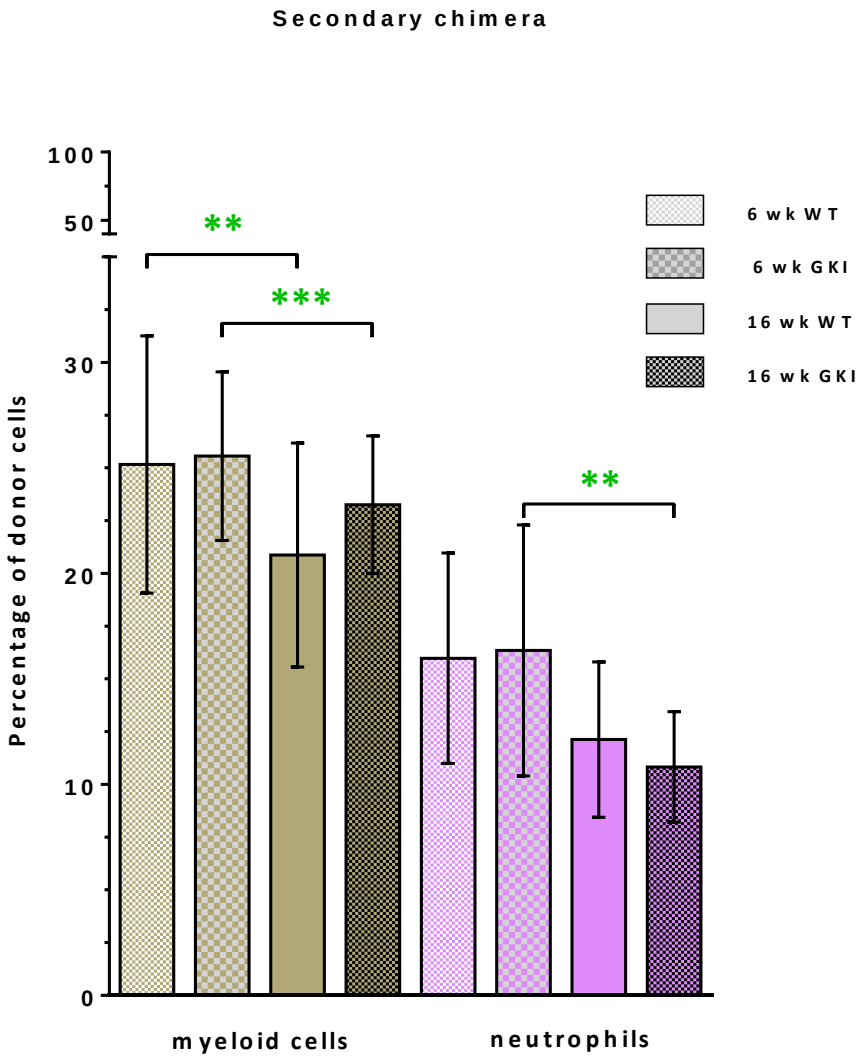

Figure 6.20 Percentage of myeloid cell types in peripheral blood of secondary chimeric mice

Mice from the secondary chimera were assessed by flow cytometry of peripheral blood for the percentage of total myeloid and neutrophil leukocytes at six and 16 weeks after irradiation. There were no differences observed between GKI-origin groups compared to WT-origin groups. There were significant differences between the 6 and 16 week time-points (green asterisks) for myeloid cells and GKI-origin neutrophils. Graphs are represented as mean percentages where n = 9 for the WT-origin group and n = 10 for the GKI-origin group for both time-points. Error bars denote SD and significance was assigned where $p < 0.05$ (*), $p < 0.01$ (**), $p < 0.001$ (***).

percentages. This could result in a reduced ratio of donor cell chimerism in the T cell compartment for the secondary chimera. However, this is unlikely since the overall levels are comparable for both chimeras and are close to the normal expected level of 20% for peripheral blood. With its stable T cell numbers, the secondary chimeric mice should be able to generate an effective T cell response against pathogens and cancers. This could be investigated in future experiments.

Unlike the primary chimera, the overall peripheral blood leukocytes of both myeloid and lymphoid lineages (Figure 6.22) showed little variation between the 6 and 16 week time-points with a strong bias towards the lymphoid lineages. This suggests a more limited self-renewal capacity of the HSCs and is consistent with the reduced flexibility of progenitor cell commitment in bone marrow transplants over fetal liver transplants. However, the pattern is the same for both WT-origin and GKI-origin groups which implies that this effect is not related to the absence of DPP9 enzymatic activity in the regenerating immune system.

6.3.4 Immune challenge with Influenza

DPP9-origin chimeric mice have not previously been subjected to an immune challenge. The aim of this challenge was to assess whether the reconstituted immune systems of the chimeric mice were capable of normal immune function. For these studies, it was decided to infect the mice from both the primary and secondary chimera experiments with influenza virus. [PR8], which was used for the immune challenge, represents the A/Puerto Rico/8/1934 (H1N1) strain, an influenza A virus of

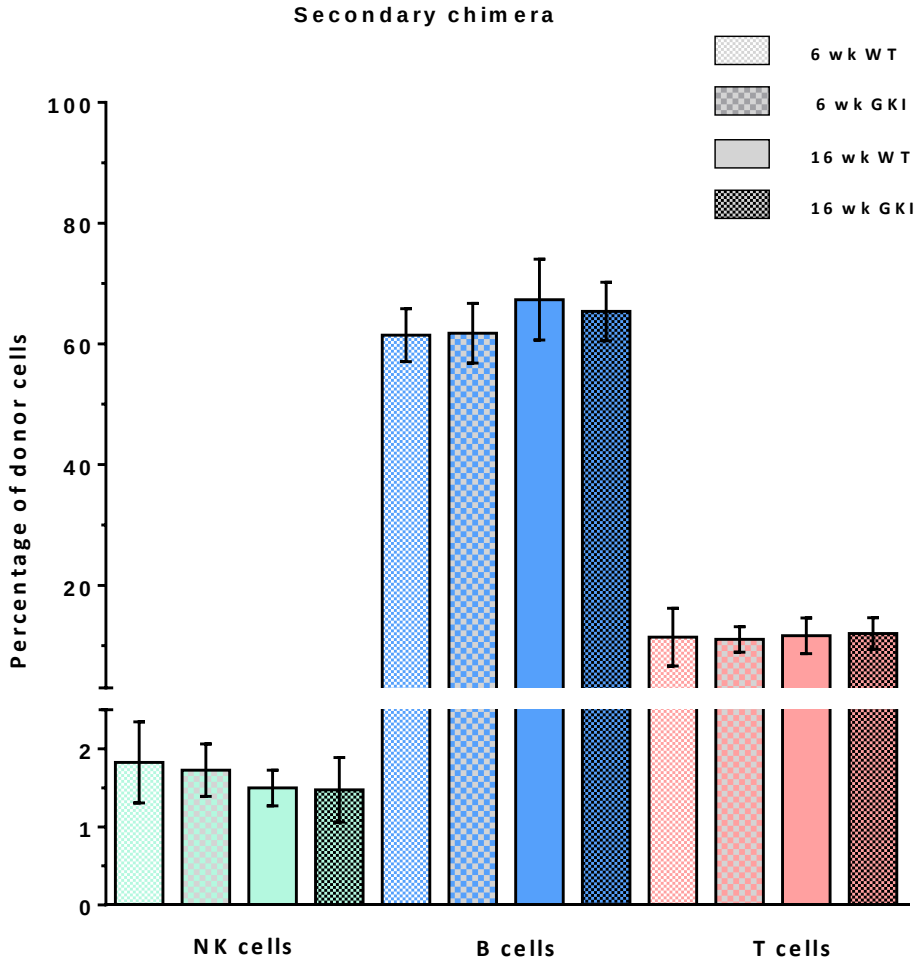

Figure 6.21: Percentage of lymphoid cell types in peripheral blood of secondary chimeric mice

Mice from the secondary chimera were assessed by flow cytometry of peripheral blood for the percentage of lymphoid lineage leukocytes at six and 16 weeks after irradiation. There were no significant differences observed for any cell type between genotype-origin groups at either time-point. Graphs are represented as mean percentages where n = 9 for the WT-origin group and n = 10 for the GKI-origin group for both time-points. Error bars denote SD.

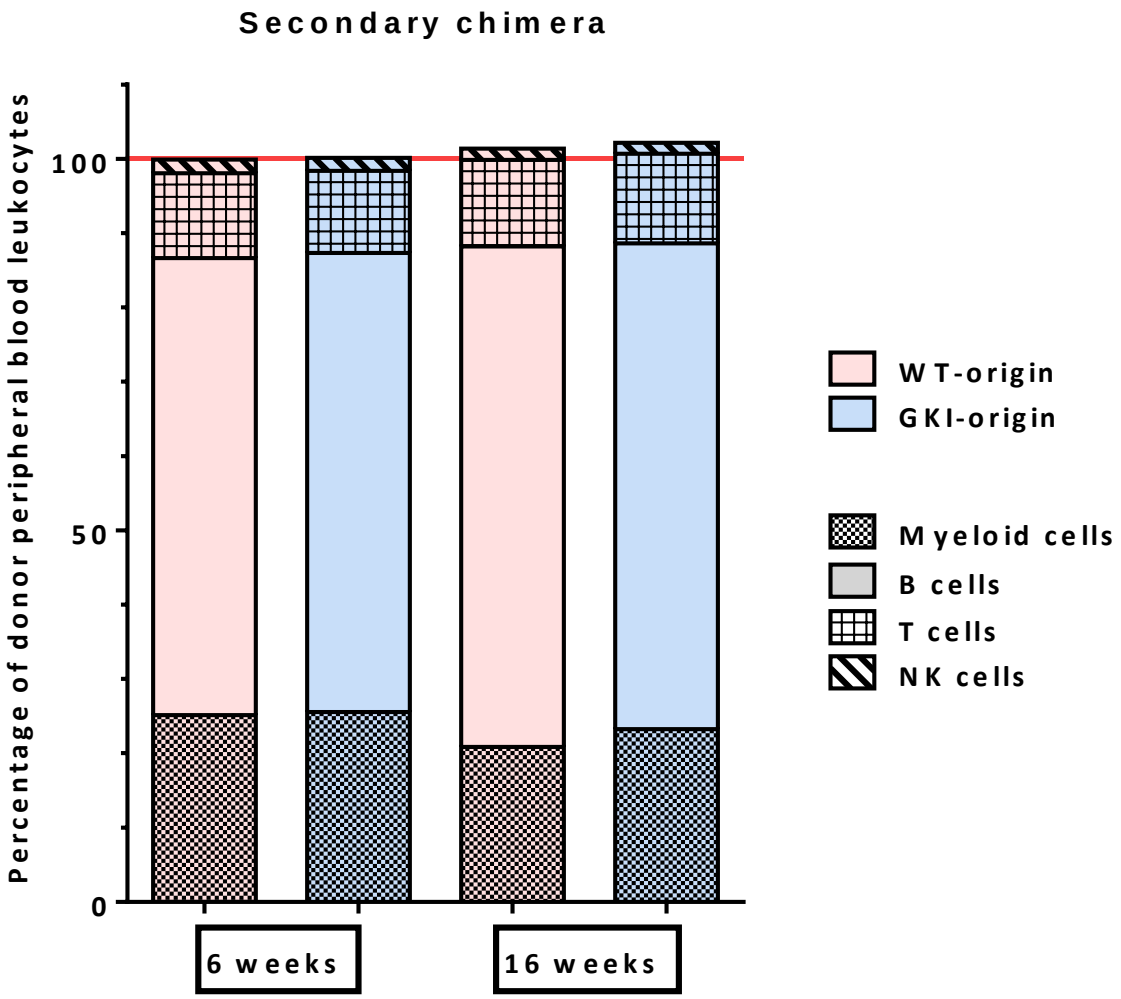

Figure 6.22: Total donor peripheral blood leukocytes of secondary chimeric mice

This graph represents the cell type analysis of total peripheral blood leukocytes of donor-origin at six and 16 weeks after irradiation and adult bone marrow cell transplant. From six weeks to 16 weeks, both WT-origin and GKI-origin groups show very little change between lymphoid and myeloid lineage cell proportions. The cell percentages added up to slightly more than 100% (designated by the red line) for the 16 week time-point as a result of the univariate analysis used by the FlowJo software to preserve the relative relationship between groups.

H1N1 subtype. While host resistance to influenza is a complex multigenic trait, C57BL/6 mice are susceptible to infection with this virus and the clinical signs, such as weight loss and lethargy, make tracking the progress of the disease possible (Bouvier and Lowen, 2010).

At 30 weeks post-irradiation, the primary chimeric mice were inoculated intra-nasally with influenza virus and monitored for weight loss. By this time, the reconstitution of the mouse immune systems would be expected to be complete and peripheral blood donor cells should be long-term HSCs. The pattern of weight loss was identical for both genotype-origin groups with a maximum mean loss of approximately 25% of original body weight before signs of weight recovery around 13 days after infection (Figure 6.23). This suggests that the regenerated immune system in each group was equally functional and able to cope with the immune challenge.

The experiment was repeated with the secondary chimeric mice which were produced by irradiation of recipient mice and transplantation of adult bone marrow cells for immune regeneration. As the infection weight loss results for the primary chimeric mice were quite severe, it was decided to reduce the virus infection dose to 25 pfu to ensure mouse survival.

Of note for this experiment is the mean start weight discrepancy between the two genotype-origin groups, with the GKI-origin group displaying a statistically significantly higher mean start weight than the WT-origin groups (as mentioned in Section 6.3.3.1). Despite this, there was no difference in the percentage weight change between the two groups for the first 5 days post-infection, with both groups showing a 5% loss

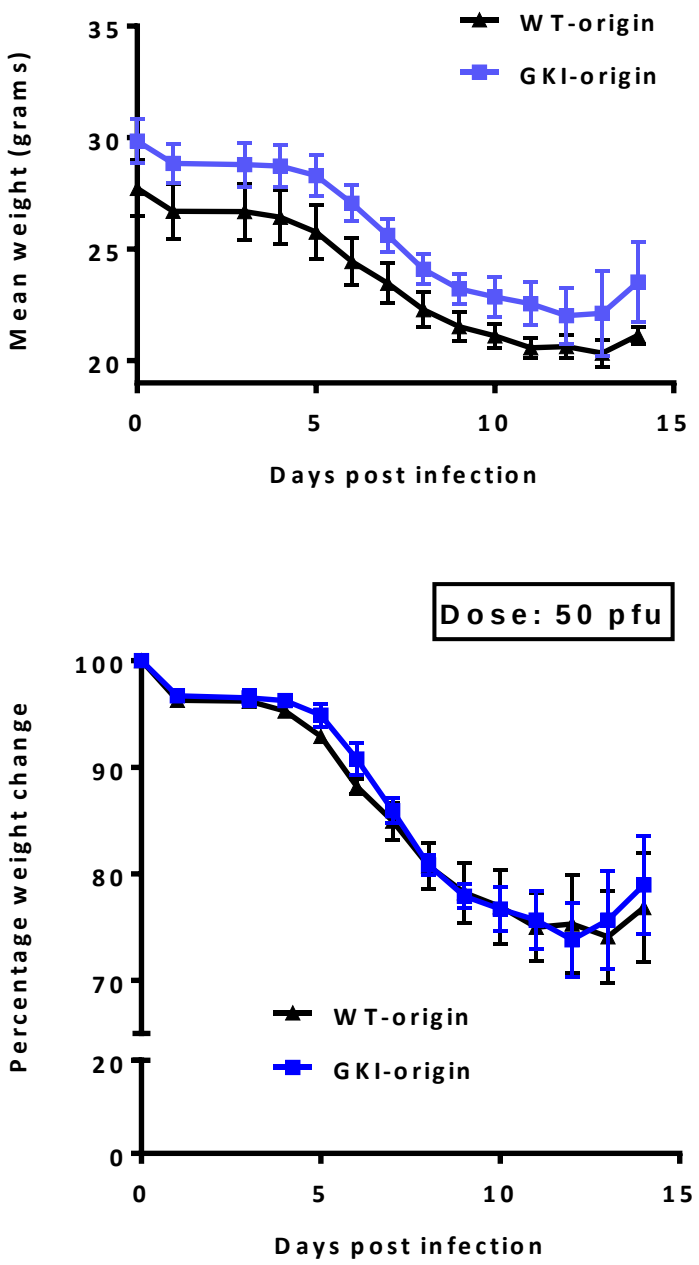

Figure 6.23: Weight monitoring of primary chimeric mice after influenza infection

Mice from the primary chimera experiment were inoculated intra-nasally with 50 pfu of [PR8] influenza virus at 30 weeks after irradiation and fetal liver cell transplant. There were no significant differences for either mean weight change or percentage weight change between WT-origin or GKI-origin groups. Graphs represent group means where n = 7 for the WT-origin group and n = 5 for the GKI-origin group. Error bars denote SEM.

(Figure 6.24). The WT-origin group continued to lose weight until day 10 in a similar fashion to the primary chimeric mice. The weight loss for the WT-origin secondary chimeric mice was not as high (maximum loss around 20%) as for the primary chimeric mice and recovery began several days earlier. This is consistent with a lower starting dose of influenza in the secondary chimeric mice and, hence, a lower viral load.

Interestingly, from day 6 onwards, there was a divergence of the two groups, with the GKI-origin mice maintaining a relatively steady weight for the duration of the experiment (Figure 6.24). Theoretically, the higher start weight of the GKI-origin group may have increased their resistance to the influenza infection. However, the identical percentage weight change of the two groups for the first five days of infection tends to suggest this is not the reason for the difference.

Another possibility for consideration is an advantage in the GKI-origin secondary chimeric mice which increased their resistance to the immune challenge of influenza

Figure 6.24: Weight monitoring of secondary chimeric mice after influenza infection

Mice from the secondary chimera experiment were inoculated intra-nasally with 25 pfu of [PR8] influenza virus at 25 weeks after irradiation and adult bone marrow cell transplant. While there were no significant differences for percentage weight change between WT-origin or GKI-origin groups for the first 5 days post infection, the two groups differed from day 6 onwards. The GKI-origin groups maintained a stable weight while the WT-group followed a more typical loss-and-recovery pattern. Graphs represent group means where n = 9 for the WT-origin group and n = 9 for the GKI-origin group. Error bars denote SEM.

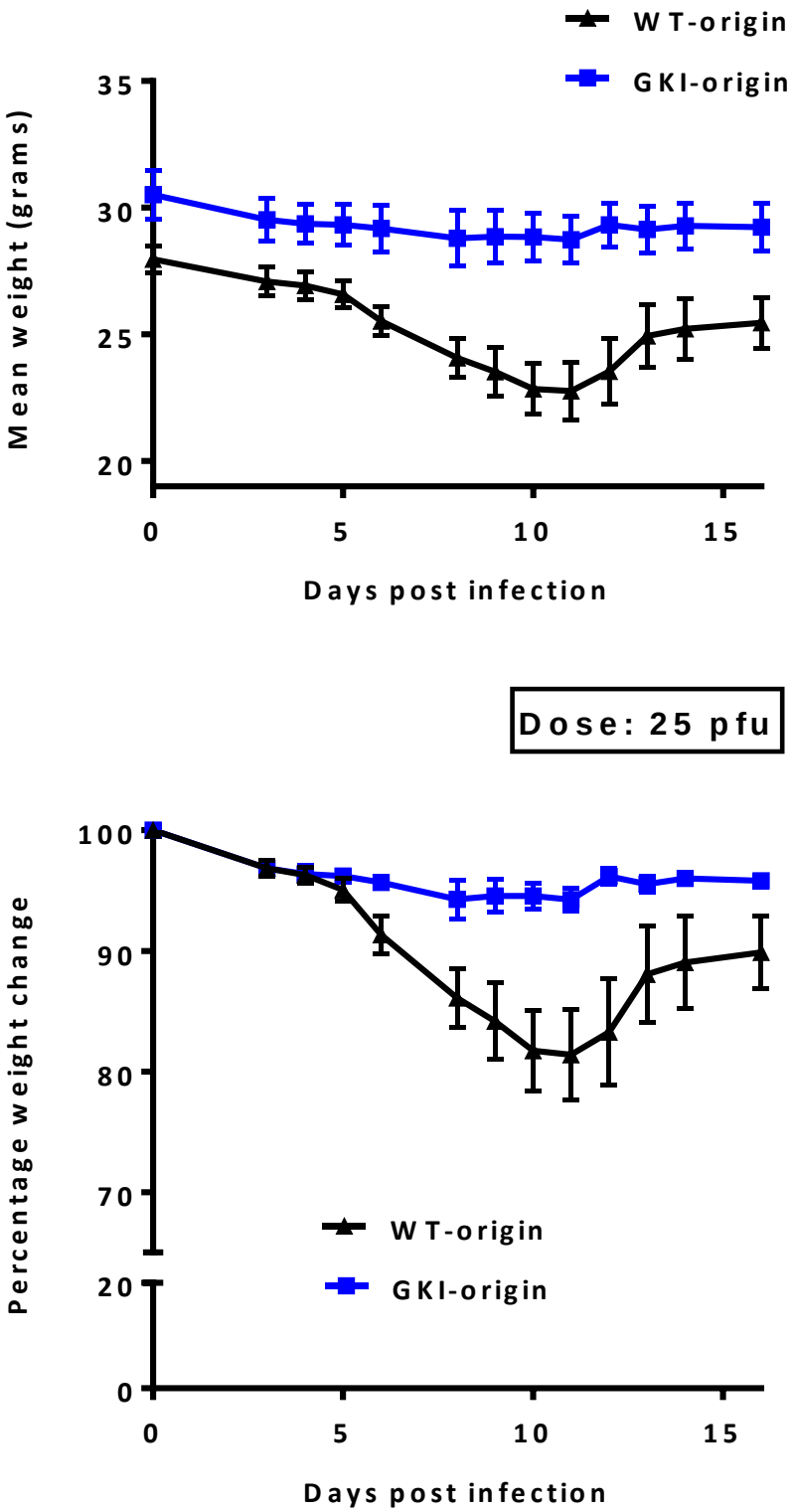
WT-origin
GKI-origin
Mean weight (grams)
35
30
25
20
0
5
10
15
Days post infection
Dose: 25 pfu
Percentage weight change
100
90
80
70
20
0
WT-origin
GKI-origin
0
5
10
15
Days post infection

infection. Future experiments will need to be undertaken to investigate whether this is the case. Either way, neither the primary nor the secondary chimeric mice of GKI-origin show any disadvantage in carrying the DPP9-GKI mutant allele and, thus, the absence of DPP9 enzymatic activity in immune cells does not impair immune function.

6.4 Discussion

The murine immune system is essential to protect the mouse from the many toxic and pathogenic elements to which it is exposed in the environment. To this end, normal function is required of both the perennially-present innate immune responses and the activated adaptive immune system. DPP9 has been shown to have roles in the mouse in both the innate and adaptive immune system (Lankas et al., 2005, Reinhold et al., 2009, Tang et al., 2009, Yu et al., 2009, Geiss-Friedlander et al., 2009, Chowdhury et al., 2013). By creating chimeric mice using normal tissue and tissue lacking DPP9 enzymatic activity from both fetal and adult mice, this chapter aims to explore the possible functions of DPP9 in mouse immune regeneration and hematopoiesis.

The first consideration before undertaking this experiment was whether the fetal liver cells of DPP9-WT and DPP9-GKI genotype origin showed any differences which may affect the experimental outcome and result in incorrect conclusions being drawn regarding the negative or positive impact of DPP9 enzymatic activity. However, both cell inoculum groups showed the same proportions of erythroid and non-erythroid lineage HSCs. This provided a common starting point for creation of the chimeric mice and assessment and quantification of HSC numbers and functionality.

Weight tracking is an important monitoring tool to assess the impact of irradiation on the recipient mice and indicate potential graft failure after fetal liver or adult bone marrow transplant. The use of percentage weight change data normalises the weights from each group to overcome mouse-to-mouse variation and provide a common start point. The primary chimeric mice showed no differences in the weight loss-and-gain pattern after irradiation between the two genotype-origin groups. While there was a difference in the start weight of the two groups for the secondary chimera, the percentage weight change showed no difference between the groups in their recovery from irradiation over the period of the experiment. These data confirm the success of the grafts of both the fetal liver cell and adult bone marrow cell chimeras.

Although there were no differences between WT-origin and GKI-origin groups in weight change data, the time taken to regain the initial lost body weight after irradiation was different between the primary and secondary chimeric mice. The primary chimeric mice took 5 weeks to reach the original start weight, while the secondary mice achieved the same in just over a week. This difference is most likely due to the dose of initial irradiation and the use of supplementary cells to boost immune regeneration. The primary chimeric mice were subjected to a lethal myelo-ablative dose of irradiation and inoculated with only donor cells. As these were fetal liver cells, which possess an enhanced ability to initiate immune regeneration, the engraftment was successful but the time to reach the original start weight was delayed. For the secondary chimeric mice, however, irradiation was at a sub-lethal dose and the inoculum was supplemented with $PTPRC^{A}$ competitor cells which assured mouse survival and also greatly reduced the time taken to regain body weight to the

original start weight in both groups. Despite this disparity between the primary and secondary chimera in the time taken to attain original start weight, the overall pattern of weight gain throughout the experimental period was the same for all groups.

Another indicator of successful engraftment in recipient mice is the percentage of chimerism in peripheral blood, in this study shown by the donor cells present identified with the CD 45.2 allelic marker and flow cytometric analysis. The degree of chimerism of the primary mice was very high at both the six and 16 week time-points with only small percentages of residual recipient cells present after irradiation. This was consistent with the lethal irradiation regime employed and suggested that, as well as the success of engraftment, there was no impairment in the DPP9-GKI HSCs ability to engraft.

For the secondary chimeric mice, the percentage chimerism is harder to interpret. There is no difference between the early and late time points for each matching origin group but a noticeable difference between the WT-origin and GKI-origin competitor:donor ratios for each time-point. The WT-origin group has a higher proportion of competitor cells (which comprise residual recipient cells plus introduced competitor cells) over donor cells, when compared with the original inoculum. This predominance of competitor cells may arise from the contribution of increased levels of residual recipient cells surviving after sub-lethal irradiation or an enhanced regenerative ability of the competitor cells over the donor cells. A separate point to consider is that some studies have shown alloreactivity and variable cell subpopulations in bone marrow chimeras when using congenic CD 45.1 and CD 45.2

mice, and this may affect competitor:donor cell ratios (Chen et al., 1998, Xu et al., 2004, Basu et al., 2013).

However, the GKI-origin group shows a competitor:donor ratio for both time-points much more closely matched to the original inoculum ratio. As both the WT-origin and GKI-origin chimeric groups were inoculated with the same competitor cells, received the same irradiation dose and, therefore, most likely had the same proportion of residual recipient cells, it is more likely that the sole differing variable of cell-origin genotype is influencing this result. If so, then the GKI-origin donor cells may possess an enhanced engraftment ability in the secondary chimera. This would need to be shown by repeating the experiment. Now that successful engraftment and survival of the secondary chimeric mice has been shown, a future secondary chimera could be carried out with lethal irradiation and/or a non-competitive strategy using only donor cells for transplant, thereby removing the confounding effects of competitor and residual recipient cells.

Having confirmed effective engraftment of donor cells by mouse husbandry methods and degree of donor chimerism, it is then necessary to determine the contribution of the different hematopoietic cell lineages to the development and repopulation of the reconstituting immune system. By six weeks post-irradiation, the peripheral blood cells that arise from the original donor cells can be the progeny of short-term HSCs or long-lived progenitor cells (Duran-Struuck and Dysko, 2009, Mayle et al., 2013). Most HSCs that repopulate the ablated immune system are short-lived and the length of time they function has shown to be proportional to donor species lifespan (Morrison and

Weissman, 1994). By 16 weeks, however, all donor cells present are long-term HSCs capable of self-renewal and are the progeny of short-term HSCs. Hence, it is possible to determine if the self-renewal capacity of the donor HSCs is stable or transient and whether the transition from short term to long term immune regeneration has occurred. The cell types chosen as a broad indicator of lineage development were general myeloid cells and neutrophils as representative of the myeloid lineage and NK cells, B cells and T cells as representative of the lymphoid lineage. Analysis of these few cell types was sufficient to show hematopoietic and immune regeneration after irradiation. In-depth analysis of cell subpopulations would be necessary for complete analysis of immune regeneration but was beyond the scope of the present study.

At 6 and 16 weeks post-irradiation, in both the primary and secondary chimeric mice, all myeloid and lymphoid cell types considered in this study were present for both genotype-origin groups. This confirms that the progenitor cell pool was intact and both the primary and secondary HSCs showed no defect in self-renewal or proliferation capability.

No differences in myeloid lineage cells were seen between genotype-origin groups in either time-point or chimera. However, a significant reduction in myeloid cells was seen between the 6 and 16 week time-points for both genotype-origin groups in both chimeras. This result was supportive of the resolution of irradiation-induced inflammation at the later time-point. It was also consistent with reduced myeloid cell output as HSCs are reprogrammed after six weeks to an adult gene expression pattern (Bowie et al., 2007).

Neutrophils represented around 60% of the total myeloid cells in both the WT-origin and GKI-origin groups in the primary and secondary chimeric mice at the 6 week time-point. While this proportion remained the same at the 16 week time-point for the primary chimeric and WT-origin secondary chimeric mice, the proportion of neutrophils decreased significantly in the secondary GKI-origin mice suggesting an increase in other granulocytes and, hence, normalisation of the myeloid cell compartment. Whether this is indicative of a hematopoietic reconstitution advantage is unclear and would require further investigation.

The cells of lymphoid lineage targetted for analysis in this study were NK cells, B cells and T cells. NK cells are reported to regain normal cell numbers and function within a month of engraftment (Awwad, 1990, Auletta and Lazarus, 2005, Sungur and Murphy, 2014) and both the primary and secondary chimeric mice for both genotype-origin groups and time-points showed stable NK cell numbers consistent with this observation. This early establishment of NK cells would be important for protection of mice against infection with pathogens.

B cells were also present in comparable stable levels in both the primary and secondary chimeras with the only observed difference being at the 6 week time-point in the primary chimera. There was a significant reduction in the B cells numbers in the GKI-origin group compared to the WT-origin group, which normalised at 16 weeks. The reason for this difference is difficult to explain but, as it was only slight and not present at 16 weeks, it may have been due to mouse-to-mouse variations in analysis or a slight

delay in B cell re-establishment for this group. Repeating the primary chimera with a more detailed focus on B cell subsets may explain this in the future.

T cell reconstitution was the same for all genotype-origin groups for each time-point in the primary and secondary chimeras. While the secondary chimera also showed no difference between time-points, the primary chimeric mice, for both WT-origin and GKI-origin groups, showed a highly significant increase in T cells at 16 weeks compared to six weeks. The low 6 week T cell levels is consistent with the lethally irradiated primary chimeric mice being more severely depleted of residual recipient T cells than the secondary chimeric mice. Although the numbers have greatly increased at 16 weeks, they are still not at normal levels for mouse peripheral blood (Chen and Harrison, 2002), unlike the secondary chimeric mice that appear to have early full reconstitution of the T cell compartment. As was the case for the B cells, future investigation of T cell subsets during immune regeneration may shed light on the mechanisms in play. While this needs further investigation, the fact that it was consistent across both genotype-origin groups suggests that it is unrelated to the presence or absence of DPP9 activity.

The overall proportion of myeloid to lymphoid lineage cells in donor-derived peripheral blood leukocytes can provide further information about the regenerated immune system of chimeric mice (Kent et al., 2009). When the reconstituted immune system shifts from short term to long term regeneration, the self-renewal capacity of HSCs becomes more limited, as progenitor cells are produced with defined lineage potential. This is usually displayed by a trend towards a greater lymphoid-biased

output of peripheral blood leukocytes. This trend is evident in both the primary and secondary chimeric mice (Figure 6.17 and 6.22), where the change from the 6 to 16 week time-point for all groups is an increased bias towards lymphoid cells over myeloid cells.

The final assessment of immune regeneration and function in this study was the infection of primary and secondary chimeric mice with influenza virus to determine potential functional differences caused by the presence of DPP9-enzyme-activity-deficient immune cells. The primary chimeric mice displayed identical weight loss and recovery patterns for both the WT-origin and the GKI-origin groups suggesting an equivalent level of functionality of the regenerated immune systems of both groups when presented with an immune challenge. As both the primary and secondary chimeras resulted in successful engraftment and regeneration of viable immune systems in the recipient mice, it was surprising to see a very notable difference in the body weight data for the GKI-origin secondary chimeric mice after immune challenge. Although the difference in starting body weight between the secondary chimera groups was significant, it did not appear to present the GKI-origin mice any advantage in the initial five days after infection. Both groups followed a similar weight loss pattern over this period but showed divergent path from day 6.

With a reduced inoculation dose and lower viral load for the secondary chimeric mice, it would be expected that both groups would recover quickly. The WT-origin mice did show a lower percentage weight loss and an earlier upturn to weight gain than either of the primary chimeric groups. The secondary GKI-origin chimeric mice, however,

maintained a stable weight from day 6 onwards for the duration of the experiment. This data indicates that the secondary GKI-origin chimeric mice had an increased resistance to an immune challenge. Whether this was specific for influenza infection alone as the immune challenge or the result was influenced by the increased start weight of groups, and whether similar observations might be made in other infections, will need to be determined by future experiments.

Considering the combined immune challenge results, nonetheless, it is apparent that there is no weakening of immune function shown by either the primary or secondary chimeric mice of GKI-origin over the WT-origin mice. In fact, the result of the secondary immune challenge experiment tends to suggest there may be an advantage in the absence of DPP9 enzymatic activity in immune cells, certainly in relation to immune function.

CHAPTER 7:

General Discussion

7 *General Discussion*

7.1 Introduction

This study aimed to increase our understanding of the role of DPP9 in biological systems. This goal was achieved through the use of a mouse model of targetted inactivation of DPP9 enzyme activity to generate physiologically relevant *in vivo* data. This study utilised a broad strategy of histological, immuno-histochemical and molecular biological techniques which resulted in novel findings in both neonatal and adult mice. The major findings of this study were:

- the absence of DPP9 enzymatic activity in the mouse results in a lethal neonatal phenotype
- the DPP9-GKI mouse displays evidence for dysregulation in autophagy, which may contribute to the lethal phenotype
- adult heterozygous DPP9-GKI mice display reduced skin collagen levels compared to their WT littermates
- DPP9-enzyme-activity-deficient secondary chimeric mice, in which the hematopoietic tissue and immunological system derive from a different mouse than other somatic cells, may have an enhanced ability to recover from an immune challenge with influenza virus.

7.2 DPP9 in the neonatal mouse

7.2.1 Lethality in the neonatal mouse

Much of the early work in this thesis revolved around determining that inactivation of DPP9 resulted in lethality in the mouse and confirming that death occurred in the early neonatal stage (Chapter 3). After confirming that DPP9 was indeed inactivated, the focus of this study then turned to elucidating the specific cause(s) of lethality. Recently, much information regarding the roles of DPP9 *in vitro* is emerging (Zhang et al., 2013, Waumans et al., 2015, Wilson et al., 2016, Okondo et al., 2016, Justa-Schuch et al., 2016). However, *in vivo* data, especially in neonatal mice, is extremely limited. The current study resulted in a broad investigation of potential lethal effects of DPP9 enzyme inactivation starting with the most obvious causes such as defects in mouse gross morphological and/or histological development and aberrant structure and function or failure of organs. Also considered were behavioural differences in the DPP9-GKI neonates that may have caused exclusion of the pup from proper care and suckling by the mother.

While the characterisation of adult mice was focussed on aspects of DPP9 biology that are not suspected to be involved in neonate lethality, it is possible that, by elucidating roles of DPP9 in the adult mouse, we can gain further clues into the cause of lethality at that particular developmental stage. For example, the finding that adult heterozygous DPP9-GKI mouse skin shows reduced levels of collagen may indicate reduced levels in the neonatal mouse. If true, this could have implications for organ function. It has been shown that cardiovascular abnormalities often lead to neonate-

lethal phenotypes (Turgeon and Meloche, 2009) as dramatic changes occur in the circulatory system immediately after birth. Working with our collaborator, close inspection of the internal valve structure of the neonates showed a possible aortic valve defect in the DPP9-GKI neonatal mice (Chapter 4). Normal valve function could be affected by reduced collagen levels, if present. While the gross morphological and histological make-up of organs may appear normal, the strength, and hence functionality of organ structures, may be impaired. Collagenolytic activity is necessary for skeletal and extra-skeletal connective tissue modelling and reduced collagen turnover and/or low collagen levels in neonates has been shown to affect normal function and result in many defects including dwarfism, osteopenia, arthritis, heart valve dysfunction and connective tissue disease (Holmbeck et al., Joyce et al., 2009). Also, many disorders exist, in both humans and mice, that are related to collagen depletion in connective tissues (Royce and Steinmann, 2002, Turgeon and Meloche, 2009). Thus, it would be beneficial to measure collagen content in neonate organs and other adult organs besides skin in the future. While the impact of reduced collagen in skin may not be detrimental to long term survival, reduced collagen in other organs may have a greater impact, especially at the early neonate stage.

The lack of a selective DPP9 inhibitor is an ongoing roadblock to understanding this protease. Inhibitors have been developed that are selective for DPP8 and DPP9 over DPP4 and FAP (Lankas et al., 2005, Wu et al., 2009, Jiaang et al., 2005, Van der Veken et al., 2008, Van Goethem et al., 2011) but none are selective for DPP9 alone. If an effective DPP9-specific inhibitor is found, then several future experiments could be undertaken that may contribute to our understanding of DPP9 function *in vivo* at the

neonatal stage. One such study could be to administer inhibitor from birth into WT neonatal mice to establish if the lethality experienced by the DPP9-GKI homozygous mice can be induced. Alternatively, DPP9 inhibitor could be administered at later pre-weaning time-points to determine if the lack and/or reduced level of DPP9 enzymatic activity affects survival after the early neonatal starvation period once milk metabolism is established. This result, in conjunction with findings from our lab's study into the influences of DPP9 expression on neonatal metabolic genes (Chen et al., 2016), may enable better definition of the metabolic time-point when DPP9 enzymatic activity is critical for survival.

7.2.2 Autophagy in the neonatal mouse

Dysregulation in autophagy was shown in DPP9-GKI neonate mouse tissues (Chapter 4) with up-regulation in some organs and down-regulation in others relative to DPP9-WT tissues. Enzyme activity of DPP8/ 9 has been shown to be present in all organs that displayed autophagy dysregulation in the neonate mouse, that is, heart muscle, lung, gut, brain and liver (Yu et al., 2009) and, like LC3, are found in both nucleus and cytoplasm. DPP9 nuclear localisation was evident, although unpublished at the time of this work, both *in vivo* in immune-histochemical DPP9 tissue staining (Figure 3.2 B) and *in vitro* in WT and DPP9-GKI MEFs (Figure 3.4 C and D). DPP9 is known to exist in two isoforms (Ajami et al., 2004), short and long, that are found predominantly in the cytoplasm and nucleus respectively, and it has been shown that the long isoform of DPP9 may be involved in the regulation of the activity or stability of nuclear transcription factors (Justa-Schuch et al., 2014). Many autophagy genes, including LC3,

are regulated at the transcriptional level with autophagy in the cytosol inducing their activation via nuclear-cytosolic shuttling (Fullgrabe et al., 2014). The occurrence, in normal tissue, of the autophagy marker LC3 in the same cellular locations as both DPP9 isoforms may be coincidental. It does, however, raise the question as to whether the absence of DPP9 activity in the DPP9-GKI mouse may directly influence autophagic processes. Further staining of neonate tissues using both DPP9 and autophagy protein antibodies concurrently with more advanced microscopy may show whether an exact co-localisation exists.

The organs in which LC3B was most up-regulated without DPP9 activity were heart muscle, lung and gut. All of these organs are subject to enormous functional adjustments in the early neonate period and autophagic processes are maximised to provide resources for drastic metabolic changes (Mizushima et al., 2004, Turgeon and Meloche, 2009). The high levels of autophagy displayed by these organs in the DPP9-GKI mouse may have been induced to overcome a shortfall in resources at this time-point caused by an unidentified metabolic dysfunction. However, it is known that high levels of autophagy can lead to an overload of cellular components and an accumulation of debris that disrupts cellular function (Sivridis et al., 2010). Thus, rather than an attempt to alleviate the metabolic shortfall, the increased autophagy, in this case, may actually be exaggerating the problem. This could suggest that the presence of DPP9 may be a limiting factor in preventing excessive increases in autophagy.

Similarly, brain and liver, which displayed down-regulation of autophagy in DPP9-GKI mice, may be unable to induce the necessary level of autophagy for normal

requirements due to the same dysfunction, depending on the metabolic pathways affected. Both brain and liver show high levels of DPP9 in early neonate mice (Gall et al., 2013) and autophagy is normally upregulated in these organs in order to maintain an adequate amino acid pool to be used as an energy source (Kuma et al., 2004).

While the number of autophagosomes in neurons is not increased during the neonate starvation period (Mizushima et al., 2004), autophagy can be induced in cortical neurons, Purkinje cells (Alirezaei et al., 2010) and neurons of the hypothalamus (Kaushik et al.) in a fasting state. Due to technical limitations of our study, comparison of the level of autophagy between the DPP9-GKI and WT neonatal mouse brains was difficult to evaluate as only the diencephalon was consistently present across all samples. Future investigations to identify the exact regions of the brain and specific cell types that display up- and down-regulation of autophagy in the early neonatal stage need to be undertaken.

Autophagy in the liver is known to aid in the prevention of hepatocellular degeneration, remove lipid droplets, suppress tumour formation and play a part in gluconeogenesis (Mizushima and Komatsu, 2011). In the neonatal mouse, where efficient function of the liver is extremely important, any down-regulation in autophagy may impair its ability to produce ketones. This could result in an indirect effect on the brain due to an autophagy dysregulation in liver. The link between liver and brain is still unclear, but it is known that autophagy-deficient mice show the formation of ubiquitin-inclusions in the liver and brain and the protein, p62/A170/SQSTM1 links autophagy with inclusion formation (Waguri and Komatsu).

Therefore, it is possible that the reduced LC3B staining in DPP9-GKI mouse liver and brain are linked by metabolic interactions between the two organs. A future study could be undertaken using conditional Atg-7 deficient mice to study autophagy in a tissue-specific manner in both liver and brain. The addition of immunohistochemical double-staining to show the presence of both autophagy proteins and DPP9 in those mice may provide further insights into the potential involvement of DPP9 in autophagic processes.

Obvious dysregulation in autophagy, as displayed by up- and down-regulation in organs, provides clues about affected organ function. However, those tissues that displayed no apparent difference in the positivity of overall tissue immunoreactivity, but rather localisation variations of LC3B staining, can also hint to the influence of the absence of DPP9 enzyme activity on autophagy. Both the liver and adrenal gland DPP9-GKI samples showed unusual immunoreactivity localisation compared to the WT tissue with little or no difference in overall tissue reactivity.

In the adrenal gland, the presence of many secretory granules in the DPP9-GKI adrenal gland may be indicative of either increased production or dysfunctional release of catecholamines from the granules in these animals. Increased production of catecholamines could arise as a physiological stress response in the DPP9-GKI mice due to whatever event(s) are causing their impending death. Alternatively, reduced catecholamine release could contribute to lethality. It is known that, immediately after birth, catecholamine release sharply increases due to labour-induced hypoxia when the umbilical cord is severed. The increase in catecholamines decreases the insulin/

glucagon ratio in the neonate, resulting in the induction of metabolic changes essential to survival during the early starvation period until milk metabolism can contribute to energy production (Medina et al., 1992).

One major process that can be impaired by dysfunction of catecholamine release is long-chain fatty acid (LCFA) uptake. If there are insufficient LCFAs available for β-oxidation and ketogenesis during the neonate starvation period, this will result in reduced energy supplies for all organs, especially the brain which uses ketones as the main energy source. In the mouse, the main ketogenic organ during this time is the liver (Medina et al., 1992). Our group has recently reported mRNA expression data from DPP9-GKI mouse liver that points to disrupted LCFA uptake in the neonates and a lowered ketogenesis (Chen et al., 2016). As with the suggestion of reduced autophagy in the DPP9-GKI mouse brain due to ketone deficiency discussed above, this data supports a metabolic link between the liver and the brain.

Perhaps the increased autophagy seen in the heart muscle, lung and gut and the decreased autophagy in the brain and liver in the DPP9-GKI neonates is an attempt to overcome catecholamine dysregulation during this critical phase. Future investigation of catecholamine levels in neonate organs and whether DPP9 co-localises and/or interacts with known autophagy proteins may answer this question.

While the early neonatal time-point has been proven to result in a lethal phenotype for the DPP9-enzyme-activity-deficient mice, once the cause of death is discovered it may be possible to bypass this lethality. As most heterozygous mice survive to weaning and beyond, this suggests that it is possible to survive with a lowered level of DPP9

enzymatic activity. However, if survival was achieved at this time-point with a complete deficiency of DPP9 activity, later developmental or metabolic time-points may exist where lethality is again the outcome. To date, no single factor has shown potential for causing the death of the early neonates. It is most likely that the cause of lethality is interplay between several different physiological and/or metabolic effects, including those that we have identified.

7.3 DPP9 in the adult mouse

The adult heterozygous DPP9-GKI mice appear to show no signs of disadvantage in daily life or overall survival compared to their WT littermates. However, there is a significant effect on survival to weaning in immature heterozygous mice (Gall et al., 2013). Perhaps DPP9 enzymatic activity is not completely redundant after weaning in the adult mouse. The study of adult DPP9-GKI heterozygous mice was therefore driven by what differences may exist in mice with depleted DPP9 enzyme levels as compared to WT mice with full DPP9 enzymatic function. The lack of availability of a DPP9-selective inhibitor meant that DPP9 enzyme activity levels in heterozygous mice could not be measured, so whether the heterozygous mouse tissues contain 50% of the levels of DPP9 of WT mice is not known. Hence, the production of DPP9-GKI chimeric mice had an important role in overcoming this limitation.

7.3.1 Collagen in the adult mouse

The adult DPP9-GKI mice display no overt structural or functional skin defects. DPP9 is detectable in abundance in embryonic and neonate WT mouse skin, but in lower levels in adult skin (Yu et al., 2009). The inhibition of DPP9 in epithelial cell lines *in vitro* decreases cell mobility and adhesion (Zhang et al., 2015a), which suggests a potential skin repair role, however wound healing after full thickness wounding was not impaired (Chapter 5). This is contrary to other DPP4 protein family members that have known roles in granulation tissue formation and wound healing (Garin-Chesa et al., 1990, Kohl et al., 1991, Thielitz et al., 2008, Schürmann et al., 2012, Sinagra et al., 2015).

The proper function and integrity of skin plays in integral role in providing a protective barrier against physical and biological onslaughts, such as wounds, dehydration, thermal regulation and immunological assaults. Mouse epidermis, while consisting mainly of keratinocytes, also has densely packed hair follicles. Stem cells reside in the follicular bulge and dermal papilla. These stem cells restore epidermal integrity after wounding (Kimlin and Virador, 2013). The underlying dermis is rich in extracellular matrix and contains fibroblasts and many populations of myeloid and lymphoid immune cells (Pasparakis et al., 2014). The fibrous components of the dermis include collagen and elastin fibres.

The finding that DPP9-GKI heterozygous mouse skin in the steady state has reduced collagen content as compared to the skin of WT littermates is novel. While it appears to have no survival impact on the mice, it does raise questions as to the potential

interaction between DPP9 and collagen deposition and maintenance. It has previously been shown that DPP9 influences cell behaviour, including cell–extracellular matrix interactions (Yu et al., 2006a) *in vitro* and other DPPs are known to interact with collagen (Waumans et al., 2015). However, no known data exists showing a link between collagen deposition and DPP9 enzymatic activity *in vivo*. While an *in vitro* study of keloid-derived skin fibroblasts showed that inhibition of DPP8/9 could suppress secretion of procollagen type 1 (Thielitz et al., 2008), there is no known direct link between collagen and DPP9 *in vitro*.

Whether reduced collagen levels occur in both neonatal and adult DPP9-enzyme-activity-deficient mice needs to be established as there is insufficient data at this point to use the adult skin finding to extrapolate conclusions in the neonate mouse skin without further experimental work. The lower collagen levels may arise in early developmental stages or arise subsequently after a prolonged period of depleted DPP9 enzymatic activity in the DPP9-GKI heterozygous mice that has affected new collagen deposition. It would also be of interest to determine whether the collagen fibrils in DPP9-GKI tissues are ordered or disordered. Disordered collagen fibrils confer less strength on the host tissue, since the mechanical behaviour of the connective tissue of skin is primarily determined by collagen organisation and composition (Xu et al., 2008, Bancelin et al., 2015, Smithers et al., 2016).

Once again, the availability of a DPP9-specific inhibitor could be useful for testing these theories. By administering an inhibitor long-term, it may be possible to show a gradual decline in collagen. Nevertheless, further studies are required to elucidate the timing

of collagen decline and whether fibril disorganisation exists, to attempt to determine the mechanistic link between DPP9 enzymatic activity and collagen in the skin.

7.3.2 Immune regeneration and immunity in the adult mouse

The *in vivo* expression of DPP9 in immunological tissues and cells is well documented, however the role of DPP9 in immune regeneration and immune cell repopulation has not been investigated. Protection from exposure to environmental toxins and pathogens is essential for mouse survival and involves a functional innate and adaptive immune system. The findings in this thesis in respect to donor engraftment and subsequent immune responses in chimeric mice created using DPP9 enzyme activity deficient stem cells (Chapter 6) are novel and have broadened knowledge of DPP9 enzymatic activity in immune function.

Recently, interest in DPP9 as a potential therapeutic target has increased due to the implications of a possible role in tumour growth and metastasis (Zhang et al., 2013). DPP9 is abundant in human tumour cell lines and may play a part in tumour growth (Spagnuolo et al., 2013). For future targetting of DPP9, it is important to expand *in vivo* data regarding immunity in order to assess and avoid possible off-target effects of therapy.

This study has shown that the lack of DPP9 enzymatic activity in HSCs does not impair either their ability to engraft in irradiated mice or to repopulate all major immune cell types in the regenerated immune system in both a primary and secondary chimera.

These novel findings have confirmed that DPP9 enzyme activity is not necessary for stable HSC self-renewal and proliferation.

These findings may suggest that DPP9 plays no role in immune regeneration at all but the subsequent challenge of the regenerated immune systems by influenza infection showed surprising and novel results implicating DPP9 enzyme activity in immune function. The rapid weight improvement of the DPP9-GKI-origin secondary chimeric mice compared to their WT-origin counterparts suggests an enhanced ability to recover from immune challenge when DPP9 enzymatic activity is absent. This is the first time that DPP9 has been examined in the context of infection with a virus or indeed any pathogenic organism. The result might be specific to influenza infection as opposed to other types of virus or immune challenge. This question needs to be addressed by a repeat of this experiment with influenza and then with other types of immune challenge.

Another approach to testing the impact or absence of DPP9 on immune status or function could be via the use of transgenic mice. Deleting DPP9 enzymatic activity from the immune system in this study was achieved by subjecting mice to immuno-ablative irradiation and regenerating a DPP9-enzyme-activity-deficient immune system. This method, while commonly used, is technically challenging and involves long-term experiments. If a conditional DPP9 knockout became available it could be crossed with existing Cre-Vav1 mice to cause conditional hematopoietic cell depletion of DPP9. Or, the DPP9 conditional could be crossed with other immune depleted mice, such as RAG knockouts, to produce partial loss of DPP9 in the context of immune ablation.

Induction of DPP9 deficiency could perhaps be targetted to specific immune cells, allowing in-depth analysis of immune and/or hematopoietic cell lineages. Alternatively, induction of DPP9 deficiency could be targetted to connective tissue cells to examine the role of DPP9 in supportive stromal cells. Such approaches have important implications for the potential therapeutic targetting of DPP9.

7.4 Concluding remarks

Unravelling the *in vivo* activity of a protease is a complex undertaking as proteases usually act as part of an interaction between many other proteins and pathways (Eckhard et al., 2016). It was, therefore, of great interest and significance in this study to determine the novel finding that DPP9 enzymatic activity is necessary for neonatal survival. The absence of gross morphological or histological defects in the neonates or reduced survival ability in the DPP9-GKI heterozygous and DPP9-enzyme-activity-deficient chimeric adults, suggests that the function of DPP9 enzymatic activity appears to be critical to a set time-point. The potential heart valve defects, observed dysregulation in autophagy and suggested disruption of normal catecholamine release and LCFA metabolism raised in this thesis hint at possible causes for lethality in the DPP9-GKI mice. These points, and the timing of death, allude to a metabolically crucial function of DPP9 enzymatic activity during the early neonatal starvation period. This critical function most likely influences more than one of the processes that are essential for the transition from maternal dependence of the neonate to independent metabolic autonomy. Future studies will be needed to elucidate the reason that the neonates die.

The characterisation of the adult DPP9-GKI heterozygous mice and creation of DPP9-GKI chimeric mice also provided novel findings of reduced skin collagen levels and enhanced immune function respectively. Once past the critical neonatal period, the DPP9-GKI heterozygous mice are no longer subject to reduced survival ability. However, it is evident from these results that DPP9 continues to be important in the biological processes of the mouse in ways that cannot be overcome by protease redundancy. The presence of DPP9 in the nucleus and previous studies in our lab and by others, have shown a role for DPP9 in regulatory processes. If DPP9 does have a regulatory role, then DPP9 enzymatic function would impact on many biological processes within the mouse. This suggestion needs examination by future studies.

By using *in vivo* techniques, this study has aimed at expanding the current published works of *in vitro* DPP9 function by providing physiologically relevant results. It has resulted in novel findings that have enhanced both the knowledge of DPP9 enzyme function and the overall biological roles of DPP9.

References

References

ABBOTT, C. & GORRELL, M. 2013. Dipeptidyl peptidase 8. *In:* RAWLINGS, N. L. & SALVESEN, G. (eds.) *Handbook of Proteolytic Enzymes 3rd Edition.* San Diego: Elsevier.

ABBOTT, C. A. & GORRELL, M. D. 2002. The family of CD26/DPIV and related ectopeptidases. *In:* LANGNER, J. & ANSORGE, S. (eds.) *Ectopeptidases: CD13/Aminopeptidase N and CD26/Dipeptidylpeptidase IV in Medicine and Biology.* NY: Kluwer/Plenum.

ABBOTT, C. A., MCCAUGHAN, G. W. & GORRELL, M. D. 1999. Two highly conserved glutamic acid residues in the predicted beta propeller domain of dipeptidyl peptidase IV are required for its enzyme activity. *FEBS Letters,* 458**,** 278-284.

ABBOTT, C. A., YU, D. M. T., MCCAUGHAN, G. W. & GORRELL, M. D. 2000a. Post proline peptidases having DP IV like enzyme activity. *Advances in Experimental Medicine and Biology,* 477**,** 103-109.

ABBOTT, C. A., YU, D. M. T., WOOLLATT, E., SUTHERLAND, G. R., MCCAUGHAN, G. W. & GORRELL, M. D. 2000b. Cloning, expression and chromosomal localization of a novel human dipeptidyl peptidase (DPP) IV homolog, DPP8. *European Journal of Biochemistry,* 267**,** 6140-6150.

AERTGEERTS, K., LEVIN, I., SHI, L., SNELL, G. P., JENNINGS, A., PRASAD, G. S., ZHANG, Y., KRAUS, M. L., SALAKIAN, S., SRIDHAR, V., WIJNANDS, R. & TENNANT, M. G. 2005. Structural and kinetic analysis of the substrate specificity of human fibroblast activation protein {alpha}. *Journal of Biological Chemistry,* 280**,** 19441

- 19444.

AJAMI, K., ABBOTT, C. A., MCCAUGHAN, G. W. & GORRELL, M. D. 2004. Dipeptidyl peptidase 9 has two forms, a broad tissue distribution, cytoplasmic localization and DPIV-like peptidase activity. *Biochimica et Biophysica Acta (BBA) - Gene Structure and Expression,* 1679**,** 18-28.

AJAMI, K., ABBOTT, C. A., OBRADOVIC, M., GYSBERS, V., KÄHNE, T., MCCAUGHAN, G. W. & GORRELL, M. D. 2003. Structural requirements for catalysis, expression and dimerisation in the CD26/DPIV gene family. *Biochemistry,* 42**,** 694-701. doi 10.1021/bi026846s.

AJAMI, K., PITMAN, M. R., WILSON, C. H., PARK, J., MENZ, R. I., STARR, A. E., COX, J. H., ABBOTT, C. A., OVERALL, C. M. & GORRELL, M. D. 2008. Stromal cell-derived factors 1 alpha and 1 beta, inflammatory protein-10 and interferon-inducible T cell chemo-attractant are novel substrates of dipeptidyl peptidase 8. *FEBS Letters,* 582**,** 819-825.

AKASHI, K., TRAVER, D., MIYAMOTO, T. & WEISSMAN, I. L. 2000. A clonogenic common myeloid progenitor that gives rise to all myeloid lineages. *Nature,* 404**,** 193-197.

ALIREZAEI, M., KEMBALL CC FAU - FLYNN, C. T., FLYNN CT FAU - WOOD, M. R., WOOD MR FAU - WHITTON, J. L., WHITTON JL FAU - KIOSSES, W. B. & KIOSSES, W. B. 2010. Short-term fasting induces profound neuronal autophagy. *Autophagy,* 6**,** 702-710.

ANDRADE, J., GE, S., SYMBATYAN, G., ROSOL, M. S., OLCH, A. J. & CROOKS, G. M. 2011. Effects of Sub-lethal Irradiation on Patterns of Engraftment after Murine Bone Marrow Transplantation. *Biology of Blood and Marrow Transplantation,* 17**,**

608-619.

ANNAIDH, A. N., OTTENIO, M., BRUYÈRE, K., DESTRADE, M. & GILCHRIST, M. D. 2010. Mechanical Properties of Excised Human Skin. *In:* LIM, C. T. & GOH, J. C. H. (eds.) *6th World Congress of Biomechanics (WCB 2010). August 1-6, 2010 Singapore: In Conjunction with 14th International Conference on Biomedical Engineering (ICBME) and 5th Asia Pacific Conference on Biomechanics (APBiomech).* Berlin, Heidelberg: Springer Berlin Heidelberg.

ANSORGE, S., BANK, U., HEIMBURG, A., HELMUTH, M., KOCH, G., TADJE, J., LENDECKEL, U., WOLKE, C., NEUBERT, K., FAUST, J., FUCHS, P., REINHOLD, D., THIELITZ, A. & TÄGER, M. 2009. Recent insights into the role of dipeptidyl aminopeptidase IV (DPIV) and aminopeptidase N (APN) families in immune functions. *Clinical Chemistry and Laboratory Medicine,* 47**,** 253-261.

ARIKAWA-HIRASAWA, E., WATANABE H FAU - TAKAMI, H., TAKAMI H FAU - HASSELL, J. R., HASSELL JR FAU - YAMADA, Y. & YAMADA, Y. 1999. Perlecan is essential for cartilage and cephalic development. *Nature Genetics,* 23.

AULETTA, J. & LAZARUS, H. 2005. Immune restoration following hematopoietic stem cell transplantation: an evolving target. *Bone Marrow Transplantation,* 35**,** 835-857.

AULETTA, J. J., DEVECCHIO, J. L., FERRARA, J. L. M. & HEINZEL, F. P. 2004. Distinct Phases in Recovery of Reconstituted Innate Cellular-Mediated Immunity after Murine Syngeneic Bone Marrow Transplantation. *Biology of the Blood and Marrow Transplantation,* 10**,** 834-847.

AWWAD, H. K. 1990. Early Reacting Tissues: the lymphoid tissue and the immune

systems. *Radiation Oncology: Radiobiological and Physiological Perspectives: The boundary-zone between clinical radiotherapy and fundamental radiobiology and physiology.* Dordrecht: Springer Science + Business Media.

BABOVIC, S. & EAVES, C. J. 2014. Hierarchical organization of fetal and adult hematopoietic stem cells. *Experimental Cell Research,* 329**,** 185-191.

BANCELIN, S., LYNCH, B., BONOD-BIDAUD, C., DUCOURTHIAL, G., PSILODIMITRAKOPOULOS, S., DOKLÁDAL, P., ALLAIN, J.-M., SCHANNE-KLEIN, M.-C. & RUGGIERO, F. 2015. Ex vivo multiscale quantitation of skin biomechanics in wild-type and genetically-modified mice using multiphoton microscopy. *Scientific Reports,* 5**,** 17635.

BANK, U., HEIMBURG, A., WOHLFARTH, A., KOCH, G., NORDHOFF, K., JULIUS, H., HELMUTH, M., BREYER, D., REINHOLD, D., TAGER, M. & ANSORGE, S. 2011. Outside or inside: role of the subcellular localization of DP4-like enzymes for substrate conversion and inhibitor effects. *Biological chemistry,* 392**,** 169-87.

BASU, A., KLIGMAN, L. H., SAMULEWICZ, S. J. & HOWE, C. C. 2001. Impaired wound healing in mice deficient in a matricellular protein SPARC (osteonectin, BM-40). *BMC Cell Biology,* 2**,** 1-9.

BASU, S., RAY, A. & DITTEL, B. N. 2013. Differential Representation of B Cell Subsets in Mixed Bone Marrow Chimera Mice Due to Expression of Allelic Variants of CD45 (CD45.1/CD45.2). *Journal of immunological methods,* 396**,** 163-167.

BENVENISTE, P., FRELIN, C., JANMOHAMED, S., BARBARA, M., HERRINGTON, R., HYAM, D. & ISCOVE, N. N. 2010. Intermediate-Term Hematopoietic Stem Cells with Extended but Time-Limited Reconstitution Potential. *Cell Stem Cell,* 6**,** 48-58.

BIBEN, C., WEBER, R., KESTEVEN, S., STANLEY, E., MCDONALD, L., ELLIOTT, D. A., BARNETT, L., KÖENTGEN, F., ROBB, L., FENELEY, M. & HARVEY, R. P. 2000. Cardiac Septal and Valvular Dysmorphogenesis in Mice Heterozygous for Mutations in the Homeobox Gene Nkx2-5. *Circulation Research,* 87**,** 888-895.

BILLINGS, P. C., ROMERO-WEAVER, A. L. & KENNEDY, A. R. 2014. Effect of Gender on the Radiation Sensitivity of Murine Blood Cells. *Gravitational and space research : publication of the American Society for Gravitational and Space Research,* 2**,** 25-31.

BJELKE, J., CHRISTENSEN, J., NIELSEN, P., BRANNER, S., KANSTRUP, A., WAGTMANN, N. & RASMUSSEN, B. 2006. Dipeptidyl peptidase 8 and 9 specificity and molecular characterization compared to dipeptidyl peptidase IV. *Biochemistry Journal,* 396**,** 391-399.

BOUVIER, N. M. & LOWEN, A. C. 2010. Animal Models for Influenza Virus Pathogenesis and Transmission. *Viruses,* 2010**,** 1530-1563.

BOWIE, M. B., KENT DG FAU - DYKSTRA, B., DYKSTRA B FAU - MCKNIGHT, K. D., MCKNIGHT KD FAU - MCCAFFREY, L., MCCAFFREY L FAU - HOODLESS, P. A., HOODLESS PA FAU - EAVES, C. J. & EAVES, C. J. 2007. Identification of a new intrinsically timed developmental checkpoint that reprograms key hematopoietic stem cell properties. *Proceedings of the National Academy of Sciences of the United States of America,* 104**,** 5878-5882.

BRADSHAW, A. D., PUOLAKKAINEN, P., WIGHT, T. N., HELENE SAGE, E., DASGUPTA, J. & DAVIDSON, J. M. 2003. SPARC-Null Mice Display Abnormalities in the Dermis Characterized by Decreased Collagen Fibril Diameter and Reduced Tensile

Strength. *Journal of Investigative Dermatology,* 120**,** 949-955.

BRENNEN, W. N., ISAACS, J. T. & DENMEADE, S. R. 2012. Rationale Behind Targeting Fibroblast Activation Protein–Expressing Carcinoma-Associated Fibroblasts as a Novel Chemotherapeutic Strategy. *Molecular Cancer Therapeutics,* 11**,** 257-266.

BROUGHTON, N. G., JANIS, J. E. & ATTINGER, C. E. 2006. The basic science of wound healing. *Plastic and reconstructive surgery,* 117**,** 12S-34S.

BROXMEYER, H. E., HOGGATT J FAU - O'LEARY, H. A., O'LEARY HA FAU - MANTEL, C., MANTEL C FAU - CHITTETI, B. R., CHITTETI BR FAU - COOPER, S., COOPER S FAU - MESSINA-GRAHAM, S., MESSINA-GRAHAM S FAU - HANGOC, G., HANGOC G FAU - FARAG, S., FARAG S FAU - ROHRABAUGH, S. L., ROHRABAUGH SL FAU - OU, X., OU X FAU - SPETH, J., SPETH J FAU - PELUS, L. M., PELUS LM FAU - SROUR, E. F., SROUR EF FAU - CAMPBELL, T. B. & CAMPBELL, T. B. 2012. Dipeptidylpeptidase 4 negatively regulates colony-stimulating factor activity and stress hematopoiesis. *Nature medicine,* 18.

BUHLING, F., KUNZ, D., REINHOLD, D., ULMER, A. J., ERNST, M., FLAD, H. D. & ANSORGE, S. 1994. Expression and functional rol of dipeptidyl peptidase IV (CD26) on human natural killer cells. *Nature Immunology,* 13**,** 270-279.

BURKEY, B. F., HOFFMANN, P. K., HASSIEPEN, U., TRAPPE, J., JUEDES, M. & FOLEY, J. E. 2008. Adverse effects of dipeptidyl peptidases 8 and 9 inhibition in rodents revisited. *Diabetes, Obesity and Metabolism,* 10**,** 1057-1061.

CALOGERO, S., GRASSI, F., AGUZZI, A., VOIGTLANDER, T., FERRIER, P., FERRARI, S. & BIANCHI, M. E. 1999. The lack of chromosomal protein Hmg1 does not disrupt cell growth but causes lethal hypoglycaemia in newborn mice. *Nature Genetics,*

22**,** 276-280.

CHAGRAOUI, J., LEPAGE-NOLL A FAU - ANJO, A., ANJO A FAU - UZAN, G., UZAN G FAU - CHARBORD, P. & CHARBORD, P. 2003. Fetal liver stroma consists of cells in epithelial-to-mesenchymal transition. *Blood,* 101**,** 2973-2982.

CHEN, J. & HARRISON, D. E. 2002. Quantitative trait loci regulating relative lymphocyte proportions in mouse peripheral blood. *Blood,* 99**,** 561.

CHEN, T., AJAMI, K., MCCAUGHAN, G. W., GAI, W.-P., GORRELL, M. D. & ABBOTT, C. A. 2005. Molecular Characterization of a novel Dipeptidyl Peptidase Like 2 short form (DPL2-s) that is highly expressed in the brain and lacks dipeptidyl peptidase activity. *Biochimica et Biophysica Acta,* 1764**,** 33-43.

CHEN, T., SHEN, X.-F., CHEGINI, F., GAI, W.-P. & ABBOTT, C. A. 2008. Molecular characterisation of a novel dipeptidyl peptidase like protein: its pathological link to Alzheimer's disease. *Clinical Chemistry and Laboratory Medicine,* 46**,** A13.

CHEN, W., CHATTA, G. S., RUBIN, W. D., CLARK, J. G., HACKMAN, R. C., MADTES, D. K., LIGITT, D. H., KUSUNOKI, Y., MARTIN, P. J. & CHEEVER, M. A. 1998. T Cells Specific for a Polymorphic Segment of CD45 Induce Graft-Versus-Host Disease with Predominant Pulmonary Vasculitis. *The Journal of Immunology,* 161**,** 909-918.

CHEN, Y. 2013. *Functional Characterisation of Dipeptidyl Peptidase 9 using mouse models.* Doctor of Philosophy, University of Sydney.

CHEN, Y., GALL, M. G., ZHANG, H., KEANE, F. M., MCCAUGHAN, G. W., YU, D. M. & GORRELL, M. D. 2016. Dipeptidyl Peptidase 9 Enzymatic Activity Influences the Expression of Neonatal Metabolic Genes. *Experimental Cell Research,* 342**,** 72-

82.

CHOUDHARY, C., KUMAR, C., GNAD, F., NIELSEN, M. L., REHMAN, M., WALTHER, T. C., OLSEN, J. V. & MANN, M. 2009. Lysine Acetylation Targets Protein Complexes and Co-Regulates Major Cellular Functions. *Science,* 325**,** 834-840.

CHOWDHURY, S., CHEN, Y., YAO, T.-W., AJAMI, K., WANG, X. M., POPOV, Y., SCHUPPAN, D., BERTOLINO, P., MCCAUGHAN, G. W., YU, D. M. & GORRELL, M. D. 2013. Regulation of dipeptidyl peptidase 8 and 9 expression in activated lymphocytes and injured liver. *World Journal of Gastroenterology,* 19**,** 2883-2893.

CHRISTIANSEN, V. J., JACKSON, K. W., LEE, K. N., DOWNS, T. D. & MCKEE, P. A. 2013. Targeting Inhibition of Fibroblast Activation Protein-α and Prolyl Oligopeptidase Activities on Cells Common to Metastatic Tumor Microenvironments. *Neoplasia,* 15**,** 348-358.

CLARK, S. J. 1957. Cellular Differentiation In The Kidneys Of Newborn Mice Studied With The Electron Microscope. *The Journal of Biophysical and Biochemical Cytology,* 3.

COLLINS, P. J., MCMAHON, G., O'BRIEN, P. & O'CONNOR, B. 2004. Purification, identification and characterisation of seprase from bovine serum. *International Journal of Biochemistry & Cell Biology,* 36**,** 2320-33.

COLLOMBAT, P., MANSOURI, A., HECKSHER-SØRENSEN, J., SERUP, P., KRULL, J., GRADWOHL, G. & GRUSS, P. 2003. Opposing actions of Arx and Pax4 in endocrine pancreas development. *Genes & Development,* 17**,** 2591-2603.

CONARELLO, S., LI, Z., RONAN, J., ROY, R., ZHU, L., JIANG, G., LIU, F., WOODS, J., ZYCBAND, E., MOLLER, D., THORNBERRY, N. & ZHANG, B. 2003. Mice lacking

dipeptidyl peptidase IV are protected against obesity and insulin resistance. *Proceedings of the National Academy of Sciences United States of America,* 100**,** 6825-6830.

CONWAY, S. J., KRUZYNSKA-FREJTAG, A., KNEER, P. L., MACHNICKI, M. & KOUSHIK, S. V. 2003. What cardiovascular defect does my prenatal mouse mutant have, and why? *genesis,* 35**,** 1-21.

CRAWFORD, L. W., FOLEY, J. F. & ELMORE, S. A. 2010. Histology Atlas of the Developing Mouse Hepatobiliary System with Emphasis on Embryonic Days 9.5-18.5. *Toxicologic Pathology,* 38**,** 872-906.

CRONIN, S., BERGER, S., DING, J., SCHYMICK, J. C., WASHECKA, N., HERNANDEZ, D. G., GREENWAY, M. J., BRADLEY, D. G., TRAYNOR, B. J. & HARDIMAN, O. 2008. A genome-wide association study of sporadic ALS in a homogenous Irish population. *Human Molecular Genetics,* 17**,** 768-774.

CUNNINGHAM, D. F. & O'CONNOR, B. 1997. Proline specific peptidases. *Biochimica et Biophysica Acta,* 1343**,** 160-186.

DAVIDSON, J. M. 2001. Experimental Animal Wound Models. *Wounds: a compendium of clinical research and practice* 13**,** 9-23.

DEACON, C. F. 2011. Dipeptidyl peptidase-4 inhibitors in the treatment of type 2 diabetes: a comparative review. *Diabetes, Obesity and Metabolism,* 13**,** 7-18.

DORE, B. A., GROGAN, W. M., MADGE, G. E. & WEBB, S. R. 1981. Biphasic development of the postnatal mouse pancreas. *Biology of the Neonate,* 40**,** 209-217.

DREW, A. F., LIU, H., DAVIDSON, J. M., DAUGHERTY, C. C. & DEGEN, J. L. 2001. Wound-healing defects in mice lacking fibrinogen. *Blood,* 97**,** 3691-3698.

DUBOIS, V., GINNEKEN, C. V., DE COCK, H., LAMBEIR, A.-M., VAN DER VEKEN, P., AUGUSTYNS, K., CHEN, X., SCHARPÉ, S. & DE MEESTER, I. 2009. Enzyme activity and immunohistochemical localization of dipeptidyl peptidase 8 and 9 in male reproductive tissues. *Journal of Histochemistry and Cytochemistry,* 57**,** 531-541.

DUBOIS, V., LAMBEIR, A.-M., VANDAMME, S., MATHEEUSSEN, V., GUISEZ, Y., SCHARPÉ, S. & DE MEESTER, I. 2010. Dipeptidyl peptidase 9 (DPP9) from bovine testes: Identification and characterization as the short form by mass spectrometry. *Biochimica et Biophysica Acta - Proteins & Proteomics,* 1804**,** 781-788.

DURAN-STRUUCK, R. & DYSKO, R. C. 2009. Principles of Bone Marrow Transplantation (BMT): Providing Optimal Veterinary and Husbandry Care to Irradiated Mice in BMT Studies. *Journal of the American Association for Laboratory Animal Science : JAALAS,* 48**,** 11-22.

ECKHARD, U., HUESGEN, P. F., SCHILLING, O., BELLAC, C. L., BUTLER, G. S., COX, J. H., DUFOUR, A., GOEBELER, V., KAPPELHOFF, R., KELLER, U. A. D., KLEIN, T., LANGE, P. F., MARINO, G., MORRISON, C. J., PRUDOVA, A., RODRIGUEZ, D., STARR, A. E., WANG, Y. & OVERALL, C. M. 2016. Active site specificity profiling of the matrix metalloproteinase family: Proteomic identification of 4300 cleavage sites by nine MMPs explored with structural and synthetic peptide cleavage analyses. *Matrix Biology,* 49**,** 37-60.

EFEYAN, A., ZONCU R FAU - CHANG, S., CHANG S FAU - GUMPER, I., GUMPER I FAU - SNITKIN, H., SNITKIN H FAU - WOLFSON, R. L., WOLFSON RL FAU - KIRAK, O., KIRAK O FAU - SABATINI, D. D., SABATINI DD FAU - SABATINI, D. M. & SABATINI, D. M. 2013. Regulation of mTORC1 by the Rag GTPases is necessary for neonatal

autophagy and survival. *Nature,* 493**,** 679-683.

EMA, H. & NAKAUCHI, H. 2000. Expansion of hematopoietic stem cells in the developing liver of a mouse embryo. *Hematopoiesis,* 95**,** 2284-2288.

ERICKSON, R. H., SUZUKI, Y., SEDLMAYER, A. & KIM, Y. S. 1992. Biosynthesis and degradation of altered immature forms of intestinal dipeptidyl peptidase IV in a rat strain lacking the enzyme. *Journal of Biological Chemistry,* 267**,** 21623-9.

FINGERLIN, T. E., MURPHY, E., ZHANG, W., PELJTO, A. L., BROWN, K. K., STEELE, M. P., LOYD, J. E., COSGROVE, G. P., LYNCH, D., GROSHONG, S., COLLARD, H. R., WOLTERS, P. J., BRADFORD, W. Z., KOSSEN, K., SEIWERT, S. D., DU BOIS, R. M., GARCIA, C. K., DEVINE, M. S., GUDMUNDSSON, G., ISAKSSON, H. J., KAMINSKI, N., ZHANG, Y., GIBSON, K. F., LANCASTER, L. H., COGAN, J. D., MASON, W. R., MAHER, T. M., MOLYNEAUX, P. L., WELLS, A. U., MOFFATT, M. F., SELMAN, M., PARDO, A., KIM, D. S., CRAPO, J. D., MAKE, B. J., REGAN, E. A., WALEK, D. S., DANIEL, J. J., KAMATANI, Y., ZELENIKA, D., SMITH, K., MCKEAN, D., PEDERSEN, B. S., TALBERT, J., KIDD, R. N., MARKIN, C. R., BECKMAN, K. B., LATHROP, M., SCHWARZ, M. I. & SCHWARTZ, D. A. 2013. Genome-wide association study identifies multiple susceptibility loci for pulmonary fibrosis. *Nature Genetics,* 45**,** 613-620.

FRERKER, N., WAGNER, L., WOLF, R., HEISER, U., HOFFMAN, T., RAHFELD, J.-U., SCHADE, J., KARL, T., NAIM, H. Y., ALFALAH, M., DEMUTH, H. U. & VON HORSTEN, S. 2007. Neuropeptide Y (NPY) cleaving enzymes: Structural and functional homologues of dipeptidyl peptidase 4. *Peptides,* 28**,** 257-268.

FULLGRABE, J., KLIONSKY, D. J. & JOSEPH, B. 2014. The return of the nucleus:

transcriptional and epigenetic control of autophagy. *Nat Rev Mol Cell Biol,* 15**,** 65-74.

FUNK, L. 2007. *Tendon Healing Mechanobiology* [Online]. Lennard Funk Consultant Shoulder & Upper Limb Surgeon. [Accessed 19 Aug 2016].

GALL, M. G., CHEN, Y., RIBEIRO, A. J. V. D., ZHANG, H., BAILEY, C. G., SPIELMAN, D., YU, D. M. & GORRELL, M. D. 2013. Targeted inactivation of Dipeptidyl Peptidase 9 enzyme activity causes mouse neonate lethality. *PLOS ONE,* 8**,** e0078378.

GARG, V., MUTH, A. N., RANSOM, J. F., SCHLUTERMAN, M. K., BARNES, R., KING, I. N., GROSSFELD, P. D. & SRIVASTAVA, D. 2005. Mutations in *NOTCH1* cause aortic valve disease. *Nature,* 437**,** 270-274.

GARIN-CHESA, P., OLD, L. J. & RETTIG, W. J. 1990. Cell surface glycoprotein of reactive stromal fibroblasts as a potential antibody target in human epithelial cancers. *Proceedings of the National Academy of Sciences of the United States of America,* 87**,** 7235-7239.

GEISS-FRIEDLANDER, R., PARMENTIER, N., MOELLER, U., URLAUB, H., VAN DEN EYNDE, B. J. & MELCHIOR, F. 2009. The cytoplasmic peptidase DPP9 Is rate-limiting for degradation of proline-containing peptides. *Journal of Biological Chemistry,* 284**,** 27211-27219.

GHOSN, E. E. B., WATERS, J., PHILLIPS, M., YAMAMOTO, R., LONG, B. R., YANG, Y., GERSTEIN, R., STODDART, C. A., NAKAUCHI, H. & HERZENBERG, L. A. 2016. Fetal Hematopoietic Stem Cell Transplantation Fails to Fully Regenerate the B-Lymphocyte Compartment. *Stem Cell Reports,* 6**,** 137-149.

GORRELL, M. D. 2005. Dipeptidyl peptidase IV and related enzymes in cell biology and

liver disorders. *Clinical Science,* 108**,** 277-292.

GORRELL, M. D., GYSBERS, V. & MCCAUGHAN, G. W. 2001. CD26: A multifunctional integral membrane and secreted protein of activated lymphocytes. *Scandinavian Journal of Immunology,* 54**,** 249-264.

GORRELL, M. D., WICKSON, J. & MCCAUGHAN, G. W. 1991. Expression of the rat CD26 Antigen (dipeptidyl peptidase IV) on subpopulations of rat lymphocytes. *Cellular Immunology,* 134**,** 205-215.

GORRELL, M. D. & YU, D. M. T. 2005. Diverse functions in a conserved structure: The dipeptidyl peptidase IV gene family. *In:* ROBINSON, J. W. (ed.) *Trends in Protein Research.* New York: Nova Science Publishers, Inc.

GROMPE, M., AL-DHALIMY, M., FINEGOLD, M., OU, C.-N., BURLINGAME, T., KENNAWAY, N. G. & SORIANO, P. 2011. Loss of fumarylacetoacetate hydrolase is responsible for the neonatal hepatic dysfunction phenotype of lethal albino mice. *Genes & Development,* 7**,** 2298-2307.

GUDMUNDSSON, K. O., STULL, S. W. & KELLER, J. R. 2012. Transplantation of Mouse Fetal Liver Cells for Analyzing the Function of Hematopoietic Stem and Progenitor Cells. *In:* SINGH, R. S. (ed.) *Somatic Stem Cells: Methods and Protocols.* Totowa, NJ: Humana Press.

HADI, A. M., MOUCHAERS, K. T. B., SCHALIJ, I., GRUNBERG, K., MEIJER, G. A., VONK-NOORDEGRAAF, A., VAN DER LAARSE, W. J. & BELIËN, J. A. M. 2011. Rapid quantification of myocardial fibrosis: a new macro-based automated analysis. *Cellular Oncology (Dordrecht),* 34**,** 343-354.

HAMSON, E. J., KEANE, F. M., THOLEN, S., SCHILLING, O. & GORRELL, M. D. 2014.

Understanding Fibroblast Activation Protein (FAP): substrates, activities, expression and targeting for cancer therapy. *PROTEOMICS – Clinical Applications,* 8**,** 454-463.

HARDY, I. 1997. Possible factors influencing vertebrate sex ratios: an introductory overview. *Applied Animal Behaviour Science,* 51**,** 217-241.

HARRISON, D. E., ZHONG RK FAU - JORDAN, C. T., JORDAN CT FAU - LEMISCHKA, I. R., LEMISCHKA IR FAU - ASTLE, C. M. & ASTLE, C. M. 1997. Relative to adult marrow, fetal liver repopulates nearly five times more effectively long-term than short-term. *Experimental Hematology,* 25**,** 293-297.

HARSTAD, E. B., ROSENBLUM, J. S., GORRELL, M. D., ACHANZAR, W. E., MINIMO, L., WU, J., ROSINI-MARTHALER, L., GULLO, R., ORDWAY, N. D., KIRBY, M. S., CHADWICK, K. D., COSMA, G. N. & MOYER, C. F. 2013. DPP8 and DPP9 expression in cynomolgus monkey and Sprague Dawley rat tissues. *Regulatory Peptides,* 186**,** 26-35.

HAUB, P. & MECKEL, T. 2015. A Model based Survey of Colour Deconvolution in Diagnostic Brightfield Microscopy: Error Estimation and Spectral Consideration. *Scientific Reports,* 5**,** 12096.

HEIMBURG, A., REINHOLD, D., FAUST, J., FUCHS, P., NEUBERT, K., TAGER, M., ANSORGE, S. & BANK, U. 2008. Differential expression of DPIV-like enzymes during the course of T cell activation. *Clinical Chemistry and Laboratory Medicine,* 46**,** A12.

HELMUTH, M., REINHOLD, D., STEFIN, S., TAGER, M., ANSORGE, S. & BANK, U. 2006. Tissue distribution of DPIV-like activities in wild type mice and CD26 knock out mice under physiological and pathological conditions. *Clinical Chemistry and*

Laboratory Medicine, 46**,** A26.

HESS, M. W., STONER, R. D. & COTTIER, H. 1967. Growth Characteristics of Mouse Thymus in the Neonatal Period. *Nature,* 215**,** 426-428.

HEYMANN, E. & MENTLEIN, R. 1978. Liver dipeptidyl aminopeptidase IV hydrolyzes substance P. *FEBS Letters,* 91**,** 360-4.

HINTON, R. B., JR., ALFIERI CM FAU - WITT, S. A., WITT SA FAU - GLASCOCK, B. J., GLASCOCK BJ FAU - KHOURY, P. R., KHOURY PR FAU - BENSON, D. W., BENSON DW FAU - YUTZEY, K. E. & YUTZEY, K. E. 2008. Mouse heart valve structure and function: echocardiographic and morphometric analyses from the fetus through the aged adult. *American Journal of Physiology - Heart and Circulatory Physiology,* 294**,** H2480-H2488.

HO, L., AYTAC, U., STEPHENS, L. C., OHNUMA, K., MILLS, G. B., MCKEE, K. S., NEUMANN, C., LAPUSHIN, R., CABANILLAS, F., ABBRUZZESE, J. L., MORIMOTO, C. & DANG, N. H. 2001. In vitro and in vivo antitumor effect of the anti-CD26 monoclonal antibody 1F7 on human CD30+anaplastic large cell T-cell lymphoma Karpas 299. *Clinical Cancer Research,* 7**,** 2031-2040.

HUANG, R. & LIU, W. 2015. Identifying an essential role of nuclear LC3 for autophagy. *Autophagy,* 11**,** 852-853.

HUNG, S.-Y., HUANG, W.-P., LIOU, H.-C. & FU, W.-M. 2015. LC3 overexpression reduces Aβ neurotoxicity through increasing α7nAchR expression and autophagic activity in neurons and mice. *Neuropharmacology,* 93**,** 243-251.

INAMOTO, T., YAMADA, T., OHNUMA, K., KINA, S., TAKAHASHI, N., YAMOCHI, T., INAMOTO, S., KATSUOKA, Y., HOSONO, O., TANAKA, H., DANG, N. H. &

MORIMOTO, C. 2007. Humanized Anti-CD26 Monoclonal Antibody as a Treatment for Malignant Mesothelioma Tumors. *Clinical Cancer Research,* 13**,** 4191-4200.

INAMOTO, T., YAMOCHI, T., OHNUMA, K., IWATA, S., KINA, S., INAMOTO, S., TACHIBANA, M., KATSUOKA, Y., DANG, N. H. & MORIMOTO, C. 2006. Anti-CD26 Monoclonal Antibody–Mediated G1-S Arrest of Human Renal Clear Cell Carcinoma Caki-2 Is Associated with Retinoblastoma Substrate Dephosphorylation, Cyclin-Dependent Kinase 2 Reduction, p27kip1 Enhancement, and Disruption of Binding to the Extracellular Matrix. *Clinical Cancer Research,* 12**,** 3470-3477.

ITO, K., KOMAZAKI, S., SASAMOTO, K., YOSHIDA, M., NISHI, M., KITAMURA, K. & TAKESHIMA, H. 2001. Deficiency of triad junction and contraction in mutant skeletal muscle lacking junctophilin type 1. *The Journal of Cell Biology,* 154**,** 1059-1067.

IVKOVIC, S., YOON BS FAU - POPOFF, S. N., POPOFF SN FAU - SAFADI, F. F., SAFADI FF FAU - LIBUDA, D. E., LIBUDA DE FAU - STEPHENSON, R. C., STEPHENSON RC FAU - DALUISKI, A., DALUISKI A FAU - LYONS, K. M. & LYONS, K. M. 2003. Connective tissue growth factor coordinates chondrogenesis and angiogenesis during skeletal development. *Development,* 130**,** 2779-2791.

JIAANG, W. T., CHEN, Y. S., HSU, T., WU, S. H., CHIEN, C. H., CHANG, C. N., CHANG, S. P., LEE, S. J. & CHEN, X. 2005. Novel isoindoline compounds for potent and selective inhibition of prolyl dipeptidase DPP8. *Bioorg Med Chem Lett,* 15**,** 687-91.

JONES, B., ADAMS, S., MILLER, G. T., JESSON, M. I., WATANABE, T. & WALLNER, B. P. 2003. Hematopoietic stimulation by a dipeptidyl peptidase inhibitor reveals a novel regulatory mechanism and therapeutic treatment for blood cell deficiencies. *Hematopoiesis,* 102**,** 1641-1648.

JUSTA-SCHUCH, D., MÖLLER, U. & GEISS-FRIEDLANDER, R. 2014. The amino terminus extension in the long dipeptidyl peptidase 9 isoform contains a nuclear localization signal targeting the active peptidase to the nucleus. *Cellular and Molecular Life Sciences,* 71**,** 3611-3626.

JUSTA-SCHUCH, D., SILVA-GARCIA, M., PILLA, E., ENGELKE, M., KILISCH, M., LENZ, C., MÖLLER, U., NAKAMURA, F., URLAUB, H. & GEISS-FRIEDLANDER, R. 2016. DPP9 is a novel component of the N-end rule pathway targeting the tyrosine kinase Syk. *eLife,* 5**,** e16370.

KARSENTY, G. & WAGNER, E. F. 2002. Reaching a genetic and molecular understanding of skeletal development. *Developmental Cell,* 2**,** 389-406.

KAUFMAN, M., NIKITIN, A. Y. & SUNDBERG, J. P. 2010. *Histological Basis of Mouse Endocrine System Development : A Comparative Analysis,* Boca Raton, CRC Press.

KAUSHIK, S., RODRIGUEZ-NAVARRO, JOSE A., ARIAS, E., KIFFIN, R., SAHU, S., SCHWARTZ, GARY J., CUERVO, ANA M. & SINGH, R. Autophagy in Hypothalamic AgRP Neurons Regulates Food Intake and Energy Balance. *Cell Metabolism,* 14**,** 173-183.

KEANE, F. M., CHOWDHURY, S., YAO, T.-W., NADVI, N. A., GALL, M. G., CHEN, Y., OSBORNE, B., VIEIRA DE RIBEIRO, A. J., CHURCH, W. B., MCCAUGHAN, G. W.,

GORRELL, M. D. & YU, D. M. T. 2012. Targeting Dipeptidyl Peptidase-4 (DPP-4) and Fibroblast Activation Protein (FAP) for diabetes and cancer therapy. *In:* DUNN, B. (ed.) *Proteinases as Drug Targets.* Cambridge, UK: Royal Society of Chemistry.

KEANE, F. M., NADVI, N. A., YAO, T.-W. & GORRELL, M. D. 2011. Neuropeptide Y, B-type natriuretic peptide, substance P and peptide YY are novel substrates of fibroblast activation protein-α. *FEBS Journal,* 278**,** 1316-1332.

KEANE, F. M., YAO, T.-W., SEELK, S., GALL, M. G., CHOWDHURY, S., POPLAWSKI, S. E., LAI, J. H., LI, Y., WU, W., FARRELL, P., VIEIRA DE RIBEIRO, A. J., OSBORNE, B., YU, D. M. T., SETH, D., RAHMAN, K., HABER, P., TOPALOGLU, A. K., WANG, C., THOMSON, S., HENNESSY, A., PRINS, J., TWIGG, S. M., MCLENNAN, S. V., MCCAUGHAN, G. W., BACHOVCHIN, W. W. & GORRELL, M. D. 2014. Quantitation of fibroblast activation protein (FAP)-specific protease activity in mouse, baboon and human fluids and organs(). *FEBS open bio,* 4**,** 43-54.

KENT, D. G., COPLEY MR FAU - BENZ, C., BENZ C FAU - WOHRER, S., WOHRER S FAU - DYKSTRA, B. J., DYKSTRA BJ FAU - MA, E., MA E FAU - CHEYNE, J., CHEYNE J FAU - ZHAO, Y., ZHAO Y FAU - BOWIE, M. B., BOWIE MB FAU - ZHAO, Y., ZHAO Y FAU - GASPARETTO, M., GASPARETTO M FAU - DELANEY, A., DELANEY A FAU - SMITH, C., SMITH C FAU - MARRA, M., MARRA M FAU - EAVES, C. J. & EAVES, C. J. 2009. Prospective isolation and molecular characterization of hematopoietic stem cells with durable self-renewal potential. *Blood,* 113**,** 6342-6350.

KIM, I., HE, S., YILMAZ, Ö. H., KIEL, M. J. & MORRISON, S. J. 2006. Enhanced purification of fetal liver hematopoietic stem cells using SLAM family receptors. *Blood,* 108**,**

737.

KIMLIN, L. & VIRADOR, V. 2013. Cellular Populations Isolated from Newborn Mouse Skin Including Mesenchymal Stem Cells. *In:* TURKSEN, K. (ed.) *Skin Stem Cells: Methods and Protocols.* Totowa, NJ: Humana Press.

KINA, T., IKUTA K FAU - TAKAYAMA, E., TAKAYAMA E FAU - WADA, K., WADA K FAU - MAJUMDAR, A. S., MAJUMDAR AS FAU - WEISSMAN, I. L., WEISSMAN IL FAU - KATSURA, Y. & KATSURA, Y. 2000. The monoclonal antibody TER-119 recognizes a molecule associated with glycophorin A and specifically marks the late stages of murine erythroid lineage. *British Journal of Haematology,* 109**,** 280-287.

KIRBY, M. S., YU, D. M., O'CONNOR, S. P. & GORRELL, M. D. 2010. Inhibitor selectivity in the clinical application of dipeptidyl peptidase-4 inhibition. *Clinical Science,* 118**,** 31-41.

KLEMANN, C., WAGNER, L., STEPHAN, M. & VON HÖRSTEN, S. 2016. Cut to the chase: a review of CD26/dipeptidyl peptidase-4's (DPP4) entanglement in the immune system. *Clinical & Experimental Immunology,* 185**,** 1-21.

KOHL, A., VOLK, H. D., BUNTROCK, P., KOHL, G., DIAMANTSTEIN, T. & VON BAEHR, R. 1991. The role of dipeptidylpeptidase IV positive T cells in wound healing and angiogenesis. *Agents and Actions,* 32**,** 125-127.

KOMATSU, M., WAGURI S FAU - UENO, T., UENO T FAU - IWATA, J., IWATA J FAU - MURATA, S., MURATA S FAU - TANIDA, I., TANIDA I FAU - EZAKI, J., EZAKI J FAU - MIZUSHIMA, N., MIZUSHIMA N FAU - OHSUMI, Y., OHSUMI Y FAU - UCHIYAMA, Y., UCHIYAMA Y FAU - KOMINAMI, E., KOMINAMI E FAU - TANAKA, K., TANAKA K FAU - CHIBA, T. & CHIBA, T. 2005. Impairment of starvation-induced and

constitutive autophagy in Atg7-deficient mice. 169**,** 425-434.

KONDO, M., WEISSMAN, I. L. & AKASHI, K. 1997. Identification of Clonogenic Common Lymphoid Progenitors in Mouse Bone Marrow. *Cell,* 91**,** 661-672.

KORKHOV, V. M. 2009. GFP-LC3 labels organised smooth endoplasmic reticulum membranes independently of autophagy. *Journal of Cellular Biochemistry,* 107**,** 86-95.

KOTOULAS, O. B., KALAMIDAS, S. A. & KONDOMERKOS, D. J. 2006. Glycogen autophagy in glucose homeostasis. *Pathology - Research and Practice,* 202**,** 631-638.

KRAPP, A., KNÖFLER, M., LEDERMANN, B., BÜRKI, K., BERNEY, C., ZOERKLER, N., HAGENBÜCHLE, O. & WELLAUER, P. K. 1998. The bHLH protein PTF1-p48 is essential for the formation of the exocrine and the correct spatial organization of the endocrine pancreas. *Genes & Development,* 12**,** 3752-3763.

KREIDBERG, J. A., DONOVAN, M. J., GOLDSTEIN, S. L., RENNKE, H., SHEPHERD, K., JONES, R. C. & JAENISCH, R. 1996. Alpha 3 beta 1 integrin has a crucial role in kidney and lung organogenesis. *Development,* 122**,** 3537-3547.

KUMA, A., HATANO, M., MATSUI, M., YAMAMOTO, A., NAKAYA, H., YOSHIMORI, T., OHSUMI, Y., TOKUHISA, T. & MIZUSHIMA, N. 2004. The role of autophagy during the early neonatal starvation period. *Nature,* 432**,** 1032-1036.

KUROKAWA, Y., MATOBA, R., TAKEMASA, I., NAKAMORI, S., TSUJIE, M., NAGANO, H., DONO, K., UMESHITA, K., SAKON, M., UENO, N., KITA, H., OBA, S., ISHII, S., KATO, K. & MONDEN, M. 2003. Molecular features of non-B, non-C hepatocellular carcinoma: a PCR-array gene expression profiling study. *Journal of Hepatology,* 39**,** 1004-1012.

LAFOREST, B., ANDELFINGER, G. & NEMER, M. 2011. Loss of Gata5 in mice leads to bicuspid aortic valve. *The Journal of Clinical Investigation,* 121**,** 2876-2887.

LANKAS, G., LEITING, B., ROY, R., EIERMANN, G., BECONI, M., BIFTU, T., CHAN, C., EDMONDSON, S., FEENEY, W., HE, H., IPPOLITO, D., KIM, D., LYONS, K., OK, H., PATEL, R., PETROV, A., PRYOR, K., QIAN, X., REIGLE, L., WOODS, A., WU, J., ZALLER, D., ZHANG, X., ZHU, L., WEBER, A. & THORNBERRY, N. 2005. Dipeptidyl peptidase IV inhibition for the treatment of type 2 diabetes - Potential importance of selectivity over dipeptidyl peptidases 8 and 9. *Diabetes,* 54**,** 2988-2994.

LEE, E.-F., JACOBS, R. E., DINOV, I., LEOW, A. & TOGA, A. W. 2005. Standard atlas space for C57BL/6J neonatal mouse brain. *Anatomy and Embryology,* 210**,** 245-263.

LEE, H. J., CHEN, Y. S., CHOU, C. Y., CHIEN, C. H., LIN, C. H., CHANG, G. G. & CHEN, X. 2006a. Investigation of the dimer interface and substrate specificity of prolyl dipeptidase DPP8. *Journal of Biological Chemistry,* 281**,** 38653-62.

LEE, K. H., LO, H. L., TANG, W. C., HSIAO, H. H. & YANG, P. M. 2014. A gene expression signature-based approach reveals the mechanisms of action of the Chinese herbal medicine berberine. *Scientific Reports,* 4**,** 6394.

LEE, K. N., JACKSON, K. W., CHRISTIANSEN, V. J., LEE, C. S., CHUN, J. G. & MCKEE, P. A. 2006b. Antiplasmin-cleaving enzyme is a soluble form of fibroblast activation protein. *Blood,* 107**,** 1397-404.

LEITCH, V. D., STRUDWICK, X. L., MATTHAEI, K. I., DENT, L. A. & COWIN, A. J. 2008. IL-5-overexpressing mice exhibit eosinophilia and altered wound healing through mechanisms involving prolonged inflammation. *Immunol Cell Biol,* 87**,** 131-140.

LEVINE, B. 2005. Eating oneself and uninvited guests: autophagy-related pathways in cellular defense. *Cell,* 120**,** 159-162.

LEVINE, B. & KLIONSKY, D. J. 2004. Development by Self-Digestion: Molecular Mechanisms and Biological Functions of Autophagy. *Developmental Cell,* 6**,** 463-477.

LEVINE, B. & KROEMER, G. 2008. Autophagy in the pathogenesis of disease. *Cell,* 132**,** 27-42.

LEVY, M., GORRELL, M., ABBOTT, C., PARK, J., RETTIG, W. & MCCAUGHAN, G. 1997. The cell surface oligopeptidase fibroblast activation protein is expressed by stellate cells at the tissue remodelling interface in human cirrhosis. *Hepatology,* 26**,** 449A.

LIU, Z.-J., HOFFMEISTER, K. M., HU, Z., MAGER, D. E., AIT-OUDHIA, S., DEBRINCAT, M. A., PLEINES, I., JOSEFSSON, E. C., KILE, B. T., ITALIANO, J., RAMSEY, H., GROZOVSKY, R., VENG-PEDERSEN, P., CHAVDA, C. & SOLA-VISNER, M. 2014. Expansion of the neonatal platelet mass is achieved via an extension of platelet lifespan. *Blood,* 123**,** 3381-3389.

LU, C., TILAN, J. U., EVERHART, L., CZARNECKA, M., SOLDIN, S. J., MENDU, D. R., JEHA, D., HANAFY, J., LEE, C. K., SUN, J., IZYCKA-SWIESZEWSKA, E., TORETSKY, J. A. & KITLINSKA, J. 2011. Dipeptidyl Peptidases as Survival Factors in Ewing Sarcoma Family of Tumors: Implications for tumor biology and therapy. *The Journal of Biological Chemistry,* 286**,** 27494-27505.

MADER, S. L., LIBAL, N. L., PRITCHETT-CORNING, K., YANG, R. & MURPHY, S. J. 2009. Refining timed pregnancies in two strains of genetically engineered mice. *Lab*

animal, 38**,** 305-310.

MADUENO, J. A., MUNOZ, E., BLAZQUEZ, V., GONZALEZ, R., APARICIO, P. & PENA, J. 1993. The CD26 antigen is coupled to protein tyrosine phosphorylation and implicated in CD16-mediated lysis in natural killer cells. *Scandinavian Journal of Immunology,* 37**,** 425-9.

MAES, M.-B., DUBOIS, V., BRANDT, I., LAMBEIR, A.-M., VAN DER VEKEN, P., AUGUSTYNS, K., CHENG, J. D., CHEN, X., SCHARPÉ, S. & MEESTER, I. D. 2007. Dipeptidyl peptidase 8/9-like activity in human leukocytes. *Journal of Leukocyte Biology,* 81**,** 1252-7.

MAO, J. R., TAYLOR, G., DEAN, W. B., WAGNER, D. R., AFZAL, V., LOTZ, J. C., RUBIN, E. M. & BRISTOW, J. 2002. Tenascin-X deficiency mimics Ehlers-Danlos syndrome in mice through alteration of collagen deposition. *Nat Genet,* 30**,** 421-425.

MARGUET, D., BAGGIO, L., KOBAYASHI, T., BERNARD, A. M., PIERRES, M., NIELSEN, P. F., RIBEL, U., WATANABE, T., DRUCKER, D. J. & WAGTMANN, N. 2000. Enhanced insulin secretion and improved glucose tolerance in mice lacking CD26. *Proceedings of the National Academy of Sciences of the United States of America,* 97**,** 6874-6879.

MARTINET, W., SCHRIJVERS, D. M., TIMMERMANS, J.-P., BULT, H. & DE MEYER, G. R. Y. 2013. Immunohistochemical analysis of macroautophagy: Recommendations and limitations. *Autophagy,* 9**,** 386-402.

MATHEEUSSEN, V., BAERTS, L., DE MEYER, G., DE KEULENAER, G., VAN DER VEKEN, P., AUGUSTYNS, K., DUBOIS, V., SCHARPE, S. & DE MEESTER, I. 2011. Expression and spatial heterogeneity of dipeptidyl peptidases in endothelial cells of

conduct vessels and capillaries. *Biological Chemistry,* 392**,** 189-198.

MATHEEUSSEN, V., WAUMANS, Y., MARTINET, W., VAN GOETHEM, S., VAN DER VEKEN, P., SCHARPE, S., AUGUSTYNS, K., DE MEYER, G. R. & DE MEESTER, I. 2013. Dipeptidyl peptidases in atherosclerosis: expression and role in macrophage differentiation, activation and apoptosis. *Basic Research in Cardiology,* 108**,** 350.

MATSUBARA, J., SUGIYAMA, S., SUGAMURA, K., NAKAMURA, T., FUJIWARA, Y., AKIYAMA, E., KUROKAWA, H., NOZAKI, T., OHBA, K., KONISHI, M., MAEDA, H., IZUMIYA, Y., KAIKITA, K., SUMIDA, H., JINNOUCHI, H., MATSUI, K., KIM-MITSUYAMA, S., TAKEYA, M. & OGAWA, H. 2012. A Dipeptidyl Peptidase-4 Inhibitor, Des-Fluoro-Sitagliptin, Improves Endothelial Function and Reduces Atherosclerotic Lesion Formation in Apolipoprotein E–Deficient Mice. *Journal of the American College of Cardiology,* 59**,** 265-276.

MAYLE, A., LUO, M., JEONG, M. & GOODELL, M. A. 2013. Flow Cytometry Analysis of Murine Hematopoietic Stem Cells. *Cytometry Part A,* 83A**,** 27-37.

MEDINA, J. M., VICARIO, C., JUANES, M. C. & FERNANDEZ, E. 1992. Biochemical Adaptations to Early Extrauterine Life. *In:* HERRERA, E. & KNOPP, R. H. (eds.) *Perinatal Biochemistry.* Boca Raton: CRC Press.

MENTLEIN, R. 1999. Dipeptidyl-peptidase IV (CD26): role in the inactivation of regulatory peptides. *Regulatory Peptides,* 85**,** 9-24.

MENTLEIN, R., GALLWITZ, B. & SCHMIDT, W. E. 1993. Dipeptidyl-peptidase IV hydrolyses gastric inhibitory polypeptide, glucagon-like peptide-1(7-36)amide, peptide histidine methionine and is responsible for their degradation in human serum. *European Journal of Biochemistry,* 214**,** 829-35.

MIKKOLA, H. K. & ORKIN, S. H. 2006. The journey of developing hematopoietic stem cells. *Development,* 133**,** 3733-3744.

MILNER, J., HUI, W., DAVIDSON, R., GILMORE, B., WALKER, B., CLARK, I. & ROWAN, D. 2008. Inhibition of FAP and dipeptidyl peptidase enzymes blocks cartilage restoration. *Clinical Chemistry and Laboratory Medicine,* 46**,** A31.

MINETTE, M. S. & SAHN, D. J. 2006. Ventricular Septal Defects. *Circulation,* 114**,** 2190-2197.

MIYAMOTO, N., YOSHIDA, M., KURATANI, S., MATSUO, I. & AIZAWA, S. 1997. Defects of urogenital development in mice lacking Emx2. *Development,* 124**,** 1653-1664.

MIZUSHIMA, N. & KOMATSU, M. 2011. Autophagy: Renovation of Cells and Tissues. *Cell,* 147**,** 728-741.

MIZUSHIMA, N., YAMAMOTO, A., MATSUI, M., YOSHIMORI, T. & OHSUMI, Y. 2004. In Vivo Analysis of Autophagy in Response to Nutrient Starvation Using Transgenic Mice Expressing a Fluorescent Autophagosome Marker. *Molecular Biology of the Cell,* 15**,** 1101-1111.

MONTECINO-RODRIGUEZ, E. & DORSHKIND, K. 2012. B-1 B Cell Development in the Fetus and Adult. *Immunity,* 36**,** 13-21.

MORRISON, S. J., HEMMATI, H. D., WANDYCZ, A. M. & WEISSMAN, I. L. 1995. The purification and characterization of fetal liver hematopoietic stem cells. *Proceedings of the National Academy of Sciences of the United States of America,* 92**,** 10302-10306.

MORRISON, S. J. & WEISSMAN, I. L. 1994. The Long-Term Repopulating Subset of Hematopoietic Stem Cells Is Deterministic and lsolatable by Phenotype

Immunity, 1**,** 661-673.

NAKAI, S., SUGITANI, Y., SATO, H., ITO, S., MIURA, Y., OGAWA, M., NISHI, M., JISHAGE, K.-I., MINOWA, O. & NODA, T. 2003. Crucial roles of Brn1 in distal tubule formation and function in mouse kidney. *Development and disease,* 130**,** 4751-4759.

NGUYEN, D. H., ZHOU, T., SHU, J. & MAO, J.-H. 2013. Quantifying chromogen intensity in immunohistochemistry via reciprocal intensity. *Cancer InCytes,* 2**,** e.

NIEDERMEYER, J., GARIN-CHESA, P., KRIZ, M., HILBERG, F., MUELLER, E., BAMBERGER, U., RETTIG, W. J. & SCHNAPP, A. 2001. Expression of the fibroblast activation protein during mouse embryo development. *International Journal of Developmental Biology,* 45**,** 445-7.

NIEDERMEYER, J., KRIZ, M., HILBERG, F., GARIN-CHESA, P., BAMBERGER, U., LENTER, M. C., PARK, J., VIERTEL, B., PUSCHNER, H., MAUZ, M., RETTIG, W. J. & SCHNAPP, A. 2000. Targeted disruption of mouse fibroblast activation protein. *Molecular and Cellular Biology,* 20**,** 1089-1094.

OHNUMA, K., ISHII, T., IWATA, S., HOSONO, O., KAWASAKI, H., UCHIYAMA, M., TANAKA, H., YAMOCHI, T., DANG, N. H. & MORIMOTO, C. 2002. G1/S cell cycle arrest provoked in human T cells by antibody to CD26. *Immunology,* 107**,** 325-333.

OKONDO, M. C., JOHNSON, D. C., SRIDHARAN, R., GO, E. B., CHUI, A. J., WANG, M. S., POPLAWSKI, S. E., WU, W., LIU, Y., LAI, J. H., SANFORD, D. G., ARCIPRETE, M. O., GOLUB, T. R., BACHOVCHIN, W. W. & BACHOVCHIN, D. A. 2016. DPP8 and DPP9 inhibition induces pro-caspase-1-dependent monocyte and macrophage pyroptosis. LID - 10.1038/nchembio.2229 [doi]. *Nature chemical biology*.

OLSEN, C. & WAGTMANN, N. 2002. Identification and characterization of human Dpp9, a novel homologue of dipeptidyl peptidase IV. *Gene,* 299**,** 185-93.

PANTANO, S., DUBOST, V., DARRIBAT, K., COUTTET, P., GRENET, O., BUSCH, S. & MOULIN, P. 2013. Differential expression of dipeptidyl peptidase IV in human versus cynomolgus monkey skin eccrine sweat glands. *Journal of Molecular Histology,* 44**,** 733-747.

PARK, J., KNOTT, H. M., NADVI, N. A., COLLYER, C. A., WANG, X. M., CHURCH, W. B. & GORRELL, M. D. 2008. Reversible inactivation of human dipeptidyl peptidases 8 and 9 by oxidation. *The Open Enzyme Inhibition Journal,* 1**,** 52-60.

PARK, J. E., LENTER, M. C., ZIMMERMANN, R. N., GARIN-CHESA, P., OLD, L. J. & RETTIG, W. J. 1999. Fibroblast activation protein: A dual-specificity serine protease expressed in reactive human tumor stromal fibroblasts. *Journal of Biological Chemistry,* 274**,** 36505-36512.

PASPARAKIS, M., HAASE, I. & NESTLE, F. O. 2014. Mechanisms regulating skin immunity and inflammation. *Nat Rev Immunol,* 14**,** 289-301.

PILLA, E., KILISCH, M., LENZ, C., URLAUB, H. & GEISS-FRIEDLANDER, R. 2013. The SUMO1-E67 Interacting Loop Peptide Is an Allosteric Inhibitor of the Dipeptidyl Peptidases 8 and 9. *The Journal of Biological Chemistry,* 288**,** 32787-32796.

PILLA, E., MÖLLER, U., SAUER, G., MATTIROLI, F., MELCHIOR, F. & GEISS-FRIEDLANDER, R. 2012. A novel SUMO1-specific interacting motif in Dipeptidyl peptidase 9 (DPP9) that is important for enzymatic regulation. *Journal of Biological Chemistry,* 287**,** 44320-44329.

PITMAN, M. R., MENZ, R. I. & ABBOTT, C. A. 2010. Hydrophilic residues surrounding the

S1 and S2 pockets contribute to dimerisation and catalysis in human dipeptidyl peptidase 8 (DPP8). *Biological Chemistry,* 391**,** 959-72.

PUTAALA, H., SOININEN, R., KILPELAINEN, P., WARTIOVAARA, J. & TRYGGVASON, K. 2001. The murine nephrin gene is specifically expressed in kidney, brain and pancreas: inactivation of the gene leads to massive proteinuria and neonatal death. *Human Molecular Genetics,* 10**,** 1-8.

QI, S. Y., RIVIERE, P. J., TROJNAR, J., JUNIEN, J. L. & AKINSANYA, K. O. 2003. Cloning and characterization of dipeptidyl peptidase 10, a new member of an emerging subgroup of serine proteases. *Biochemical Journal,* 373**,** 179-89.

REBEL, V. I., MILLER, C. L., EAVES, C. J. & LANSDORP, P. M. 1996. The Repopulation Potential of Fetal Liver Hematopoietic Stem Cells in Mice Exceeds That of Their Adult Bone Marrow Counterparts. *Blood,* 87**,** 3500-3507.

REINHOLD, D., GOIHL, A., WRENGER, S., REINHOLD, A., KÜHLMANN, U. C., FAUST, J., NEUBERT, K., THIELITZ, A., BROCKE, S., TÄGER, M., ANSORGE, S. & BANK, U. 2009. Role of dipeptidyl peptidase IV (DPIV)-like enzymes in T lymphocyte activation: investigations in DPIV/CD26 knockout mice. *Clinical Chemistry and Laboratory Medicine,* 47**,** 268-74.

REN, X., HAYASHI, Y., YOSHIMURA, N. & TAKIMOTO, K. 2005. Transmembrane interaction mediates complex formation between peptidase homologues and Kv4 channels. *Mol Cell Neurosci,* 29**,** 320-32.

RÖHNERT, P., SCHMIDT, W., EMMERLICH, P., GOIHL, A., WRENGER, S., BANK, U., NORDHOFF, K., TAEGER, M., ANSORGE, S., REINHOLD, D. & STRIGGOW, F. 2012. Dipeptidyl peptidase IV, aminopeptidase N and DPIV/APN-like proteases in

cerebral ischemia. *Journal of Neuroinflammation,* 9**,** 44.

RUGH, R. 1968. *The Mouse: Its Reproduction and Development,* Minneapolis, Burgess Publishing Company.

RUMMEY, C. & METZ, G. 2007. Homology models of dipeptidyl peptidases 8 and 9 with a focus on loop predictions near the active site. *Proteins,* 66**,** 160-71.

SABOL, F., DANCAKOVA, L., GAL, P., VASILENKO, T., NOVOTNY, M., SMETANA, K. & LENHARDT, L. 2012. Immunohistochemical changes in skin wounds during the early periods of healing in a rat model. *Veterinarni Medicina,* 57**,** 77-82.

SCHADE, J., STEPHAN, M., SCHMIEDL, A., WAGNER, L., NIESTROJ, A. J., DEMUTH, H. U., FRERKER, N., KLEMANN, C., RABER, K. A., PABST, R. & VON HORSTEN, S. 2008. Regulation of expression and function of dipeptidyl peptidase 4 (DP4), DP8/9, and DP10 in allergic responses of the lung in rats. *Journal of Histochemistry and Cytochemistry,* 56**,** 147-55.

SCHAFER, M. & WERNER, S. 2008. Cancer as an overhealing wound: an old hypothesis revisited. *Nat Rev Mol Cell Biol,* 9**,** 628-638.

SCHEUNER, D., SONG, B., MCEWEN, E., LIU, C., LAYBUTT, R., GILLESPIE, P., SAUNDERS, T., BONNER-WEIR, S. & KAUFMAN, R. J. 2001. Translational Control Is Required for the Unfolded Protein Response and In Vivo Glucose Homeostasis. *Molecular Cell,* 7**,** 1165-1176.

SCHIAFFINO, S., MAMMUCARI, C. & SANDRI, M. 2008. The role of autophagy in neonatal tissues: just a response to amino acid starvation? *Autophagy,* 4**,** 727-730.

SCHINDELIN, J., ARGANDA-CARRERAS, I., FRISE, E., KAYNIG, V., LONGAIR, M., PIETZSCH,

T., PREIBISCH, S., RUEDEN, C., SAALFELD, S., SCHMID, B., TINEVEZ, J.-Y., WHITE, D. J., HARTENSTEIN, V., ELICEIRI, K., TOMANCAK, P. & CARDONA, A. 2012. Fiji: an open-source platform for biological-image analysis. *Nat Meth,* 9**,** 676-682.

SCHLAGER, G. & RODERICK, T. 1968. Secondary Sex Ratio in Mice. *Journal of Heredity,* 59**,** 363-365.

SCHÜRMANN, C., LINKE, A., ENGELMANN-PILGER, K., STEINMETZ, C., MARK, M., PFEILSCHIFTER, J., KLEIN, T. & FRANK, S. 2012. The Dipeptidyl Peptidase-4 Inhibitor Linagliptin Attenuates Inflammation and Accelerates Epithelialization in Wounds of Diabetic ob/ob Mice. *Journal of Pharmacology and Experimental Therapeutics,* 342**,** 71-80.

SEITA, J. & WEISSMAN, I. L. 2010. Hematopoietic stem cell: self-renewal versus differentiation. *Wiley Interdisciplinary Reviews: Systems Biology and Medicine,* 2**,** 640-653.

SHANLEY, D. P., AW, D., MANLEY, N. R. & PALMER, D. B. 2009. An evolutionary perspective on the mechanisms of immunosenescence. *Trends in Immunology,* 30**,** 374-381.

SHEN, F. W., SAGA, Y., LITMAN, G., FREEMAN, G., TUNG, J. S., CANTOR, H. & BOYSE, E. A. 1985. Cloning of Ly-5 cDNA. *Proceedings of the National Academy of Sciences of the United States of America,* 82**,** 7360-7363.

SHINGU, K., HELFRITZ, A., ZIELINSKA-SKOWRONEK, M., MEYER-OLSON, D., JACOBS, R., SCHMIDT, R. E., MENTLEIN, R., PABST, R. & VON HORSTEN, S. 2003. CD26 expression determines lung metastasis in mutant F344 rats: involvement of NK cell function and soluble CD26. *Cancer Immunol Immunother,* 52**,** 546-54.

SHIZURU, J. A., NEGRIN RS FAU - WEISSMAN, I. L. & WEISSMAN, I. L. 2005. Hematopoietic stem and progenitor cells: clinical and preclinical regeneration of the hematolymphoid system. *Annual review Of medicine,* 56**,** 509-538.

SIERRO, F., BIBEN, C., MARTÍNEZ-MUÑOZ, L., MELLADO, M., RANSOHOFF, R. M., LI, M., WOEHL, B., LEUNG, H., GROOM, J., BATTEN, M., HARVEY, R. P., MARTÍNEZ-A, C., MACKAY, C. R. & MACKAY, F. 2007. Disrupted cardiac development but normal hematopoiesis in mice deficient in the second CXCL12/SDF-1 receptor, CXCR7. *Proceedings of the National Academy of Sciences of the United States of America,* 104**,** 14759-14764.

SINAGRA, T., MERLO, S., SPAMPINATO, S. F., PASQUALE, R. D. & SORTINO, M. A. 2015. High mobility group box 1 contributes to wound healing induced by inhibition of dipeptidylpeptidase 4 in cultured keratinocytes. *Frontiers in Pharmacology,* 6**,** 126.

SIVRIDIS, E., KOUKOURAKIS MI FAU - ZOIS, C. E., ZOIS CE FAU - LEDAKI, I., LEDAKI I FAU - FERGUSON, D. J. P., FERGUSON DJ FAU - HARRIS, A. L., HARRIS AL FAU - GATTER, K. C., GATTER KC FAU - GIATROMANOLAKI, A. & GIATROMANOLAKI, A. 2010. LC3A-positive light microscopy detected patterns of autophagy and prognosis in operable breast carcinomas. *American Journal of Pathology,* 176**,** 2477-2489.

SMITHERS, B., OATES, M. E., TOMPA, P. & GOUGH, J. 2016. Three reasons protein disorder analysis makes more sense in the light of collagen. *Protein Science,* 25**,** 1030-1036.

SPAGNUOLO, P. A., HURREN, R., GRONDA, M., MACLEAN, N., DATTI, A., BASHEER, A., LIN, F. H., WANG, X., WRANA, J. & SCHIMMER, A. D. 2013. Inhibition of

intracellular dipeptidyl peptidases 8 and 9 enhances parthenolide's anti-leukemic activity. *Leukemia,* 27**,** 1236-1244.

SPANGRUDE, G. J. 2001. Assessment of Lymphocyte Development in Radiation Bone Marrow Chimeras. *Current Protocols in Immunology.* John Wiley & Sons, Inc.

STARCHER, B., AYCOCK, R. L. & HILL, C. H. 2005. Multiple Roles for Elastic Fibers in the Skin. *Journal of Histochemistry & Cytochemistry,* 53**,** 431-443.

STREMENOVA, J., KREPELA, E., MARES, V., TRIM, J., DBALY, V., MAREK, J., VANICKOVA, Z., LISA, V., YEA, C. & SEDO, A. 2007. Expression and enzymatic activity of dipeptidyl peptidase-IV in human astrocytic tumours are associated with tumour grade. *International Journal of Oncology,* 31**,** 785-92.

STREMENOVA, J., MARES, V., LISA, V., HILSER, M., KREPELA, E., VANICKOVA, Z., SYRUCEK, M., SOULA, O. & SEDO, A. 2010. Expression of dipeptidyl peptidase-IV activity and/or structure homologs in human meningiomas. *International Journal of Oncology,* 36**,** 351-8.

SUGRUE, T., LOWNDES, N. F. & CEREDIG, R. 2013. Mesenchymal stromal cells: radio-resistant members of the bone marrow. *Immunol Cell Biol,* 91**,** 5-11.

SULDA, M. L., ABBOTT, C. A., MACARDLE, P. J., HALL, R. K. & KUSS, B. J. 2010. Expression and prognostic assessment of dipeptidyl peptidase IV and related enzymes in B-cell chronic lymphocytic leukemia. *Cancer Biology & Therapy,* 10**,** 180-189.

SUNGUR, C. M. & MURPHY, W. J. 2014. Positive and Negative Regulation by NK Cells in Cancer. *Critical reviews in oncogenesis,* 19**,** 57-66.

TADJE, J., HEIMBURG, A., KOCH, G., HELMUTH, M., REINHOLD, D., FUCHS, P., FAUST, J., NEUBERT, K., TAGER, M., ANSORGE, S. & BANK, U. 2008. Expression pattern and

inhibition of DASH proteins T cell subsets and related cell lines *Clinical Chemistry and Laboratory Medicine,* 46**,** A36.

TAI, X., GUINTER, T. & SINGER, A. 2012. Bone marrow transplantation. *In:* HTTPS://CCROD.CANCER.GOV/CONFLUENCE/DOWNLOAD/ATTACHMENTS/80677524/XUGUANG%20TAI.PDF?VERSION=1 (ed.) *Pdf.* Bethseda: Center for Cancer Research.

TAKEUCHI, M. & MIYAJIMA, A. 2004. Fetal liver hematopoiesis. *Japanese journal of clinical hematology,* 45**,** 355-364.

TANG, H.-K., TANG, H.-Y., HSU, S. C., CHU, J. R., CHIEN, C. H., SHU, C. H. & CHEN, X. 2009. Biochemical properties and expression profile of human prolyl dipeptidase DPP9. *Archives of Biochemistry and Biophysics,* 485**,** 120-127.

TANG, H. K., CHEN, K. C., LIOU, G. G., CHENG, S. C., CHIEN, C. H., TANG, H. Y., HUANG, L. H., CHANG, H. P., CHOU, C. Y. & CHEN, X. 2011. Role of a propeller loop in the quaternary structure and enzymatic activity of prolyl dipeptidases DPP-IV and DPP9. *FEBS Letters,* 585**,** 3409-3414.

TAYLOR, P. A., MCELMURRY, R. T., LEES, C. J., HARRISON, D. E. & BLAZAR, B. R. 2002. Allogenic fetal liver cells have a distinct competitive engraftment advantage over adult bone marrow cells when infused into fetal as compared with adult severe combined immunodeficient recipients. *Blood,* 99**,** 1870-1872.

THEILER, K. 1989. *The house mouse: atlas of embryonic development,* New York, Springer-Verlag.

THIELITZ, A., VETTER, R. W., SCHULTZE, B., WRENGER, S., SIMEONI, L., ANSORGE, S., NEUBERT, K., FAUST, J., LINDENLAUB, P., GOLLNICK, H. P. M. & REINHOLD, D.

2008. Inhibitors of Dipeptidyl Peptidase IV-Like Activity Mediate Antifibrotic Effects in Normal and Keloid-Derived Skin Fibroblasts. *Journal of Investigative Dermatology,* 128**,** 855-866.

TRAVER, D., MIYAMOTO, T., CHRISTENSEN, J., IWASAKI-ARAI, J., AKASHI, K. & WEISSMAN, I. L. 2001. Fetal liver myelopoiesis occurs through distinct, prospectively isolatable progenitor subsets. *Blood,* 98**,** 627-635.

TURGEON, B. & MELOCHE, S. 2009. Interpreting Neonatal Lethal Phenotypes in Mouse Mutants: Insights Into Gene Function and Human Diseases. *Physiological Reviews***,** 1-26.

VAN DER MEEREN, A., MONTI, P., LEBARON-JACOBS, L., MARQUETTE, C. & GOURMELON, P. 2001. Characterization of the Acute Inflammatory Response after Irradiation in Mice and Its Regulation by Interleukin 4 (Il4). *Radiation Research,* 155**,** 858-865.

VAN DER VEKEN, P., DE MEESTER, I., DUBOIS, V., SOROKA, A., VAN GOETHEM, S., MAES, M. B., BRANDT, I., LAMBEIR, A. M., CHEN, X., HAEMERS, A., SCHARPE, S. & AUGUSTYNS, K. 2008. Inhibitors of dipeptidyl peptidase 8 and dipeptidyl peptidase 9. Part 1: identification of dipeptide derived leads. *Bioorganic & Medicinal Chemistry Letters,* 18**,** 4154-8.

VAN DER VEKEN, P., SOROKA, A., BRANDT, I., CHEN, Y. S., MAES, M. B., LAMBEIR, A. M., CHEN, X., HAEMERS, A., SCHARPE, S., AUGUSTYNS, K. & DE MEESTER, I. 2007. Irreversible inhibition of dipeptidyl peptidase 8 by dipeptide-derived diaryl phosphonates. *Journal of Medicinal Chemistry,* 50**,** 5568-70.

VAN GOETHEM, S., MATHEEUSSEN, V., JOOSSENS, J., LAMBEIR, A. M., CHEN, X., DE

MEESTER, I., HAEMERS, A., AUGUSTYNS, K. & VAN DER VEKEN, P. 2011. Structure-activity relationship studies on isoindoline inhibitors of dipeptidyl peptidases 8 and 9 (DPP8, DPP9): is DPP8-selectivity an attainable goal? *Journal of Medicinal Chemistry,* 54**,** 5737-46.

VINCE, J. E., WONG, W. W., KHAN, N., FELTHAM, R., CHAU, D., AHMED, A. U., BENETATOS, C. A., CHUNDURU, S. K., CONDON, S. M., MCKINLAY, M., BRINK, R., LEVERKUS, M., TERGAONKAR, V., SCHNEIDER, P., CALLUS, B. A., KOENTGEN, F., VAUX, D. L. & SILKE, J. 2007. IAP antagonists target cIAP1 to induce TNFalpha-dependent apoptosis. *Cell,* 131**,** 682-93.

WAGNER, L., GUNDEL, D., ZEITSCHEL, U., ROSSNER, S., FRERKER, N., SCHADE, J., STILLER, J., NIESTROJ, A. J., THUMMLER, A., WOLF, R., GARTNER, U. T., MANHART, S., KEHLEN, A., RAHFELD, J.-U., HOFFMAN, T., VON HORSTEN, S. & DEMUTH, H. U. 2006a. Tissue-distribution of dipeptidyl peptidase 4-like enzymes in distinct brain areas and neuronal tissue. *Clinical Chemistry and Laboratory Medicine,* 46**,** A11.

WAGNER, L., HOFFMAN, T., RAHFELD, J.-U. & DEMUTH, H. U. 2006b. Distribution of dipeptidyl peptidase IV-like activity enzymes in canine and porcine tissue sections by RT-PCR. *In:* LENDECKEL, U., REINHOLD, D. & BANK, U. (eds.) *Dipeptidyl Aminopeptidases: Basic Science and Clinical Applications*

New York: Kluwer.

WAGURI, S. & KOMATSU, M. Biochemical and Morphological Detection of Inclusion Bodies in Autophagy-Deficient Mice. *In:* KLIONSKY, D. (ed.) *Methods in Enzymology: Autophagy in Disease and Clinical Applications, Part C.* San Diego:

Elsevier.

WALSH, M. P., DUNCAN, B., LARABEE, S., KRAUSS, A., DAVIS, J., CUI, Y., KIM, S. Y., GUIMOND, M., BACHOVCHIN, W. & FRY, T. J. 2013. Val-BoroPro Accelerates T Cell Priming via Modulation of Dendritic Cell Trafficking Resulting in Complete Regression of Established Murine Tumors. *PLoS ONE,* 8**,** e58860.

WANG, A., DORSO, C., KOPCHO, L., LOCKE, G., LANGISH, R., HARSTAD, E., SHIPKOVA, J. M., HAMANN, L. & KIRBY, M. S. 2012. Potency, selectivity and prolonged binding of saxagliptin to DPP4: maintenance of DPP4 inhibition by saxagliptin in vitro and ex vivo when compared to a rapidly-dissociating DPP4 inhibitor. *BMC Pharmacology,* 12:2.

WANG, N.-D., FINEGOLD, M. F., BRADLEY, A., OU, C. N., ABDELSAYED, S. V., WILDE, M. D., TAYLOR, L. R., WILSON, D. R. & DARLINGTON, G. J. 1995. Impaired Energy Homeostasis in C/EBPα Knockout Mice. *Science,* 269.

WANG, X. M., CORDOBA, S., MARGUET, D., RETTIG, W., SCHNAPP, A., MCCAUGHAN, G. W. & GORRELL, M. D. 2007. Reduced hepatic fibrosis is associated with fewer intrahepatic B cells in Fibroblast Activation Protein and dipeptidyl peptidase IV gene knockout mice. *Hepatology,* 46**,** 299A.

WANG, X. M., YU, D. M. T., MCCAUGHAN, G. W. & GORRELL, M. D. 2005. Fibroblast activation protein increases apoptosis, cell adhesion and migration by the LX-2 human stellate cell line. *Hepatology,* 42**,** 935-945.

WANG, Z. & BUNTING, K. D. 2008. Hematopoietic Stem Cell Transplant into Non-Myeloblated *W/W^{v}* Mice to Detect Steady-State Engraftment Defects. *In:* BUNTING, K. D. (ed.) *Methods in Molecular Biology.* Totowa, New Jersey:

Humana Press.

WAUMANS Y, BAERTS L, KEHOE K, LAMBEIR A-M & I, D. M. 2015. The Dipeptidyl Peptidase Family, Prolyl Oligopeptidase, and Prolyl Carboxypeptidase in the Immune System and Inflammatory Disease, Including Atherosclerosis. *Frontiers in Immunology,* 6**,** 387.

WAUMANS, Y., BAERTS, L., KEHOE, K., LAMBEIR, A.-M. & DE MEESTER, I. 2015. The Dipeptidyl Peptidase Family, Prolyl Oligopeptidase and Prolyl Carboxypeptidase in the Immune System and Inflammatory Disease, including Atherosclerosis. *Frontiers in Immunology,* 6**,** 387-405.

WAUMANS, Y., VLIEGEN, G., MAES, L., ROMBOUTS, M., DECLERCK, K., VEKEN, P. V. D., BERGHE, W. V., MEYER, G. R. Y. D., SCHRIJVERS, D. & MEESTER, I. D. 2016. The Dipeptidyl Peptidases 4, 8, and 9 in Mouse Monocytes and Macrophages: DPP8/9 Inhibition Attenuates M1 Macrophage Activation in Mice. *Inflammation***,** epub ahead of print 10 Oct.

WHITTEN, W. K. 1956. MODIFICATION OF THE OESTROUS CYCLE OF THE MOUSE BY EXTERNAL STIMULI ASSOCIATED WITH THE MALE. *Journal of Endocrinology,* 13**,** 399-404.

WILSON, C. & ABBOTT, C. 2012a. Expression profiling of dipeptidyl peptidase 8 and 9 in breast and ovarian carcinoma cell lines. *International Journal of Oncology,* 41**,** 919-932.

WILSON, C., ZHANG, H., GORRELL, M. & ABBOTT, C. 2016. Dipeptidyl peptidase 9 substrates and their discovery: current progress and the application of mass spectrometry-based approaches. *Biological Chemistry,* 397**,** 837-856.

WILSON, C. H. & ABBOTT, C. A. 2012b. Dipeptidyl Peptidases: Substrates and Therapeutic Targeting in Human Health and Disease. *In:* DUNN, B. (ed.) *Proteinases as Drug Targets.* Cambridge UK: Royal Society of Chemistry.

WILSON, C. H., INDARTO, D., DOUCET, A., POGSON, L. D., PITMAN, M. R., MENZ, R. I., MCNICHOLAS, K., OVERALL, C. M. & ABBOTT, C. A. 2013. Identifying natural substrates for dipeptidyl peptidase 8 (DP8) and DP9 using terminal amine isotopic labelling of substrates, TAILS, reveals in vivo roles in cellular homeostasis and energy metabolism. *Journal of Biological Chemistry,* 288**,** 13936-13949.

WOGNUM, A. W. & SZILVASSY, S. J. 2015. Hematopoietic Stem and Progenitor Cells. *In:* TECHNOLOGIES, S. (ed.) Version 6.0.0 ed. Vancouver: STEMCELL Technologies.

WONG, P. F., GALL, M. G., BACHOVCHIN, W. W., MCCAUGHAN, G. W., KEANE, F. M. & GORRELL, M. D. 2016. Neuropeptide Y is a physiological substrate of fibroblast activation protein: Enzyme kinetics in blood plasma and expression of Y2R and Y5R in human liver cirrhosis and hepatocellular carcinoma. *Peptides,* 75**,** 80-95.

WRENGER, S., FAUST, J., MRESTANI-KLAUS, C., BRANDT, W., THIELITZ, A., NEUBERT, K. & REINHOLD, D. 2008. Non-substrate peptides influencing dipeptidyl peptidases IV/CD26 activity and immune cell function. *Frontiers in Bioscience,* 13**,** 3194-3201.

WU, J.-J., TANG, H.-K., YEH, T.-K., CHEN, C.-M., SHY, H.-S., CHU, Y.-R., CHIEN, C.-H., TSAI, T.-Y., HUANG, Y.-C., HUANG, Y.-L., HUANG, C.-H., TSENG, H.-Y., JIAANG, W.-T., CHAO, Y.-S. & CHEN, X. 2009. Biochemistry, pharmacokinetics, and toxicology of a potent and selective DPP8/9 inhibitor. *Biochemical Pharmacology,* 78**,** 203-

210.

WU, W., LIU, Y., MILO JR, L. J., SHU, Y., ZHAO, P., LI, Y., WOZNICA, I., YU, G., SANFORD, D. G., ZHOU, Y., POPLAWSKI, S. E., CONNOLLY, B. A., SUDMEIER, J. L., BACHOVCHIN, W. W. & LAI, J. H. 2012. 4-Substituted boro-proline dipeptides: Synthesis, characterization, and dipeptidyl peptidase IV, 8, and 9 activities. *Bioorganic & Medicinal Chemistry Letters,* 22**,** 5536-5540.

XU, F., LU, T. J. & SEFFEN, K. A. 2008. Biothermomechanical behavior of skin tissue. *Acta Mechanica Sinica,* 24**,** 1-23.

XU, H., EXNER BG FAU - CHILTON, P. M., CHILTON PM FAU - SCHANIE, C., SCHANIE C FAU - ILDSTAD, S. T. & ILDSTAD, S. T. 2004. CD45 congenic bone marrow transplantation: evidence for T cell-mediated immunity. *Stem Cells,* 22**,** 1039-1048.

XU, J. 2005. Preparation, Culture and Immortalization of Mouse Embryonic Fibroblasts. *Current Protocols in Molecular Biology,* Supplement 70**,** 28.1.1-28.1.8.

YANG, W., SHERMAN, V. R., GLUDOVATZ, B., SCHAIBLE, E., STEWART, P., RITCHIE, R. O. & MEYERS, M. A. 2015. On the tear resistance of skin. *Nat Commun,* 6.

YAO, T.-W., KIM, W.-S., YU, D. M., SHARBEEN, G., MCCAUGHAN, G. W., CHOI, K.-Y., XIA, P. & GORRELL, M. D. 2011. A Novel Role of Dipeptidyl Peptidase 9 in Epidermal Growth Factor Signaling. *Molecular Cancer Research,* 9**,** 948-959.

YAZBECK, R., SULDA, M. L., HOWARTH, G. S., BLEICH, A., RABER, K., VON HÖRSTEN, S., HOLST, J. J. & ABBOTT, C. A. 2010. Dipeptidyl peptidase expression during experimental colitis in mice. *Inflammatory Bowel Diseases,* 16**,** 1340-1351.

YU, D. M. T., AJAMI, K., GALL, M. G., PARK, J., LEE, C. S., EVANS, K. A., MCLAUGHLIN, E.

A., PITMAN, M. R., ABBOTT, C. A., MCCAUGHAN, G. W. & GORRELL, M. D. 2009. The in vivo expression of dipeptidyl peptidases 8 and 9. *Journal of Histochemistry and Cytochemistry,* 57**,** 1025-1040.

YU, D. M. T., WANG, X. M., AJAMI, K., MACCAUGHAN, G. & GORRELL, M. D. 2006a. DP8 and DP9 have Extra-Enzymatic Roles in Cell Adhesion, Migration and Apoptosis. *Advances in experimental medicine and biology,* 575**,** 63-72.

YU, D. M. T., WANG, X. M., MCCAUGHAN, G. W. & GORRELL, M. D. 2006b. Extra-enzymatic functions of the dipeptidyl peptidase (DP) IV related proteins DP8 and DP9 in cell adhesion, migration and apoptosis. *FEBS Journal,* 273**,** 2447-61.

YU, D. M. T., YAO, T.-W., CHOWDHURY, S., NADVI, N. A., OSBORNE, B., CHURCH, W. B., MCCAUGHAN, G. W. & GORRELL, M. D. 2010. The Dipeptidyl Peptidase IV family in cancer and cell biology. *FEBS Journal,* 277**,** 1126-1144.

ZHANG, H., CHEN, Y., KEANE, F. M. & GORRELL, M. D. 2013. Advances in understanding the expression and function of dipeptidyl peptidase 8 and 9. *Molecular Cancer Research,* 11**,** 1487-1496.

ZHANG, H., CHEN, Y., WADHAM, C., MCCAUGHAN, G. W., KEANE, F. M. & GORRELL, M. D. 2015a. Dipeptidyl peptidase 9 subcellular localization and a role in cell adhesion involving focal adhesion kinase and paxillin. *Biochimica et Biophysica Acta (BBA) - Molecular Cell Research,* 1853**,** 470-480.

ZHANG, H., MAQSUDI, S., RAINCZUK, A., DUFFIELD, N., LAWRENCE, J., KEANE, F. M., JUSTA-SCHUCH, D., GEISS-FRIEDLANDER, R., GORRELL, M. D. & STEPHENS, A. N. 2015b. Identification of novel dipeptidyl peptidase 9 substrates by two-dimensional differential in-gel electrophoresis. *FEBS Journal,* 282**,** 3737-3757.

ZHU, H., ZHOU, Z. M., LU, L., XU, M., WANG, H., LI, J. M. & SHA, J. H. 2005. Expression of a novel dipeptidyl peptidase 8 (DPP8) transcript variant, DPP8-v3, in human testis. *Asian Journal of Andrology,* 7**,** 245-55.

Appendices

Appendix 1

Statement of Author Contribution

Publication:

Margaret G Gall and Mark D Gorrell (2016) The multifunctional post-proline dipeptidyl peptidase, DPP9, in mice, cell biology and immunity. In: Pathophysiological aspects of proteases. Editors: Sajal Chakraborti and Naranjan S. Dhalla. Publisher: Springer, New York. In press.

Author contributions:

MGG conceived and prepared the figures and wrote the final manuscript

MDG conceived, supervised and assisted in revising the final manuscript

- *In addition to the statements above, in cases where I am not the corresponding author of a published item, permission to include the published material has been granted by the corresponding author*

Student Name: Margaret G. Gall

Signature: 

Date:

- *As supervisor for the candidature upon which this thesis is based, I can confirm that the authorship attribution statements above are correct.*

Supervisor Name: A/Prof Mark D. Gorrell

Signatu[redacted]

Date: 12-12-16.

Appendix 2

Statement of Author Contribution

Publication:

Gall MG, Chen Y, Vieira de Ribeiro AJ, Zhang H, Bailey CG, Spielman DS, et al. (2013) Targeted Inactivation of Dipeptidyl Peptidase 9 Enzymatic Activity Causes Mouse Neonate Lethality. PLoS ONE 8(11): e78378. doi:10.1371/journal.pone.0078378

Author contributions:

MGG conceived, designed and performed the experiments, analysed the data and wrote the manuscript.

DY conceived, designed and performed the experiments and wrote the manuscript.

MDG conceived and designed the experiments, analysed the data and wrote the manuscript.

YC performed the experiments, analysed the data and wrote the manuscript.

AJR performed the experiments.

HZ performed the experiments and analysed the data.

CGB performed the experiments.

DSS analysed the data.

- *In addition to the statements above, in cases where I am not the corresponding author of a published item, permission to include the published material has been granted by the corresponding author*

Student Name: Margaret G. Gall

Signature: [redacted]

Date:

- *As supervisor for the candidature upon which this thesis is based, I can confirm that the authorship attribution statements above are correct.*

Supervisor Name: A/Prof Mark D. Gorrell

Signatu [redacted]

Date: